Endothelial cell culture in microfluidically perfused biochips enables the recreation of microphysiological conditions of the human vasculature *in vitro*

Dissertation

To Fullfill the

Requirements for the Degree of

“doctor rerum naturalium” (Dr. rer. nat.)

Submitted to the Council of the Faculty

of Biological Sciences

of the Friedrich Schiller University of Jena

by M. Sc. Martin Raasch

born on 05.05.1987 in Altenburg

1st Reviewer: PD Dr. Alexander Mosig; Jena University Hospital

2nd Reviewer: Prof. Dr. Otmar Huber; Jena University Hospital

3rd Reviewer: Jun.-Prof. Dr. Peter Loskill; Eberhard Karls University Tübingen

Date of the public disputation: December 14th, 2020

I. Index

II. List of Figures

III. List of Abbreviations

3D	three-dimensional
ADAMTS-13	a disintegrin and metalloproteinase with a thrombospondin type 1 motif, member 13 (von Willebrand factor-cleaving protease)
ADME	absorption, distribution, metabolism, excretion
BBB	blood-brain barrier
CAM	cell adhesion molecule
CD	cluster of differentiation
CFD	computational fluid dynamic
CNS	central nervous system
COC	cyclic olefin copolymer
COP	cyclic olefin polymer
CSI	cell shape index
CX3CL1	fractalkine
(p)DNA	(plasmid) deoxyribonucleic acid
EC	endothelial cell
ECM	extracellular matrix
ET-1	endothelin-1
EPR effect	enhanced permeability and retention effect
FITC	fluorescein isothiocyanate
GSH	glutathione
hCMEC	human cerebral microvascular endothelial cell
ICAM-1	intercellular adhesion molecule-1 / CD54
IL	interleukin
INFγ	interferon gamma
iPSC	induced pluripotent stem cell
ITO	indium tin oxide

JAM-A	junctional adhesion molecule-A
LDH	lactate dehydrogenase
LDL	low density lipoprotein
LPS	lipopolysaccharide
MAPK	mitogen-activated protein kinase
MCP-1	monocyte chemoattractant protein-1
MOTiF	multi-organ-tissue-flow
MPS	microphysiological system
NP	nanoparticle
NO	nitric oxide
PAX6	paired box 6
PDMAEMA	poly((methyl methacrylate)-*co*-(2-dimethylamino ethylmethacrylate))
PDMS	polydimethylsiloxane
PECAM-1	platelet endothelial cell adhesion molecule-1 / CD31
PEG	polyethylene glycol
PEI	poly (ethylene imine)
PLGA	Poly(lactic-co-glycolic acid)
PMAA	poly((methyl methacrylate)-*co*-(methacrylic acid))
PRINT	particle replication in nonwetting templates
PS	polystyrene
RAFT	reversible addition-fragmentation chain transfer
(m/si)RNA	(messenger / small interfering) ribonucleic acid
RES	reticuloendothelial system
RGD	arginine-glycine-aspartate (peptide sequence)
ROS	reactive oxygen species
SMC	smooth muscle cell
SSRE	shear stress responsive element
µTAS	micro total analysis system
TAT	trans-activator of transcription

Tbr 1/2	T-box brain
TEER	transendothelial electrical resistance
TIMP1	tissue inhibitor of metalloproteinase 1
TNF	tumor necrosis factor
VCAM-1	vascular cell adhesion molecule-1 / CD106
VE	vascular endothelial
VEGF(R-2)	vascular endothelial growth factor (receptor-2)
vWf	von Willebrand factor
WPB	Weibel-Palade body
ZO	*zonula occludens*

IV. Summary

The endothelium lines the inner surface of all blood vessels representing an important tissue with vital functions to mediate tissue homeostasis [1, 2]. Tissue-tissue interfaces play an critical role throughout the human body where endothelial cells (ECs) contribute by creating vital barriers with tight and adherens junctions to regulate permeability of macromolecules and fluids while protecting and nourishing adjacent tissue [3, 4]. They are the most prominent cell type to experience physical forces of shear, stretch and strain through the laminar pulsatile nature of the bloodstream [5, 6]. Alterations in physiological flow profiles has a strong impact on EC pathology contributing to diseases like atherosclerosis and coronary heart disease as well as inflammatory conditions [6-8]. Further, they are among the first cell types to interact with xenobiotics. Endothelial endocytosis and barrier regulation have profound impact on drug-tissue interactions. Although first attempts to study EC biology under physiological conditions of shear stress have already been made in the 1970s, the field hast stayed very small and never really left focus from just investigating morphological and molecular changes on a cellular level for a long time. There is still the need for technological innovations and improvements to study EC biology, EC-epithelial and EC-nanocarrier interactions in more complex settings that take physiological biophysical and biochemical cues into account.

For this purpose, the *Multi-Organ-Tissue-Flow* (MOTiF) biochip has been invented and its design has been finalised during the beginning of this thesis. The objective was to develop handling and cellular seeding protocols for the biochip and to subsequently establish more *in vivo*-like and more complex *in vitro* EC culture approaches. Within the scope of this thesis, the biochip has been characterised for perfused EC culture. Complex co-cultures with tissue-resident macrophages and further with murine cortical spheroids present in liver sinusoidal structures and at the blood-brain barrier (BBB) have been established, respectively. Additionally, first applications under physiological parameters of shear stress have been made. We focused on nanocarrier uptake profiles and microvascular endothelial barrier interaction.

Initially, perfused ECs have been characterised under low and high shear forces. Results were compared to standard flow chambers and static cell culture (manuscript I). The data on the biochip regarding EC morphology, marker expression, cytoskeletal changes and barrier integrity was found to be much more superior compared to the other approaches. In fact, we discovered that a three-dimensional (3D) perfusion of ECs benefits their biology at the most.

Immune cell recruitment is an important process and tissue-resident macrophages are prominent in many vessels and organs. With the newly established perfusion protocols, we investigated EC-macrophage-interaction influence on xenobiotics such as nanoparticles (NPs) (manuscript II). We chose various shear forces to represent conditions of different vascular beds. We gained interesting insight in shear force dependent and co-culture dependent NP

uptake. Most intriguing is the fact, that high flow and shear rates do not necessarily decrease EC-NP interactions and uptake as we initially hypothesised. Secondly macrophages had a profound impact and dampened endothelial NP uptake presumably due to paracrine signalling. Finally, in this study we could demonstrate that observations made in the perfused *in vitro* system could be found in *in vivo* models of mice.

The multi-layered design of the MOTiF biochip is intentionally and favours more complex co-cultures on several levels and in particular supports questions of barrier integrity. Hence, we were eager to test the culture of ECs from unique vascular beds like the microvasculature of the BBB. Additionally, we further developed the biochip design with an additional membrane enabling the immobilisation of cortical spheroids representing neural tissue (manuscript III). We were able to demonstrate the successful establishment of a simple perfused BBB-like model. We could functionally prove that inflammation induced microvascular barrier breakdown had profound impact on the differentiation and survival of adjacent neural tissue. Thus, the MOTiF biochip facilitates complex perfused co-cellular culture and crosstalk.

In a concluding study we used these insights to simulate nanocarrier delivery across the BBB. We investigated the influence of glutathione (GSH) functionalisation on polyplex-forming polymers (manuscript IV). We obtained best results for maintaining microvascular barrier integrity with simultaneous barrier passage capacity for GSH-decorated polyplexes with secondary amino-functionality. Most importantly, we could demonstrate the model's feasibility to improve studies on EC-NP interaction.

Concluding the results of this thesis, the MOTiF biochip development was successfully completed and culture conditions for improved perfused EC cultures were established. The biochips' feasibility could be demonstrated in an exemplary way with nanocarriers representing applications for xenobiotic screenings. Comparative analysis to studies performed in animals demonstrate the potential of the newly developed tool to minimize or close the data transferability gap between *in vitro and in vivo* experiments. Further, the gained insights in handling perfused EC cultures and the obtained results suggest various future possibilities for complex multi-cellular cultures to implement different microphysiological systems (MPS) with a vascular component in the MOTiF biochip.

V. Zusammenfassung

Endothelzellen kleiden die Oberfläche aller Blutgefäße aus und üben lebenswichtige Funktionen aus, mit denen sie die Homöostase des Blutgefäßgewebes regulieren [1, 2]. Gewebe-Grenzflächen spielen im gesamten menschlichen Körper eine wichtige Rolle und Endothelzellen tragen dazu bei, diese Barrieren mit Zellkontakten der *tight* und *adherens junctions* abzudichten. Darüber hinaus regulieren sie die Permeabilität von Makromolekülen und Flüssigkeiten [3, 4]. Sie stellen den prominentesten Zelltyp dar, bei dem physikalische Kräfte wie Scherstress, zelluläre Dehnung und Verformung durch die laminar-pulsatilen Kräfte des Blutstroms hervorgerufen werden [5, 6]. Darüber hinaus gehören Endothelzellen zu den ersten Zelltypen, die mit körperfremden Stoffen interagieren und deren Verbleib beeinflussen. Obwohl bereits in den 1970er Jahren physiologische Flusskulturbedingungen von Endothelzellen untersucht wurden, blieb das Forschungsgebiet lange Zeit sehr klein und nur auf die Untersuchung morphologischer und molekularer Veränderungen beschränkt. Es besteht demzufolge ein Bedarf an technologischen Neuerungen, um Endothelzellbiologie als auch Wechselwirkung mit angrenzendem Epithelgewebe und körperfremden Stoffen in einem komplexen physiologischen Umfeld unter Berücksichtigung biochemischer und biophysikalischer Parameter zu untersuchen.

Um dies zu realisieren, wurde der MOTiF-Biochip erfunden und zu Beginn dieser Arbeit in seinem Design finalisiert. Die Ziele waren die Entwicklung von Protokollen für das Chip-*handling* und eine perfundierte Endothelzellkultur. Zellkulturen mit gewebeständigen Makrophagen, die die sinusoidalen Strukturen der Leber repräsentieren, und ferner mit kortikalen Sphäroiden, die einfache neuronale Gewebestrukturen an der Blut-Hirn-Schranke repräsentieren, wurden darauf aufbauend etabliert. Zusätzlich wurden erste Anwendungen demonstriert. Der Fokus lag hierbei auf Nanoträgerstrukturen und deren zelluläre Aufnahme sowie die Interaktion mit der mikrovaskulären Endothelzellbarriere der Blut-Hirn-Schranke.

Zunächst wurden Kulturprotokolle entwickelt und Endothelzellen unter niedrigen und hohen Scherkräften charakterisiert. Die Ergebnisse wurden mit standardisierten einkanaligen Biochips und statischen Zellkulturen verglichen (Manuskript I). Die aus dem MOTiF-Biochip gewonnenen Daten bezüglich Endothelzellmorphologie, Marker-Expression, Zytoskelettausbildung und endothelialer Barriereintegrität erwiesen sich als überlegener. Tatsächlich stellten wir fest, dass die Endothelzellen von einer dreidimensionalen Perfusion, welche das Chipdesign erlaubt, am besten profitieren.

Die Rekrutierung von Immunzellen ist ein wichtiger Prozess innerhalb des Blutgefäßsystems. Mit den neu etablierten Kulturprotokollen untersuchten wir den Einfluss von Endothelzell-Makrophagen-Kokultur auf die Interaktion mit körperfremden Stoffen wie z.B. Nanopartikel (Manuskript II). Hierfür haben wie ein Spektrum verschiedener Scherstresswerte gewählt,

welche die Bedingungen in verschiedenen Blutgefäßen darstellen. Scherkräfte und Makrophagen prägten die Nanopartikelaufnahme signifikant. Am überraschendsten ist das Ergebnis, dass hohe Fluss- und Schergeschwindigkeiten nicht unbedingt die Wechselwirkungen von Nanopartikeln an Endothelzellen verringern, wie ursprünglich vermutet. Darüber hinaus schwächten Makrophagen die Aufnahme von Nanopartikeln durch das Endothel maßgeblich. Dies ist vermutlich auf parakrine Signalwege zurückzuführen. Schließlich konnten wir in dieser Studie zeigen, dass die *in vitro* gewonnenen Ergebnisse in *in vivo*-Mausversuchen nachvollzogen werden konnten.

Das Design des MOTiF-Biochips begünstigt ferner die Etablierung komplexerer Kokulturen. Die frei hängende Membran ermöglicht eine Zellkultur auf mehreren Ebenen und unterstützt insbesondere Fragestellungen der Barriereintegrität. Daher waren wir bestrebt, die Kultur von Endothelzellen mit besonderer Barrierefunktion wie z.B. der Blut-Hirn-Schranke zu testen. Dafür wurde das Biochip-Design mit einer zusätzlichen Membranebene weiterentwickelt, welche die Immobilisierung kortikaler Sphäroide ermöglichte (Manuskript III). Wir konnten die erfolgreiche Etablierung eines einfachen perfundierten Blut-Hirn-Schranke Modells demonstrieren und funktionell nachweisen, dass entzündliche Prozesse die mikrovaskulären Barriere zusammenbrechen lassen und einen tiefgreifenden Einfluss auf die Differenzierung und das Überleben des benachbarten Nervengewebes haben. Somit ermöglicht der MOTiF-Biochip auch den Aufbau komplexer perfundierter Zellkulturmodelle und zelluläre Kommunikation.

In einer abschließenden Studie haben wir mit diesem Modell die Passage von Glutathion-funktionalisierten Nanoträgersystemen über die Blut-Hirn-Schranke simuliert (Manuskript IV). Die besten Ergebnisse für die Aufrechterhaltung der mikrovaskulären Barriereintegrität bei gleichzeitiger Fähigkeit die Barriere zu passieren, erhielten wir für Glutathion-funktionalisierte Polyplexe mit sekundärer Aminfunktionalität. Weiterhin konnten wir damit die Nützlichkeit zur Evaluierung von Endothelzell-Nanopartikel-Interaktionen demonstrieren.

Zusammengefasst wurde die Etablierung des MOTiF-Biochips für endotheliale perfundierte Mono- und Kozellkulturen erfolgreich umgesetzt. Die spezifische Anwendung der Systeme konnte beispielhaft an Studien mit Nanoträgerstrukturen demonstriert werden, die eine mögliche Form von Wirkstoffapplikationen und Therapieformen darstellen. Vergleichbare Ergebnisse zu tierexperimentellen Studien von Kollegen zeigen das Potenzial des neu entwickelten Biochips, die Lücke bei der Datenübertragung aus *in vitro*-Versuchen in *in vivo*-Experimente zu minimieren oder zu schließen. Darüber hinaus belegen die gewonnenen Erkenntnisse im Umgang mit perfundierten Endothelzellkulturen und die erzielten Ergebnisse aus den multizellulären Versuchen, dass mit Hilfe des MOTiF-Biochips innovative, komplexe mikrophysiologische Systeme implementierbar sind.

1. Introduction

1.1 The Endothelium

The endothelium is a thin layer of cells lining the inner lumen of both blood and lymphatic vessels in the human body [1, 2, 4]. It is comprised of ECs and the subendothelium, i.e. primarily extracellular matrix (ECM) proteins like collagen, fibronectin, laminin, glycosaminoglycans and von Willebrand factor (vWf), all secreted by ECs [2]. With approximately 1 x 10^{13} cells yielding a total mass of approximately 1 kg and a surface area of approximately 5,000 m² it is one of the largest tissues within the human body [1, 2]. Its main functions are the regulation of blood vessel barrier integrity, vasomotor tone, organisation of angiogenesis, the mediation and regulation of immune cell trafficking and inflammation, and the regulation of coagulation [1, 2, 9]. Hence, a healthy endothelium is inevitable for maintaining body homeostasis. EC dysfunction contributes to a variety of pathological conditions, mainly cardiovascular diseases (atherosclerosis, hypertension, allograft vasculopathy), diabetes, sepsis and associated inflammatory syndromes [1, 2].

Moreover, the endothelium and its associated ECM provide a site- and time-specific regulation of various molecular processes through the secretion of soluble factors into the blood stream [9]. Additionally, they are further characterised by a high degree of plasticity [1]. Both features cause a phenomenon to be known as EC heterogeneity [4] and strongly contributing to organ-specific microenvironments [10]. In consequence, the endothelium is legitimately discussed to classify as an organ [2, 4, 11].

1.1.1 Endothelial cells form a biologically active monolayer

ECs are flattened, rhomboid cells and grow physiologically as monolayer [2]. Although ECs can differ significantly in protein and gene expression along the vascular tree, the majority of ECs share common ultrastructural characteristics like Weibel-Palade bodies (WPBs), fenestrae, caveolae, vesiculo-vacuolar organelles and trans-endothelial channels [9, 10, 12, 13] as well as immunohistochemical marker proteins like CD31 (PECAM-1), CD144 (VE-Cadherin), vWf, vascular endothelial growth factor receptor-2 (VEGFR-2), claudin-5 and other cell adhesion molecules (CAMs) like ICAM-1 (CD54) and VCAM-1 (CD106), and E-selectin (CD62e) [2, 12, 13] (fig. 1). They also secrete bioactive molecules like NO and prostacyclin (PGI_2) at high levels, reactive oxygen species (ROS) at low levels, endothelin (ET)-1, and interleukin (IL)-8 upon inflammation [2, 12].

Endothelial integrity is mainly mediated by CD31 at the vessel wall, together with CD144 [12]. It is concentrated at endothelial junctions and plays a major role in mediating endothelial cell-

cell contact [9, 13] as well as leukocyte trafficking [4, 9, 14]. Moreover, it has been shown that CD31 is involved in angiogenesis [13] and that the protein also plays a crucial role in signalling events with integrins [15], hence, mediating mechanotransduction [14]. It is a central protein in EC biology.

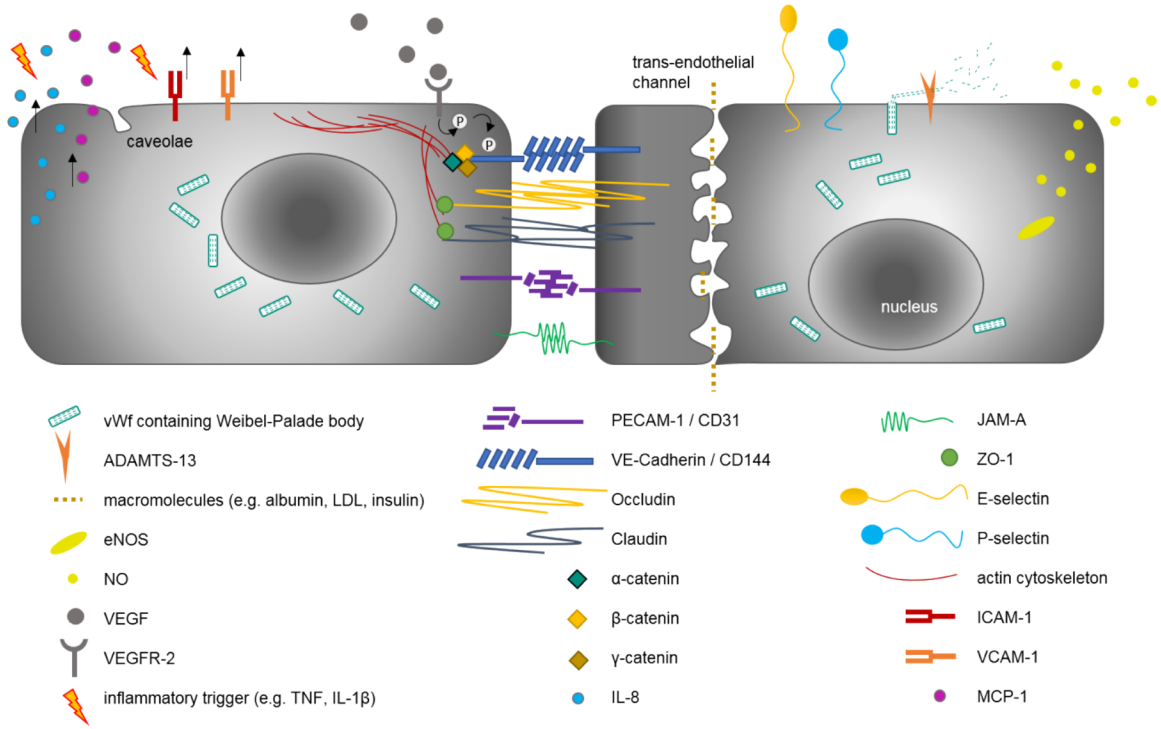

Figure 1. *Common endothelial cell ultrastructural and protein markers.* Along the vascular tree ECs share characteristic markers for cellular transport mechanisms, barrier integrity, modulation of vascular tone, regulating blood coagulation and mediating immune cell interactions.

Von Willebrand factor is synthesised by ECs and stored in the form of ultralarge multimers in WPBs [13]. Upon release, vWf is cleaved at the EC surface by the metalloprotease ADAMTS-13 into smaller, globular structures [12] (fig. 1) mainly regulating blood coagulation by binding to factor VIII and mediating platelet adhesion at sites of endothelial injury [13].

ECs are further highly responsive to VEGF that plays a key role in the formation and maintenance of fenestrae [4] and angiogenesis [12, 13]. Further, EC permeability is modulated by VEGF-Receptor-2 (VEGFR2)-dependent CD144 phosphorylation [12] contributing to barrier integrity and further vessel wall modulation (fig. 1). Both are important functions performed by ECs. Claudin-5 also acts as abundantly present junctional molecule maintaining endothelial barrier [13]. These processes are necessary for regulating metabolic needs of tissues, especially via the microcirculation, and in maintaining overall homeostasis [2]. In consequence, they even guarantee leukocyte trafficking at the endothelial barrier without impairing it's functionality [16]. During inflammation, either systemically or local, ECs have a crucial role in leukocyte trafficking across the vessel wall into the tissue via IL-8 and monocyte

chemoattractant protein (MCP)-1 chemoattractant guidance [2, 17]. Leukocyte adhesion is a multistep process involving endothelial cell adhesion molecules (CAMs) like ICAM-1, VCAM-1 and selectins like E-selectin and P-selectin. Resting ECs do not consecutively express these molecules, but they are immediately upregulated upon injury or inflammatory stimuli [9] (fig. 1). Sequentially, endothelial selectins and CAMs mediate leukocyte tethering, rolling, adhesion, arrest and eventually extravasation into the tissue [9, 17], mainly at the site of postcapillary venules [4].

Further, ECs regulate blood fluidity [11] and set vascular tone via NO, prostacyclin and ET-1 secretion [18, 19]. The first two phenomena act in a vasodilative way and inhibit platelet activation, the latter one act in a vasoconstrictive manner [19].

Taken together, the endothelium is a highly active tissue with a variety of different functions to regulate and maintain homeostasis both locally and systemically. Thus, in this thesis two important aspects of EC biology are introduced in more detail: the endothelial barrier and endothelial mechanosensitivity.

1.1.2 Endothelial cells form a selective barrier

The supply with oxygen, nutrient and hormones, and the removal of catabolites and waste products is regulated at the blood-tissue interface represented by the endothelium. An intact endothelial barrier is vital for a proper function of these processes [20]. The endothelium forms a tight semipermeable barrier and can be classified into continuous, (non-)fenestrated and discontinuous endothelial layers [12, 20]. Mainly macromolecules like albumin, transferrin and low density lipoprotein (LDL) are not able to translocate freely through the vessel wall [4], in special cases like the BBB (continuous non-fenestrated) even very small hydrophilic molecules [21] are prevented from translocation under physiological conditions. Macromolecular exchange thus mainly occurs via receptors, transporters and in vesicles [20] via clathrin-mediated endocytosis [4] and vesiculo-vacuolar organelles [22]. Solutes pass through the endothelial barrier via transendothelial channels or transcytosis mediated by caveolae [4, 12].

1.1.2.1 Adherens and tight junctions regulate the endothelial barrier

Barrier integrity is mediated by a set of adherens and tight junctions, whereas the former are common to all ECs, but the latter are graduated within different sites of the vascular bed. Adherens junctions maintain mechanical integrity while tight junctions seal intercellular space [3]. Additionally, tight junctions are necessary to maintain EC polarity [4] and adherens junctions participate in contact-dependent growth inhibition [23]. Typically, tight junctions are concentrated at the apical side of a cell and adherens junctions are located below, however in ECs both junction proteins are found to be mixed [23, 24]. Adherens junctions are composed

of cadherin-catenin complexes formed by VE-Cadherin and α-, β- or γ-catenin [3, 24, 25]. Mainly β- and γ-catenin bind directly to the cytoplasmic tail of VE-Cadherin, whereas α-catenin binds those two and mediates anchorage to the peripheral actin cytoskeleton of the cell (also called dense peripheral band) [3, 24]. During vascular remodelling β-catenin can be further relocate to endothelial nuclei acting as signalling molecule [23]. Tight junctions are composed of integral membrane proteins like occludin, claudins and junctional adhesion molecule-A (JAM-A) and associated intracellular proteins like *zonula occludens* (ZO)-1, -2 and cingulin [23, 26](fig. 1). Occludin participates in maintaining intercellular adhesion as well as the regulation of paracellular permeability [26]. Claudins comprise more than 20 proteins [26] and are thus the major tight junctional transmembrane proteins [23]. They function either as sealed walls or can form pores in the endothelial barrier [26]. Claudin-5 is specifically and highly expressed in endothelial tight junctions [23, 25]. The cytoplasmic tails of claudins and occludin are connected to ZO-1 mediating attachment to actin filaments of the cellular cytoskeleton and the linkage to adherens junctions [3]. Tight junctional JAM-A has mainly adhesive properties and is involved in leukocyte-endothelial interaction [26], two functions that are shared with PECAM-1 [3, 23]. However, PECAM-1 is only functionally associated and not considered as a adherens or tight junction protein component [3].

1.1.2.2 The blood-brain barrier is a highly restrictive barrier

The manifestation of endothelial tight and adherens junctions differs within the vascular tree [23-25] which directly contributes to the regulation of the endothelial barrier. Peripheral beds show increased permeability, especially post-capillary venules [23], whereas the BBB represents a highly restrictive exception and is impermeable for molecules larger than 400 kDa [27]. Its main task is the regulation of the local environment to support neural function. The BBB separates the peripheral from the central transmitter pool, protects neural tissue from macromolecules, regulates the CNS ion composition and brain nutrition via specific transporters and channels and shields the CNS from neurotoxic substances (endogenous metabolites and xenobiotics) [28]. Claudin-1, -3 and -5, and occludin mainly contribute to the maintenance of the BBB tightness [21, 23, 28]. The formation of an intact physiological BBB further requires two adjacent cell types: a) astrocytes with end feet connecting the BBB, and b) pericytes secreting barrier strengthening factors [21, 23]. At the luminal site ECs of the BBB exhibit a low expression rate of CAMs that significantly reduces the number of adherent leukocytes [12]. However, it was shown that to some extent leucocytes could still transmigrate through the BBB via diapedesis directly through the endothelial cytoplasm avoiding endothelial rearrangement and opening of tight junctions [28].

1.1.2.3 Endothelial barrier modulation

There are a variety of endothelial barrier-modulating factors mainly contributing to alterations in endothelial barrier function during pathological conditions and chronic diseases [20, 23]. In general, hyperpermeability is induced by vasoactive agents and cytokines upon injury and inflammation and can either be transient or prolonged and accompanied by leukocyte extravasation [20]. Histamine (trauma, burns, infection) and thrombin (thrombosis) are leakage-inducing agents during injury [29] and can cause transient or prolonged hyperpermeability associated with stress fibre formation [20]. VEGF is a cytokine commonly found during ischemia-reperfusion injury (common after septic shock [30]) and angiogenesis [29] and has also significant impact on the endothelial barrier through VE-Cadherin phosphorylation [12, 23]. Under inflammatory conditions, specifically during sepsis, high levels of the cytokines tumour necrosis factor (TNF) and IL-1β are rapidly released by leukocytes at target sites in tissues [31]. Both contribute to barrier breakdown via phosphorylation of the VE-Cadherin complex [23, 32], redistribution of PECAM-1 [3], reorganization of the cellular cytoskeleton [31] and shedding of the endothelial glycocalyx associated with a loss in mechanosensing and vascular control [33]. But in contrast to the former mentioned agents, cytokines are generally long-lasting [3]. This is a huge problem in sepsis and associated inflammatory syndromes causing prolonged vascular leakage and bacterial translocation eventually leading to severe multiple organ dysfunction or failure [30].

In contrast, intended endothelial barrier modulation is important for CNS-targeted drug delivery. Over 20 years ago, the BBB was less well represented in academic neuroscience or industry programs, however, it sets the bottleneck for treating CNS disorders. A variety of biotechnologically manufactured large molecules like monoclonal antibodies, gene therapeutics and recombinant proteins do not cross the BBB [27]. Various strategies to overcome the BBB have been discussed such as focused ultrasound supported BBB opening [34], non-invasive nasal delivery [35], or receptor- and carrier-mediated transport by functionalised chemical drug carriers via the BBB transporter system [27, 36, 37]. This strategy, best described as a molecular Trojan horse, has already been tested for gene therapy strategy to treat Parkinson’s disease and brain cancer [38].

1.1.3 Mechanical stimulation of endothelial cells and mechanotransduction

Unlike other cell types and tissues in the human body, the endothelium is exceptionally exposed to mechanical stimulation through the bloodstream resulting in shear forces and tension that directly act upon ECs. This has extensive consequences on EC phenotype and functionality. Hemodynamic shear forces induce shear stress on the endothelial membrane with additional pressure and deformation (strain) as well as cytoskeletal manipulation (tension)

characteristics [5, 6]. Cellular and vessel deformations by pressure gradients result in distension and tension, and can be described by Laplace's law [5]. Shear stress mainly occurs at the vessel wall (commonly referred to as wall shear stress), displays a frictional (tangential) force as a result of the blood flow, is mathematically described by Poiseuille's law (cf. 1.3.3) and mainly depends on vessel diameter and blood viscosity. Typical shear stress values are 0.1 – 0.6 Pa (also commonly found in the literature as dyn/cm²; 1 dyn/cm² = 0.1 Pa) for veins and 1 – 7 Pa for arteries in the human body [6]. However, the literature is still lacking comprehensive data sets for the human circulation, especially the microcirculation within organs.

1.1.3.1 Endothelial cells phenotypically adapt to shear forces

Alterations in vessel geometry could result in three distinctive flow patterns within the human circulation: laminar, disturbed and turbulent (oscillatory) flow [39-41]. In the healthy vasculature laminar flow is predominately present but arterial bifurcations also induce turbulent and disturbed flow patterns [39, 41]. Shear stress and flow patterns induce tremendous adaptive changes on EC morphology and EC function [5, 42]. Under flow conditions ECs elongate and align with the direction of flow, *in vivo* [43-45] as well as *in vitro* [39, 41, 42]. This is accompanied with extensive remodelling of the EC cytoskeleton and the formation of F-actin stress fibres coaligned in the direction of flow [46-48]. Additionally, changes in integrin distribution can be observed and both contribute to enhanced EC adhesion under mechanical manipulation [5]. Laminar shear stress decreases cellular turnover [49] and inhibits apoptosis [50] promoting a quiescent EC layer. Endothelial CAMs are differentially and specifically regulated by shear stress. Under laminar shear stress ICAM-1 is upregulated [51, 52], whereas VCAM-1 and E-selectin are reported to be unaffected [52] or downregulated [53]. However, oscillatory shear stress induces enhanced expression of all three molecules and thereby promotes leukocyte adhesion [54]. Shear stress is known to increase the endothelial permeability of small and macro-molecules [41]. Further, Ca^{2+}-specific and K^{+}-specific ion channels are activated immediately upon onset of shear forces applied on ECs [5, 41]. Barrier shaping molecules like PECAM-1 [55], occludin and ZO-1 are upregulated by mechanical stimulation [56] (fig. 2). Similarly, the release of substances like NO and prostacyclin, both inducing flow-dependent vasodilation [5], or the release of endothelial-derived neurotransmitter bradykinin [57] is triggered by shear stress.

1.1.3.2 Mechanotransduction and the mechanosensory complex

Molecules of the EC plasma membrane projecting into the luminal side of blood vessels made them already in early flow experiments to speculative candidates for mechanosensing and -transduction. The endothelial glycocalyx represents a significant structure in mechanosensing

events [57] as well as integrins, G protein coupled receptors, ion channels, VEGFR-2 and adhesion molecules [42, 47, 55]. Integrins are connected extracellularly to the ECM and intracellularly to focal adhesion sites enabling inside-out and outside-in signalling as well as mechanosensing and -transduction [42]. A central role for shear stress dependent regulation of EC functions plays the mechanosensory complex comprised of VE-Cadherin, PECAM-1 and VEGFR-2 [55, 58] (fig. 2). In this complex, PECAM-1 mediates mechanosensing via conformational changes directly triggered by shear stress leading to PECAM-1 tyrosine phosphorylation [42, 55]. VE-Cadherin resembles the complex but has itself no mechanosensing capacity. However, VE-Cadherin acts as mechnotransducing element to stimulate VEGFR-2 upon PECAM-1 phosphorylation [58].

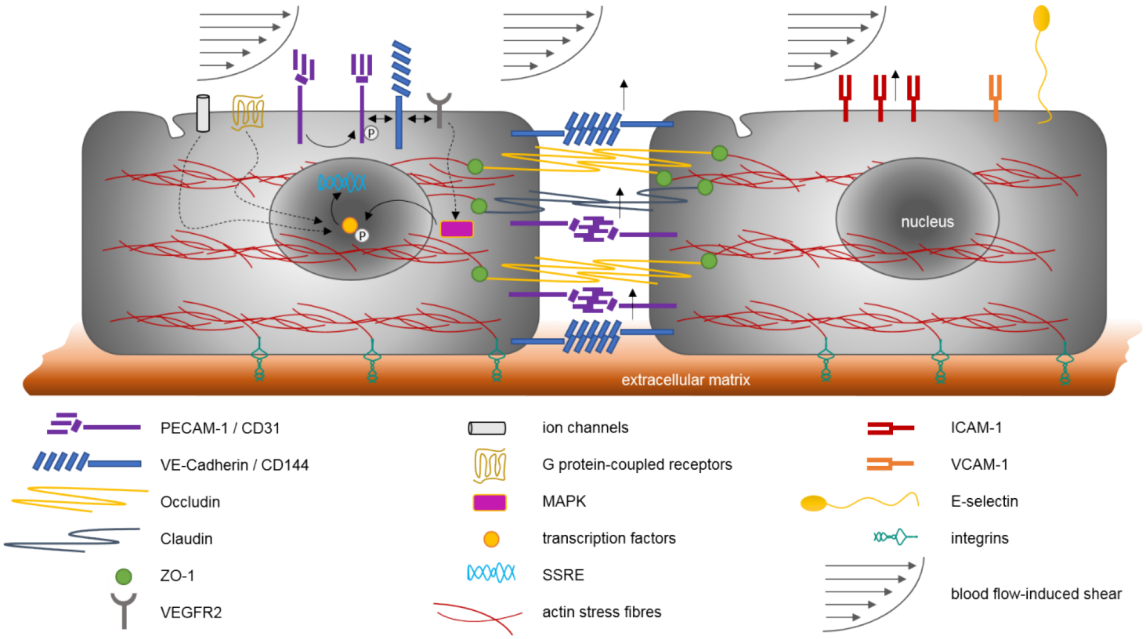

Figure 2. *ECs are highly responsive to shear stress.* ECs adapt to shear stress extensively by cytoskeletal rearrangements, barrier tightening, and by upregulation of surface receptors like CAMs and anchorage proteins like integrins. Mechanosensory elements like ion channels, G protein-coupled receptors or the mechanosensory complex (PECAM-1, VE-Cadherin and VEGFR2) and subsequent signaling cascades (dotted lines) leading to MAPK activation, transcription factor phosphorylation and activation of SSREs play a central role in endothelial mechanosensing and -transduction.

Following mechanosensing, mechanotransduction is mediated by several intracellular pathways including extracellular-signalling regulated kinase (Erk) and Akt kinase [58], and mainly cumulating in the induction of mitogen-activated protein kinase (MAPK) leading to phosphorylation of transcription factors. These transcription factors bind to shear stress responsive elements (SSRE) of mechanosensitive genes [39] (fig. 2). Many EC genes have been identified to be regulated positively or negatively by a SSRE like platelet-derived growth factor-BB, NO synthase, PECAM-1, VEGFR-2, MCP-1, VCAM-1 and angiotensin converting

enzyme-1 [59].

1.1.3.3 Pathological conditions associated with non-laminar flow patterns

Non-laminar flow patterns, mainly of turbulent / oscillatory nature, are reported to be associated with endothelial dysfunction [6, 39, 60]. Oscillatory flow-prone regions are arterial bifurcations and curvatures [6, 39, 55] with flow separation zones and recirculation [61]. They depict two distinctive sites of the vascular bed to be susceptible for atherosclerotic changes of the vessel wall [7]. Turbulent flow increases EC DNA synthesis, proliferation and turnover [40]. In this context, Smad 1/5 has proven to be oscillatory flow-specifically upregulated, contributing to EC cycle progression and it further can be found increasingly in atherosclerotic regions [60]. Moreover, low oscillatory flow increases CAM expression, ET-1 and ROS production, LDL uptake and oxidation, ECM degradation, vascular remodelling, and MCP-1 expression, all promoting EC - monocyte and - T-lymphocyte interaction as well as immune cell adherence with subsequent vascular remodelling and atherosclerotic plaque formation [39, 42, 55]. Similar processes induced by decelerated or altered flow patterns can be observed in venous pathologies like telangiectasias, reticular and varicose veins [62] and in the coronary microcirculation during the pathogenesis of myocardial ischemia [8]. In this context, mainly endothelial- and neutrophil-derived ROS decrease vasoreactivity and trigger an inflamed endothelium after reperfusion, known as ischemia-reperfusion injury [63], also common in sepsis.

1.2 Nanoparticles in clinical research

Nanoparticles are a promising new technology for drug delivery and the research area focusing of the improvement of these delivery tools has rapidly developed within recent years. Their unique properties allow the carriage and delivery of drugs to specific target sites within tissues [64]. The agents transported can either be classic chemical and biological drugs or biological material such as pDNA, mRNA or siRNA for gene therapy. Up to date, the majority of NP-based drugs are anti-cancer and anti-inflammatory agents [65]. Drugs can either be laden onto the surface of the NP or they can be dissolved, entrapped, absorbed or encapsulated into the NP matrix [66]. The combination of small sizes and biodegradable materials support several advantages of NPs: targeted drug delivery with increased uptake, suitability for intravenous application, improved bioavailability with higher therapeutic efficacy, protection against enzymatic degradation, establishment of long-lasting local drug depots and reduced toxicity towards off-target tissues [64, 66]. Despite their benefits and broad application range, the pre-clinical evaluation of NP uptake efficiency and biodistribution remains a major challenge to be addressed. Additionally, guidelines for relevant biological testing are missing [67].

1.2.1 Characteristics and types of Nanoparticles

A NP is a small structure below 100 nm in size in at least one direction [64, 68, 69]. There are various kinds of NPs with different shapes and sizes ranging from spherical to rod-shaped, nanochains as well as nanoboxes [68, 70, 71]. Despite their specific molecular structure, NPs in general are composed of a core, a shell and several optional surface modifications giving the shell specific characteristics or acting as “ligands” for a directed uptake after binding a specific receptor or transporter protein (fig. 3).

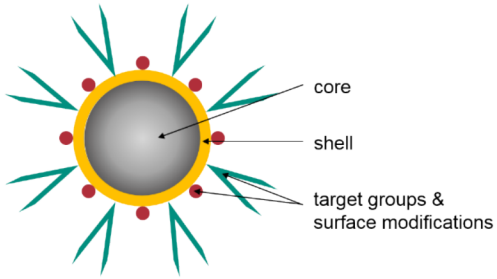

Figure 3. *Basic structure of a NP.* The most common composition of a NP comprises a core and a shell with implemented target groups and surface modifications that can vary to a different extent.

Size and structure are usually determined by photo-correlation spectroscopy and dynamic light scattering and are verified by scanning or transmission electron microscopy. Particle size and size distribution influence the biodistribution, targeting ability, biological fate and potential toxicity [66]. Furthermore, it determines the surface area-to-volume ratio with profound impact on drug release. Small vehicles with drugs loaded to the surface facilitate fast release rates, whereas large particles with drugs encapsulated into the core result in slow and sustained release rates. However, smaller fast-acting particles tend to be more toxic [66, 68].

1.2.1.1 Nanoparticle performance depends on surface charge

The surface charge properties of a NP are characterized by the zeta-potential. It represents the charge of a NP at the surface in relation to its environment. This parameter is e.g. dependent on particle composition and the pH of the surrounding environment [66, 72]. Charge density and charge polarity play an important role in NP fate [73]. In general, NPs with a zeta potential above ± 30 mV are considered to be stable [66]. Charged NPs show more side effects than neutral formulations with positively charged particles being more toxic than negatively charged ones [64, 67]. Another important factor is the hydrophobicity of a NP. It determines the amount of blood components binding to the particle surface like opsonins [66] and other proteins forming a protein corona [74]. Especially opsonins mark particles, antigens or dead cell material for immune responses and degradation. Hence, charge, hydrophobicity and the resulting protein corona are important issues to be taken into account during the designing process of a NP [74].

1.2.1.2 Types of nanoparticles

So far, several NP platforms have been developed (fig. 4) [64]. Each of them has unique properties influencing their behaviour as a drug carrier and towards biodistribution and -availability.

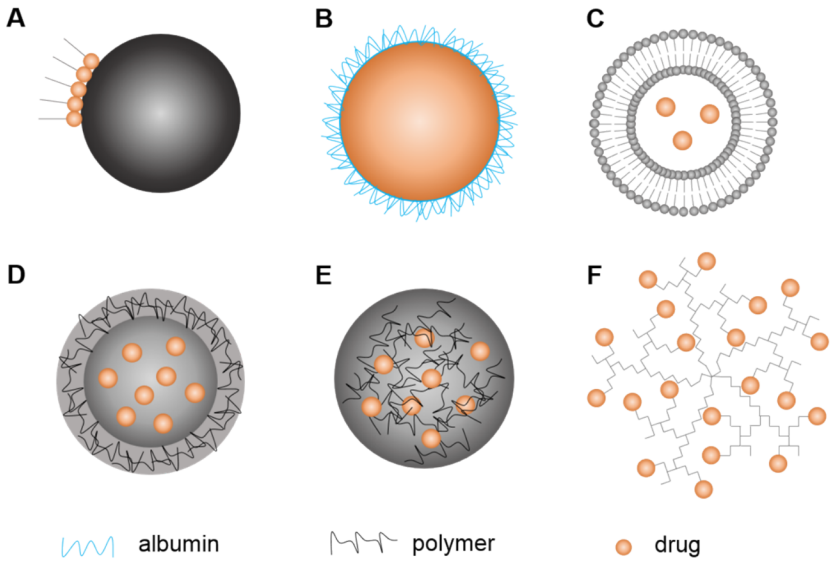

Figure 4. *Different types of NPs.* Several types and formulas of NPs for drug administration have been developed: (A) metallic NPs, (B) NP albumin-bound [nab], (C) liposomes, (D + E) polymeric NP technology including (D) nanocapsules and (E) nanospheres, and (F) dendrimers.

NPs based on metal ions (fig. 4A) represent a classic approach among NPs. They consist of a core formed by metal ion compounds loaded with drugs, but they might trigger toxic side-effects upon accumulation within the tissue [64, 74]. The NP albumin-bound technology (fig. 4B) uses albumin as a carrier for the delivery of therapeutics. Furthermore, albumin can bind the glycoprotein receptor and facilitate transcytosis of bound drugs [64]. Albumin coating may also reduce cytotoxicity [67]. Liposomes (fig. 4C) were one of the first NP formulations to be applied in medical treatments. They have a bilayered membrane structure enwrapping an aqueous core [64]. The bilayered shell mediates “contact-facilitated drug delivery” enhancing drug release and depot effects [66]. Polymeric NPs (fig. 4D + 4E) are usually made of biocompatible and biodegradable materials [64, 68], either of synthetic or of natural origin [66, 68]. But there are non-degradable formulations as well. As polymers might challenge the immune system, non-ionic surfactant coating is required [68]. Poly(lactic-co-glycolic acid) (PLGA) is the most common biodegradable polymer approved for use in humans and degrades via hydrolysis into lactic and glycolic acid metabolized easily by the body [65, 68]. Drugs can be encapsulated in the core and shell (nanocapsules) of polymeric NPs or they can be uniformly dispersed within a polymeric matrix (nanosphere), respectively [66]. Furthermore,

drugs can be immobilized onto the surface. These different options facilitate various release strategies and therapeutic applications [66, 68] rendering polymeric NP application a diverse field. Dendritic structures have been observed in many biological systems hence their architecture was adapted to well-defined, regularly branched NPs (fig. 4F). Key components are a core, dendrons (arms) and surface-active groups for various ligand modifications and drug immobilization [64, 68]. In early studies with encapsulated drugs their release was difficult to control leading to the incorporation of degradable links and to the usage of dendronized polymers (linear polymers with dendrons) with enhanced circulation time [66]. Moreover, there are further requirements to be met for clinical applications: stability of the nanotransporter within blood without activation of the reticuloendothelial system (RES) as well as non-toxicity, non-thrombogenicity, non-immunogenicity, non-proinflammatory properties to guarantee its safe application as a treatment option for patients [68]. Nanoparticle shape, size and formulation thus represent important characteristics influencing the NP platform and its usability. Nanoparticles used in this thesis are polymeric NPs (manuscript II) and polyplexes (manuscript IV). Polymeric NPs can be formed via particle replication in nonwetting templates (PRINT) [75], via reversible addition-fragmentation chain transfer (RAFT) polymerization, polymeric self-assembly or a combination of RAFT and self-assembly [76]. Polyplexes are cationic polymers used for gene delivery. Positively charged polymers form complexes by binding negatively charged DNA while keeping a positive net charge. This allows them to still interact with cells and bind to their negative membranes [67].

1.2.2 Factors influencing nanoparticle uptake and biodistribution

Cellular NP uptake is either mediated actively or passively. Passive uptake is rather rare and most NPs enter the cells via endocytosis on four different routes: macropinocytosis, clathrin-mediated endocytosis, caveolae-mediated endocytosis and clathrin- and caveolae-independent endocytosis [67]. But NPs do not only interact with their designated target tissues or target cells. On their way through the circulation they inevitably interact with a variety of molecules and cells as well as they face physical conditions like shear. Among intrinsic properties of shape, size and charge, these extrinsic factors additionally influence NP uptake strongly.

1.2.2.1 Biological traps: immune cells, protein coronas and the EPR effect

The tissue macrophages of the RES (or mononuclear phagocyte system) are of most importance to NP clearance [65, 77]. The RES comprises bone marrow progenitors, blood monocytes and tissue macrophages with focus on Kupffer cells of the liver and macrophages of the spleen [64]. These cells recognize opsonins adsorbed to NPs which fosters their phagocytosis and clearance from the blood. Especially NPs above the size of 100 nm are

cleared by the RES [77]. A common strategy to apply a ‘stealth mode’ to NPs is a polyethylene glycol (PEG) coating [64, 65, 74, 77]. Nanoparticle uptake by phagocytic cells is increased by the presence of serum in general and NPs adsorb serum proteins independent from their charge, but the final coverage may differ [67]. Interestingly, the formation of a protein corona suppresses the NP uptake by non-phagocytic cells as well. Proteins may shield NPs and prevent cellular surface receptor interaction. Even proteins with pronounced receptor-mediated uptake by cells do not enhance NP uptake upon binding while conserving their conformation, but a disruption in protein conformation might facilitate uptake rates [74]. Hence, the protein corona and its influence in general as well as by specific composition on the uptake of NPs remains an important factor that is not fully understood up to now. Additionally, to the NP clearance from the blood by the RES, an enhanced permeability and retention (EPR) effect may lead to nonspecific NP accumulation. The EPR effect is a phenomenon known from cancer with high accumulation of NPs within tumours [64, 77]. A high proliferation rate of ECs and a decreased number of pericytes render a leaky tumour vasculature with pores of several hundred nm in size. Nanoparticles enter the tumour tissue easily and accumulate due to an impaired lymphatic drainage [64, 65, 78]. The EPR effect is used for passive tumour targeting but requires additional NP modifications when other tissues than the tumour are of therapeutic interest. Hence, the EPR might lead to unspecific blood clearance of NPs decreasing final dosages.

1.2.2.2 Shear forces likely influence nanoparticle uptake

The endothelial environment is highly dynamic and mainly influenced by its hemodynamic conditions. Thus, flow conditions are expected to influence NP interaction and uptake by ECs [65]. Laminar shear stress has a profound influence on endothelial biology modulating cell shape and size [44, 79, 80], focal adhesion [81], adhesion molecule expression [51], glycocalyx deposition [82, 83], barrier function [84, 85], and action of G-proteins and ion channels [57]. However, to date only a few studies have taken mechanical forces into account, especially shear stress and its impact on EC-NP interaction and uptake. The majority of studies were performed in static cell culture assays to evaluate NP uptake. Factors that influence NP uptake the most are particle composition, shear magnitude and exposure time [65]. In this context it is also noteworthy that differently charged NPs show unique uptake patterns under various shear rates [86]. Different factors of the endothelial microenvironment influence this process as well as each other partially, i.e. the state of the cell surface, shear stress, protein content of the circulation and the presence of phagocyting cells. Thus, the endothelium constitutes a highly complex system locally as well as throughout the vascular bed and its main components should be carefully considered when evaluating EC-NP interaction and uptake.

1.2.3 Modifications of nanoparticles and applications

Directed, specific drug delivery to sites of diseased tissues (i.e. inflammation, neoplastic and degenerated tissue, functionally impaired signalling pathways) depicts the ultimate goal in nanomedicine. However, this is only achieved by unique NP formulations involving both basic composition and additional surface modifications to increase target specificity. Furthermore, NPs are subject to rapid clearance which is desired to be prevented [65]. In this context, polymeric NPs have gained special attention due to their stability and their simplicity to modify them [66]. Coating nanoparticles with surfactants or designing them from biodegradable polymers like PEG or polysorbate 80 prolongs their body circulation time and prevents their fast opsonisation associated with an increased phagocytosis rate [66, 77] and reduces their inflammatory potential [77]. Antibodies are predestined for targeted cellular delivery of drugs. For endothelial targeting, anti-VCAM-1, -ICAM-1, -PECAM-1, -E-selectin and -P-selectin antibodies have been successfully applied [65]. Antibodies generally constitute large proteins facilitating targeting and binding but might interfere with cellular uptake. Hence, smaller peptides or amino acids are favourable. Highly cationic cell-penetrating peptides like HIV-TAT, transportan or c-Jun have been used as alternatives on NPs for magnetic resonance imaging, bioimaging or liposomal drug delivery [77, 87]. RGD-peptides have shown to enhance integrin interaction and endocytosis efficiency on cancer cells [88]. Further, amino acids have also been identified to improve biocompatibility in treating amyloid diseases [89] and to support eco-friendly NP design and production [90]. In contrast, magnetic NPs have been widely used to explore and study cancer treatment. They qualify for easy manipulation techniques. For instance the desired distribution can be achieved when using active targeting of magnetic NPs by applying external magnetic fields for tissue specific enrichment of typically superparamagnetic iron oxide containing particles [77]. Variations in substrate formulation and composition, i.e. creating whole NP libraries, is also a common strategy to explore specificity, efficacy and possible side effects [91, 92]. This represents more of a reverse application approach to identify a NP composition hit for an application rather than optimize a sole formulation until it fits. This strategy has been applied in manuscript II to investigate flow-dependent NP uptake. Moreover, small molecule (peptide) decoration has been applied in manuscript IV to overcome highly specialised tissue barriers in a directed way.

1.3 Biochip-based cell culture

For many decades researchers got used to culture cells *ex vivo* solely under static conditions in a classic petri dish setting. Dynamic cell culture emerged from the convergence of different fields from physics, chemistry and biology/medicine. The understanding of the underlying physical theoretical aspects of fluid properties set ground for further sophisticated

developments of especially analysis equipment in chemistry (gas-phase chromatography, high-pressure liquid chromatography) and molecular biology (high-throughput DNA sequencing) [93]. Adaptation of concepts of fluid flow to cell biology emerged from clinically relevant questions about the manifestation of atherosclerosis. For this purpose, parallel plate flow chambers, one of the first devices for flow-based cell culture, were invented with the beginning 1970s. Krueger et al. investigated MDBK cell performance under a range of minimal and high shear stress to shed some light onto the physical integrity of cell layers and alterations of cells exposed to flow [94]. The behaviour of EC morphology and EC performance under laminar and oscillatory or turbulent flow profiles subsequently emerged as field for first broad flow studies and applications [40, 44, 50, 79, 80, 95]. Later on, concepts for new and more complex 3D cell culture systems, tissue engineering [96] and lab-on-a-chip systems (µTAS, microchemical total analysis systems) emerged [97] and high-maintenance macroscale setups were scaled down [98]. Microfabrication processes, soft lithography and surface patterning techniques became quite prominent for designing perfusable cell culture devices at the microscale [97, 99] facilitating biochip-based cell culture and microphysiological system (MPS) devices. Biochip-based cell culture has the advantages of streamlining experimentation, recreating the physiological microenvironment *in vitro* and revealing cellular responses not to be seen in conservative cell culture settings.

1.3.1 MOTiF biochip design

The biochip used for this thesis was developed within a joint research project designated *Multi-Organ-Tissue-Flow*. The MOTiF biochip comprises two cell culture cavities integrated into a plastic carrier in the size of a microscope slide (fig. 5A + 5C). Each cavity is separated by a 11 µm thin porous PET membrane (8 µm pore diameter, 10^5 pores/ cm²) into an upper (blue) and a lower (orange) channel. The membrane serves as cell culture substrate (scaffold) where cells can be arranged and co-cultured in a layer-wise fashion on both sides. Both channels can be individually perfused with cell culture media (fig. 5A). Both channels, above and below the membrane, are rectangular-shaped to support a laminar physiologic flow profile and they are 0.7 mm and 0.8 mm in height, respectively (fig. 5B). The membrane provides an area of 0.7 cm² for cell culture in MOTiF biochips version 2 (fig. 5A + 5C) and 1.1 cm² in MOTiF biochips version 3 (fig. 5D + 5E). Version 2 was further developed to version 3 supporting larger cell culture constructs. This has the advantage of culturing more cells for assay-based analysis like cytokine profiling and substrate turnover.

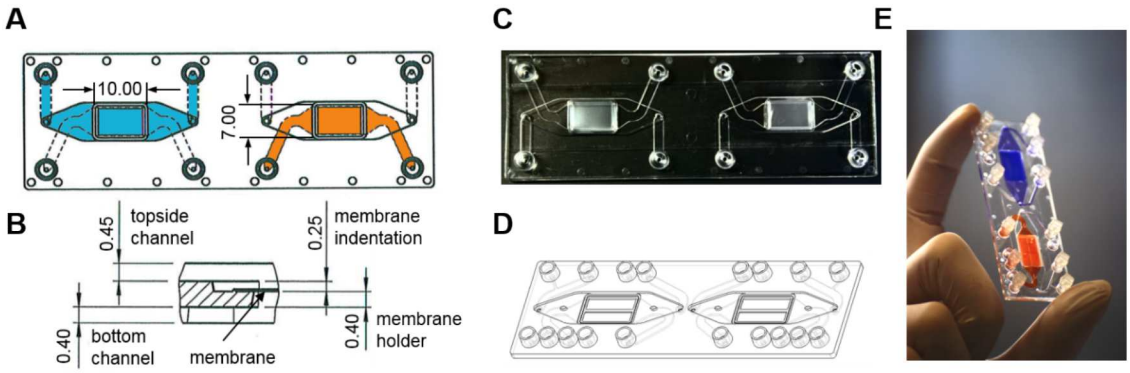

Figure 5. *MOTiF biochip design and further development.* (A) Version 2 of the biochip design with membrane dimensions indicated. The membrane separates the top channel (blue) and the bottom channel (orange) and serves as cell culture area. (B) The top channel has a height of 0.7 mm above the membrane and the bottom channel is 0.8 mm in height below the membrane. (C) Photograph of version 2 of the biochip. (D) Scheme of improved version 3 comprised of a larger membrane area and additional sampling ports. (E) Photograph of version 3 of the biochip with coloured top channel (blue) and bottom channel (orange). Dimensions indicated in mm. Pictures A-D kindly provided by research group INSPIRE / University Hospital Jena, picture E self-taken.

Both applications are further supported by the integration of additional sampling ports on each channel making sampling more feasible. The larger cell culture area enables an analysis of multiple immunofluorescence markers as well by cutting it into pieces. MOTiF biochips version 2 were used for the studies in manuscript I. MOTiF biochips version 3 were used for the studies in manuscript III and IV.

1.3.2 Injection molding vs. rapid prototyping: material preferences

MOTiF biochips are manufactured by injection molding of cyclic olefin polymer (COP, ZEONOR®/ ZEONEX®), cyclic olefin copolymer (COC, Topas®) or polystyrene (PS). These polymers are widely used in cell culture, show high biocompatibility, are further certified for clinical applications and have superior optical characteristics suitable for fluorescence and bright field microscopy [100]. The injection molding technique provides standardized high-quality biochips in large quantities (GMP quality). It further enables the precise production of rather complex biochip designs in one piece. Detailed descriptions of the manufacturing process of MOTiF biochips are given in the method section of manuscript I. However, this procedure requires a cost-intensive template for each design variant and is thus not suitable for rapid prototyping. That is why the majority of groups working in the field of microfluidics and dynamic cell culture choose soft lithography to produce their biochips [98, 101-106]. Polydimethylsiloxane (PDMS) is a standard material used for these techniques due to its low costs, feasibility and high compliance [101]. Still, PDMS inherits several disadvantages especially for cell culture applications. PDMS monomers tend to not fully polymerize and

remain agile within the chip body. Surface modifications such as hydrophilization with oxygen plasma show only short-lasting effects [107, 108]. It was further shown that remaining PDMS monomers negatively influence cellular behaviour [109, 110]. PDMS has not only drawbacks on cell behaviour, but as ground material within flow devices of any kind it might counteract their intentional purpose: ECs are exposed to different kinds of shear stress throughout the vasculature, hence a precise control of the applied shear stress within experimental settings is necessary. However, this is not supported by PDMS due to its high flexibility and deformation capacities [101]. Consequently, biochips designed for the studies on flow-mediated EC behaviour in the present thesis were made of COC (manuscript I) and PS (manuscript III and IV).

1.3.3 Calculation of shear values in channel systems

The MOTiF biochip design supports laminar flow conditions upon the perfusion of cells. A uniform, laminar flow in turn is suitable to induce shear stress on EC layers. *In vivo* vascular fluid flow is a rather complex process including pulsatile to continuous flow properties, a diverse vessel geometry (tapered, branched and curved) and interdependencies of physical quantities like fluid shear rate, fluid viscosity, vessel elasticity and radius [111]. However, the predominant nature of blood flow is a continuous laminar flow due to the “Windkessel” effect [112]. Laminar flow induced shear stress is considered to support a healthy endothelial phenotype while disturbed flow with low wall shear stress is associated with atherosclerosis susceptible regions [113]. Thus, shear stress applied in EC experimentation must be predictable and precisely calculable to set obtained results into the right context. Hence, channel and cavity geometries in microfluidic devices are kept simple [98] as it is for MOTiF biochips. Shear stress is a tangential force applied on the surface of ECs (fig. 6) and it is calculated based on Poiseuilles law (eq. 1) *in vitro* as well as *in vivo* [113, 114] by

$$\tau = \frac{4\eta q}{\pi r^3} \qquad \textit{eq. 1}$$

where η is the medium viscosity, q is the flow rate and r is the vessel radius. This equation applies for cylindric, duct-like structures. Most channels in microfluidic devices comprise parallel flat plates with a gap of narrow height. Thus, Poiseuilles law can be modified to

$$\tau = \frac{6\eta q}{w h^2} \qquad \textit{eq. 2}$$

where *w* and *h* are channel width and height, respectively. This case assumes infinite flat plates, but fluid channels are in fact confined by side walls causing a deviation of shear stress from eq. 2 at near-wall regions. This effect heavily depends on the cross-sectional aspect ratio

$$\alpha = \frac{h}{w} \qquad \textit{eq. 3}$$

where low α implies a slit-like geometry with negligible side wall effects in a two-dimensional model. For 3D velocity profiles within microfluidic channels, eq. 2 can be modified in a simple approximation to

$$\tau = \frac{2\eta q}{wh^2}\left(\frac{m+1}{m}\right)(n+1) \qquad \textit{eq. 4}$$

with

$$m = 1.7 + 0.5\alpha^{-1.4} \qquad \textit{eq. 5}$$

where n = 2 for aspect ratios α < 1/3 [98].

Another important parameter specifying the nature of the obtained flow profile at any given velocity is the Reynolds number, *Re*, which is defined by

$$Re = \frac{\rho UL}{\eta} \qquad \textit{eq. 6}$$

where *ρ* is the fluid density, *U* is the flow velocity and *L* the characteristic channel length. Low values (Re < 10^3) indicate a uniform laminar flow profile whereas high values (Re > 10^4) indicate a chaotic turbulent flow profile [98].

Based on eq. 1 to 6, shear stress values and corresponding flow profiles were calculated for the perfusion channels of the MOTiF biochip. These approximations to calculate shear stress hold for microfluidic *in vitro* applications, but not for the complex *in vivo* situation with branching and curved vessels as well as the non-Newtonian fluid nature of blood [113]. A comprehensive theoretical analysis on the calculation of *in vivo* wall shear stress can be found elsewhere [111].

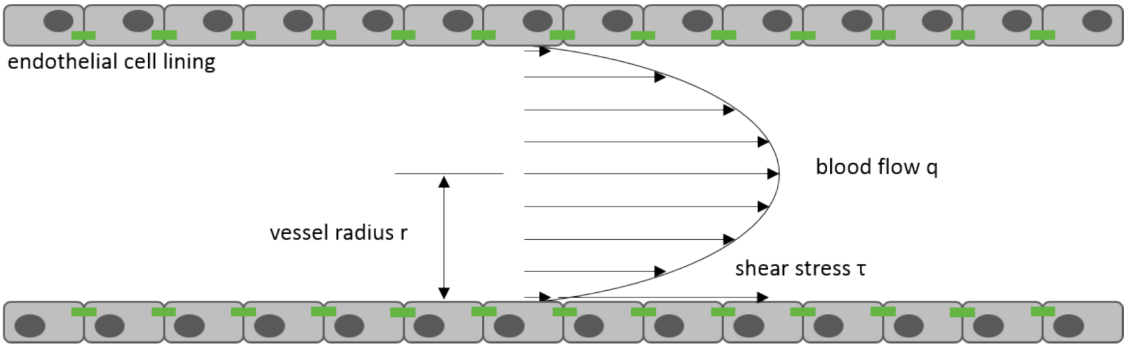

Figure 6. *Endothelial wall shear stress and its determinants*. Fluid flow results in a parabolic velocity profile based on fundamental fluid mechanics where the velocity of a fluid upon a surface is zero (no-slip condition) and the established velocity gradient leads to a maximum in the center of a tube or channel [114].

To derive actual wall shear rates from *in vivo* blood flow, several techniques have been applied. A laser Doppler velocimeter [115] and fluorescently labelled particles have been developed to trace flow in the microcirculation as well as for larger vessels ultrasound or magnetic resonance imaging have been applied [113, 114, 116]. Shear stress values used as orientation in this thesis have been taken from the literature [114, 116].

1.3.4 Applications of biochips in cell culture: recreating the cellular microenvironment

The cellular microenvironment (biological, chemical and physical) plays an important role for cell function, cell polarity and cell communication. Two-dimensional cell culture approaches solely include cellular monolayers and stationary medium supply thereby neglecting multiple cell type arrangements, cellular crosstalk and secretion as well as physical stimuli through ECM components and flowing body fluids. This has an overall impact on cellular morphology, differentiation, viability, proliferation, gene expression, protein synthesis and drug metabolism limiting experimental and clinical studies [117]. Classic 3D cell culture techniques (hanging drop, hydrogels, matrices and scaffolds, agitation-based) have been combined with microfluidic technology profoundly improving cellular physiologic-like microenvironments. Fluid flow across cell layers does not only facilitate nutrient transport positively influencing cell viability and function, but microfluidic concepts can be used to specifically apply gradients on cells. In a biochip with three parallel inlets entering one main channel, it is possible to maintain three distinct fluid streams side by side in that channel by precisely controlling fluid rates. A cell positioned in the centre of the main channel experiences all three fluid streams thereby being exposed to either different concentrations of a molecule or to different substances creating a polarized environment within the cell [118]. Single cell manipulation depicts one extreme side of microfluidic device application, culturing whole tissue constructs certainly the

opposite. Microfluidic devices designed to support complex tissue arrangements usually have an integrated membrane dividing the main chamber into individually perfusable channels. The membrane serves as cell culture scaffold and allows the construction of tissue-tissue interfaces on opposed sites crucial for proper function in many organs like liver, gut, kidney and lung. It shields epithelial cells sensitive to shear stress from fluid flow as presented in models mimicking liver functionality [119] while allowing close contact and cross-communication to other cell types such as the endothelium [120]. It further supports barrier functionality crucial in gut models [121], cell polarization in gut [122] and kidney models [123, 124] and the membrane is also feasible for creating an air-liquid-interface while allowing mechanical stimulation of cell layers in lung models [102]. Tissue-tissue interfaces clearly help recreating cellular microenvironments – a concept which can also be adapted to rather complex cell cultures like 3D spheroids.

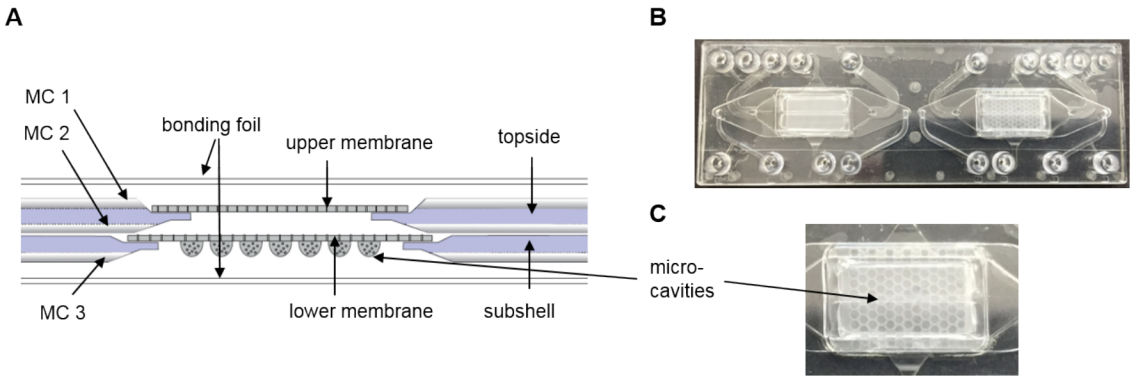

Figure 7. *Adaptation of the MOTiF biochip version 3 for spheroid culture.* (A) Cross-section through the biochip. A second layer has been attached at the bottom of the original biochip providing an additional membrane for cell culture and a third perfusable microchannel (MC). (B) Photograph of the adapted biochip version. (C) Porous microcavities for spheroid immobilization are included in the lower membrane providing flow-based nutrient exchange while protection spheroids from shear forces.

Within this thesis, the MOTiF biochip design was further developed to support spheroid culture (fig. 7). A second chip body with another membrane was attached to the former chip design from below creating multiple tissue culture sites and three perfusable microchannels (fig. 7A). The newly introduced membrane comprised microcavities of 800 µm in diameter (fig. 7C) suitable for immobilizing spheroids and allowing sufficient nutrient exchange through microchannel three while protecting these complex tissues from direct flow-induced shear. This complex chip design was used in manuscript III to further develop endothelial cultures into a microfluidic concept of a blood-brain barrier model.

2. Objective

2.1 Problem

In basic research, toxicology and drug screening, animal models are elaborately and time consuming. Further they are lastingly challenged by ethical concerns with increasingly less support by the public and by the scientific community itself. About 60 years ago, William Russel and Rex Burch defined the principles of 3R in a publication where they made basic suggestions for scientific research. The background of 3R is to substitute animal experimentation (replacement), to decrease the number of animals being used (reduce) and to constantly improve scientific research techniques and tools (refine) to limit animal suffering [125]. Although scientists have been recognising these suggestions, they became legally approved just in 2010 in an EU directive (2010/63/EU) on the dealings with animals in scientific research. Since then, the focus on the development of new tools to fit the 3R principle has been intensified.

However, not only legal frameworks and governments set the tone for new innovations but also intrinsic motivation in the field of cell biology, biochemistry and drug development. Animal physiology differs significantly from human physiology, hence there is a problem of data transfer from animal models to prepare following clinical trials, a so-called *transferability gap* [126]. Moreover, some human diseases cannot be adequately simulated in small animal models like atherosclerosis or liver and lung fibrosis [127-129]. Further, standard *in vitro* cell culture does not take physiological parameters like shear forces, cyclic stretch of tissue and multi-cellular cross-talk sufficiently into account [126]. However, due to their inherent nature of forming a cellular mono-layer directly in contact with the blood stream, ECs would benefit the most from emulated flow properties and the resulting mechanical forces *ex vivo*. Additionally, there is a need for methods to enable microfluidically supported multi-cellular cultures as it is the fact that since the early 1970s the field of flow-based mono-cell culture did not evolve substantially in complexity during the following 30 years.

2.2 Approach to solution

Following, in the joint research project MOTiF, a biochip for more physiologic *in vitro* cell culture was developed.

Within this thesis, the objective is to initially characterise MOTiF biochips for perfused vascular EC culture. The focus is to develop handling strategies for the biochip and developing protocols for mono-cell culture as well as cellular co-cultures. ECs culture within MOTiF biochips will be characterised regarding growth behaviour, typical EC marker expression, EC barrier formation

and how to deal with different perfusion regimes. Further, the development of perfused cellular co-culture and of 3D multi-cellular models will be demonstrated. Eventually, the established perfused cellular *in vitro* systems will be tested for responsiveness to inflammatory conditions and for their feasibility in drug screenings by the testing of different nanocarrier-systems in two different settings: the endothelial lining of liver sinusoidal structures and the microvascular endothelial BBB.

The implementation will be achieved by establishing microfluidic perfusion culture in the MOTiF biochips, by imaging techniques such as brightfield and immunofluorescence microscopy, by flow cytometry and quantification of microscopy data for cell growth, EC biomarker expression and modulation and nanocarrier interaction.

Eventually, the newly developed biochip tool and its characterisation for EC culture will be discussed in the context to support *in vitro* studies in a more physiological way, to support the further development of more complex microphysiological systems and how it bears the possibility to minimize the data transferability gap between *in vitro* research and *in vivo* human biology.

3. Manuscripts

Manuscript I

Raasch M, Rennert K, Jahn T, Peters S, Henkel T, Huber O, Schulz I, Becker H, Lorkowski S, Funke H, Mosig A. (2015)

Microfluidically supported biochip design for culture of endothelial cell layers with improved perfusion conditions.

Biofabrication. 7(1): p. 015013 Journal Impact Factor: 7.236

Manuscript II

Rinkenauer AC, Press AT, **Raasch M**, Pietsch C, Schweizer S, Schworer S, Rudolph KL, Mosig A, Bauer M, Traeger A, Schubert US. (2015)

Comparison of the uptake of methacrylate-based nanoparticles in static and dynamic in vitro systems as well as in vivo.

J Control Release. 216: p. 158-68. Journal Impact Factor: 7.901

Manuscript III

Raasch M, Rennert K, Jahn T, Gärtner C, Schönfelder G, Huber O, Seiler AE, Mosig AS. (2016)

An integrative microfluidically supported in vitro model of an endothelial barrier combined with cortical spheroids simulates effects of neuroinflammation in neocortex development.
Biomicrofluidics. 10(4): p. 044102. Journal Impact Factor: 2.531

Manuscript IV

Englert C, Trutzschler AK, **Raasch M,** Bus T, Borchers P, Mosig AS, Traeger A, Schubert US. (2016)

Crossing the blood-brain barrier: Glutathione-conjugated poly(ethylene imine) for gene delivery.

J Control Release. 241: p.1-14. Journal Impact Factor: 7.901

Manuscript I

Microfluidically supported biochip design for culture of endothelial cell layers with improved perfusion conditions

Raasch, M., Rennert, K., Jahn, T., Peters, S., Henkel, T., Huber, O., Schulz, I., Becker, H., Lorkowski, S., Funke, H. and Mosig, A. (2015)

Biofabrication 7(1): 015013

Here, we describe the development and design of the microfluidically supported MOTiF biochip and characterise its potential to improve EC cell culture under physiological perfusion conditions. The MOTiF biochip is made of Topas® and has the dimensions of a microscopic slide to enable its use with standard lab hardware. An integrated porous membrane serves as cellular scaffold separating an upper from a lower channel system. Computational fluid dynamic (CFD) simulations verified laminar flow conditions within the MOTiF biochip. ECs were subjected to bidirectional perfusion conditions and were characterised for expression of typical endothelial marker proteins (PECAM-1, von-Willebrand factor, ZO-1) and morphological adaption to flow conditions. Further, responsiveness to cytokine treatment (TNF and IFNγ) was demonstrated based on meassurement of cell adhesion molecule (CAM) expression, related immune cell recruitment and adhesion as well as endothelial barrier modulation. Results were compared to static cell culture conditions and two-dimensional standard flow chambers. We found EC culture in MOTiF chips to be superior over conventional culture approaches in terms of cellular morphology and protein expression, which was similar to the *in vivo* situation. We conclude that improved bilateral perfusion conditions exhibit beneficial effects on perfused EC culture.

author contribution (80 %): Cell culture and HUVEC isolation from umbilical cords, biochip preparation (sterilisation, cell seeding and maintenance), evaluation of culture conditions within the MOTiF biochip, performing biochip perfusion experiments, calculation of shear stress levels, immunofluorescence staining and microscopy, cell shape index analysis, permeability assays, THP-1 adhesion assays, flow cytometry analysis of CAMs, analysis of data, co-writing the manuscript.

IOP Publishing Biofabrication 7 (2015) 015013 doi:10.1088/1758-5090/7/1/015013

Biofabrication

PAPER

Microfluidically supported biochip design for culture of endothelial cell layers with improved perfusion conditions

RECEIVED
17 September 2014

REVISED
15 January 2015

ACCEPTED FOR PUBLICATION
28 January 2015

PUBLISHED
2 March 2015

Martin Raasch[1,7], **Knut Rennert**[1], **Tobias Jahn**[4], **Sven Peters**[2], **Thomas Henkel**[3], **Otmar Huber**[1,7], **Ingo Schulz**[4], **Holger Becker**[4], **Stefan Lorkowski**[5], **Harald Funke**[6] **and Alexander Mosig**[1,7]

[1] Institute of Biochemistry II, Jena University Hospital, Nonnenplan 2-4, D-07743 Jena, Germany
[2] Department of Ophthalmology, Jena University Hospital, Bachstraße 18, D-07743 Jena, Germany
[3] Institute of Photonic Technology (IPHT), Albert Einstein Straße 9, D-07745 Jena, Germany
[4] microfluidic ChipShop GmbH, Stockholmer Straße 20, D-07747 Jena, Germany
[5] Institute of Nutrition, Friedrich Schiller University Jena, Dornburger Str. 25, D-07743 Jena, Germany
[6] Molecular Hemostaseolgy, Jena University Hospital, Bachstraße 18, D-07743 Jena, Germany
[7] Center for Sepsis Control and Care, Jena University Hospital, Erlanger Allee 101, D-07747 Jena, Germany

E-mail: alexander.mosig@med.uni-jena.de

Keywords: endothelial cells, microfluidic, dynamic cell culture

Supplementary material for this article is available online

Abstract

Hemodynamic forces generated by the blood flow are of central importance for the function of endothelial cells (ECs), which form a biologically active cellular monolayer in blood vessels and serve as a selective barrier for macromolecular permeability. Mechanical stimulation of the endothelial monolayer induces morphological remodeling in its cytoskeleton. For *in vitro* studies on EC biology culture devices are desirable that simulate conditions of flow in blood vessels and allow flow-based adhesion/permeability assays under optimal perfusion conditions. With this aim we designed a biochip comprising a perfusable membrane that serves as cell culture platform multi-organ-tissue-flow (MOTiF biochip). This biochip allows an effective supply with nutrition medium, discharge of catabolic cell metabolites and defined application of shear stress to ECs under laminar flow conditions. To characterize EC layers cultured in the MOTiF biochip we investigated cell viability, expression of EC marker proteins and cell adhesion molecules of ECs dynamically cultured under low and high shear stress, and compared them with an endothelial culture in established two-dimensionally perfused flow chambers and under static conditions. We show that ECs cultured in the MOTiF biochip form a tight EC monolayer with increased cellular density, enhanced cell layer thickness, presumably as the result of a rapid and effective adaption to shear stress by remodeling of the cytoskeleton. Moreover, endothelial layers in the MOTiF biochip express higher amounts of EC marker proteins von-Willebrand-factor and PECAM-1. EC layers were highly responsive to stimulation with TNFα as detected at the level of ICAM-1, VCAM-1 and E-selectin expression and modulation of endothelial permeability in response to TNFα/IFNγ treatment under flow conditions. Compared to static and two-dimensionally perfused cell culture condition we consider MOTiF biochips as a valuable tool for studying EC biology *in vitro* under advanced culture conditions more closely resembling the *in vivo* situation.

Introduction

Endothelial cells (ECs) lining the inner lumen of blood vessels form a barrier for ions, nutrients, water and macromolecules and are responsible for important homeostatic functions such as the regulation of the vessel tonus or coagulation by secretion of bioactive molecules. Endothelial layers are also important regulators of vascular inflammation due to their ability to recruit immune cells from the circulation via expression of cell adhesion molecule (CAM) in response to tissue damage or infection. Shear stress is a critical factor for endothelial function as mechanic stimulation of the EC membrane has been demonstrated to mediate morphological adaptations (Flaherty *et al* 1972, Davies *et al* 1976, Goode *et al* 1977), and

to regulate endothelial permeability (Kwei *et al* 2004). Moreover, shear stress is involved in the regulation of inflammatory reactions at the onset of cardiovascular diseases such as atherosclerosis (Traub and Berk 1998).

Endothelial adaption to dynamic cell culture under flow conditions includes the modulation of the cytoskeleton in response to shear stress. F-actin microfilaments have been shown to reorganize under flow conditions into long, dense stress fibers crossing the cells in a direction perpendicular to flow. During this process the cytoskeleton forms bridges between mechanosensors on the luminal apical side and the integrins on the basal side, which also have been described as mechanotransducers (Davies 1995, Geiger *et al* 2001). One of these sensors is the platelet endothelial cell adhesion molecule-1 (PECAM-1), the major constituent of the EC intercellular junctions which has been shown to transmit mechanical forces via PI3K/Akt-mediated integrin activation and actin microfilament alignment (Tzima *et al* 2005). Beyond, PECAM-1 is involved in the maintenance of endothelial integrity preserving barrier function and preventing alterations of the cellular environment that could contribute to organ dysfunction (Harhaj and Antonetti 2004). In addition, shear stress has been reported to regulate expression of CAMs and to modulate monocyte adhesion to the vascular endothelium. Under flow conditions cell surface expression of intercellular adhesion molecule-1 (ICAM-1) is selectively up-regulated (Nagel *et al* 1994), whereas expression of vascular cell adhesion molecule-1 (VCAM-1) and E-selectin is reported to be decreased in response to shear stress (Chiu *et al* 2004).

In vitro studies in EC biology rely on reproducible culture conditions that resemble critical parameters of the *in vivo* state. Microfluidically supported flow chambers have emerged as advanced tools for EC culture within the last decade. Micro-scaled flow chambers offer the advantages of low consumption of reagents and biological samples, a high flexibility in the design of integrated structures, and optimal control of cell patterning (El-Ali *et al* 2006, Whitesides 2006, Wang *et al* 2011). Established two-dimensionally perfused flow chambers mostly comprise rhombic shaped cavities with a tight bottom serving as cell culture area that is perfused with cell culture medium under laminar flow conditions. However, these two-dimensionally perfused flow chambers provide only the option of apical perfusion and therefore lack the opportunity for flow-based studies on permeability or investigations of e.g. cytokine actions on the basal cell membrane during dynamic culture.

The vast majority of flow chambers used for the culture of EC layers is based on polydimethylsiloxane (PDMS) due to its ease of use for a rapid manufacturing of prototypes (Young and Simmons 2010). PDMS is biological compatible, transparent and exibits low autofluorescence which makes it suitable for on-chip fluorescence microscopy (Berthier *et al* 2012). However, elastic PDMS possess a couple of drawbacks, e.g. hydrophobic molecules can adsorb to the bulk of the PDMS and uncrosslinked monomers tend to migrate from the bulk to the surface, allowing to recover surface hydrophobicity even after oxygen plasma treatment (Eddington *et al* 2006, Toepke and Beebe 2006). Uncrosslinked PDMS monomers have also been found to leach out from the bulk, into the media and affecting cellular behavior (Regehr *et al* 2009). Furthermore, PDMS is permeable to gases and water vapor, causing changes in the osmolarity of the cell culture medium (Thuenauer *et al* 2014).

We designed a chip architecture that uses porous membranes as also utilized in Transwell filter inserts serving as cell culture substrate (Ramello *et al* 2011, Huh *et al* 2013, Jang *et al* 2013, Ramadan *et al* 2013) allowing apical and basolateral perfusion of EC layers in parallel during cell culture within the biochip. Cyclic olefin copolymers (COCs) have been used for manufacturing of cell culture devices to overcome limitations of PDMS. COCs do not unspecifically absorb medium contents and bulk surfaces of biochips can easily been functionalized by long lasting plasma treatment for hydrophilization. Furthermore COC possess high stability, ideal optical characteristics for bright field as well as fluorescence microscopy and is frequently used in medical devices due to its proven biocompatibility (van Midwoud *et al* 2012). For the first time, we here systemically characterize and compare the impact of the different cell culture methods of expression on endothelial marker proteins and cell growth under static and dynamic conditions in established two-dimensionally perfused flow chambers and MOTiF biochips to proof the benefits of EC culture within membrane-containing biochips.

Methods

HUVEC and THP-1 cells

ECs were isolated from human umbilical cord veins (HUVEC) as described elsewhere (Jaffe *et al* 1973). Donors were informed about the aim of the study and gave written informed consent. The study was approved by the ethics committee of the Friedrich-Schiller-University Jena, Germany. Experiments were performed with HUVEC cells up to passage four cultured in EC medium (Promocell, Heidelberg, Germany). THP-1 cells were obtained from DSMZ (Braunschweig, Germany) and cultured in RPMI 1640 supplemented with 10% FCS (Life Technologies, Karlsruhe, Germany).

Multi-organ-tissue-flow (MOTiF) biochip fabrication and surface treatment

MOTiF biochips and flow chamber chips were manufactured by and obtained from microfluidic ChipShop GmbH (Jena, Germany). The microfluidic devices

were made from Topas®, a COC. The chip was manufactured by injection molding using a modular mold base with exchangeable metallic mold inserts. The mold inserts were structured using ultra-precision mechanical machining using a 100 μm diameter machining bit for the smallest features and finishing. As first fabrication step the microstructured part with microfluidic channels network, fluidic interfaces and the area for membrane integration are made by injection molding. Afterwards the integration of the 11 μm thick polyethylene-terephthalate (PET) membrane with a pore diameter of 8 μm and a pore density of 2×10^5 pores/cm^2 (TRAKEDGE Sabeu, Radeberg, Germany) was carried out. The parts were then sealed on top and bottom side with an extruded 140 μm thick COC film using a low-temperature proprietary bonding method.

Surface oxidation for hydrophilization was accomplished by treatment with oxygen plasma using a T200G plasma generator (PVA Tepla AG, Wettenberg, Germany). The surface of the 2D perfusion chamber was oxidized as described for MOTiF chips. COC foils used for sealing in both chip designs show significant oxygen permeability. Gas permeable silicon tubing was used for two- and three-dimensional (3D) perfusion allowing oxygen equilibration during experimentation. Ramping structures have been introduced in the biochip design between membrane and membrane framing of the bulk to avoid unfavorable flow conditions and trapping of stationary bubbles. Bubble formation was reduced by oxygen plasma treatment of the whole chip surface and perfusion medium was stirred and equilibrated over night under perfusion conditions before use.

Meassurement of contact angles

Measurement of contact angles was done on injection-molded biochips without usage of any mold release agents. Contact angles were measured using a Dino-Lite AD4113TL (Long Working Distance) microscope camera and analyzed with the Dino Capture 2.0 software.

Antibodies, flow cytometry and vitality stain

The following antibodies were used for immunofluorescence microscopy: anti-CD31 (CellSignaling, MA, USA), anti-von Willebrand factor (vWF) (DAKO, Hamburg, Germany), anti-zonula occludens-1 (ZO-1), goat-anti-mouse-Cy3, goat-anti-rabbit-AF488 (Life Technologies), and goat-anti-rabbit-AF647 (Dianova, Hamburg, Germany). Actin was stained with phalloidin-AF633 (Life Technologies). Immunofluorescence microscopy was performed with Axio Observer Z1 (Zeiss, Jena) controlled by AxioVision 4.8.2 software (Zeiss, Jena). Z-stack imaging was done with a Zeiss LSM 710 confocal microscope (Zeiss, Jena, Germany). Fluorescence analysis, quantification of immunofluorescence staining and cell shape analysis was performed with ImageJ 1.46r. Calcein-AM (Life Technologies)-staining was performed according to manufacturer's recommendations. For flow cytometry the antibodies anti-CD31-FITC, anti-CD62e-PECy5, anti-CD106-V450 (BD Pharmingen, Heidelberg, Germany), anti-CD54-AF647 (BioLegend, San Diego, CA, USA) and isotype control antibodies mouse IgG1-FITC, mouse IgG1-PE (Miltenyi Biotec, Bergisch-Gladbach, Germany), mouse IgG1-APC (BioLegend), mouse IgG1-PECy5 and rat IgG2a-eFluor450 (eBioscience, San Diego, CA, USA) were used. Flow cytometry was done using a BD FACS-Canto™ II (BD BioScience, Heidelberg, Germany) and data were analyzed with FlowJo v7.6.5 (TreeStar, Ashland, OR, USA).

Computational fluid dynamic (CFD) simulations

CFD simulations were performed using the OpenFOAM CFD-toolkit (the OpenFoamFoundation, http://www.openfoam.org) in combination with the ParaView Toolkit (Henderson 2004) for data visualization and analysis. Surface triangulated meshes were obtained from the geometry models using the gmsh utility (Geuzaine and Remacle 2009). Volume hexaeder meshes were generated using the snappyHexMesh utility of OpenFoam. Transient simulations have been performed using the interFoam solver as provided by OpenFOAM Version 2.2.0 for a flow rate of 20 μl s^{-1}. with aqueous phase Reynolds number Re of 28 in the inflow and outflow cylinders, Re of 12 in the inflow section of the main chamber and Re of 5.5 in the main section of the chamber. Time step size was adjusted dynamically to a fluid and interface Courant number below 0.15. Final tolerance limits were set in the fvSolution parameter dictionary of the solver to 1 10-9 for the p_rghFinal iterations and to 1 10-10 for the UFinal iterations. Interface compression defined by the parameter cALPHA was switched off by setting the value to zero.

Flow culture experiments

Microfluidic cell culture experiments were performed under a specialized clean bench for microfluidic applications with environment control of 5% CO_2, 70% air humidity and 37 °C under sterile cell culture conditions (Automated Lab Solutions GmbH, Jena, Germany). HUVECs were seeded on MOTiF biochips and flow chambers with a density of 1.3×10^5 cells/cm^2. Static cell culture was performed in 24 well plates with 13 mm glass coverslips (Menzel, Braunschweig, Germany). Cells were cultured for 72 h until reaching confluence. Medium was changed on a daily basis in the wells or chips. ECs were cultivated under static conditions within the chips until reaching confluence. Chips then were perfused with medium using peristaltic pumps (Ismatec REGLO digital MS-CA-4/12-100, Wertheim, Germany). Shear stress of 0.7 and 10 dyn cm^{-2} was applied for 24 h.

Calculation of shear stress levels

Shear stress was calculated with the equation:

$$\tau = \frac{2^{*}\mu^{*}Q}{w^{*}h^{2}}{}^{*}\left(\frac{m+1}{m}\right)^{*}(n+1)$$

(τ: shear stress, h: height and ω: width of the microfluidic chamber, Q: flow rate of the medium). The values for m and n are empirical constants with $m = 1.7 + 0.5^{*}\alpha^{-1.4}$, and $n = 2$ for $\alpha < 1/3$, where cross sectional aspect ratio $\alpha = h/w$ with $0 \leqslant \alpha \leqslant 1$ (Young and Simmons 2010).

Permeability assay

EC were treated with 20 ng ml^{-1} TNFα (Calbiochem, Billerica, MA, USA) and 10 ng ml^{-1} IFNγ (Peprotech, Hamburg, Germany) through the lower perfusion channel. After cytokine treatment endothelial layers were incubated with 10 mg ml^{-1} of FITC-dextran for 30 min under static conditions. FITC-dextran that permeates through the layer was collected via the lower perfusion channel and analyzed with an iEMS Reader MF & Multiskan and Ascent Software version 2.6 (Thermo Scientific, Waltham, MA, USA).

THP-1 adhesion assay

THP-1 cells were labeled with 1 μM CellTracker green CMFDA (Life Technologies, Karlsruhe, Germany). EC layers were perfused at the apical cell membrane via the upper perfusion channel with indicated shear stress and simultaneously stimulated at the basal cell membrane with 20 ng ml^{-1} TNFα perfused via the lower perfusion channel of the MOTiF biochips through membrane pores with 8 μm diameter for 24 h. Within the last 30 min of the experiment EC layers were simultaneously perfused at the apical side with 2×10^{6}/(ml $\times$ h) labeled THP-1 using a neMESYS syringe pump with stirring module (Cetoni, Korbußen, Germany). After flushing with PBS, the cell layers were fixed for 10 min with 4% PFA (Sigma-Aldrich, MO, USA), mounted and nuclei were stained with DAPI (Life Technologies) and samples were mounted in fluorescent mounting medium (DAKO). THP-1/HUVEC ratio was calculated by counting labeled adherent THP-1 cells and DAPI stained HUVEC.

Cell shape index (CSI) analysis

CSI analysis was performed by fluorescence staining of the CD31 membrane protein to locate cellular boundaries, analyzed with ImageJ and calculated using the formula $\mathrm{CSI} = 4\pi^{*}\frac{A}{P^{2}}$ (P: cellular perimeter, A: area) (Malek and Izumo 1996). CSI defines cellular morphological shape ranging from 0 corresponding to circular shape to 1 corresponding to a straight line.

Statistical analysis

All results are reported as average of the performed experiments with standard deviation. Where indicated multiple comparison analysis was performed using one-way-ANOVA testing with Tukey's multiple testing. Direct comparison of two conditions was done with two-tailed, non-paired Student's t-test. Statistical analysis was performed using GraphPad Prism 6 software (Graphpad Software, La Jolla, CA, USA).

Results

Microfluidic chips are a promising tool to investigate endothelial layers and their interaction with immune cells. Here, we developed a microfluidically supported biochip, allowing a 3D perfusion of EC layers under defined shear stress conditions thereby providing enhanced nutrition supply and preventing enrichment of catabolic metabolite. To prove that the design of the MOTiF biochip allows culture of EC layers under conditions that resemble the natural situation we analyzed cell morphology, EC marker protein expression and functional responsiveness to chemokines and compared it with established two-dimensionally perfused flow chamber designs (figure 1(A)) and static culture conditions, respectively.

The MOTiF biochip consists of an upper and a lower flow chamber horizontally separated by a microporous PET membrane (figure 1(B)). The membrane acts as culture area for ECs. The integrated pores of 8 μm diameter allow basal perfusion and medium exchange to cultured EC layers through a lower perfusion channel, and in parallel apical perfusion via a separate upper perfusion channel (figures 1(B) and (C)). Dependent on the maximum local Reynolds numbers and Dean numbers above 50 in the inflow region, the formation and downstream propagation of Dean vortices can be expected. These fluid structures may superpose the laminar profile in the capillary slit at the endothelial layer resulting in non-predictable local shear stress variations in this zone. This effect has been considered in the design of the geometry of the vertical inflow region. Therefore, the cylindrical inflow was rounded in a direction-dependent way in order to increase the characteristic radius of the curvature in this region and secondly to decrease the average fluid velocity in this region. The geometry of the MOTiF biochip cavity generates laminar flow conditions during EC layer perfusion as verified by CFD analyses. CFD was calculated on the basis of measured contact angles for EC Medium with the bulk wall that has been treated with oxygen plasma for reducing hydrophobicity. Contact angle between flow medium and oxygen plasma-treated bulk wall was 43° ± 2° (supplementary figure 1(A)) and with the EC layer seeded on the membrane of the MOTiF biochip at 22° ± 2°, (supplementary figure 1(B)). CFD simulation based on these contact angels revealed that the formation of bubbles and turbulent flow on the channel inlet is prevented under these conditions. Filling characteristics in the inflow region of the main

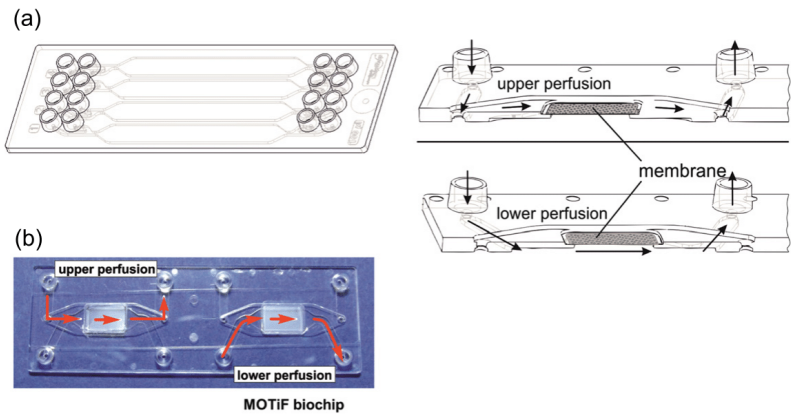

Figure 1. *2D Flow Chamber and MOTiF biochip design.* (A) Design of two-dimensionally perfused flow chambers. (B) MOTiF biochips contain two cavities, each comprising an integrated membrane serving as cell culture area. Cells cultured on the membrane are perfusable independently from both the apical or basal side through upward directed (upper perfusion) and downward directed (lower perfusion) channels. (B) Prototype of MOTiF biochips produced by injection molding with cyclic olefin polymers with welded membrane of polyethylene terephthalate.

chamber for the exchange of air by aqueous medium was investigated for surface contact angles in the range between 15 and 105° with a contact angle stepping of 15°. Bubble free exchange of the air by aqueous medium was observed for contact angles below 60°. At higher contact angle configurations an air bubble was formed in the pocket between the end of the top microchannel and the junction of the cylindrical inflow channel into the main channel (video 1). The same analysis has been performed for the exchange of air by aqueous medium for the outlet region of the main chamber. In this case, air exchange by aqueous buffer without remaining air bubbles was observed for contact angles below 75° (video 2). The complete fluid exchange and interface evolution for the main chamber was analyzed in the third simulation for the targeted contact angle configuration of the chip wall material of 82° and the membrane section with a contact angle of 22°. The contact line of the interface to the membrane precedes the interface contact line to the channel walls. The interface contact lines are orthogonal to the fluid transport direction. No tendency for inclusion air bubble formation is observed (video 3). In the video sequence the outflow section was not included since this aspect is always covered by the results of the outflow fluid exchange characteristics simulation.

In a first step we studied growth and vitality of endothelial layers on the chips under static and dynamic culture conditions. We used COC as bulk material for molding of two-dimensionally perfused flow chambers as well as MOTiF biochips in order to enable a direct comparison between both chip designs and to prevent polymer-related bias in the obtained results. To distinguish between the specific effects of continuous medium exchange and mechano-transduced effects of shear stress, we compared endothelial layers under low shear stress of 0.7 dyn cm^{-2} with only minimal flow related mechanical stimulation, and high shear stress with 10 dyn cm^{-2}. The chosen high shear stress rate corresponds to the human *in vivo* situation in larger arteries and venules and represents the mean shear stress rate of common human carotid artery (Cheng *et al* 2007). ECs exhibit the typical cobblestone shape in static cell culture whereas in dynamic cell culture under perfusion the shear stress induces adaption within 24 h detectable as elongation of EC along the flow direction (figure 2(A)). Typical percentage of vital ECs under all culture conditions was above 97% as verified by calcein-AM staining (figure 2(B)) and flow cytometry (data not shown). ECs were characterized based on their morphology using the CSI. A CSI of 1 describes a circle and CSI of 0 describes a line. Although we observed no differences of ECs cultured in flow chambers and MOTiF biochips under low shear stress conditions, an improved adaption to high shear stress was detectable for ECs cultured in MOTiF biochips in respect to cell elongation and an increased cell density compared to flow chamber culture was detectable. Stimulation of ECs with high shear stress even reduced cell density in endothelial layers cultured in two-dimensionally perfused flow chambers (figures 2(C) and (D)).

Dynamic cell culture is known to mediate cytoskeleton rearrangements within ECs in response to shear stress (Malek and Izumo 1996). We therefore investigated endothelial actin microfilament organization under static conditions and after adaption of ECs to

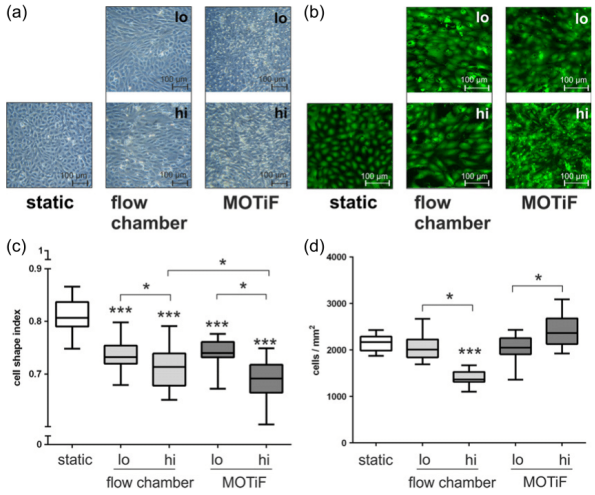

Figure 2. *Morphology and vitality of EC.* (A) Bright field images of EC cultured under static and dynamic conditions (lo: low shear stress, hi: high shear stress). (B) Viability staining of ECs with calcein-AM (C) cell density. (D) * $p < 0.05$; *** $p < 0.001$ versus static or between conditions as indicated (Student's t-test).

flow conditions within two-dimensionally perfused flow chambers and MOTiF biochips. Z-stack imaging of EC layers illustrates that endothelial layers within MOTiF biochips exhibit an increased mono-cell-layer thickness compared to corresponding conditions in flow chambers or static culture, respectively. Increased cell heights and densities were found associated with an intensified cytoskeleton remodeling, increased expression of F-actin and the formation of prominent stress fibers (figures 3(A) and (B)). F-actin fiber content correlated positively with increasing shear stress. In addition, endothelial F-actin expression was found significantly increased by MOTiF biochip culture compared to other culture conditions (figure 3(C)). In agreement with previous reports (Galbusera *et al* 1997), we observed increasing protein levels of vWF that correlated with the intensity of shear stress stimulation. Endothelial layers cultured in MOTiF biochips showed a significantly increased expression of vWF and a unique accumulation and intracellular localization of Weibel–Palade bodies (WPB) along with the appearance of extracellular patches and formation of vWF macrofilamentous strings (figures 3(D) and (E)). Similar to vWF we found an elevated expression of PECAM-1 on EC layers cultured within MOTiF biochips. Our observation that increased levels of vWF and PECAM-1 were predominantly found on areas of the culture membrane with a high pore density (figure 4(A)), supports the idea that apical and basal perfusion within MOTiF biochips not only improve supply of cell layers with nutritional culture medium but also favors rapid adaption of ECs to flow culture conditions.

The MOTiF biochips further provide the possibility to perform permeability assays under flow conditions. PECAM-1 and zonula occludens-1 (ZO-1) are critical regulators of endothelial permeability and associated pathophysiology (Harhaj and Antonetti 2004). We found elevated expression levels of PECAM-1 (figures 4(B) and (C)) and ZO-1 (figures 4(D) and (E)) on endothelial layers correlating with increasing shear stress stimulation (figure 4(E)). Flow-based permeability assays using FITC-labeled 40 kDa dextran revealed that EC layers cultured with high shear stress stimulation formed a tighter cell layer compared to low shear stress stimulation (figure 4(G)). It has been shown that treatment of EC layers with the proinflammatory cytokines TNFα and IFNγ mediated a loss in barrier function (Lopez-Ramirez *et al* 2012). In agreement with these observations we found a significant elongation of cell morphology (figure 4(F)) upon treatment with TNFα/IFNγ that was further accompanied with a nearly complete breakdown of PECAM-1 and ZO-1 protein expression (figures 4(B)–(E)). The disintegration of cell connective proteins in consequence resulted in an increased permeability for dextran and breakdown of endothelial barrier function (figure 4(G)).

Inflammation within the vascular system not only involves leakage of endothelial layers but also mediates active recruitment of immune cells from the circulation depending on the interaction with CAM proteins. We therefore characterized endothelial layers in

IOP Publishing Biofabrication 7 (2015) 015013 M Raasch et al

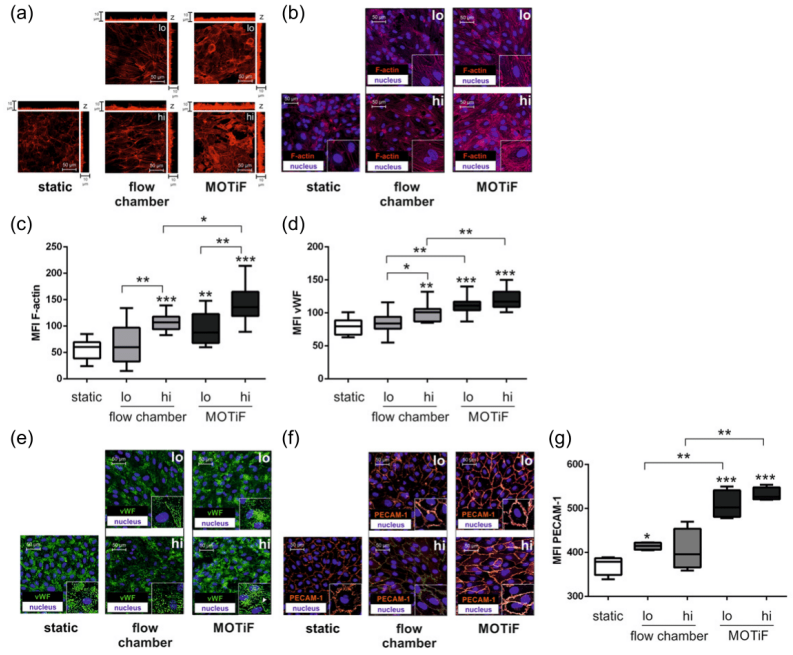

Figure 3. *Adaption of endothelial layers to shear stress.* F-actin arrangement and cytoskeleton remodeling visualized by (A) confocal Z-stack imaging and (B) two-dimensional immunofluorescence microscopy. Quantification of (C) actin and (D) vWF expression. (E) Expression of vWF. (F) Visualization and (G) quantification of PECAM-1 expression. * $p < 0.05$; ** $p < 0.01$, *** $p < 0.001$ versus static or between conditions as indicated (one-way ANOVA with Tukey's multiple testing comparison).With Tukey's multiple testing comparison * $p < 0.05$; ** $p < 0.01$, *** $p < 0.001$ compared to static or between indicated conditions.

MOTiF biochips for their cell surface expression of ICAM-1, VCAM-1 and E-selectin in response to pro-inflammatory TNFα stimulation. Without cytokine stimulation ICAM-1 expression was found up-regulated only under high shear stress conditions, whereas VCAM-1 expression declined under low as well as high shear stress conditions in MOTiF biochips compared to static cell culture. Expression of E-selectin was not effected by shear stress in the absence of cytokine stimulation. However, when cells were cultured under flow conditions, expression of all three CAMs declined in response to TNFα stimulation compared to static conditions (figures 5(A)–(C)). Functional relevance of altered CAM expression was tested by flow-based adhesion assays. Fluorescence-labeled THP-1 cells were continuously perfused through the upper channel of MOTiF biochips thereby overflowing the apical site of the EC layer equivalent to the lumen of a blood vessel. Simultaneously to THP-1 incubation with the endothelial layer, TNFα was applied through the lower perfusion channel. TNFα treatment activated ECs and mediated a significantly increased proportion of adhesive THP-1 cells under static and dynamic culture conditions (figures 5(D)). Highest amounts of adhesive THP-1 cells were found under static culture conditions. Within 30 min, THP-1 cells already formed filopodia on the endothelial layer that were not observed in the dynamic cell culture even with low shear stress stimulation (supplementary figure 1(C)). Furthermore, the number of THP-1 cells interacting with unstimulated as wells as TNFα-activated endothelial layers decreased with increasing shear stress.

Discussion

The development of cell culture technologies that better mimic the *in vivo* context for specific cell types are of great value for a better understanding of signaling pathways, the development of therapeutic strategies and for toxicity studies. This is mainly a consequence of the possibility to control experimental conditions much better, at least for proof of principle studies, than it is possible in living animals. As reported previously by other groups ECs exhibit remarkable changes in cell morphology when adapted to flow conditions (Levesque and Nerem 1985, Girard

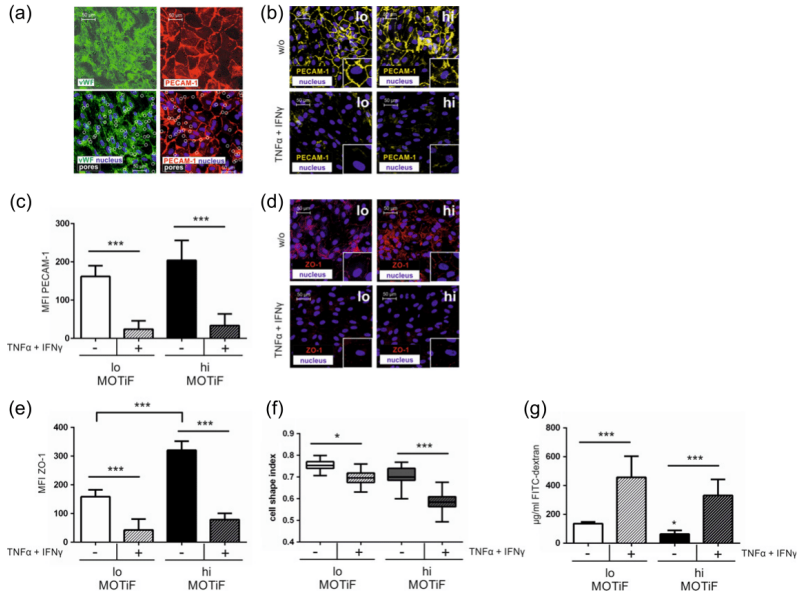

Figure 4. *Expression of vWF, PECAM-1 and ZO-1 in ECs cultured in MOTiF biochips.* (A) Expression of vWF and PECAM-1 in dependence of membrane pore density. For visualization and comparison purposes pores were marked in the lower images. (B) and (D) Expression of PECAM-1 (B) and ZO-1 (D) in dependence of shear stress and TNFα/IFNγ treatment in ECs cultured in MOTiF biochips. Quantification of PECAM-1 (C) and ZO-1 (E) expression in ECs cultured in MOTiF biochips. (F) Cell shape index. (G) Permeability of endothelial layers for 40 kDa FITC-labeled dextan. * $p < 0.05$; ** $p < 0.01$, *** $p < 0.001$ between conditions as indicated (Student's t-test).

and Nerem 1995). To ensure the best possible comparability and transferability between *in vitro* and *in vivo* studies, critical *in vitro* cell culture parameters such as the application of physiological shear stress and optimal perfusion conditions of the cells layers have to be taken into account. Therefore, flow chamber systems are being used more frequently for *in vitro* studies on EC biology instead of static cell culture conditions that lack the option to apply mechano-stimulatory effects. Although two-dimensionally perfused flow chambers provide an improved nutrition supply compared to static culture and allow the application of physiological shear stress these devices do not implement effects induced by flow-based permeability or transmigration. Further, cell culture within conventional dishes as well as two-dimensionally perfused flow chambers mostly includes growth of adherent cells on a tight and inflexible plastic substrate that prevents perfusion of the basal side of the cell membrane and limits nutrition supply and dynamic removal of cellular metabolites and catabolites. We therefore developed the MOTiF biochip design that offers improved perfusion conditions for the EC layers. Due to the option of stimulation with dynamically adjustable gradient concentrations during permeability or adherence/transmigration experiments from different cell membrane sides, the immune cell recruitment and modulation of endothelial permeability in response to cytokine stimulation from different luminal or basal derived sources can be investigated separately or in parallel. To characterize the MOTiF design for culture of endothelial layers we compared ECs under dynamic culture within MOTiF biochips in respect to viability, adaption to flow conditions and expression of endothelial marker proteins with static and dynamic culture conditions in two-dimensionally perfused flow chambers, respectively.

Inhomogeneous aggregation of EC cultured within MOTiF biochips could possibly influence flow dynamics across the membrane. However microscopic analysis revealed the formation of a tight, confluent and homogenous EC layer during culture in MOTiF biochips and a disturbed flow through inhomogeneous cell aggregation was not observed. ECs adapted to flow conditions in established flow chambers as well as in MOTiF biochips within 24 h. This became apparent by a change in cell morphology compared to static cell culture. In addition, ECs cultured in MOTiF biochips revealed an intensive modulation of

IOP Publishing Biofabrication 7 (2015) 015013 M Raasch et al

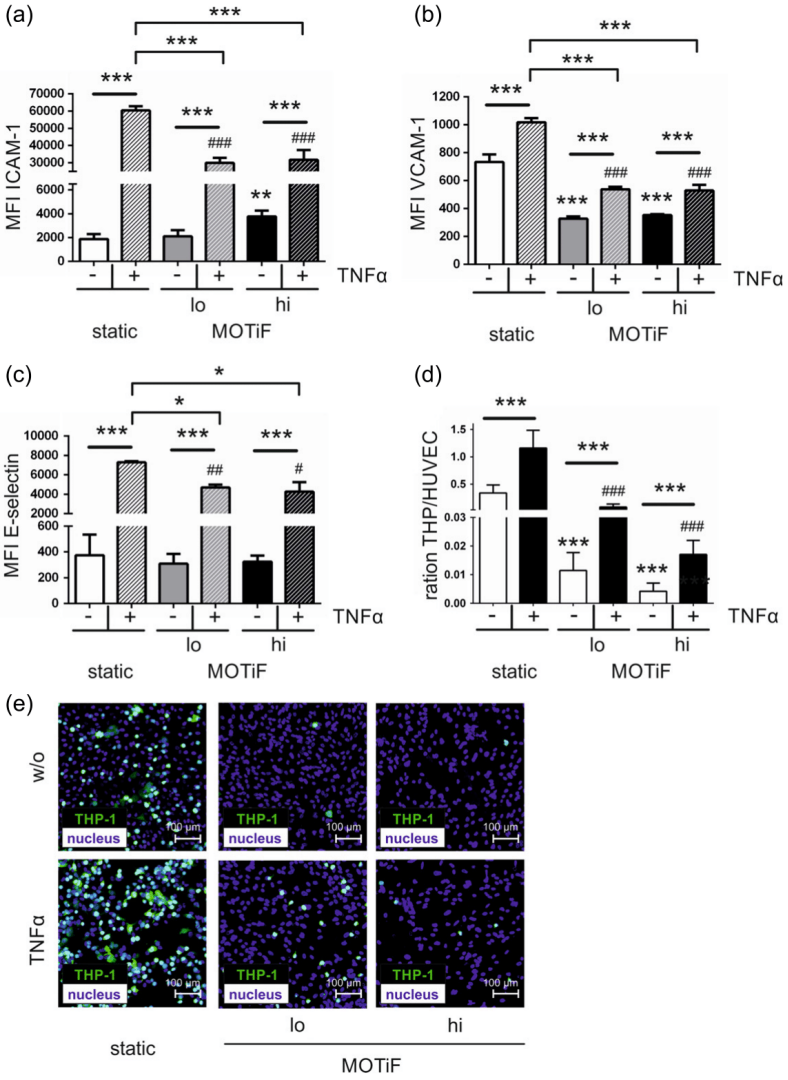

Figure 5. *Expression of endothelial CAMs and adhesion of THP-1 lymphocytes to ECs cultured in MOTiF biochips*. Expression of (A) ICAM-1, (B) VCAM-1, (C) E-selectin in ECs cultured in MOTiF biochips. (D)–(E) Adherent fluorescence-labeled THP-1 cells on HUVEC cell layer. (D) Ratio of adherent THP-1 cells to confluent EC. (E) Fluorescence microscopic images of adherent THP-1 to endothelial layer. * $p < 0.05$; ** $p < 0.01$, *** $p < 0.001$ between conditions as indicated (Student's t-test).

the cytoskeleton in response to flow and exhibited an increased cell height corresponding to enhanced polarity. The remodeling of the cytoskeleton was even more prominent in the MOTiF biochips when compared with standard flow chambers with identical shear stress application. Remodeling of the cytoskeleton in response to force from outside is induced by the generation of signals to the inside of a cell which subsequently induces the reorganization of the cytoskeleton and thereby reinforces the strength of cell attachment (Zhao *et al* 1995).

In addition, we observed that the expression of vWF was increased in the endothelial layers when grown in the MOTiF biochips. However, expression of

vWF was enhanced independently from shear stress stimulation within MOTiF biochips and was significantly increased when compared to two-dimensional flow chamber perfusion. Strongest expression of vWF was detectable in MOTiF biochips within areas of high pore-density on the membrane allowing improved basal medium perfusion. The impact of improved culture conditions also became apparent during the analysis of the cellular distribution of vWF on ECs in flow chambers and MOTiF biochips. Recently, multigranular exocytosis of vWF has been proposed to be a significant mode of exocytosis in which WPBs coalesce into a 'secretory pod' before fusing with the plasma membrane (Valentijn *et al* 2010). In ECs, the formation of secretory pods facilitates vWF string formation by accumulating the content of multiple WPBs before their release. The unique intracellular distribution of vWF within ECs cultured in MOTiF biochips shows remarkable morphological similarities with these secretory pods, and vWF macrofilament secretion colocalizes with these structures. The vWF string formation is dependent on neutral extracellular pH and is impaired if the pH within the WPBs is increased e.g. by pretreatment with monensin, which causes the disappearance of vWF strings (Valentijn *et al* 2010). Improved perfusion conditions in MOTiF biochips might thus contribute to a stable neutral extracellular pH thereby facilitating vWF string secretion. Exocytosis of vWF also depends on the interaction of WPBs with microtubules and actin cytoskeleton (Manneville *et al* 2003). Extensive remodeling as observed in MOTiF biochips assumed to contribute to increased vWF secretion. In addition exocytosis of WPBs is regulated by hypertensive stretch through VEGF-receptor 2 (VEGFR2) signaling pathways. In contrast to ECs cultured within two-dimensionally perfused flow chambers where cells are attached to an inflexible culture area, mechanical forces to endothelial layers can be generated when grown on the free-hanging membrane within MOTiF biochips. We speculate that flow conditions in the dynamic culture induce a limited stretching of the PET membrane and the cultured endothelial layer thereon. Stretch of the endothelium is known to trigger a rapid release of vWF strings from WPBs (Xiong *et al* 2013) that have been shown to remain associated with cells for a considerable time (Michaux *et al* 2006, Huang *et al* 2008). These vWF strings are a physiological requirement in the healthy endothelium and known to prevent coagulopathy and impaired wound healing (Federici and Mannucci 2007).

Furthermore, multigranular exocytosis of vWF strings has been shown to constitute an important pathway for the regulated release of VWF by vascular ECs (Valentijn *et al* 2010). vWF string formation and secretion was not observed under static cell culture conditions and only to a limited extent in two-dimensionally perfused flow chambers. In this context we want to note, that ultra-large von Willebrand fibers that are formed under pathophysiological conditions from vWF strings were reported to be important in the initial pathogenic step of *S.aureus*-induced endocarditis in patients with an apparently intact endothelium (Pappelbaum *et al* 2013). Although we do not know the exact mechanisms by which vWF string formation is induced in MOTiF biochips we suppose that endothelial layers obtained therein might be an interesting *in vitro* model for studies on immune cell interactions with EC layers under improved perfusion conditions and with new methodical possibilities compared to two-dimensionally perfused flow chambers.

In regard to immune cell interactions with ECs the maintenance and regulation of endothelial barrier function is one of the most imported tasks at the vessel wall. PECAM-1 is known to be a critical regulator of immune cell trafficking and maintenance of EC junctional integrity (Privratsky *et al* 2010). PECAM-1 is known to be protective in ECs during inflammation due to its ability to inhibit pro-inflammatory cytokine signaling and maintaining of vascular integrity (Carrithers *et al* 2005, Maas *et al* 2005, Privratsky *et al* 2010). Furthermore, ZO-1 which connects to and stabilizes endothelial tight junctions within lateral cell-cell contact and thereby contributes to endothelial barrier function (Chattopadhyay *et al* 2014) was found up-regulated by high shear stress in ECs cultured within MOTiF biochips. Thus, increased expression of PECAM-1 as well as ZO-1 likely contributes to improved barrier function observed in response to high shear stress stimulation within MOTiF biochips. In addition, also the prolonged lateral cell–cell contacts of thickened EC monolayers (mediated by amplified cytoskeleton rearrangement) further contribute to elevated barrier function of EC layers stimulated with high shear stress. Similar observations were made with microfluidic models using kidney epithelial cells that responded to fluid shear stress by increasing their cell height and actin cytoskeleton rearrangement, also resulting in the formation of tighter cell layers (Jang *et al* 2011, Jang *et al* 2013). During inflammation PECAM-1 is redistributed and down-regulated from lateral junctions (Stewart *et al* 1996) resulting in a loos of endothelial barrier function (Fernández-Martín *et al* 2012). We reproduced this phenomenon by basal application of proinflammatory cytokines TNFα and IFNγ to EC layers, demonstrating the feasibility of MOTiF biochips for usage in flow-based permeability assays. The basal stimulation of ECs with cytokines in the dynamic cell culture was associated with an elongation of stimulated ECs. It was recently shown that EC activation by TNFα is not only accompanied with augmented cell elongation under flow conditions but also with a dynamic shifts of the cytoskeleton and reduced cell stiffness (Stroka *et al* 2012). Thus, the observed leakage of endothelial layers in response to TNFα/IFNγ treatment is likely mediated by loos of PECAM-1 and ZO-1 expression combined with reduced cytoskeleton stiffness.

Activation of ECs also includes alterations in CAM expression. EC layers in MOTiF biochips exhibited a characteristic CAM expression profile in response to shear stress. In accordance with previous reports ECs adapt to high shear stress by up-regulation of ICAM-1 expression and down-regulation of VCAM-1 (Morigi *et al* 1995, Tsao *et al* 1996). Concordant with this we observed a diminished expression of ICAM-1, VCAM-1 and E-selectin in the dynamic cell culture in MOTiF biochips under low as well as high shear stress conditions in response to TNFα treatment compared to static culture. Down-regulation of CAM expression has been shown to be mediated by release of nitric oxide by ECs in response to shear stress (De Caterina *et al* 1995). Furthermore, laminar shear stress attenuates the expression of E-selectin and VCAM-1 in response to TNFα modulation by NF-κB-dependent signaling pathways (Chiu *et al* 2004, Partridge *et al* 2007).

However, in these studies the authors show an increased ICAM-1 expression in response to TNFα by shear stress whereas in our studies a down-regulation of ICAM-1 expression after TNFα treatment during low as well as high shear stress stimulation was detectable. We speculate that the observed differences might be due to different stimulation times used. Partridge *et al* and Chiu *et al* stimulated HUVEC with TNFα for 2 h and 4 h, respectively. In our setting endothelial layers were stimulated during the entire 24 h shear stress stimulation (Chiu *et al* 2004, Partridge *et al* 2007).

We have shown that endothelial layers cultured in MOTiF biochips exhibit an improved expression of EC marker proteins. We used different flow rates in perfusion experiments with two-dimensional and 3D perfusion. Generally, increasing flow rate resulted in higher cell density and expression of EC markers irrespective of the chip design and material used. However, additional basal perfusion in MOTiF chips had higher impact on EC density and marker expression than apical perfusion alone at identical flow rates. From this we conclude that improved basal perfusion of cell layers is beneficial to EC cell culture.

It is reasonable that rigidity of the substrate has effects on cell physiology. We observed increased expression of actin, vWF and PECAM-1 compared to solely apical perfusion already by low basal shear stress perfusion in MOTiF biochips. These low shear stress conditions are considered to not result in significant stretching of the membrane and thereby should not induce additional mechanostimulatory effects from the basal side. However, by increasing basal flow rate in MOTiF chips we observed a further improvement of cellular parameters compared to conditions with only apical perfusion. Under these conditions an additional mechanical stimulation of ECs through stretching of the membrane surface might have a relevant effect, thus further contributing to improved cell function. Although we cannot explain the underlying mechanism, we can conclude that enhanced perfusion in MOTiF biochips significantly contributes to the improved EC function observed under dynamic flow culture conditions.

Expression and cellular distribution of vWF in MOTiF biochips share similarities to the *in vivo* state that are not observed in two-dimensionally perfused flow chambers or under static culture conditions. In addition, the MOTiF biochips allow simultaneous perfusion through both microchannels with dynamically adjustable flow rates and flow modes such as oscillatory or continuous flow that can be individually adjusted to the respective microchannel and side of cell layer perfusion. Moreover, MOTiF chips are suitable for advanced studies on immune cell interaction with adherent cell layers under flow conditions. The MOTiF biochips device allows the dynamic adjustment of substance concentrations during perfusion and basal stimulation of MOTiF biochips embedded cell layers together with a simultaneous application of suspension cells overflowing and interacting with the adherent cell layer. The MOTiF biochips design thus combines the advantages of the widely used cell culture filter membrane inserts for culturing polarized cell types such as ECs thereby enabling studies of transport, secretion, absorption and permeability combined with the features of flow chamber systems offering flow-based permeability and adhesion/transmigration assays.

We have shown that the MOTiF biochips represent a valuable tool for dynamic cell culture with improved perfusion conditions that overcome some limitations of two-dimensionally perfused flow chambers. One of the most important limitations of 3D tissue culture even under dynamic conditions within two-dimensionally perfused flow chambers is the sufficient supply of cells with nutrients and oxygen as well as the removal of unwanted cell metabolites/catabolites. This is mainly due to increased diffusion ranges from the apical tissue side to the bottom of the cell culture device throughout the tissue as simultaneous apical and basal perfusion is not possible in these devices. The MOTiF biochip design allows individually adjustable flow conditions for both, upper and lower microdevice channels and an overall improved perfusion condition for cell layers when compared to static cell culture or two-dimensionally perfused flow chambers. Thus MOTiF biochips might also be a suitable device for long-term 3D cell culture approaches. Studies are currently underway to elucidate the potential of the MOTiF biochips design for long-term culture of e.g. multilayered 3D tissues.

Acknowledgments

We are grateful to the excellent technical work of Maria Franke and Margot Voigt. We thank the team of the Placenta Laboratory of the Jena University Hospital for supplying umbilical cords for HUVEC isolation.

The authors would further like to acknowledge support of this work by 2011 VF 0005 grant of the Thüringer Aufbaubank. This work was further supported by the FK 3 1329-470 grant from the Federal Agency on Risk Assessment and in part by the Federal Ministry of Education and Research (BMBF), Germany, FKZ: 01EO1002.

References

Berthier E, Young E W K and Beebe D 2012 Engineers are from PDMS-land, biologists are from polystyrenia *Lab Chip* **12** 1224–37

Carrithers M, Tandon S, Canosa S, Michaud M, Graesser D and Madri J A 2005 Enhanced susceptibility to endotoxic shock and impaired STAT3 signaling in CD31-deficient mice *Am. J. Pathol.* **166** 185–96

Chattopadhyay R, Dyukova E, Singh N K, Ohba M, Mobley J A and Rao G N 2014 Vascular endothelial tight junctions and barrier function are disrupted by 15(S)-hydroxyeicosatetraenoic acid partly via protein kinase C ε-mediated zona occludens-1 phosphorylation at threonine 770/772 *J. Biol. Chem.* **289** 3148–63

Cheng C *et al* 2007 Large variations in absolute wall shear stress levels within one species and between species *Atherosclerosis* **195** 225–35

Chiu J-J, Lee P-L, Chen C-N, Lee C-I, Chang S-F, Chen L-J, Lien S-C, Ko Y-C, Usami S and Chien S 2004 Shear stress increases ICAM-1 and decreases VCAM-1 and E-selectin expressions induced by tumor necrosis factor-[alpha] in endothelial cells *Arterioscler. Thromb. Vasc. Biol.* **24** 73–9

Davies P F 1995 Flow-mediated endothelial mechanotransduction *Physiol. Rev.* **75** 519–60

Davies P F, Reidy M A, Goode T B and Bowyer D E 1976 Scanning electron microscopy in the evaluation of endothelial integrity of the fatty lesion in atherosclerosis *Atherosclerosis* **25** 125–30

de Caterina R, Libby P, Peng H B, Thannickal V J, Rajavashisth T B, Gimbrone M A, Shin W S and Liao J K 1995 Nitric oxide decreases cytokine-induced endothelial activation. Nitric oxide selectively reduces endothelial expression of adhesion molecules and proinflammatory cytokines *J. Clin. Invest.* **96** 60–8

Eddington D T, Puccinelli J P and Beebe D J 2006 Thermal aging and reduced hydrophobic recovery of polydimethylsiloxane *Sensors Actuators* B **114** 170–2

El-Ali J, Sorger P K and Jensen K F 2006 Cells on chips *Nature* **442** 403–11

Federici A B and Mannucci P M 2007 Management of inherited von Willebrand disease in 2007 *Ann. Med.* **39** 346–58

Fernández-Martín L *et al* 2012 Crosstalk between reticular adherens junctions and platelet endothelial cell adhesion molecule-1 regulates endothelial barrier function *Arterioscler. Thromb. Vasc. Biol.* **32** e90–102

Flaherty J T, Pierce J E, Ferrans V J, Patel D J, Tucker W K and Fry D L 1972 Endothelial nuclear patterns in the canine arterial tree with particular reference to hemodynamic events *Circ. Res.* **30** 23–33

Galbusera M, Zoja C, Donadelli R, Paris S, Morigi M, Benigni A, Figliuzzi M, Remuzzi G and Remuzzi A 1997 Fluid shear stress modulates von Willebrand factor release from human vascular endothelium *Blood* **90** 1558–64

Geiger B, Bershadsky A, Pankov R and Yamada K M 2001 Transmembrane crosstalk between the extracellular matrix–cytoskeleton crosstalk *Nat. Rev. Mol. Cell Biol.* **2** 793–805

Geuzaine C and Remacle J-F 2009 Gmsh: a 3D finite element mesh generator with built-in pre- and post-processing facilities *Int. J. Numer. Methods Eng.* **79** 1309–31

Girard P R and Nerem R M 1995 Shear stress modulates endothelial cell morphology and F-actin organization through the regulation of focal adhesion-associated proteins *J. Cell. Physiol.* **163** 179–93

Goode T B, Davies P F, Reidy M A and Bowyer D E 1977 Aortic endothelial cell morphology observed in situ by scanning electron microscopy during atherogenesis in the rabbit *Atherosclerosis* **27** 235–51

Harhaj N S and Antonetti D A 2004 Regulation of tight junctions and loss of barrier function in pathophysiology *Int. J. Biochem. Cell Biol.* **36** 1206–37

Henderson A 2004 *The ParaView Guide: A Parallel Visualization Application* (Clifton Park, NY: Kitware) p 1

Huang R-H, Wang Y, Roth R, Yu X, Purvis A R, Heuser J E, Egelman E H and Sadler J E 2008 Assembly of Weibel–Palade body-like tubules from *N*-terminal domains of von Willebrand factor *Proc. Natl Acad. Sci. USA* **105** 482–7

Huh D, Kim H J, Fraser J P, Shea D E, Khan M, Bahinski A, Hamilton G A and Ingber D E 2013 Microfabrication of human organs-on-chips *Nat. Protocols* **8** 2135–57

Jaffe E A, Nachman R L, Becker C G and Minick C R 1973 Culture of human endothelial cells derived from umbilical veins. Identification by morphologic and immunologic criteria *J. Clin. Invest.* **52** 2745–56

Jang K-J, Cho H S, Kang D H, Bae W G, Kwon T-H and Suh K-Y 2011 Fluid-shear-stress-induced translocation of aquaporin-2 and reorganization of actin cytoskeleton in renal tubular epithelial cells *Integr. Biol.* **3** 134–41

Jang K-J, Mehr A P, Hamilton G A, McPartlin L A, Chung S, Suh K-Y and Ingber D E 2013 Human kidney proximal tubule-on-a-chip for drug transport and nephrotoxicity assessment *Integr. Biol.* **5** 1119–29

Kwei S, Stavrakis G, Takahas M, Taylor G, Folkman M J, Gimbrone M A J and García-Cardeña G 2004 Early adaptive responses of the vascular wall during venous arterialization in mice *Am. J. Pathol.* **164** 81–9

Levesque M J and Nerem R M 1985 The elongation and orientation of cultured endothelial cells in response to shear stress *J. Biomech. Eng.* **107** 341–7

Lopez-Ramirez M A, Fischer R, Torres-Badillo C C, Davies H A, Logan K, Pfizenmaier K, Male D K, Sharrack B and Romero I A 2012 Role of caspases in cytokine-induced barrier breakdown in human brain endothelial cells *J. Immunology* **189** 3130–9

Maas M, Stapleton M, Bergom C, Mattson D L, Newman D K and Newman P J 2005 Endothelial cell PECAM-1 confers protection against endotoxic shock *Am. J. Physiol. Heart Circ. Physiol.* **288** H159–64

Malek A M and Izumo S 1996 Mechanism of endothelial cell shape change and cytoskeletal remodeling in response to fluid shear stress *J. Cell. Sci.* **109** 713–26

Manneville J-B, Etienne-Manneville S, Skehel P, Carter T, Ogden D and Ferenczi M 2003 Interaction of the actin cytoskeleton with microtubules regulates secretory organelle movement near the plasma membrane in human endothelial cells *J. Cell. Sci.* **116** 3927–38

Michaux G, Abbitt K B, Collinson L M, Haberichter S L, Norman K E and Cutler D F 2006 The physiological function of von Willebrand's factor depends on its tubular storage in endothelial Weibel–Palade bodies *Dev. Cell* **10** 223–32

Morigi M, Zoja C, Figliuzzi M, Foppolo M, Micheletti G, Bontempelli M, Saronni M, Remuzzi G and Remuzzi A 1995 Fluid shear stress modulates surface expression of adhesion molecules by endothelial cells *Blood* **85** 1696–703

Nagel T, Resnick N, Atkinson W J, Dewey C F J and Gimbrone M A J 1994 Shear stress selectively upregulates intercellular adhesion molecule-1 expression in cultured human vascular endothelial cells *J. Clin. Invest.* **94** 885–91

Pappelbaum K I *et al* 2013 Ultralarge von Willebrand factor fibers mediate luminal *Staphylococcus aureus* adhesion to an intact endothelial cell layer under shear stress *Circulation* **128** 50–9

Partridge J *et al* 2007 Laminar shear stress acts as a switch to regulate divergent functions of NF-kappaB in endothelial cells *FASEB J.* **21** 3553–61

Privratsky J R, Newman D K and Newman P J 2010 PECAM-1: conflicts of interest in inflammation *Life Sci.* **87** 69–82

Ramadan Q *et al* 2013 NutriChip: nutrition analysis meets microfluidics *Lab Chip* **13** 196–203

Ramello C, Paullier P, Ould-Dris A, Monge M, Legallais C and Leclerc E 2011 Investigation into modification of mass transfer kinetics by acrolein in a renal biochip *Toxicology In Vitro* **25** 1123–31

Regehr K J, Domenech M, Koepsel J T, Carver K C, Ellison-Zelski S J, Murphy W L, Schuler L A, Alarid E T and Beebe D J 2009 Biological implications of polydimethylsiloxane-based microfluidic cell culture *Lab Chip* **9** 2132–9

Stewart R J, Kashour T S and Marsden P A 1996 Vascular endothelial platelet endothelial adhesion molecule-1 (PECAM-1) expression is decreased by TNF-alpha and IFN-gamma. Evidence for cytokine-induced destabilization of messenger ribonucleic acid transcripts in bovine endothelial cells *J. Immunology* **156** 1221–8

Stroka K M, Vaitkus J A and Aranda-Espinoza H 2012 Endothelial cells undergo morphological, biomechanical, and dynamic changes in response to tumor necrosis factor-α *Eur. Biophys. J.* **41** 939–47

Thuenauer R, Rodriguez-Boulan E and Römer W 2014 Microfluidic approaches for epithelial cell layer culture and characterisation *Analyst* **139** 3206–18

Toepke M W and Beebe D J 2006 PDMS absorption of small molecules and consequences in microfluidic applications *Lab Chip* **6** 1484–6

Traub O and Berk B C 1998 Laminar shear stress: mechanisms by which endothelial cells transduce an atheroprotective force *Arterioscler. Thromb. Vasc. Biol.* **18** 677–85

Tsao P S, Buitrago R, Chan J R and Cooke J P 1996 Fluid flow inhibits endothelial adhesiveness nitric oxide and transcriptional regulation of VCAM-1 *Circulation* **94** 1682–9

Tzima E, Irani-Tehrani M, Kiosses W B, Dejana E, Schultz D A, Engelhardt B, Cao G, DeLisser H and Schwartz M A 2005 A mechanosensory complex that mediates the endothelial cell response to fluid shear stress *Nature* **437** 426–31

Valentijn K M, van Driel L F, Mourik M J, Hendriks G-J, Arends T J, Koster A J and Valentijn J A 2010 Multigranular exocytosis of Weibel–Palade bodies in vascular endothelial cells *Blood* **116** 1807–16

van Midwoud P M, Janse A, Merema M T, Groothuis G M M and Verpoorte E 2012 Comparison of biocompatibility and adsorption properties of different plastics for advanced microfluidic cell and tissue culture models *Anal. Chem.* **84** 3938–44

Wang L, Zhang Z-L, Wdzieczak-Bakala J, Pang D-W, Liu J and Chen Y 2011 Patterning cells and shear flow conditions: convenient observation of endothelial cell remoulding, enhanced production of angiogenesis factors and drug response *Lab Chip* **11** 4235

Whitesides G M 2006 The origins and the future of microfluidics *Nature* **442** 368–73

Xiong Y *et al* 2013 Hypertensive stretch regulates endothelial exocytosis of Weibel–Palade bodies through VEGF receptor 2 signaling pathways *Cell Res.* **23** 820–34

Young E W K and Simmons C A 2010 Macro- and microscale fluid flow systems for endothelial cell biology *Lab Chip* **10** 143–60

Zhao S, Suciu A, Ziegler T, Moore J E, Bürki E, Meister J J and Brunner H R 1995 Synergistic effects of fluid shear stress and cyclic circumferential stretch on vascular endothelial cell morphology and cytoskeleton *Arterioscler. Thromb. Vasc. Biol.* **15** 1781–6

Manuscript II

Comparison of the uptake of methacrylate-based nanoparticles in static and dynamic *in vitro* systems as well as *in vivo*

Rinkenauer, A.C., Press, A. T., Raasch, M., Pietsch, C., Schweizer, S., Schwörer, S., Rudolph, K. L., Mosig, A., Bauer, M., Träger, A. and Schubert, U. S. (2015)

Journal of Controlled Release 216: 158-168

In this manuscript, the established microfluidic platform of our lab is tested in a first application. For this purpose, we performed a study comparing the uptake of methacrylate-based NPs in dependence of their systematically altered physicochemical properties. A well-defined poly((methyl methacrylate)-*co*-(methacrylic acid)) (PMAA) and poly((methyl methacrylate)-*co*-(2-dimethylamino ethylmethacrylate)) (PDMAEMA) based NP library was chosen. The following basic principles to assess the suitability of the system are taken into account: (i) influence of NP composition regarding polymers and corresponding surface charges on uptake behaviour, (ii) influence of perfusion culture with different types of shear stress representing different sites of the human body, (iii) influence of macrophage co-culture on NP distribution and (iv) finally comparison of *in-vitro* obtained data to *in-vivo* systemic administration with focus on the liver as main xenobiotic metabolising tissue. We were able to show that increasing NP surface charge promotes cellular uptake by ECs in *in-vitro* static as well as perfusion culture. Furthermore, distinct applied shear stress alters *in-vitro* uptake behaviour significantly. Coculture with tissue-resident macrophages revealed a significant impairment of HUVEC NP uptake compared to mono-cell culture. Finally, *in-vivo* obtained data on polymer-dependent and endothelial as well as macrophage cell type specific NP uptake verify *in-vitro* perfused cell culture models as promising screening tools for NP uptake and distribution.

author contribution (25 %): HUVEC isolation from umbilical cords, HUVEC and macrophage cell culture, performance of whole blood monocyte isolation, macrophage differentiation and fluorescence labelling, biochip preparation of HUVEC mono-cell and HUVEC-macrophage co-culture, performing biochip NP uptake studies, immunofluorescence microscopy, quantification of NP uptake, analysis of data, preparation of figures, co-writing the manuscript.

Journal of Controlled Release 216 (2015) 158–168

Contents lists available at ScienceDirect

Journal of Controlled Release

journal homepage: www.elsevier.com/locate/jconrel

Comparison of the uptake of methacrylate-based nanoparticles in static and dynamic *in vitro* systems as well as *in vivo*

Alexandra C. Rinkenauer [a,b,1], Adrian T. Press [b,c,1], Martin Raasch [c,d], Christian Pietsch [a], Simon Schweizer [a], Simon Schwörer [b,e], Karl L. Rudolph [b,e], Alexander Mosig [b,c,d], Michael Bauer [b,c], Anja Traeger [a,b,*], Ulrich S. Schubert [a,b,*]

[a] Laboratory of Organic and Macromolecular Chemistry (IOMC), Friedrich Schiller University Jena, Humboldtstrasse 10, 07743 Jena, Germany
[b] Jena Center for Soft Matter (JCSM), Friedrich Schiller University Jena, Philosophenweg 7, 07743 Jena, Germany
[c] Center for Sepsis Control and Care (CSCC), Jena University Hospital, Erlanger Allee 101, 07747 Jena, Germany
[d] Institute of Biochemistry II, Jena University Hospital, Friedrich Schiller University Jena, Nonnenplan 2, 07743 Jena, Germany
[e] Leibniz Institute for Age Research, Fritz Lipmann Institute Jena, Beutenbergstrasse 11, 07745 Jena, Germany

ARTICLE INFO

Article history:
Received 27 April 2015
Received in revised form 23 July 2015
Accepted 4 August 2015
Available online 12 August 2015

Keywords:
Methacrylate
Nanoparticle
In vivo
Shear stress
Microfluidics
Uptake
Pharmacokinetic

ABSTRACT

Polymer-based nanoparticles are promising drug delivery systems allowing the development of new drug and treatment strategies with reduced side effects. However, it remains a challenge to screen for new and effective nanoparticle-based systems *in vitro*. Important factors influencing the behavior of nanoparticles *in vivo* cannot be simulated in screening assays *in vitro*, which still represent the main tools in academic research and pharmaceutical industry. These systems have serious drawbacks in the development of nanoparticle-based drug delivery systems, since they do not consider the highly complex processes influencing nanoparticle clearance, distribution, and uptake *in vivo*. In particular, the transfer of *in vitro* nanoparticle performance to *in vivo* models often fails, demonstrating the urgent need for novel *in vitro* tools that can imitate aspects of the *in vivo* situation more accurate. Dynamic cell culture, where cells are cultured and incubated in the presence of shear stress has the potential to bridge this gap by mimicking key-features of organs and vessels. Our approach implements and compares a chip-based dynamic cell culture model to the common static cell culture and mouse model to assess its capability to predict the *in vivo* success more accurately, by using a well-defined poly((methyl methacrylate)-*co*-(methacrylic acid)) and poly((methyl methacrylate)-*co*-(2-dimethylamino ethylmethacrylate)) based nanoparticle library. After characterization in static and dynamic *in vitro* cell culture we were able to show that physiological conditions such as cell–cell communication of co-cultured endothelial cells and macrophages as well as mechanotransductive signaling through shear stress significantly alter cellular nanoparticle uptake. In addition, it could be demonstrated by using dynamic cell cultures that the *in vivo* situation is simulated more accurately and thereby can be applied as a novel system to investigate the performance of nanoparticle systems *in vivo* more reliable.

1. Introduction

Drug delivery *via* polymer-based nanoparticles has the potential to be used for novel treatment strategies offering improved pharmacological properties, higher efficiencies as well as reduced side effects, compared to direct drug application [1]. In order to develop optimized nanoparticle-based drug delivery systems, the investigation of key-factors influencing their pharmacokinetic and pharmacodynamic properties is necessary. Numerous factors affect the uptake of nanoparticles *in vitro*, including the protein corona, surface charge, size and shape [2–5]. For instance, it is well-known that nanoparticles with 50 to 200 nm in diameter are internalized by a wide variety of cells [6]. However, direct translation of their uptake efficiency *in vitro* to their behavior *in vivo* is challenging. In particular, the prediction concerning biodistribution and interaction with the reticuloendothelial system (RES) remains a challenge [7,8]. Thus, resource and time consuming *in vivo* experiments are applied to evaluate new nanoparticle systems and to answer the question, whether they improve the biodistribution and the availability of a compound to the target cell and whether a reduced uptake by off-target tissues and cells is realized to limit detrimental effects. As a consequence, different targeting moieties such as antibodies, aptamers, metabolites, and anti-genes were used to coat the nanoparticle surface, creating new cell-type specific nanotherapeutics, -diagnostics, and -theranostic systems. [9–13] The

* Corresponding authors at: Laboratory of Organic and Macromolecular Chemistry (IOMC), Friedrich Schiller University Jena, Humboldtstrasse 10, 07743 Jena, Germany.
E-mail addresses: anja.traeger@uni-jena.de (A. Traeger), ulrich.schubert@uni-jena.de (U.S. Schubert).
[1] Authors contribute equally to this work.

http://dx.doi.org/10.1016/j.jconrel.2015.08.008
0168-3659/

biodistribution of nanoparticles is influenced by the RES as nanoparticles once in the circulation interact with various plasma proteins such as opsonins (immune globulins and complement factor) as well as albumins influencing their fate in different manners [14,15]. The formed protein corona is strongly under investigation, but so far only a few interacting proteins were identified resulting in a predictable impact on the fate of nanoparticles [16,17]. Due to the complexity of the plasma protein composition with more than 3.700 proteins and several other factors, the corona is still rarely understood and its dynamic makes it difficult to analyze [14]. An important role in the RES for drug- and nanoparticle clearance plays the liver [18]. In particular Kupffer cells, the local tissue-macrophages but although their endothelial cells, possess phagocytic or endocytic activity against blood-borne materials entering the liver and contribute to tissue modulation and regulation of the immune system in response to stimulants [19–21]. Their close cellular interaction and communication was described as relevant for different diseases [22]. For a rational drug development, possible immunemodulatory effects as well as nanoparticle clearance are key factors that need to be investigated under physiological conditions [23].

Promising new developments to more accurately model the *in vivo* environments are dynamic (co)-cultures where cells are cultured and incubated under shear stress and different cell-types might interact with each other. Endothelial cells line the inner layer of the blood vessels and are in direct contact with the bloodstream. For this purpose, their cell biology as morphology, cytoskeleton, permeability, and the expression of important markers and surface proteins as well as cellular interactions are affected by shear stress [24,25]. This mechanical force evolved to an important factor investigating physiological processes in the context of endothelial substance interaction and internalization. Endothelial cells represent the first tissue barrier nanoparticles have to overcome to reach parenchymal target cells as it is often aimed. Not only endothelial cells but also local macrophages, in particular in the liver but also in other vessels, have direct contact to nanoparticles and might clear them, why we co-cultured primary macrophages with human umbilical vein endothelial cells (HUVECs) to better understand their influence on uptake. In particular new screening methods to test toxicity, permeability and transport of drugs are under investigation [23,26]. In a recent study, where liver-specific PLGA-based nanoparticles were used, the relevance of shear stress on nanoparticle-uptake in an artificial liver was presented [13]. To gain more insight into the impact of shear stress and co-culture of HUVECs and primary macrophages, well-known methacrylate-based nanoparticles can be applied. Methacrylates are non-biodegradable and, thus, particularly suited to analyze the internalization behavior depending on structural properties of nanoparticles, *e.g.*, surface charge or size. In addition, poly(methyl methacrylates) (PMMA) are proposed for vaccination [6,27].

Herein, we used a library consisting of co-polymers for nanoparticle preparation, poly((methyl methacrylate)-*co*-(methacrylic acid)) (P(MMA-*co*-MAA)) and poly((methyl methacrylate)-*co*-(2-dimethylamino ethyl-methacrylate)) (P(MMA-*co*-DMAEMA)) representing polymers with pH dependent anionic and cationic charges, respectively. Moreover, in the case of P(MMA-*co*-MAA) the amount of methacrylic acid was varied. Nanoparticles were formed *via* nanoprecipitation to circumvent the use of surfactants and to obtain narrow size distribution [28–30]. Previous results gathered from *in vitro* studies are only of limited use to screen nanoparticles for drug applications, since the results hardly represent the *in vivo* situation [31,32], revealing the lack of appropriate methods allowing investigation of nanoparticle uptake and clearance under physiological relevant conditions. In the case of the applied methacrylate-based nanoparticle library with comparable size we were able to demonstrate a different internalization. On one hand attributed to different charge density (3% PMAA *vs.* 13% PMAA) and on the other hand due to different charges (PMAA *vs.* PDMAEMA) were investigated under static *in vitro* and dynamic cell culture. The impact of particle charge and the influence of shear stress on nanoparticle internalization *in vitro* were systematically characterized. Finally, the results were compared to an *in vivo* mouse model verifying the dynamic co-cell culture as promising tool for screening nanoparticle uptake and clearance.

2. Results and discussion

2.1. Polymer and nanoparticle preparation and characterization

The co-polymers were synthesized *via* the reversible addition–fragmentation chain transfer (RAFT) polymerization technique [33,34] to obtain polymers with narrow molar mass distribution and tailored polymer properties, *i.e.*, a defined amount of carboxylic acid or amines and, therefore, a defined number of charges within the polymer. Here, pH dependent co-polymers were synthesized consisting on the one hand of negatively charged MAA units at basic conditions and on the other hand of cationic charges (DMAEMA units) at acidic conditions. The amount of charges of the polymer represents a crucial parameter for the nanoparticle formation and stability. Nanoparticles with zeta potentials above $\pm$20 mV are more stabilized by the repulsion forces compared to particles with zeta potentials below [35]. A fine-tuning of the pH dependency, which goes hand in hand with negative charges (–COOH groups), as well as the hydrophobicity (MMA units) was realized by synthesizing co-polymer libraries with a systematic variation in the compositions. Thus, MAA amounts of 3, 5, 8 and 13%, as well as 20% of DMAEMA were used as a co-monomer in the polymerization procedure. Both monomers MMA and MAA (or DMAEMA) were statistically distributed along the polymer chain due to the same reactivity ratio [36]. The low amounts of MAA or DMAEMA ensure the formation and stability of hydrophobic particles under physiological pH values. In the case of 20% PDMAEMA nanoparticles a swelling is assumed due to the protonation of the amine group at a decreased pH value (PDMAEMA $pK_a = 7.5$) [37,38] in endosomes/lysosomes [39].

Molar masses between $M_n = 11.700$ g mol^{-1} to 12.700 g mol^{-1} with dispersities lower than 1.2 were determined by size exclusion chromatography (SEC) for the final co-polymers (Table 1 and Fig. S1). The compositions (content of MMA and MAA or MMA and DMAEMA) were calculated using ^{1}H NMR spectroscopy. The observed values agree well with prospected theoretical amounts and are listed in Table 1. The benefit of these polymers for preparation of defined nanoparticles *via* nanoprecipitation was already demonstrated earlier [28,40,41]. An advantage of nanoprecipitation is the absence of surfactants, as they can influence the properties of nanoparticles and their biological impact [42,43]. Furthermore, nanoparticles with different diameters with narrow size distributions can easily be obtained. In this study nanoparticles of around 200 nm in diameter were chosen as at this size cellular internalization *via* endocytosis could be assumed [28]. The characterization of the nanoparticles was performed using dynamic light scattering (DLS) as well as scanning electron microscopy (SEM) measurements (Table 1, Figs. 1 and S2). The zeta potential measurements confirm the negative surface charges of nanoparticles consisting of PMMA-*co*-PMAA and positive charges for PMMA-*co*-PDMAEMA nanoparticles (Table S2).

2.2. Internalization of methacrylate-based nanoparticles in static cell cultures

Initially, the nanoparticles were investigated regarding their internalization in HEK293 cells. For this purpose, flow cytometry and confocal microscopy was used. Methacrylate-based particles are known to lead to an increased granularity or rather increased side scatter (SSC) in flow cytometry after internalization [28,44]. To exclude the influence of cell size (forward scatter, FSC) the relative SSC/FSC was used as indication for successful nanoparticle internalization as it was also confirmed by nile red fluorescent intensity, encapsulated into different nanoparticles as a cargo. A clear correlation of cellular internalization rates depending on the PMAA amount of nanoparticles was observed.

Table 1
Polymer and nanoparticle characterization.

Polymer	M_n[a]	$Đ$[a]	Theo. ratio[b] MAA/D [%]	Exp. ratio[c] MAA/D [%]	Nanoparticle	D_H [nm][d]	PDI_P
P(MMA-*co*-MAA)	11.700	1.17	3.0	3.3	3% PMAA	196	0.061
P(MMA-*co*-MAA)	12.200	1.20	5.0	5.1	5% PMAA	193	0.097
P(MMA-*co*-MAA)	12.700	1.19	7.5	8.2	8% PMAA	207	0.099
P(MMA-*co*-MAA)	12.600	1.19	10.0	13.3	13% PMAA	205	0.079
P(MMA-*co*-DMAEMA)	11.000	1.10	20.0	20.8	20% PDMAEMA	207	0.101

[a] Calculated from SEC ($CHCl_3$), PMMA calibration.
[b] Molar ratio in the polymer feed solutions, MAA = methacrylic acid and D = dimethylamino ethyl methacrylate.
[c] Calculated from ^{1}H NMR spectroscopy. The homopolymer PMMA was used as reference (adjustment of the broad backbone integral from 0.5 to 2.5 ppm to exclude impurities like water) and all spectra were corrected with this ratio between $-OCH_3$ to the backbone signal of PMMA (correction factor 0.964).
[d] D_H represents the Z-average intensity weighted diameter.

Increasing amounts of PMAA resulted in an increased uptake of nanoparticles (Fig. 2A). In particular, the differences in the uptake behavior of 3% PMAA (rel. SSC/FSC = 1.2) and 13% PMAA (rel. SSC/FSC = 1.7) is remarkable. The differences in polymer composition and related negative charge increase of the particle surface as well as a decreased hydrophobicity appear to be beneficial for the cellular uptake. The cationic charged nanoparticles (20% PDMAEMA) displayed the highest cellular uptake (rel. SSC/FSC = 2). Increased internalization rate might be explained by the cationic charges that are known to be beneficial for interaction with the cell membrane [5]. Nanoparticles carrying negative as well as positive charges show an adsorption of serum proteins that impact their uptake efficiency [14,18]. The question arises whether the different cellular uptake of the methacrylate-based nanoparticles can be ascribed to the interaction with the cell membrane or rather to different protein coronas. Therefore, we tested the nanoparticle uptake of 3% PMAA, 13% PMAA and 20% PDMAEMA in the presence of fetal calf serum (FCS) in the cell culture medium (Fig. 2B). We found no impact of FCS on internalization of 13% PMAA and 20% PDMAEMA nanoparticles. In contrast, we observed a more efficient cellular uptake of 3% PMAA in the absence of FCS. Thus, we speculate that differences in cellular uptake of 3% and 13% PMAA nanoparticle are triggered by varying protein coronas depending on the exposed surface charges of nanoparticles and their interaction with the cell membrane. That the cellular uptake rates of 13% PMAA and 20% PDMAEMA are independent of the presence of proteins was not expected before, as in general a decreased uptake due to an increased protein interaction is assumed for nanoparticles formed of hydrophobic polymers [45,46]. Thus, further investigations are required to characterize the formation of the protein corona depending on surface charge density and the impact of its composition on cellular internalization. SDS-PAGE of nanoparticle bound proteins reveals a lack of distinct protein binding as well as a total reduction of bound proteins to the higher charged nanoparticles irrespectively if positively or negatively charged (Fig. S 3A, B).

As the sensitivity of relative SSC/FSC is limited and, moreover, restricted to flow cytometry analysis the hydrophobic dye nile red was encapsulated into the nanoparticles. The encapsulation efficiency varies depending on the hydrophobicity of the polymers. We tackled this obstacle by applying a correction factor determined for each nanoparticle batch (Table S3) [47]. To confirm the uptake measured by the relative SSC/FSC, the fluorescence intensity was also used showing a good correlation (Fig. S4). In addition, confocal microscopy was performed to verify the internalization of nanoparticles measured by flow cytometry (Fig. 3). All investigated nanoparticles were detectable inside the cells. 20% PDMAEMA shows higher fluorescence intensity and a more diffuse distribution compared to PMAA nanoparticle. This supports the assumption of swelling of nanoparticles under acidic conditions within the endosome.

The dependency of cellular uptake on charge amount and type were further confirmed in various cell types, including primary murine muscle cells (Table 2). Beside cell-type specific variations concerning the amount of internalized nanoparticles, two general trends were observed: With increasing negative charge, the cellular uptake was increased; however, the cationic charged nanoparticles were internalized more efficiently. Thus, the performance of the nanoparticles is mainly influenced by the particle composition depending on the polymer chemistry with an impact on the protein corona [48–50]. Therefore, the observed trends are independent of the used cell-types or if co-culture is used (Figs. 4 and S6). The nanoparticle uptake of HUVECs is significantly decreased due to cellular interactions. Further a significant decreased uptake in both cell-types was observed in contrast to the mono-culture.

Cytotoxicity is another highly relevant parameter for *in vivo* application of nanoparticles. Therefore, the hemo-compatibility of the nanoparticle library was tested using erythrocytes. We observed no release of hemoglobin or aggregation of erythrocytes promoting the nanoparticles suitable for *in vivo* investigations (Fig. S5).

Taken together, static *in vitro* studies depict relevant properties of nanoparticles: (i) Uptake effectiveness depending on nanoparticle characteristics, (ii) they enable crucial assays to understand the interaction of nanoparticles with soluble molecules of, *e.g.*, serum proteins, and (iii) they allow a first assessment of nanoparticle toxicity. In addition, by analyzing the cellular uptake in different cell types the same trend concerning an enhanced uptake of charged nanoparticles was observed. Interaction of particles and proteins were shown by SDS-PAGE,

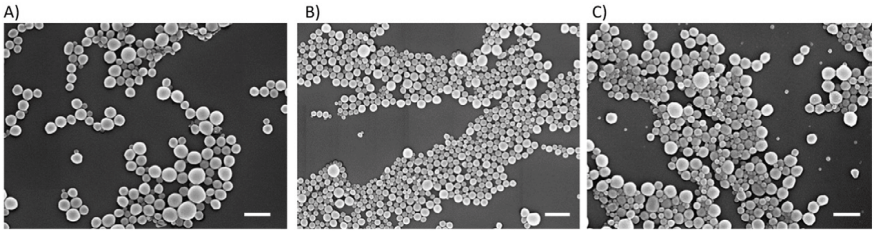

Fig. 1. SEM micrographs of methacrylate-based nanoparticles A (3% PMAA), B (13% PMAA) and C (20% PDMAEMA) confirm their spherical shape. Scale bar = 500 nm.

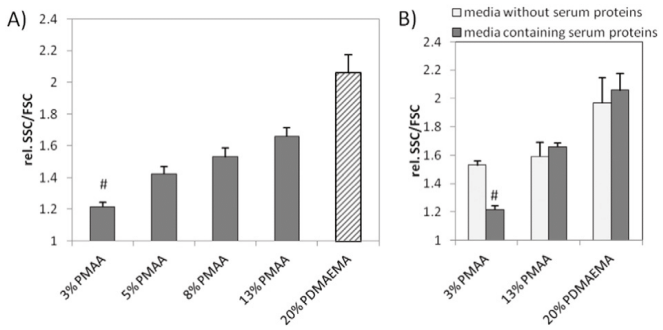

Fig. 2. Internalization of methacrylate-based nanoparticles in HEK293 cells treated for 24 h with 100 μg mL^{-1} nanoparticle in media containing FCS, rel. SSC/FSC regarding the control. A) Negative and cationic charged nanoparticle uptake, # represent significant differences compared to 20% PDMAEMA and B) comparison of nanoparticle uptake in media with and without serum. A, B) bars show mean + s.e.m of three independent experiments, significance tested using A) two-way ANOVA with Turkey's post-hoc test and using B) Kruskal-Wallis and Dunn's multiple comparison test, $p < 0.05$.

indicating serum interaction as one aspect of the internalization of nanoparticles, rising evidence for opsonization and RES interaction [16]. Common used *in vitro* blood compatibility tests like complement activation can be applied for first investigations, but these tests are also known to lead in false-positive results due to the optical properties of the nanoparticles [8]. In addition, static cell culture conditions provide sedimentation effects which are strongly altered under dynamic condition, *e.g.*, in the blood stream [51].

2.3. Internalization of methacrylate-based nanoparticles in dynamic cell cultures

Cell culture under dynamic conditions allows the investigation of nanoparticle binding and internalization under physiologically relevant *in vitro* conditions. In particular, the impact of different cell phenotypes of HUVECs [52] on the nanoparticle uptake under shear stress can be investigated in dynamic cell cultures [24,25]. Shear stress values from 0.7, 3.0, 6.0 and 10.0 dyn cm^{-2} were applied representing basal nutrient exchange with minimal mechanical stimulation observed *e.g.*, in hepatic sinusoids (0.7 dyn cm^{-2}) and shear stress values observed in human veins and venules (3.0 and 6.0 dyn cm^{-2}) [53], human suprarenal aorta (6.0 dyn cm^{-2}) and human common carotid artery (10.0 dyn cm^{-2}) [54]. Interestingly, increasing shear stress positively correlates with the total amount of internalized nanoparticles in mono-cultures (Fig. 5A, B). This indicates that nanoparticle-cell interactions are sufficient to induce adhesion and internalization even at high shear stress. In comparison, other studies investigating inorganic SiO_2-nanoparticles or polystyrene nanoparticles showed a reduced uptake under increasing shear stress conditions, even when antibodies where used as targeting moiety, suggesting that these nanoparticles would have sufficient target-cell interactions *in vivo* [25,55,56]. The findings of the methacrylate-based nanoparticle concerning shear stress can be attributed to a higher frequency of nanoparticle interaction per cell compared to static *in vitro* conditions. Dynamic cell culture revealed a different nanoparticle uptake as seen under static *in vitro* conditions: Uptake of 13% PMAA nanoparticles occurred more efficiently compared to 20% PDMAEMA, whereas the uptake of 3% PMAA was of significant lower efficiency (Fig. 4B). Shear stress higher than 6 dyn cm^{-2} does not increase the uptake of 20% PDMAEMA but reaches a plateau. Nanoparticles composed of 20% PDMAEMA differ from PMAA containing particles in respect to their ability of swelling under acidic conditions. A plateau for cellular uptake was reached at 3 dyn cm^{-2} for 20% PDMAEMA indicating a sufficient interaction of nanoparticles with the cell membrane, since the uptake was significantly decreased at even higher shear stress. Thus, tendencies between different nanoparticles, which were obtained under static conditions, differ under dynamic conditions. In particular, the uptake rate of the 20% PDMAEMA under flow conditions is reduced to comparable levels as 13% PMAA. This might be due to an activation of HUVEC under

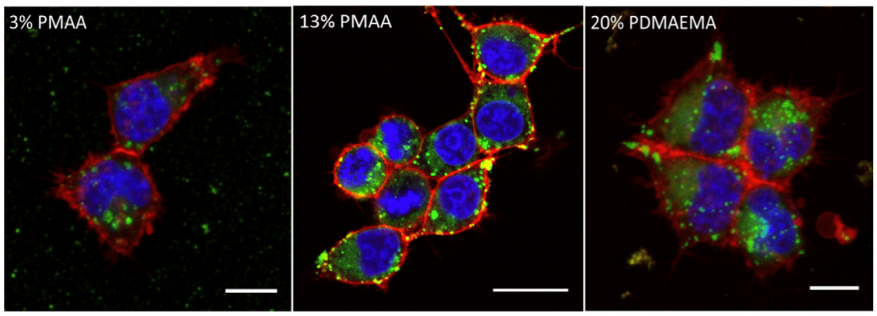

Fig. 3. Internalization of methacrylate-based nanoparticles. HEK293 cells were stained with Hoechst for DNA-staining (blue) and CellMask DeepRed (red) for plasma membrane staining previous to the addition of nanoparticles (green). Images were taken 25 to 30 min after addition of nanoparticles. Scale bar = 10 μm.

Table 2
Internalization of methacrylate-based nanoparticles in cell lines of different origin analyzed after 24 h *via* flow cytometry. The MFI was used as readout (n = 3) and was rated into very low uptake (− = MFI < 15), media uptake (+ = 15 < MFI < 50), high uptake (++ = 50 < MFI < 150) and very high uptake (+++ = MFI > 150).

	Cell line	3% PMAA	13% PMAA	20% PDMAEMA
Immortal	HEK 293	−	+	+
	L929	−	+	++
	HepG2	−	−	+
primary	Primary muscle cells	−	+	++
	Differentiated muscle cells	+	++	+++
	HUVEC	−	+	++
	MΦ	−	+	++

dynamic conditions leading to a different surface receptor expression pattern [25,33].

Furthermore cell–cell interactions, known to influence cellular physiology, have to be taken into consideration. For this purpose, a co-culture composed of MΦ and HUVEC, assembled in a reproducible composition and cultured under standardized conditions, was used for dynamic cell culture experiments (Fig. 5). In particular, the contribution of macrophages for nanoparticle uptake with consideration to heterogeneous cell interactions between macrophages and the endothelial lining was investigated. MΦs are known to be responsible for clearance of circulating nanoparticles in the blood stream by phagocytosis [8]. In the presence of MΦ, a shear stress dependent increased uptake of nanoparticles in HUVECs was observed. MΦ in general exhibited a higher uptake rate compared to HUVEC. Compared to the HUVEC mono-culture, the presence of MΦ strongly decreased the nanoparticle uptake through HUVECs (Fig. 5B). It is not likely that reduced nanoparticle uptake by HUVECs is simply due to an increased uptake rate through MΦ. It can be assumed that the proportion of nanoparticles in the medium in relation to the perfused cell cluster of HUVEC and MΦ will outbalance possible local concentration gradients formed by elevated uptake kinetics. This gains importance in particular under high perfusion conditions, where most of the prominent differences in uptake rates have been observed. The presence of primary human MΦ in co-culture was accompanied by a decreased endothelial uptake observed for all applied nanoparticles. In addition, a release mechanism for 13% PMAA can be assumed as 13% PMAA as well as 20% PDMAEMA lead to a homogeneous staining of the cytoplasm (Figs. 3, 5A). The investigations in static and dynamic cell culture conditions lead to the assumptions that the 13% PMAA as well as the 20% PDMAEMA would be also taken up by macrophages *in vivo*. In addition, the uptake of 13% PMAA and 20% PDMAEMA nanoparticles should be enhanced compared to the 3% PMAA nanoparticle. Concerning the uptake-tendencies between the different nanoparticles in the co-culture experiments, similar patterns were obtained under static and dynamic conditions at 3 and 6 dyn cm^{-2}, respectively (Figs. 4, 5). However, at 0.7 dyn cm^{-2}, which is assumed to be present in hepatic sinusoids, the uptake of 13% PMAA and 20% PDMAEMA did not significantly differ in contrast to the results under static conditions.

2.4. Internalization of methacrylate-based nanoparticles in vivo

The liver is composed of four major cell types: endothelial cells, local macrophages (Kupffer cells), stellate cells and hepatocytes. The liver sinusoidal endothelial cells (LSECs) represent a specialized subset of endothelial cells, whereas HUVEC reflect endothelial cells of the vasculature [57]. A major obstacle in *in vitro* studies and their translation to the *in vivo* situation is the missing consideration of biodistribution within an organism. It is considered as necessary to avoid the accumulation of nanoparticles in the RES, however often it is hardly discriminated, which cell type is affected. While hepatocyte mainly function as metabolic and detoxifying cells, Kupffer cells are known to clear all kinds xenobiotics effectively and trigger local and global responses to these molecules. Using intravital microscopy we could observe the cellular-distribution of 3%, 13% PMAA and 20% PDMAEMA nanoparticles in the liver. *In vivo* Kupffer cells mainly cleared all tested nanoparticles in the liver. However to a lesser extend also LSECs — liver-specific endothelial cells — took up especially 13% PMAA and 20% PDMAEMA nanoparticles (Fig. 6A). Beside the differences in the cellular distribution also the speed and kinetic of nanoparticle-uptake varies between nanoparticles. 20% PDMAEMA were taken up fastest (4.6% per min) followed by 13% PMAA nanoparticles (3.8% per min). The slowest uptake had low-charged (3% PMAA) nanoparticles (1.9% per min) (Fig. 6B). These different uptake kinetics and cellular distribution represent the different ability to unspecifically interact with cellular membranes and subsequently activate endocytotic or phagocytotic pathways. The uptake of all nanoparticles reached a plateau after 30 to 60 min reflecting a saturation of the processes or a clearance of the nanoparticles in the

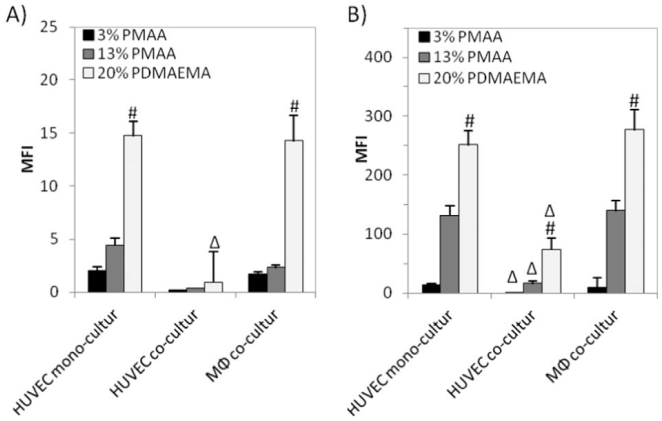

Fig. 4. Internalization of methacrylate-based nanoparticles in mono-culture and co-culture of HUVEC and MΦ treated for 1 h with 200 μg mL^{-1} nanoparticles. A) Analysis *via* flow cytometry and B) *via* microscopy # represent significant differences of 3 and 13% PMAA compared to 20% PDMAEMA within the different cultures, Δ represent significant differences of the cell types in co-culture compared to the corresponding mono-culture. The bars show mean + s.e.m of three independent experiments, significance using two-way ANOVA with Turkey's post-hoc test $p < 0.05$.

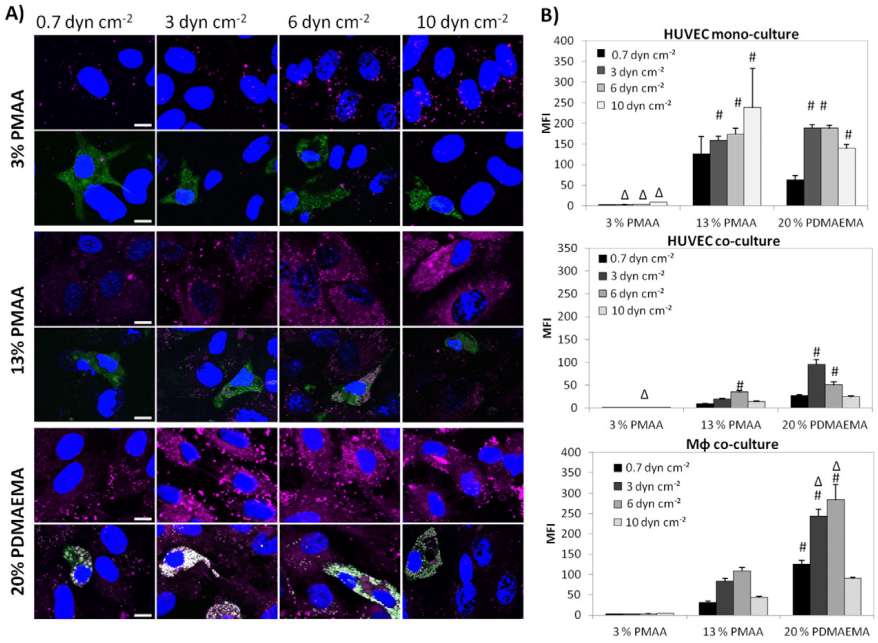

Fig. 5. Different nanoparticles in the dynamic cell culture. A, B) Uptake of different nanoparticles containing nile red in a HUVEC monoculture or a co-culture with MΦ which were subjected to different shear stress (0.7, 3, 6 or 10 dyn cm^{-2}) were analyzed after 60 min. A) Uptake and distribution of different nanoparticles (purple) in the HUVEC monoculture (upper panels) and co-culture (lower panels) with MΦ. Cells were subsequently stained with DAPI (blue) and macrophages were stained using CMFDA (green). All scale bars = 10 μm. B) Measured and analyzed MFI in HUVECs or MΦ. MFI were corrected using the calculated correction factor mentioned earlier. Differences between groups were analyzed using a two-way ANOVA with Tukey's post-hoc test performed on three independent experiments. #: $p < 0.05$ significant differences to 3% PMAA of corresponding dyn cm^{-2}. Δ: $p < 0.05$ for the differences between the 13% PMAA NP-uptake to the corresponding dyn cm^{-2}.

body (Fig. 6B). The MFI of 20% PDMAEMA even decreased constantly by 0.5% per min after 30 min within the time of observation, implying a release of nile red from 20% PDMAEMA. Finally we also compared the uptake of the nanoparticles in Kupffer cells *in vivo* revealing that higher charged ones (13% PMAA and 20% PDMAEMA) are cleared more effective than the low charged 3% PMAA and that Kupffer cells showed a higher uptake than endothelial cells. However, higher charged nanoparticles excerpt a smaller difference between the uptake in Kupffer cells and endothelial lining (Fig. 6C). The uptake in the static cell culture clearly showed a significant increased uptake of 20% PDMAEMA, which was also present in the co-culture experiments at 3 and 6 dyn cm^{-2}. However, at 0.7 dyn cm^{-2} the differences between 13% PMAA and 20% PDMAEMA are less pronounced in the co-culture (Fig. 5B).

3. Conclusion

Studies on nanoparticle uptake and transferability from *in vitro* to *in vivo* are necessary but challenging. Thus, methods for pre-screening of nanoparticle-cell interaction under physiological relevant conditions are required. In particular, the interaction of nanoparticles with immune cells responsible for unwanted clearance is important but unknown after *in vitro* investigations. It was previously shown that static *in vitro* studies underestimate effects and effectiveness of nanoparticle uptake and clearance *in vivo* [13]. In this study, we could demonstrate that the dynamic cell culture mimics shear-stress as one key-factor influencing nanoparticle uptake in general and might represent an important screening option for cell-type specific nanoparticle uptake. In particular in the case of the HUVEC mono-culture the tendencies of nanoparticle uptake were different between static and dynamic conditions. The dynamic cell culture influences the uptake tendencies of the tested nanoparticles, leading to decreased uptake of 20% PDMAEMA whereas under static conditions 20% PDMAEMA showed the highest uptake. Previously it was shown that applying shear-stress results in different surface receptor expression patterns which might lead to an increased uptake of the 13% PMAA whereas the uptake of 20% PDMAEMA seems to be not influenced by this HUVEC activation.

Diminished cell-interactions of low-charged non-targeted nanoparticles (3% PMAA) might lead to reduced and unspecific uptake. However, insufficient cellular membrane interactions might also compromise the nanoparticle uptake resulting in a shear-stress dependent decrease of uptake efficiency, demonstrated by previous studies of CdTe-quantum dots and SiO_2-based nanoparticles [25]. Another study tested vascular cell adhesion molecule (VCAM)-1-antibodies as targeting moiety conjugated to the surface of inorganic nanoparticles to address only activated endothelial cells [55]. Despite an increased uptake in cells expressing VCAM-1 under static culture conditions, subjecting these cells to flow lead to a decrease of uptake effectiveness. However, nanoparticle carrying VCAM-1-conjugated antibodies still showed a significant higher uptake. These studies reveal the importance of balancing the interaction of nanoparticles to ensure a specific uptake under certain circumstances but preventing unspecific nanoparticle interaction.

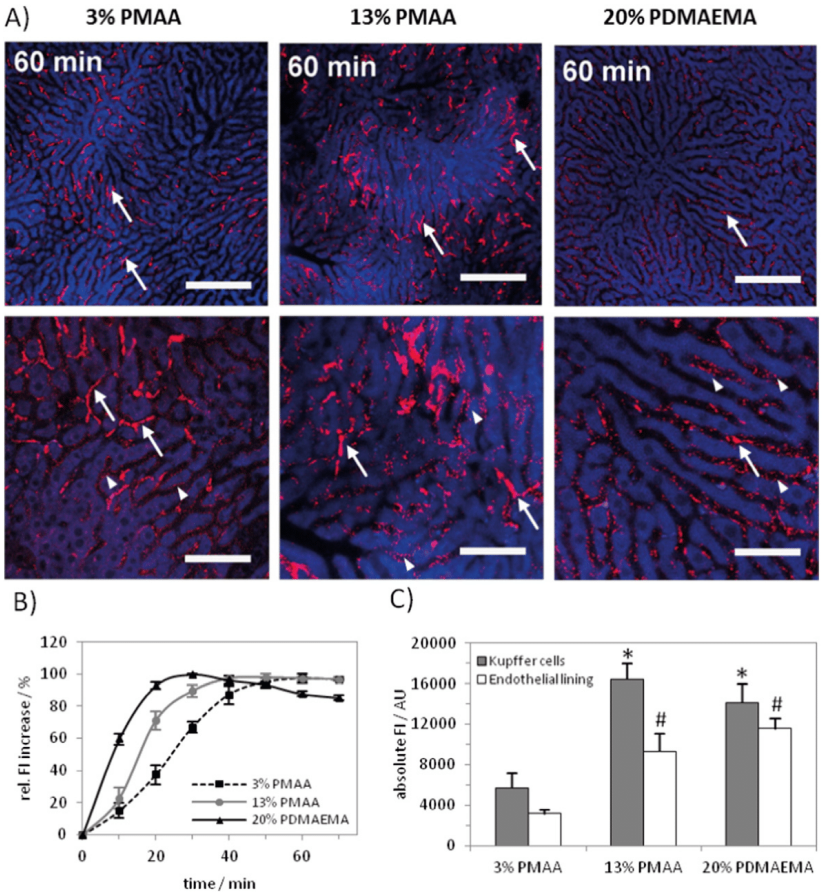

Fig. 6. A) Intravital microscopy of different nanoparticles in the liver (liver architecture: blue, nile red containing nanoparticles red) showing accumulation of nanoparticles mostly in Kupffer cells (examples marked with white arrows) and only little in endothelial cells (examples marked with a white triangle); scale bar for upper column is 250 μm, lower column is 50 μm. Contrast of all images were harmonized. B) Uptake kinetic of nile red containing nanoparticles in Kupffer cells *in vivo*; graph show mean ± s.e.m. of three independent experiments. C) Maximal fluorescence intensity of PMAA and PDMAEMA-nanoparticles containing nile red in murine Kupffer cells and endothelial lining in the liver 30 min (PDMAEMA) or 60 min (PMAAs) after administration. Significance was tested using a two-way ANOVA with Tukey's post-hoc test performed on three independent experiments; $p < 0.01$ between 13% PMAA or 20% PDMAEMA and 3% PMAA in * Kupffer cells or # endothelial lining. # $p < 0.01$ between both cell types of one nanoparticle.

Beside the influence of shear stress, monocultures lack cell–cell interactions and the resulting impact on the nanoparticle uptake. Based on the cell culture and supported by *in vivo* investigations, we showed that co-cultured macrophages have a severe impact on endothelial uptake of all nanoparticles tested. Further studies are required to characterize the underlying mechanism and to design nanoparticles in a way to prevent this inhibitory effect on endothelial cells. Besides, the question arises if also tumor-associated macrophages play a role in modulating the nanoparticle uptake in cancer cells leading to a reduced efficacy of nanoparticle-based tumor therapy or whether this is an effect restricted by the vascular endothelium [58].

This study shows that static cell cultures represent a fast and useful tool to assess nanoparticle uptake in general. Assessing nanoparticle uptake in primary endothelial cells is significantly influenced by physiological shear stress. We therefore suggest that investigation of nanoparticle uptake in endothelial cells should be performed under dynamic conditions where physiological relevant shear stress conditions could be resembled. In macrophage rich environments the effects of endothelial cell activation seems to be overwhelmed, likely due to macrophage derived factors effecting endothelial nanoparticle uptake. Considering the applied shear stress of 0.7 dyn cm^{-2} less pronounced differences between the uptake of 13% PMAA and 20% PDMAEMA under dynamic conditions were obtained in contrast to static conditions. This demonstrates the importance of shear stress on nanoparticle uptake. Since animal experiments are resource and time consuming, new models and automated systems for dynamic cell culture should be developed for screening purposes to increase the success of new animal studies.

4. Experimental section

4.1. Materials

MMA, MAA and DMAEMA were purchased from Sigma Aldrich and purified with an inhibitor-remover before use. 2,2′-azobis-(isobutyronitrile) (AIBN) was recrystallized from methanol prior to use. The chain transfer agent 2-cyano-2-propyl dithiobenzoate (CPDB) and the dye nile red was purchased from Sigma Aldrich.

4.2. Polymer synthesis and characterization

The co-polymers P(MMA-*stat*-MAA), were prepared by co-polymerization of MMA with MAA using the RAFT polymerization method [33,34]. In a typical RAFT co-polymerization experiment (3 mol% MAA as example, all polymerization conditions are listed in the SI), 5.827 g of MMA monomer (58.2 mmol), 0.155 g of MAA monomer (1.8 mmol), 24.63 mg of AIBN initiator (0.15 mmol), 132.8 mg of CPDB RAFT agent (0.6 mmol) and 5.16 mL ethanol were mixed together in a 25 mL reaction vial. The monomer concentration was kept at 4 mol L^{-1}. Subsequently, the reaction solution was placed in a preheated oil bath at 70 °C for 10 h. The copolymer was purified by precipitation into a large volume of cold diethyl-ether and dried under reduced pressure. ^{1}H NMR (CD_2Cl_2, 300 MHz): δ = 7.89 (d, Ar-H, CPDB), 7.57 (t, Ar-H, CPDB), 7.41 (t, Ar-H, CPDB), 3.60 (–OCH_3), 2.25–0.5 (backbone) ppm. SEC ($CHCl_3$, PMMA standard): M_n = 12.700 g mol^{-1}, $Đ$ = 1.17. All RAFT polymerizations and polymer analysis by SEC and ^{1}H NMR can be found in the supplementary information.

4.3. Instrumentation

Size-exclusion chromatography (SEC) experiments were performed on a Shimadzu system equipped with a SCL-10A system controller, a LC-10AD pump, a RID-10A refractive index detector, a UVD SPD-10AD UV/Vis detector and a PSS SDV linear S, 5 μm column (8 × 300 mm) with chloroform/triethylamine/2-propanol (94:4:2) as eluent at 1 mL min^{-1}, and the column oven was set to 40 °C. A calibration with low dispersity polystyrene standards (ranging Mn from 376 to 128,000 g mol^{-1}) was used.

^{1}H NMR spectra were recorded on a Bruker AC 300 (300 MHz) spectrometer at 298 K. The chemical shifts are reported in parts per million (ppm, δ scale) relative to the signals from the NMR solvents.

4.4. Preparation and characterization of nanoparticles

The nanoparticles used in this study were prepared by nanoprecipitation [28]. For this purpose, 25 to 30 mg of the distinguished polymer was dissolved in 1 mL acetone. For the preparation of nile red containing nanoparticles, 1 mg mL^{-1} nile red was diluted in acetone as stock-solution. Then, 250 to 300 μg of nile red was added from the stock- to the polymer-solution. The obtained solution was dropped into 10 mL of type 1-water. A 120 × 0.8 mm syringe was used to drop 100 to 200 μL of the polymer-solution per minute into the 10 mL type 1-water under permanent stirring (300 to 500 rpm) on a magnetic stirrer (Magnetic Stirrer MR Hei-Standard). Afterwards, the nanoparticle-suspension was stirred overnight for evaporation of acetone. The acetone-free nanoparticles with encapsulated nile red were shortly centrifuged for 10 to 20 s at 1620 ×*g* to remove all non-encapsulated nile red. Finally, the supernatant was diluted with type 1-water to the desired concentration.

The sizes of the nanoparticles were characterized by DLS on a Zetasizer Nano ZS (Malvern Instruments, Germany) with a He–Ne laser operating at a wavelength of λ = 633 nm. The detection of the counts occurs at an angle of 173°. All measurements were carried out at 25 °C after an equilibration time of 120 s. For analyzing the autocorrelation function the CONTIN algorithm was applied [59]. The apparent hydrodynamic diameter was calculated according to the Stokes–Einstein equation. The zeta potential of the nanoparticles was analyzed using the Zetasizer Nano ZS by applying laser doppler velocimetry. 20 runs were performed for each measurement using the slow-field reversal and fast-field reversal mode at 150 V. The experiment was performed in triplicate at 25 °C. The zeta potential (ζ) was calculated from the electrophoretic mobility (μ) according to the Henry Equation. Henry coefficient f(ka) was calculated according to Oshima [60].

Scanning electron microscopy (SEM) characterization was performed as follow: Nanoparticle suspensions were diluted with deionized water (~1.0 mg mL^{-1}). One droplet of the suspension was placed on a mica surface and dried in vacuum. Finally, the samples were coated with platinum (4 nm), using a BAL-TEC MED020 sputtering device (Bal-Tec AG, Lichtenstein). SEM measurements were performed on a Zeiss SIGMA VP Field Emission SEM equipped with the GEMINI column (Carl-Zeiss AG, Germany) operating at 3 to 7 kV using the InLens or SE2 detector.

The encapsulation efficiency and thus the fluorescence intensity vary dependent on the used polymers. For comparison of the fluorescence intensities a correction factor was applied [47]. Therefore, the nanoparticle stock solutions were diluted to 0.2 μg mL^{-1}, 100 μg mL^{-1} and 200 μg mL^{-1} and the fluorescence intensity was analyzed at the GENios Pro fluorescence microplate reader (Tecan, Germany). The nanoparticles were excited at λ_{Ex} = 488 nm (bandwidth 9 nm) and the emission was measured at λ_{Em} = 575 nm (bandwidth 20 nm). The correction factor represents the relative values of the slope of the fluorescence intensity against the nanoparticle concentration [47].

4.5. Hemolysis assay and erythrocyte aggregation

The membrane damaging properties of the polymers were quantified by analyzing the release of hemoglobin from erythrocytes. The hemolysis assay was performed as described before [41]. Briefly, blood from sheep was centrifuged at 4 500 ×*g* for 5 min and the pellet was washed three times with cold Dulbecco-PBS (DPBS). The stock solutions were diluted in DPBS and 100 μL of each nanoparticle solution at the indicated concentration were mixed and further incubated for 60 min at 37 °C. The release of hemoglobin in the supernatant was determined at 580 nm after centrifugation (2 400 ×*g* for 5 min). The absorbance was measured using a plate reader. For comparison, the collected erythrocytes were washed with DPBS and either lysed with 1% Triton X-100 (Sigma Aldrich, Germany) yielding the 100% lysis control value (A_{100}) or re-suspended in DPBS as reference (A0). The hemolytic activity of the nanoparticles was calculated as follow (1):

$$Hemolysis = \frac{100 * (A_{sample} - A_0)}{(A_{100} - A_0)}. \quad (1)$$

Here, A_{sample}, A_0, and A_{100} are the absorbance intensities of a given sample, erythrocytes incubated with DPBS, and erythrocytes lysed with Titon X-100.

For the erythrocyte aggregation 100 μL of the suspension were mixed with nanoparticle solution of the same volume and incubated for 2 h at 37 °C. bPEI 25 kDa was used as negative control at a concentration of 50 μg mL^{-1}. The erythrocytes aggregation was evaluated by microscopy. The analysis of hemolysis and erythrocyte aggregation was repeated with blood from at least three independent donors.

4.6. Culture of immortal cells

If not stated otherwise, cell culture materials, cell culture media, and solutions were obtained from Biochrom GmbH (Germany). The cells were cultured at 37 °C in a humidified 5% CO_2 atmosphere. HEK293 cells (CLR-1573, ATCC) were maintained in RPMI 1640, L929 cells (CCL-1, ATCC) in Dulbecco's MEM with stable L-glutamine and HepG2

(DSMZ, Germany) were cultured in DMEM/Ham's F-12. The media were supplemented with 10% fetal calf serum, 100 μg mL^{-1} of streptomycin, 100 IU mL^{-1} of penicillin and in the case of the HEK293 cells 2 mM L-glutamine were added.

4.7. Human umbilical vein endothelial (HUVEC) cell culture

HUVEC were isolated from human umbilical cord veins through collagenase digestion as previously described [61]. Experiments were performed with HUVECs up to passage 4 cultured in Endothelial Cell Growth Medium MV (PromoCell, Germany).

4.8. Peripheral blood mononuclear cell (PBMC) culture and macrophage differentiation

PBMCs were freshly isolated immediately after collecting donor blood from healthy volunteers. The donors were informed about the aim of the study and gave written informed consent. Blood sample volume was diluted two times with PBS without calcium and magnesium (Biochrom AG, Germany) containing 0.1% bovine serum albumin (BSA, Carl Roth, Germany) and 2 mM EDTA (Sigma-Aldrich, Germany; isolation buffer). PBMCs were obtained from density gradient centrifugation using Biocoll separating solution (Biochrom AG, Germany). The cells were washed subsequently in isolation buffer for several times and were finally strained by a 40 μm molecular mesh (BD Bioscience, Germany). For monocyte enrichment 10^7 PBMCs per well were plated on a six well plate in 2 mL X-VIVO 15 (Lonza, Germany) supplemented with 10% autologous serum, 10 ng mL^{-1} GM-CSF (PeproTech, Germany), 100 units mL^{-1} penicillin, and 100 μg mL^{-1} streptomycin (Life Technologies, Germany). The cells were washed with plain X-VIVO 15 medium after 3 h of incubation and fresh medium with supplements (stated above) was added. Including the preparation time for flow culture nanoparticle experiments, macrophage (Mϕ) differentiation was performed for five days.

4.9. Fluorescence activated cell sorting (FACS) of satellite cells and myotube differentiation

For the culture of primary myoblasts, satellite cells were purified by FACS as described elsewhere [62,63]. 8 to 12 weeks old C57BL/6 were sacrificed and the muscles from hind limbs were prepared and collected in PBS. Muscle tissue was washed in PBS, minced with scissors and digested in DMEM containing 650 U mL^{-1} collagenase-solution (Biochrom, Germany) for 90 min at 37 °C with agitation (70 rpm). Digested muscle tissue was washed with PBS supplemented with 10% fetal calf serum, triturated and incubated again in Collagenase (100 U mL^{-1}, Biochrom, Germany) and Dispase (2.4 U mL^{-1}, Life Technologies, Germany) for 30 min at 37 °C with agitation (100 rpm). The muscle slurry was further diluted with PBS supplemented with 10% fetal calf serum, filtered through 100 μm cell strainers and pelleted at 500 ×*g* for 5 min. Pellets were re-suspended in 10 mL FACS buffer (Hank's Balanced Salt Solution (HBSS), Life Technologies, Germany) containing 2% fetal calf serum (Biochrom, Germany) and filtered through 40 μm cell strainers and pelleted again at 500 ×*g* for 5 min. Pellets were re-suspended in 500 μL FACS buffer and stained with anti-mouse CD45 APC conjugate (30-F11, 1:200, eBioscience), anti-mouse CD11b APC conjugate (M1/70, 1:800, eBioscience, USA), anti-mouse Sca-1 APC conjugate (D7, 1:800, eBioscience, USA), anti-mouse/rat CD29 PE conjugate (ß1-Integrin, 1:400, Biolegend, USA) and biotinylated anti-mouse CD184 (CXCR4, 1:100, BD Bioscience, USA) for 20 min at 4 °C on a rotating wheel. Cells were washed with 5 mL FACS buffer and pelleted at 500 ×*g* for 5 min. Pellets were re-suspended in 500 μL FACS buffer and incubated with Streptavidin Cy7-PE conjugate (1:100, eBioscience, USA) for 20 min at 4 °C on a rotating wheel. Live cells were identified as calcein blue positive (1:1000, Life Technologies, Germany) and propidium iodide negative (1 μg mL^{-1}, BD Bioscience). Satellite cells were identified as $CD45^-$ $Sca\text{-}1^-CD11b^-CXCR4^+\beta1\text{-}integrin^+$ [63]. Cell sorting was performed on FACSAriaIII (BD Bioscience, USA) equipped with 405 nm, 488 nm and 633 nm lasers, respectively.

Satellite cells were sorted into growth medium comprised of F10 (Life Technologies, Germany) with 20% horse serum (PAA Laboratories), 500 U mL^{-1} penicillin/streptomycin (Life Technologies, Germany) and 5 ng mL^{-1} basic fibroblast growth factor (bFGF) (Sigma Aldrich, Germany) and maintained in 3% oxygen in collagen and laminin coated well-plates with fresh bFGF added daily. For the coating, well plates were incubated with collagen type I from rat tail (1 mg mL^{-1}, Sigma Aldrich, Germany) and laminin (10 mg mL^{-1}, Life Technologies, Germany) in type 1-water for at least 1 h at 37 °C and allowed to air-dry. To be considered as primary myoblasts, satellite cells were cultured for at least 1 week. For passaging, primary myoblasts were incubated with 0.5% trypsin (Life Technologies, Germany) in PBS for 3 min at 37 °C and collected in FACS buffer.

Primary myoblasts were passaged up to 70 to 80% confluence, and growth medium was replaced by differentiation medium comprised of DMEM with 2% horse serum and 500 U mL^{-1} penicillin/streptomycin (all Life Technologies, Germany). Myoblasts were allowed to differentiate into myotubes for five days.

4.10. Internalization of nanoparticles in static cell cultures

Cells were seeded with a density of 10^5 cells per well in 12-well plates. The growth medium was replaced by fresh medium 30 min before the addition of nanoparticles with indicated concentrations. After 24 h or 1 h incubation at 37 °C and with 5% CO_2, cells were analyzed *via* flow cytometry (FC 500, Beckman Coulter, Germany). Viable cells were identified by SSC/FSC and nanoparticle containing cells identified *via* their increased fluorescence (for nanoparticles with encapsulated nile red) or by increased side scatter (SSC). To avoid the detection of cells with attached nile red containing nanoparticles at the cell surface, 10% trypan blue (Sigma Aldrich, Germany) was added before the measurement to quench outer fluorescence. The relative SSC/FSC or mean fluorescence intensity (MFI) of at least 10^4 viable cells was used to quantify internalization of the nanoparticles. In case of the co-culture experiments (HUVECs and MΦ) the MΦ cells were stained with specific anti-human CD45 antibody (FITC-conjugated, ImmunoTools, Friesoythe, Germany). For this purpose, the cells were centrifuged at 200 *g* for 5 min at room temperature (RT), the pellet was washed with 200 μL DPBS and further centrifuged (300 *g*, 5 min, RT). Before adding 2 μL antibody, the pellet was suspended in 50 μL DPBS and afterwards incubated for 30 min on ice. Subsequently, the cells were centrifuged (300 *g*, 5 min, RT) and re-suspended in 500 μL DPBS for flow cytometry investigations. All experiments were performed independently for three times.

4.11. Confocal live-cell imaging

HEK293 cells were seeded in cell-view chamber slides (Greiner Bio-One, Germany) at a density of 10^5 cells per well and cultured as described above. After 24 h, cells were stained by adding 2 μg mL^{-1} bisBenzimide H 33258 (Sigma Aldrich, Germany) and 5 μg mL^{-1} CellMask DeepRed (Life Technologies, Germany). After 10 min under normal growth conditions cells were washed twice with pre-warmed HBSS (Life Technologies, Karlsruhe, Germany) twice and OptiMEM (Life Technologies, Germany) was added. Confocal live-cell imaging was performed on a laser scanning microscope (LSM-780, Zeiss AG, Germany) at 37 °C in a humidified 5% CO_2 atmosphere. H33258 was excited with a laser diode at 375 to 405 nm. Emitted light of 410 to 485 nm was collected on a photomultiplier tube. Different nanoparticles containing nile red at a concentration of 25 μg mL^{-1} were imaged through excitation at 488 nm (argon-ion laser) and fluorescence was detected using a gallium arsenide phosphide detector through a

500 nm long pass for 40 min. Fluorescence analysis of nanoparticle uptake were performed with ImageJ 1.46r (NIH, USA).

4.12. Internalization of nanoparticles in dynamic cell cultures

Rhombic chamber chips (RCC) were obtained from microfluidic ChipShop (Jena, Germany). Microfluidic cell culture experiments were performed under sterile environmental conditions of 5% CO_2, 70% air humidity and 37 °C. Monocytes were harvested 24 h after isolation by treatment with 4 mg mL^{-1} lidocaine (Sigma-Aldrich, Germany) and 5 mM EDTA. Confluent HUVECs were detached using trypsin. Monocytes were stained with 1 μM CellTracker green CMFDA (Life Technologies, Karlsruhe, Germany) for 45 min in serum-free X-VIVO 15. Subsequently monocytes and HUVECs were pooled 1:3 in Endothelial Growth Medium MV supplemented with 10% autologous serum, 10 ng mL^{-1} GM-CSF and 100 U mL^{-1} penicillin and 100 μg mL^{-1} streptomycin and seeded at a density of 1.3×10^5 HUVECs cm^{-2} and 0.43×10^5 monocytes cm^{-2} into RCC. Medium was changed on a daily basis. MΦ differentiation was performed in presence of GM-CSF for 72 h under static culture conditions. HUVEC were perfused using peristaltic pumps (Ismatec REGLO digital MS-CA-4/12-100, Germany). Shear stress within RCC was calculated as previously described [24]. Shear stress of 0.7, 3.0, 6.0 and 10.0 dyn cm^{-2} was applied for 24 h following 60 min nanoparticle uptake at a concentration of 200 μg mL^{-1}. Negative charged nanoparticles containing nile red were solved in Endothelial Cell Growth Medium MV without additives. Cells were mounted with VectaShield Hard Set H-1500 with DAPI (Biozol, Germany).

Immunofluorescence microscopy was performed with Axio Observer.Z1 controlled by AxioVision 4.8.2 SP 3 software (both from Zeiss, Germany). Fluorescence analysis and quantification of nanoparticle uptake were performed with ImageJ 1.46r (NIH, USA).

4.13. Protein binding to nanoparticles and SDS-PAGE

To assess serum protein binding to nanoparticles, 0.5 mg nanoparticles were added to 1 mL RPMI 1640 containing 10% fetal calf serum, mixed gently by inverting the tube several times and incubate for 10 min at 37 °C and humidified 5% CO_2 atmosphere. Afterwards, nanoparticles were washed twice using centrifugation (10 600 ×g, 10 min). Medium was removed and nanoparticles were re-suspended in 2 mL PBS without calcium and magnesium.

4.14. Animals

Animal studies were conducted in accordance with animal welfare legislation under pathogen-free conditions in the animal facility of the Jena University Hospital. During all procedures and imaging methods, animals remained under deep general anesthesia using Desflurane (Baxter, USA) and pain-reflexes were assessed to gauge the depth of anesthesia. The body temperature further was permanently kept on 37 °C using feed-back controlled heating plates.

4.15. Intravital microscopy

A tail-vein catheter was made attaching the tip of a 30 gauge-needle to polyurethane tubing (inner diameter of 0.30 mm and an outer diameter of 0.64 mm) (AgnTho's, Sweden). The catheter was then sterilized by formaldehyde fumigation before placed in the tail-vein of male FVB/NRj mice. Afterwards the left lateral abdomen was shaved and opened by a 1 cm vertical incision. The ligamentum falciforme was further dissected and the left lateral liver lobe was exposed on a cover slip. It then was fixed with a drop of *n*-butyl-2-cyanoacrylat (Histoacryl, B. Braun Melsungen AG, Germany) on the cover slide to avoid movements. For the analysis an inverted confocal laser scanning microscope (LSM-780, Zeiss AG, Jena, Germany) was used.

The liver architecture was visualized using the NAD(P)H/H^+ autofluorescence of hepatocytes by excitation with a laser diode at 375 to 405 nm, and collecting emitted light of 410 to 485 nm with a photomultiplier tube. Different nanoparticles containing nile red were imaged as described above. After localizing ≥3 areas of interest of each liver, different nanoparticles containing nile red were administered *via* the tail-veil catheter. Then, images were taken every 5 min to monitor kinetics. Analysis of >30 Kupffer cells or of the endothelial lining from 3 areas of interest per mouse and three mice resulted in the mean gray values shown in the table. The analysis was done at 30 min (PDMAEMA) or 60 min (PMAA) when kinetic analysis showed a plateau in the fluorescence intensity. Fluorescence analysis of nanoparticle uptake was performed with ImageJ 1.46r (NIH, MD, USA).

4.16. Statistical analysis

All results are reported as average of the performed experiments with standard error of mean (s.e.m.). All tests were performed using a significance level of 0.05. Detailed test information is stated in the figure legends. The analysis was performed using GraphPad Prism 6 software (Graphpad Software, USA).

Acknowledgment

We acknowledge funding from Carl Zeiss Foundation (Strukturantrag JCSM) (grant #0563-2.8/335/4) and the Thuringian Ministry for Education, Science and Culture (TMBWK; grants #B514-09051, NanoConSens and ProExzellence II, NanoPolar) as well as the German Federal Ministry of Education and Research (BMBF) (grants #13N13416, SmartDyeLivery) and the Center for Sepsis Control and Care for providing the LSM-780. We thank U. Vetterling for assistance with the animal experiments. This work was further supported by the European Union (ERC advanced grant to K. L. Rudolph, grant 323136 — StemCellGerontoGenes) and the State of Thuringia (FZ-12001-514).

Appendix A. Supplementary data

Supporting information available: Additional experimental section, polymerization of copolymer as well as further data regarding polymer and nanoparticle characterization, hemolysis and aggregation assay. Supplementary data associated with this article can be found, in the online version, at http://dx.doi.org/10.1016/j.jconrel.2015.08.008.

References

[1] A.Z. Wang, R. Langer, O.C. Farokhzad, Annu. Rev. Med. 63 (2012) 185–198.
[2] L. Treuel, X.E. Jiang, G.U. Nienhaus, J. R. Soc. Interface 10 (2013) 1–9.
[3] A. Lesniak, A. Salvati, M.J. Santos-Martinez, M.W. Radomski, K.A. Dawson, C. Aberg, J. Am. Chem. Soc. 135 (2013) 1438–1444.
[4] Z. Zhang, C. Wang, Y. Zha, W. Hu, Z. Gao, Y. Zang, J. Chen, J. Zhang, L. Dong, ACS Nano 9 (2015) 2405–2419.
[5] J. Voigt, J. Christensen, V.P. Shastri, PNAS 111 (2014) 2942–2947.
[6] V. Mailander, K. Landfester, Biomacromolecules 10 (2009) 2379–2400.
[7] C. Chen Weihsu, X. Zhang Andrew, S.-D. Li, Eur. J. Nanomed. 4 (2012) 89–93.
[8] M.A. Dobrovolskaia, P. Aggarwal, J.B. Hall, S.E. McNeil, Mol. Pharm. 5 (2008) 487–495.
[9] B.B. Wang, C.V. Galliford, P.S. Low, Nanomedicine 9 (2014) 313–330.
[10] J. Xie, S. Lee, X.Y. Chen, Adv. Drug Deliv. Rev. 62 (2010) 1064–1079.
[11] O.C. Farokhzad, J.J. Cheng, B.A. Teply, I. Sherifi, S. Jon, P.W. Kantoff, J.P. Richie, R. Langer, PNAS 103 (2006) 6315–6320.
[12] M.E. Davis, J.E. Zuckerman, C.H.J. Choi, D. Seligson, A. Tolcher, C.A. Alabi, Y. Yen, J.D. Heidel, A. Ribas, Nature 464 (2010) 1067–1140.
[13] A.T. Press, A. Traeger, C. Pietsch, A. Mosig, M. Wagner, M.G. Clemens, N. Jbeily, N. Koch, M. Gottschaldt, N. Beziere, V. Ermolayev, V. Ntziachristos, J. Popp, M.M. Kessels, B. Qualmann, U.S. Schubert, M. Bauer, Nat. Commun. 5 (2014) 5565.
[14] P. Aggarwal, J.B. Hall, C.B. McLeland, M.A. Dobrovolskaia, S.E. McNeil, Adv. Drug Deliv. Rev. 61 (2009) 428–437.
[15] M. Lundqvist, J. Stigler, G. Elia, I. Lynch, T. Cedervall, K.A. Dawson, PNAS 105 (2008) 14265–14270.
[16] S. Tenzer, D. Docter, J. Kuharev, A. Musyanovych, V. Fetz, R. Hecht, F. Schlenk, D. Fischer, K. Kiouptsi, C. Reinhardt, K. Landfester, H. Schild, M. Maskos, S.K. Knauer, R.H. Stauber, Nat. Nanotechnol. 8 (2013) 772–1000.

[17] S. Ritz, S. Schottler, N. Kotman, G. Baier, A. Musyanovych, J. Kuharev, K. Landfester, H. Schild, O. Jahn, S. Tenzer, V. Mailander, Biomacromolecules 16 (2015) 1311–1321.
[18] M.J. Ernsting, M. Murakami, A. Roy, S.D. Li, J. Control. Release 172 (2013) 782–794.
[19] F. Alexis, E. Pridgen, L.K. Molnar, O.C. Farokhzad, Mol. Pharm. 5 (2008) 505–515.
[20] R. Kumar, I. Roy, T.Y. Ohulchanskky, L.A. Vathy, E.J. Bergey, M. Sajjad, P.N. Prasad, ACS Nano 4 (2010) 699–708.
[21] A.C. Anselmo, S. Mitragotri, J. Control. Release 190 (2014) 531–541.
[22] N.A. Hutchins, C.S. Chung, J.N. Borgerding, C.A. Ayala, A. Ayala, Am. J. Pathol. 182 (2013) 742–754.
[23] K.S. Vellonen, M. Malinen, E. Mannermaa, A. Subrizi, E. Toropainen, Y.R. Lou, H. Kidron, M. Yliperttula, A. Urtti, J. Control. Release 190 (2014) 94–114.
[24] M. Raasch, K. Rennert, T. Jahn, S. Peters, T. Henkel, O. Huber, I. Schulz, H. Becker, S. Lorkowski, H. Funke, A. Mosig, Biofabrication 7 (2015) 015013.
[25] S.P. Samuel, N. Jain, F. O'Dowd, T. Paul, D. Kashanin, V.A. Gerard, Y.K. Gun'ko, A. Prina-Mello, Y. Volkov, Int. J. Nanomedicine 7 (2012) 2943–2956.
[26] S.H. Au, M.D. Chamberlain, S. Mahesh, M.V. Sefton, A.R. Wheeler, Lab Chip 14 (2014) 3290–3299.
[27] J. Kreuter, J. Control. Release 16 (1991) 169–176.
[28] A. Vollrath, A. Schallon, C. Pietsch, S. Schubert, T. Nomoto, Y. Matsumoto, K. Kataoka, U.S. Schubert, Soft Matter 9 (2013) 99–108.
[29] I. Perevyazko, A. Vollrath, S. Hornig, G.M. Pavlov, U.S. Schubert, J. Polym. Sci. Polym. Chem. 48 (2010) 3924–3931.
[30] S. Hornig, T. Heinze, C.R. Becer, U.S. Schubert, J. Mater. Chem. 19 (2009) 3838–3840.
[31] J.W. Nichols, Y.H. Bae, Nano Today 7 (2012) 606–618.
[32] J.M. Lee, T.J. Yoon, Y.S. Cho, Biomed. Res. Int. 782041 (2013) 1–10.
[33] J. Chiefari, Y.K. Chong, F. Ercole, J. Krstina, J. Jeffery, T.P.T. Le, R.T.A. Mayadunne, G.F. Meijs, C.L. Moad, G. Moad, E. Rizzardo, S.H. Thang, Macromolecules 31 (1998) 5559–5562.
[34] G. Moad, E. Rizzardo, S.H. Thang, Aust. J. Chem. 62 (2009) 1402–1472.
[35] A. Shalviri, H.K. Chan, G. Raval, M.J. Abdekhodaie, Q. Liu, H. Heerklotz, X.Y. Wu, Colloids Surf. B 101 (2013) 405–413.
[36] J. Brandrup, E.H. Immergut, E.A. Grulke, Polymer Handbook, 4 ed.Wiley-Interscience, 1999.
[37] S. Agarwal, Y. Zhang, S. Maji, A. Greiner, Mater. Today 15 (2012) 388–393.
[38] P. van de Wetering, E.E. Moret, N.M.E. Schuurmans-Nieuwenbroek, M.J. van Steenbergen, W.E. Hennink, Bioconjug. Chem. 10 (1999) 589–597.
[39] T. Yildirim, A.C. Rinkenauer, C. Weber, A. Traeger, S. Schubert, U.S. Schubert, J. Polym. Sci. Polym. Chem. (2015), http://dx.doi.org/10.1002/pola.27734.
[40] I.Y. Perevyazko, A. Vollrath, C. Pietsch, S. Schubert, G.M. Pavlov, U.S. Schubert, J. Polym. Sci. Polym. Chem. 50 (2012) 2906–2913.
[41] A. Vollrath, D. Pretzel, C. Pietsch, I. Perevyazko, S. Schubert, G.M. Pavlov, U.S. Schubert, Macromol. Rapid Commun. 33 (2012) 1791–1797.
[42] L. Araujo, R. Lobenberg, J. Kreuter, J. Drug Target. 6 (1999) 373–385.
[43] A. Schrade, V. Mailander, S. Ritz, K. Landfester, U. Ziener, Macromol. Biosci. 12 (2012) 1459–1471.
[44] A. Palecanda, L. Kobzik, Methods 21 (2000) 241–247.
[45] G. Baier, C. Costa, A. Zeller, D. Baumann, C. Sayer, P.H.H. Araujo, V. Mailander, A. Musyanovych, K. Landfester, Macromol. Biosci. 11 (2011) 628–638.
[46] K. Xiao, Y.P. Li, J.T. Luo, J.S. Lee, W.W. Xiao, A.M. Gonik, R.G. Agarwal, K.S. Lam, Biomaterials 32 (2011) 3435–3446.
[47] S. Lerch, M. Dass, A. Musyanovych, K. Landfester, V. Mailander, Eur. J. Pharm. Biopharm. 84 (2013) 265–274.
[48] M. Luck, B.R. Paulke, W. Schroder, T. Blunk, R.H. Muller, J. Biomed. Mater. Res. 39 (1998) 478–485.
[49] M.A. Dobrovolskaia, S.E. Mcneil, Nat. Nanotechnol. 2 (2007) 469–478.
[50] R.A. Petros, J.M. DeSimone, Nat. Rev. Drug Discov. 9 (2010) 615–627.
[51] E.C. Cho, Q. Zhang, Y.N. Xia, Nat. Nanotechnol. 6 (2011) 385–391.
[52] E. Berthier, E.W.K. Young, D. Beebe, Lab Chip 12 (2012) 1224–1237.
[53] A.M. Malek, S.L. Alper, S. Izumo, JAMA-J. Am. Med. Assoc. 282 (1999) 2035–2042.
[54] C. Cheng, F. Helderman, D. Tempel, D. Segers, B. Hierck, R. Poelmann, A. van Tol, D.J. Duncker, D. Robbers-Visser, N.T.C. Ursem, R. van Haperen, J.J. Wentzel, F. Gijsen, A.F.W. van der Steen, R. de Crom, R. Krams, Atherosclerosis 195 (2007) 225–235.
[55] H. Yang, F.L. Zhao, Y. Li, M.M. Xu, L. Li, C.H. Wu, H. Miyoshi, Y.Y. Liu, Int. J. Nanomedicine 8 (2013) 1897–1906.
[56] A. Lin, A. Sabnis, S. Kona, S. Nattama, H. Patel, J.F. Dong, K.T. Nguyen, J. Biomed. Mater. Res. A 93 (2010) 833–842.
[57] Y. Kim, P. Rajagopalan, PLoS ONE 5 (2010).
[58] D. Alizadeh, L.Y. Zhang, J. Hwang, T. Schluep, B. Badie, Nanomed. Nanotechnol. 6 (2010) 382–390.
[59] S.W. Provencher, Comput. Phys. Commun. 27 (1982) 229–242.
[60] H. Ohshima, J. Colloid Interface Sci. 168 (1994) 269–271.
[61] E.A. Jaffe, R.L. Nachman, C.G. Becker, C.R. Minick, J. Clin. Invest. 52 (1973) 2745–2756.
[62] R.I. Sherwood, J.L. Christensen, I.M. Conboy, M.J. Conboy, T.A. Rando, I.L. Weissman, A.J. Wagers, Cell 119 (2004) 543–554.
[63] M. Cerletti, S. Jurga, C.A. Witczak, M.F. Hirshman, J.L. Shadrach, L.J. Goodyear, A.J. Wagers, Cell 134 (2008) 37–47.

Supporting Information

Microfluidically-supported cell culture as bridge between *in vitro* and *in vivo* investigations of well-defined nanoparticle libraries.

Alexandra C. Rinkenauer,[1,2,#] Adrian T. Press,[2,3,#] Martin Raasch,[3,4] Christian Pietsch,[1] Simon Schweizer,[1] Simon Schwörer,[2,5] Karl L. Rudolph,[2,5] Alexander Mosig,[2,3,4] Michael Bauer,[2,3] Anja Träger,[1,2] Ulrich S. Schubert [1,2]**

[1]Laboratory of Organic and Macromolecular Chemistry (IOMC), Friedrich Schiller University Jena, Humboldtstrasse 10, 07743 Jena, Germany

[2]Jena Center for Soft Matter (JCSM), Friedrich Schiller University Jena, Philosophenweg 7, 07743 Jena, Germany

[3]Center for Sepsis Control and Care (CSCC), Jena University Hospital, Erlanger Allee 101, 07747 Jena

[4]Institute of Biochemistry II, Jena University Hospital, Friedrich Schiller University Jena, Nonnenplan 2, 07743 Jena, Germany

[5]Leibniz Institute for Age Research, Fritz Lipmann Institute Jena, Beutenbergstrasse 11, 07745 Jena, Germany

[#]authors contribute equally to this work

*Address correspondence to: ulrich.schubert@uni-jena.de; anja.traeger@uni-jena.de

1 Polymerizations

Table S 1: Overview of the selected RAFT polymerization conditions.

Polymer sample	Feed ratio [a] MMA/MAA	Feed ratio CPDB/AIBN	m in g MMA	MAA	CPDB	AIBN	time [h]
PMMA	100/0	1/0.25	6.007	0	0.1328	0.0246	13
P(MMA-*co*-MAA)	97/3	1/0.25	5.827	0.155	0.1328	0.0246	13
P(MMA-*co*-MAA)	95/5	1/0.25	5.707	0.258	0.1328	0.0246	13
P(MMA-*co*-MAA)	92.5/7.5	1/0.25	5.557	0.387	0.1328	0.0246	13
P(MMA-*co*-MAA)	90/10	1/0.25	5.406	0.516	0.1328	0.0246	13
P(MMA-*co*-DMAEMA)	80/20	1/0.25	4.806	1.033	0.1328	0.0246	12.5

[a] Molar ratio in the polymer feed solutions between MMA and MAA or DMAEMA.

1.1 Polymer characterization:

SEC chromatograms and ^{1}H NMR spectra of the final copolymers.

PMMA:

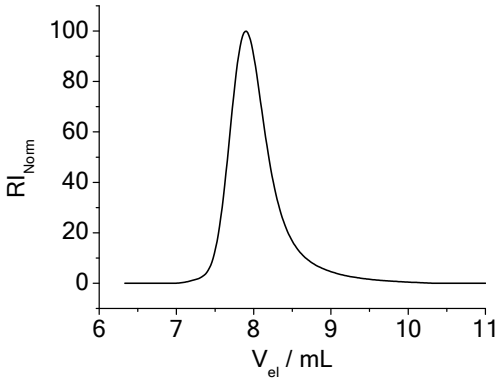
100
80
60
40
20
0
RI Norm
6
7
8
9
10
11
V el / mL

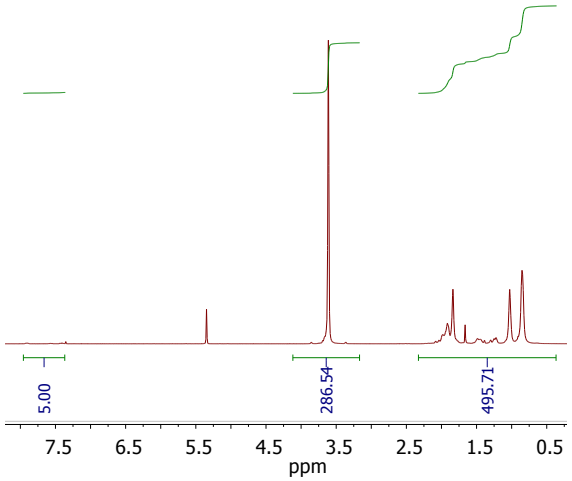
5.00
286.54
495.71
7.5
6.5
5.5
4.5
3.5
2.5
1.5
0.5
ppm

3% PMAA:

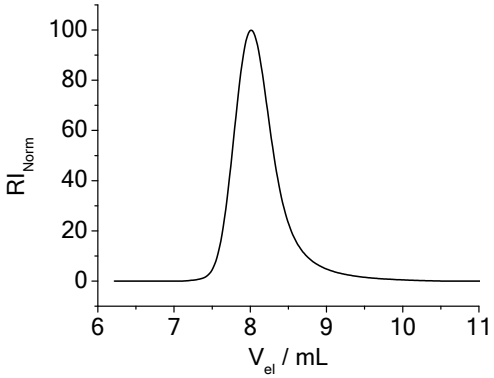
100
80
60
40
20
0
RI Norm
6
7
8
9
10
11
V el / mL

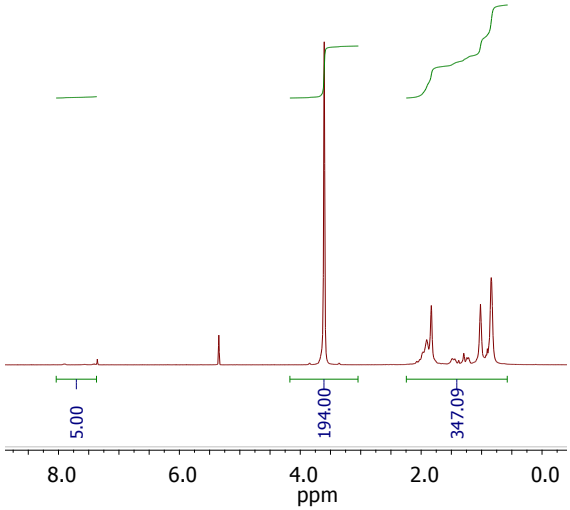
5.00
194.00
347.09
8.0
6.0
4.0
2.0
0.0
ppm

5% PMAA:

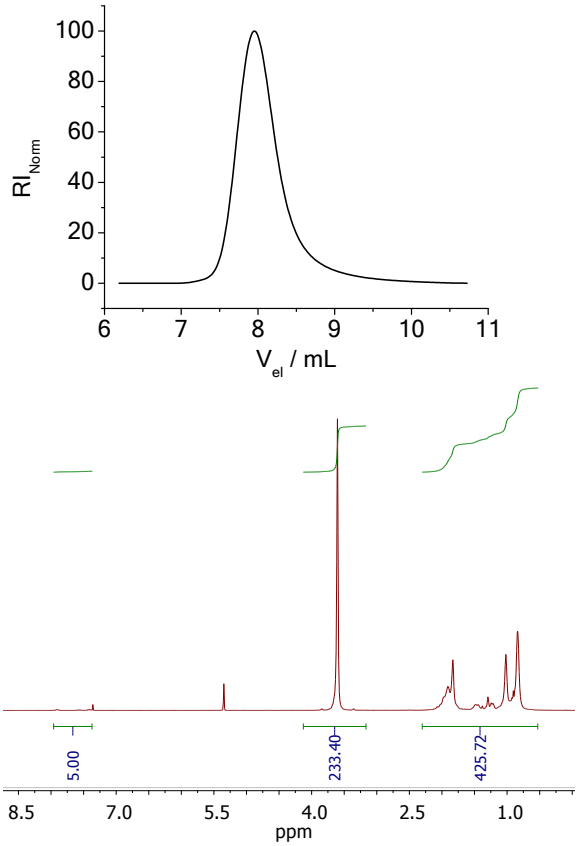
RI_Norm
100
80
60
40
20
0
6
7
8
9
10
11
V_el / mL
5.00
233.40
425.72
8.5
7.0
5.5
4.0
2.5
1.0
ppm

8% PMAA:

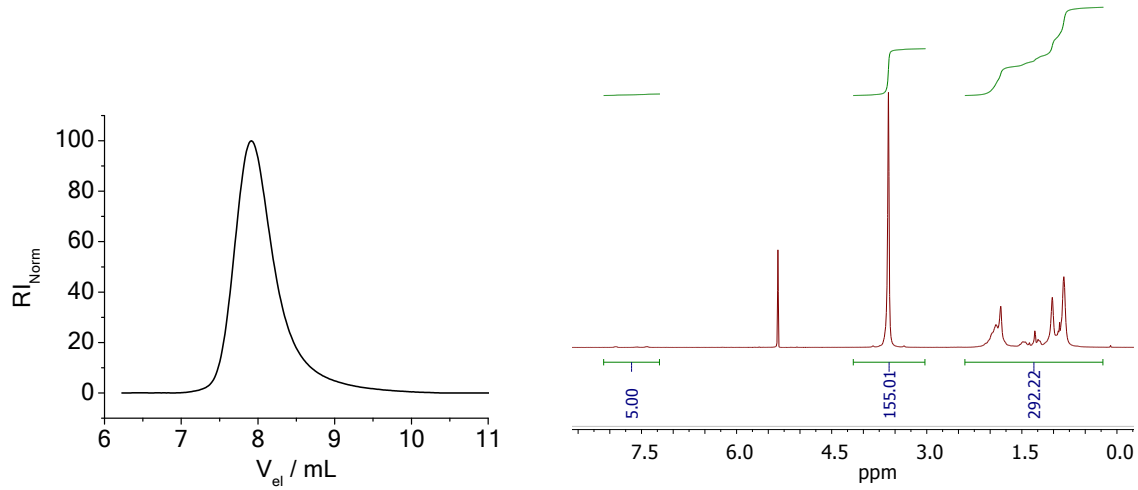
RI_Norm
100
80
60
40
20
0
6
7
8
9
10
11
V_el / mL
5.00
155.01
292.22
7.5
6.0
4.5
3.0
1.5
0.0
ppm

13% PMAA:

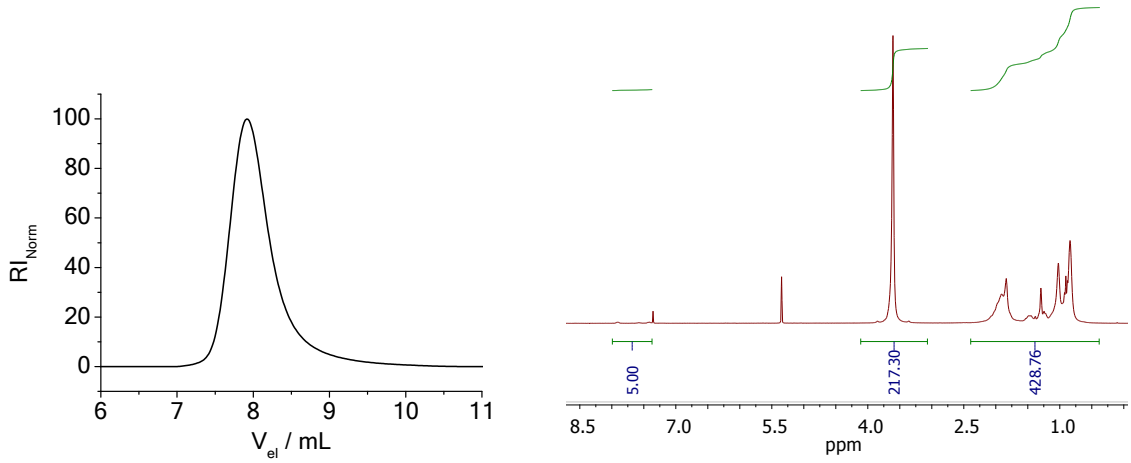

20% PDMAEMA:

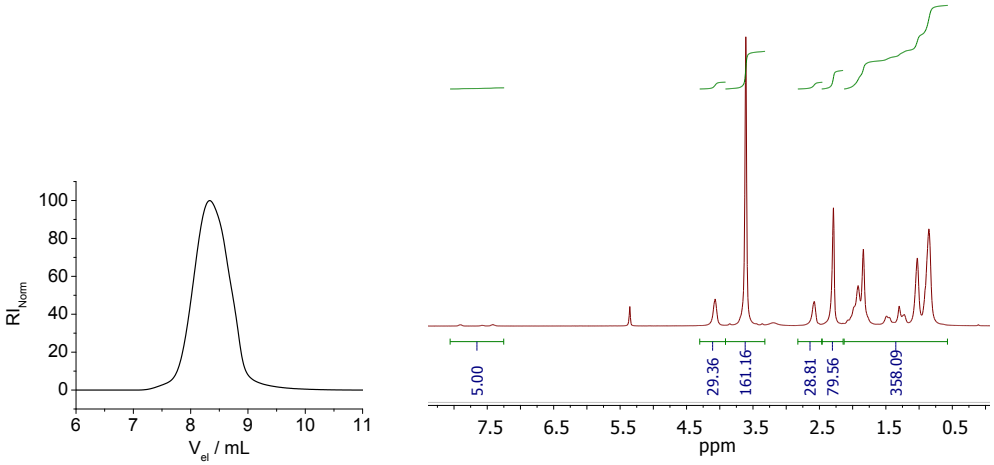

Figure S 1: SEC chromatograms and ^{1}H NMR spectra's of the final copolymers. The homopolymer PMMA was used as reference (adjustment of the broad backbone integral from 0.5 to 2.5 ppm to exclude impurities like water) and all spectra were corrected with this ratio between –OCH_3 and the backbone signal of PMMA (correction factor 0.964).

2 Nanoparticle characterization

Table S 2: Zeta potential of methacrylate-based nanoparticles with concentrations of 50 µg mL^{-1} in type 1-water.

Nanoparticle	Zeta potential [mV]
3% PMAA	– 43.3
5% PMAA	– 32.7
8% PMAA	– 32.5
13% PMAA	– 38.3
20% PDMAEMA	+ 31.3

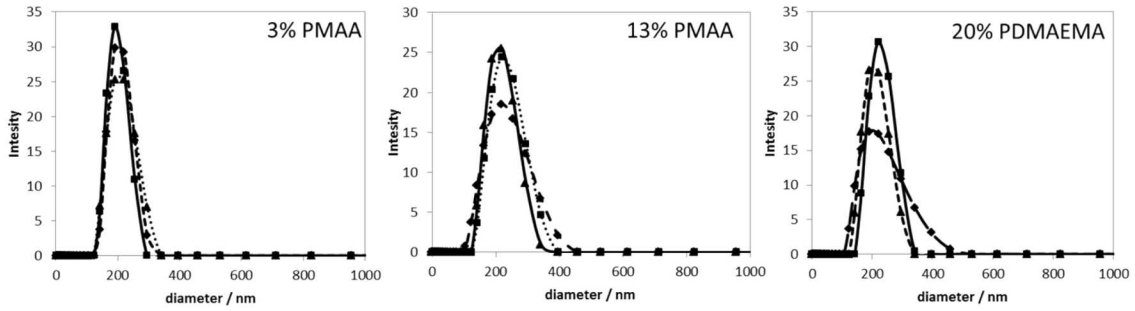

Figure S 2: DLS curves of methacrylate-based nanoparticles with concentrations of 50 µg mL^{-1} in type 1-water.

2.1 SDS-PAGE of nanoparticle incubated in serum containing media

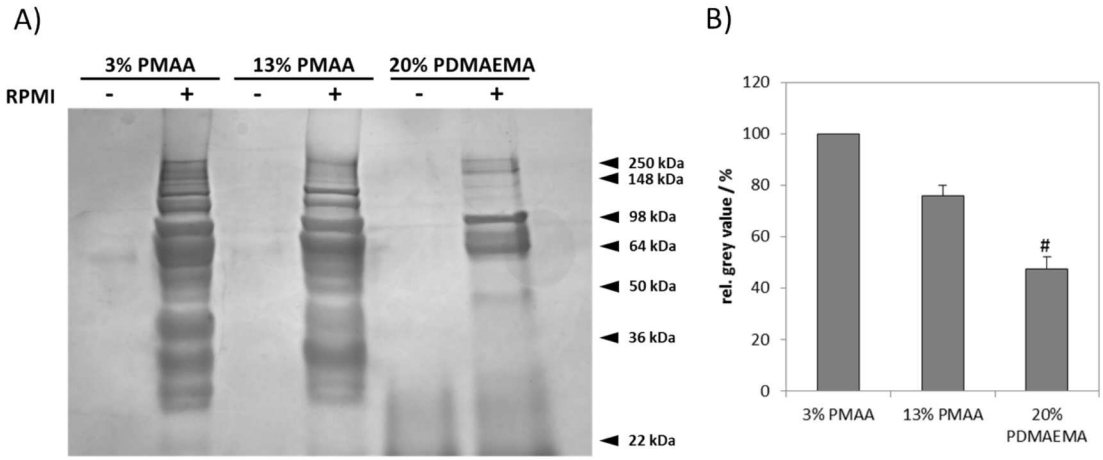

Figure S 3: *In vitro* investigation of protein binding to nanoparticles. SDS-PAGE of serum proteins bound to nanoparticles and densitometric analysis of total protein binding revealed a trend of lower protein binding to 13% PMAA and 20%DMAEMA compared to 3%PMAA. Bars show mean + s.e.m of three independent experiments, significance tested using Kruskal-Wallis and Dunn's multiple comparison test,$^{\#}p<0.05$.

2.2 Diameter and PDI of different nanoparticle batches

Table S 3: Nanoparticle batches containing nile red. Size and PDI_P are determined by DLS. The applied correction factors are given.

polymer	diameter / nm	PDI_P	correction factor
3% PMAA	206	0.099	0.49
3% PMAA	215	0.081	0.32
13% PMAA	188	0.064	1
13% PMAA	183	0.039	0.8
20% PDMAEMA	209	0.122	0.64
20% PDMAEMA	186	0.1	0.5

2.3 *Correlation of SSC/FSC using nile red.*

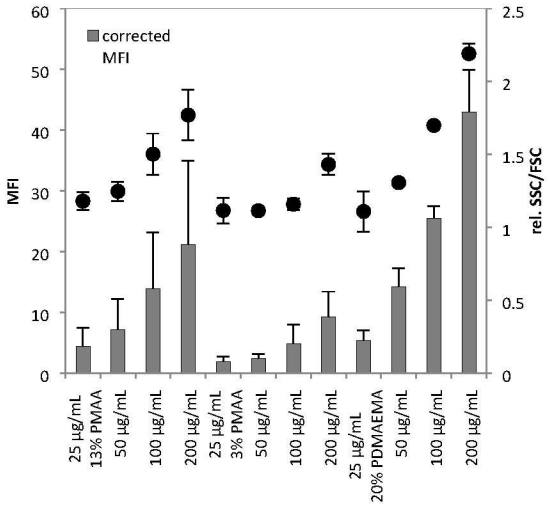

Figure S 4: Correlation of the uptake of methacrylate-based nanoparticle using rel. SSC/FSC and the corrected mean fluorescence intensity (MFI). HEK293 cells were incubated in media containing serum proteins for 24 h. Values represent the mean of three independent experiments ± SD.

2.4 *Hemolysis and aggregation*

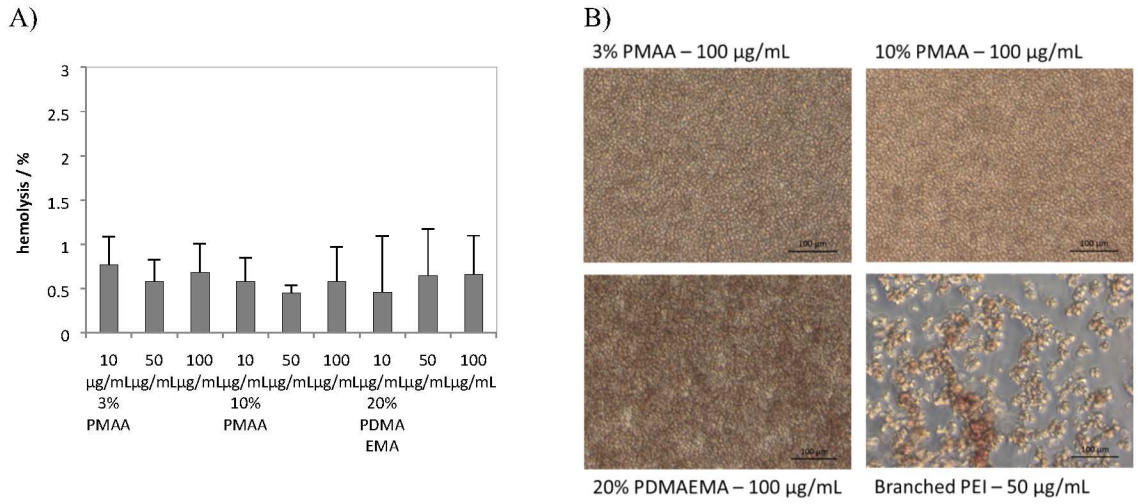

Figure S 5: Hemolysis and aggregation assay of the methacrylate-based nanoparticles.

2.5 Uptake investigations of methacrylate-based nanoparticles under static conditions

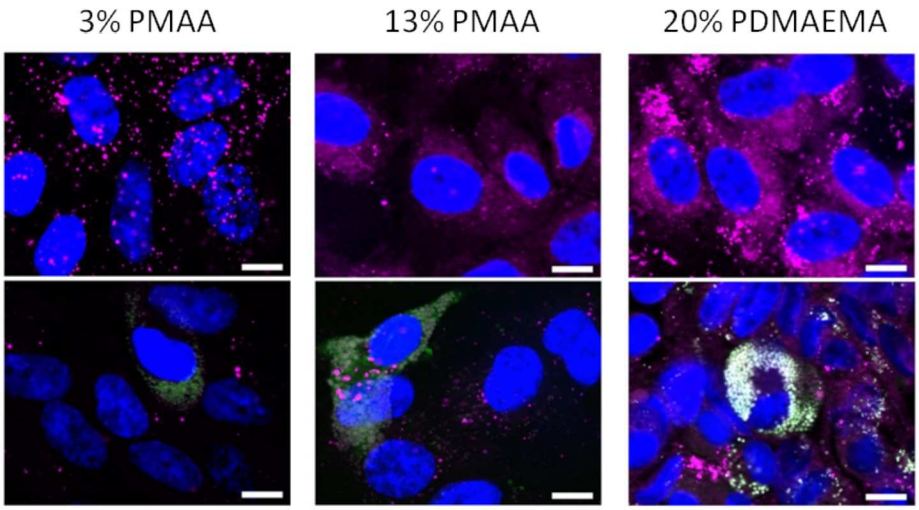

Figure S 6: Different nanoparticles in the microfluidically-assisted cell culture. Uptake of different nanoparticles containing nile red in a HUVEC monoculture or a co-culture with MΦ which were analyzed after 60 min. Uptake and distribution of different nanoparticles (purple) in the HUVEC monoculture (upper panels) and co-culture (lower panels) with MΦ. Cells were subsequently stained with DAPI (blue) and macrophages were stained using CMFDA (green). All scale bars = 10 µm.

Manuscript III

An integrative microfluidically supported *in vitro* model of an endothelial barrier combined with cortical spheroids simulates effects of neuroinflammation in neocortex development

Raasch, M., Rennert, K., Jahn, T., Gärtner, C., Schönfelder, G., Huber, O., Seiler, A. E. M. and Mosig, A. (2016)

Biomicrofluidics 10: 044102

In this manuscript we report the establishment of an integrative microfluidically supported BBB model of a human cerebral microvascular EC (hCMEC) layer co-cultured with brain cortical spheroids. The MOTiF biochip has been improved by integration of a unique second free hanging membrane comprising micro wells enabling spheroid immobilisation und flow conditions. The microvascular EC line hCMEC/D3 and cortical spheroids were adapted to a mutual medium formulation in a stepwise manner before chip integration and shear stress levels were adjusted to physiological conditions. Microvascular ECs were directly perfused, and cortical spheroids supplied with nutrition medium through the pores of the lower scaffold membrane. The microphysiological co-culture setup was characterised for expression typical cell marker proteins for each individual cell type and further barrier integrity was evaluated. Inflammatory conditions emulated by perfusion with a cytokine mixture of TNF, IL-1β, interferon gamma (INFγ) and lipopolysaccharide (LPS) resulted in an impairment of EC barrier function and related dedifferentiation of cortical spheroids. We conclude that the improvement of the MOTiF biochip design enables studies with more complex cellular arrangements helping to address each cell type or tissue culture condition individually. In particular, we could demonstrate in this study a novel tool to analyse cross-communication between the brain endothelial barrier and adjacent nerve tissue with focus on barrier integrity and inflammatory processes.

author contribution (80 %): cortical spheroid transport logistics**,** hCMEC cell culture and murine cortical spheroid differentiation, performance of medium adjustment to biochip assay co-culture medium, cortex model assembly, performing biochip perfusion experiments, viability assays, analysis and quantification of spheroid growth, permeability assays, immunofluorescence staining and microscopy, analysis of data, co-writing the manuscript.

BIOMICROFLUIDICS **10**, 044102 (2016)

An integrative microfluidically supported *in vitro* model of an endothelial barrier combined with cortical spheroids simulates effects of neuroinflammation in neocortex development

Martin Raasch,[1,2] Knut Rennert,[1,2] Tobias Jahn,[3] Claudia Gärtner,[3] Gilbert Schönfelder,[4,5] Otmar Huber,[1,2] Andrea E. M. Seiler,[4] and Alexander S. Mosig[1,2,a)]

[1]*Institute of Biochemistry II, Jena University Hospital, Jena, Germany*
[2]*Center for Sepsis Control and Care, Jena University Hospital, Jena, Germany*
[3]*microfluidic ChipShop GmbH, Jena, Germany*
[4]*Federal Institute for Risk Assessment (BfR), German Centre for the Protection of Laboratory Animals (Bf3R), Max-Dohrn-Str. 8-10, 10589 Berlin, Germany*
[5]*Department of Clinical Pharmacology and Toxicology, Charité–Universitätsmedizin Berlin, Berlin, Germany*

(Received 22 April 2016; accepted 22 June 2016; published online 5 July 2016)

The development of therapeutic substances to treat diseases of the central nervous system is hampered by the tightness and selectivity of the blood-brain barrier. Moreover, testing of potential drugs is time-consuming and cost-intensive. Here, we established a new microfluidically supported, biochip-based model of the brain endothelial barrier in combination with brain cortical spheroids suitable to detect effects of neuroinflammation upon disruption of the endothelial layer in response to inflammatory signals. Unilateral perfusion of the endothelial cell layer with a cytokine mix comprising tumor necrosis factor, IL-1β, IFNγ, and lipopolysaccharide resulted in a loss of endothelial von Willebrand factor and VE-cadherin expression accompanied with an increased leakage of the endothelial layer and diminished endothelial cell viability. In addition, cytokine treatment caused a loss of neocortex differentiation markers Tbr1, Tbr2, and Pax6 in the cortical spheroids concomitant with reduced cell viability and spheroid integrity. From these observations, we conclude that our endothelial barrier/cortex model is suitable to specifically reflect cytokine-induced effects on barrier integrity and to uncover damage and impairment of cortical tissue development and viability. With all its limitations, the model represents a novel tool to study cross-communication between the brain endothelial barrier and underlying cortical tissue that can be utilized for toxicity and drug screening studies focusing on inflammation and neocortex formation. *Published by AIP Publishing.* [http://dx.doi.org/10.1063/1.4955184]

INTRODUCTION

The development of suitable drugs for the treatment of central nervous system (CNS) diseases is challenging as the blood-brain barrier (BBB) efficiently prevents passage of nearly all polar substances from the vasculature to the brain tissue. The permeability of the BBB is determined by specialized endothelial cells of the cerebral vasculature (cerebral microvascular endothelial cell, CMEC) that only allow passage of molecules smaller than 400 Da.[1] The development of such small compounds represents an essential limitation requiring time-consuming drug-screening and preclinical studies. In consequence, suitable and reliable *in vitro* models are urgently needed to streamline the drug-screening processes and to curtail cost-intensive animal experimentation. In this context, miniaturized, microfluidically perfused BBB models attracted much attention during recent years.[2,3]

a)Author to whom correspondence should be addressed. Electronic mail: alexander.mosig@med.uni-jena.de.

Mechanotransduction induced by fluidic shear stress was demonstrated to influence endothelial cell differentiation and to regulate expression of endothelial junctional proteins necessary for the maintenance of the endothelial barrier function.[4–6] Apical junctional complex proteins determine endothelial polarity and barrier function, thereby regulating diffusion of small nutritional molecules and gases but excluding larger molecules, i.e., potential neurotoxins or microorganisms from the brain extracellular fluid.[7] Recently, the immortalized human CMEC (hCMEC)/D3 cell line has been described to express specific cerebral endothelial marker proteins including cell adhesion and tight junction (TJ) proteins as well as CNS relevant transporter systems.[8] Due to this favourable characteristics, the cell line has already been used in microfluidically perfused BBB models where it showed a transendothelial electrical resistance (TEER) of 120 Ω cm^2 with a high expression of zona occludens-1 (ZO-1), a protein of the tight junctional plaque that is important for the maintenance of BBB integrity.[9,10] Moreover, hCMEC/D3 cells were reported to mimic barrier characteristics of the BBB even in the absence of additional cell types, i.e., astrocytes or pericytes.[8]

In this context, it was shown that tight junction (TJ) protein expression is specifically down-regulated in these cells in response to pro-inflammatory cytokines such as tumor necrosis factor (TNF),[10–13] suggesting that hCMEC/D3 cells represent a reliable tool to study inflammation-related modulation of the cerebral microvascular endothelial barrier function.

For a more comprehensive modelling of events during neuroinflammatory diseases, it is essential to combine an endothelial barrier and neural tissue to see how effects on endothelial barrier function affect neural tissue and vice versa. In this proof-of-principle study, we established an integrative biochip-based model including an endothelial barrier composed of human CMECs and cortical tissue spheroids derived from murine embryonic stem cells (ESCs). We demonstrate that our model is able to reflect *in vitro* the cytokine-mediated disruption of the endothelial barrier in response to stimulation with a pro-inflammatory cytokine mix containing TNF, IL-1β, IFNγ, and lipopolysaccharide (LPS). Stimulation resulted in a diminished expression of endothelial VE-cadherin and ZO-1 indicating disruption of the endothelial barrier. In consequence, diminished expression of neural neocortex differentiation markers such as Tbr1, Tbr2, and Pax6 within cortical spheroids was observed. This demonstrates that our biochip model reflects neuroinflammatory processes at brain endothelial cell layers in association with the cortical tissue *in vitro*.

MATERIALS AND METHODS

Biochip fabrication

Biochips were made by injection moulding from polystyrene (PS) and manufactured by microfluidic ChipShop GmbH (Jena, Germany) as described previously.[6] See supplementary Figure 1 (Ref. 14) for embedded structures of the biochip with indicated lengths and heights. A 12 μm thick Polyethylene terephthalate (PET) membrane (TRAKETCH) with a pore diameter of 8 μm and a pore density of 1×10^5 pores/cm^2 (Sabeu, Radeberg, Germany) was integrated in the upper part of the biochip by heat-sealing with the bulk material. A polycarbonate membrane (300 μm, Karlsruhe, Germany) with thermo-formed micro-cavities with a diameter of 800 μm comprising pores with a diameter of 5 μm was heat-sealed in the lower part of the biochip (Figures 1 and 2).

Chips and channel structures were sealed on the top and bottom sides with an extruded 125 μm thick PS bonding foil using a low temperature bonding method. The upper and the lower parts of the biochip were assembled by a double-sided adhesive film. Oxygen plasma treatment for hydrophilization of the whole chip surface was performed to support cell adhesion and to reduce air bubble formation in the chips.

Cell culture

HCMEC/D3 cells were purchased from BIOZOL (Eching, Germany). Cells were cultured in complete EndoGRO-MV Basal Medium (endothelial cell medium (ECM)) containing 5% (v/v) fetal bovine serum (FBS), 0.2% (v/v) EndoGRO-LS supplement, 5 ng/ml recombinant

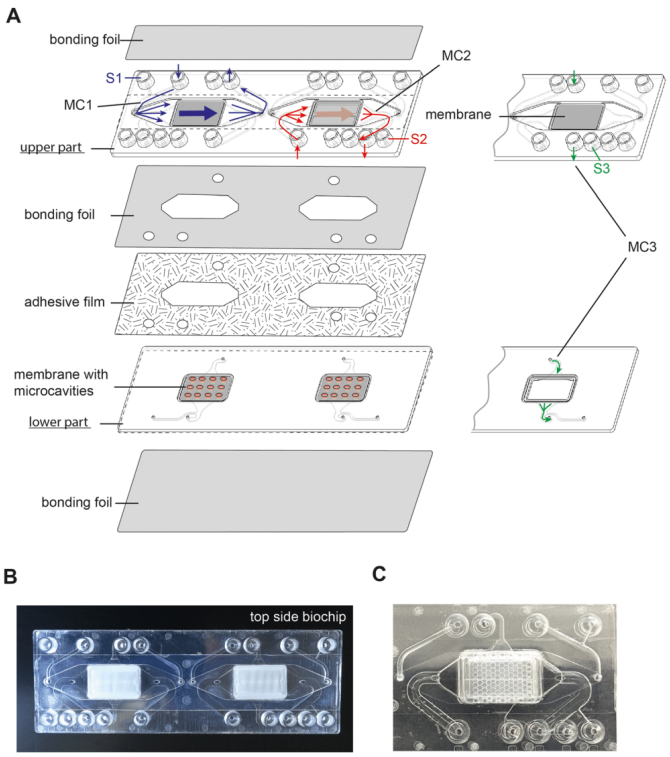

FIG. 1. Design of the components of the microfluidically supported biochip for a co-culture model of a cerebral microvascular cell layer forming an endothelial barrier and cortical structures. (a) The biochip is composed of an upper and a lower part that are combined with an adhesive film. The biochip includes two cavities. In each cavity, a planar membrane is integrated in the upper part and a membrane with micro-cavities is mounted in the lower part of the biochip. The upper and the lower chambers are sealed by bonding membranes to cover the micro-channels. The bonding foil that seals the bottom of the upper part holds openings to enable medium flow between the upper and the lower part of the biochip. Three microchannel systems are integrated in the biochip: Micro-channel 1 (MC1) perfuses the apical side of the flat membrane (blue lines). The second micro-channel (MC2) allows medium flow between both membranes (red lines). Micro-channel 3 (MC3) perfuses the basal side of the membrane with microcavities (green lines). Each micro-channel is connected to a lateral channel and a sample port that allows medium sampling during cell perfusion (sample ports S1, S2, and S3). (b) and (c) Photograph of the (b) entire biochip and (c) zoomed section of the biochip with embedded micro-cavity membrane.

human epidermal growth factor, 10 mM L-glutamine, 1 μg/ml hydrocortisone-hemisuccinate, 0.75 U/ml heparin-sulphate, and 50 μg/ml ascorbic acid (all additives were obtained from Merck-Millipore, Darmstadt, Germany).

Cortical spheroids were formed by self-aggregation as described previously.[15] Briefly, D3 mouse embryonic stem cells were seeded at a concentration of 1×10^3 cells in 100 μl per well into a 96-well PrimeSurface low adhesion cell culture plate (Sumitomo Bakelite Co., Ltd., Tokyo, Japan). Cells were differentiated in cortical differentiation medium consisting of Glasgow minimal essential medium (GMEM) supplemented with 10% (v/v) knock-out serum replacement (KSR) Non-Essential Amino Acids supplement (NEAA), pyruvate, antibiotics, and mercaptoethanol until day 7. Subsequently, cortical maturation was induced by replacing the

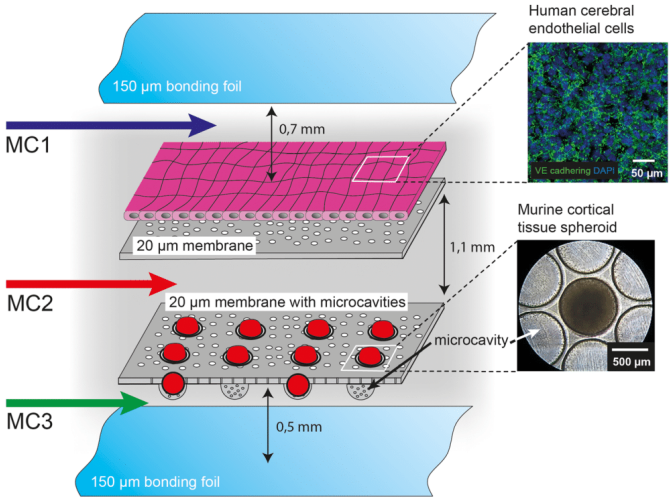

FIG. 2. Cellular setup in the biochip. On the flat membrane, human cerebral endothelial (hCMEC/D3) cells were cultured to mimic the endothelial barrier within the BBB. Murine cortical spheroids were cultured underneath the endothelial cell layer in the micro-cavities of the lower membrane simulating the cortex. Cortical spheroids were transferred into the biochip via the micro-channel 2 (MC2). HCMEC/D3 cells were perfused via the micro-channel 1 (MC1) at the apical side and spheroids were perfused via the micro-channel 3 (MC3) at the basal side. Spheroids are protected from direct impact of shear stress by the membrane that allows nutrition supply through the pores. Arrows indicate the distance between the membranes as well as the distances between the individual membranes and bonding foil.

cortical differentiation medium with cortical maturation medium (CMM) consisting of DMEM/F-12 with GlutaMAX supplemented with 1% (v/v) of N2 supplement (Thermo Fischer Scientific, Erlangen, Germany) and 100 U/ml penicillin and 100 μg/ml streptomycin (Life Technologies, Karlsruhe, Germany).

For spheroid culture in the biochips, the cell culture medium was equilibrated overnight to culture conditions of 37 °C and 5% CO_2 to reduce air bubble formation within the biochip. Gas permeable silicon tubing was used for oxygen equilibration throughout the experiments. Bright field images of cells and spheroids within the biochip were taken with a Leica DM IL LED (light-emitting diode) microscope (Leica, Wetzlar, Germany) equipped with a Canon IXUS 95 IS camera (Canon, Krefeld, Germany). Images were analysed using ImageJ2 software (Fiji; NIH, USA).

BBB/cortex model assembly

The membrane used to grow hCMEC/D3 cells within the biochip was coated with 150 μg/ml collagen A (Biochrom, Berlin, Germany) for 1 h. Subsequently, 1.5×10^5 hCMEC/D3 cells were seeded on the membrane and cultured in ECM medium for 48 h. Subsequently, the culture medium was stepwise adjusted to cortical tissue medium (CTM)/ECM medium as described in Table I.

On day 14, the cortical spheroids were transferred into the micro-cavities of the lower membrane. On day 15, the fully assembled brain endothelial layer/cortex model was cultured under perfusion conditions for 24 h. The hCMEC/D3 layer was perfused with 350 μl/min corresponding to 4 dyn/cm^2 via micro-channel 1 of the upper part of the biochip (Figure 1). A flow rate of 0.4 μl/min corresponding to a shear stress rated of 0.5 dyn/cm^2 was applied in the lower

TABLE I. Culture of hCMEC/D3 cells and cortical tissue spheroids in stepwise diluted culture medium.

Composition of cell culture medium for cortical tissue spheroids (CTM %/ECM %)				
Day 10: 100/0	*Day 11:* 90/10	*Day 12:* 80/20	*Day 13:* 70/30	*Day 14:* 50/50
Composition of cell culture medium for hCMEC/D3 (CTM %/ECM %)				
Day 10: 0/100	*Day 11:* 10/90	*Day 12:* 20/80	*Day 13:* 30/70	*Day 14:* 50/50

microfluidic channel 3 for perfusion of the cortical spheroids from their basal side. Shear stress rates were calculated as described previously.[6]

To mimic neuroinflammation, a cytokine mixture consisting of 50 ng/ml human TNF, 10 ng/ml human IL-1β, 10 ng/ml human IFNγ (all from Calbiochem, Darmstadt, Germany), and 100 ng/ml LPS (Sigma-Aldrich, Darmstadt, Germany) was added to the medium and used for the perfusion of the hCMEC/D3 layer for 24 h via micro-channel 1 of the biochip (Figure 1).

Permeability assay

To test the permeability of the endothelial cell layer, 10 mg/ml of 3 kDa fluorescein isothiocyanate (FITC)-dextran (Sigma-Aldrich) was suspended in CTM/ECM medium, injected via micro-channel 1 into the biochip, and incubated for 30 min on top of the hCMEC/D3 cell layer under static conditions. Permeated FITC-dextran was collected from micro-channel 2, and the fluorescence of the labelled dextran was measured with a Mithras LB 940 fluorometer using the Mikrowin 2000 software (Berthold Technologies, Bad Wildbach, Germany).

Viability staining and immunofluorescence analyses

Cell viability of hCMEC/D3 cells and cortical spheroids was assessed with calcein-AM (Life Technologies) and propidium iodide (PI; Sigma-Aldrich) staining. The cells were washed with phosphate buffered saline (PBS), incubated with 2.5 μM calcein-AM and 1 μg/ml PI in PBS for 15 min, washed again with PBS, and subsequently cells were imaged.

For immunofluorescence staining, cortical spheroids were collected, fixed with 2% paraformaldehyde (PFA) (Sigma-Aldrich) for 30 min, embedded, and stored in TissueTek OCT (Sakura, Staufen, Germany) at $-80\,^{\circ}$C. Samples were cut into 10 μm thick cryo-sections prior to staining. The sections were permeabilized with 0.1% (w/v) Saponin (Fluka, St. Gallen, Switzerland) and blocked with 3% (v/v) normal goat serum (Dianova, Hamburg, Germany) for 30 min. Cortical spheroids were stained with chicken anti-Tbr-1, rabbit anti-Tbr-2 (Merck-Millipore, Darmstadt, Germany), and mouse anti-Pax-6 (Santa Cruz, Heidelberg, Germany) antibodies overnight.

For analysis of cells cultured in the biochips, the cavities of the biochip were opened by cutting the bonding foils with a scalpel. HCMEC/D3 cell layers on PET membranes were fixed with 2% PFA for 5 min with subsequent methanol treatment for 10 min at $-20\,^{\circ}$C and stained with rabbit anti-human von Willebrand factor (vWf; Dako, Hamburg, Germany), mouse anti-human VE-cadherin, mouse anti-human β-catenin (both BD Biosciences, Heidelberg, Germany), and rabbit anti-human ZO-1 (Life Technologies) overnight. The following secondary antibodies were used: goat anti-chicken AF488 (Abcam, Cambridge, UK), goat anti-mouse Cy3, and goat anti-rabbit AF647 (Dianova, Hamburg, Germany). Nuclei were stained with 4′,6-Diamidine-2′-phenylindole dihydrochloride (DAPI) (Life Technologies, Karlsruhe, Germany). Fluorescence imaging was performed on an Axio Observer Z1 fluorescence microscope equipped with Apotome.2 (Carl Zeiss AG, Jena, Germany). Fluorescence images were analysed with the ImageJ2 software.

Statistics

All results are reported as average means with standard deviation of at least three independent experiments. Statistical significance was calculated with two-tailed, non-paired student's t-test using GraphPad Prism 6.07 software (GraphPad, La Jolla, CA, USA).

RESULTS

Design of the biochip to co-culture brain microvascular endothelial cells and cortical tissue spheroids

Based on our recently described Multi-Organ-Tissue-Flow (MOTiF) biochip design allowing improved endothelial cell culture conditions under flow,[6] the biochip comprises an upper part, holding a flat membrane that serves as cell substrate for the culture of hCMEC/D3 cells. This membrane is connected to two micro-channel systems that allow the independent perfusion of the membrane from the apical and basal side as recently described (Figure 1).[6] Micro-channels are sealed at the top and bottom of the upper biochip part by a bonding foil and have a height of 0.45 mm for micro-channel 1 (upper channel), 0.7 mm for micro-channel 2 (middle channel), and 0.2 mm for micro-channel 3 (lower channel) (Figures 1 and 2). For co-culture with cortical tissue spheroids, a special membrane with thermo-formed micro-cavities was integrated for immobilization of the spheroids during perfusion of the endothelial layer in the lower part of the biochip (Figure 1).[16] Each micro-channel system is connected to a separate sampling port that allows sample collection without interruption of cell culture perfusion with medium (Figure 1).

HCMEC/D3 cells were cultured on the flat membrane of the upper part of the biochip and grown to full confluence to assemble an endothelial barrier (Figure 2). Cortical tissue spheroids were cultured for 14 days in non-adhesive tissue plates to allow cell aggregation. Subsequently, spheroids were transferred into the biochip via micro-channel 2 of the lower part of the biochip and cultured in the micro-cavities of the lower membrane (Figure 2). The shear stress at the endothelial barrier within brain capillaries ranges between 3 and 20 dyn/cm^2.[17] To enable physiological mechanostimulatory conditions, the hCMEC/D3 cell layer was perfused with 350 μl/min, corresponding to a shear stress rate of 4 dyn/cm^2 via the top channel (marked as micro-channel 1 in Figures 1 and 2). The cortical spheroids were perfused from the basal side via micro-channel 3 with a low flow rate of 0.4 μl/min corresponding to a shear stress rate of 0.5 dyn/cm^2 (Figures 1 and 2) to provide sufficient medium exchange, but to prevent potential cell stress on the neural tissue spheroids.

Adjustment of cell culture medium and characterization of cell growth

To facilitate a reliable co-culture of hCMEC/D3 cells and cortical tissue spheroids, the cell culture medium for both cell types was adjusted to a 50/50 (v/v) composition of ECM and cortical tissue medium (CTM). Cortical tissue spheroids were adapted to the new cell culture medium by a daily stepwise reduction of the CTM portion in the culture medium and a concomitant increase in ECM. HCMEC/D3 cells vice versa were adapted to the co-culture medium in a similar way but with a reverse medium mix series (see Table I). Before transfer to the biochip, the cells were cultured for additional two days in the adjusted CTM/ECM medium.

We observed no adverse impact on spheroid growth after transfer and subsequent culture of spheroids to the co-culture medium (Figures 3(a) and 3(b)). Moreover, no effect of medium adjustment was detectable on cortical spheroid viability as analysed by calcein-AM staining. The number of dead cells within the spheroids was also not increased as analysed by propidium iodide (PI) staining (Figure 3(c)). Similarly, we observed no differences in cell viability or cell death in hCMEC/D3 cells cultured in adjusted CTM/ECM compared with cells grown in ECM medium (Figure 3(d)). Treatment of spheroids or hCMEC/D3 cells with 1 μM of the apoptosis inducer staurosporine for 24 h served as control in cell viability staining and cell death assays. Staurosporine treatment induced a disintegration of cortical spheroids and detachment of hCMEC/D3 cells and was associated with a decline in the calcein-AM and an increase in the PI fluorescence signals (Figures 3(c) and 3(d)).

Detection of typical cortical and endothelial cell marker proteins

We next checked the expression of Tbr1, Tbr2, and Pax6 representing important regulators of the neocortical development in cortical spheroids cultured in CTM and CTM/ECM medium.

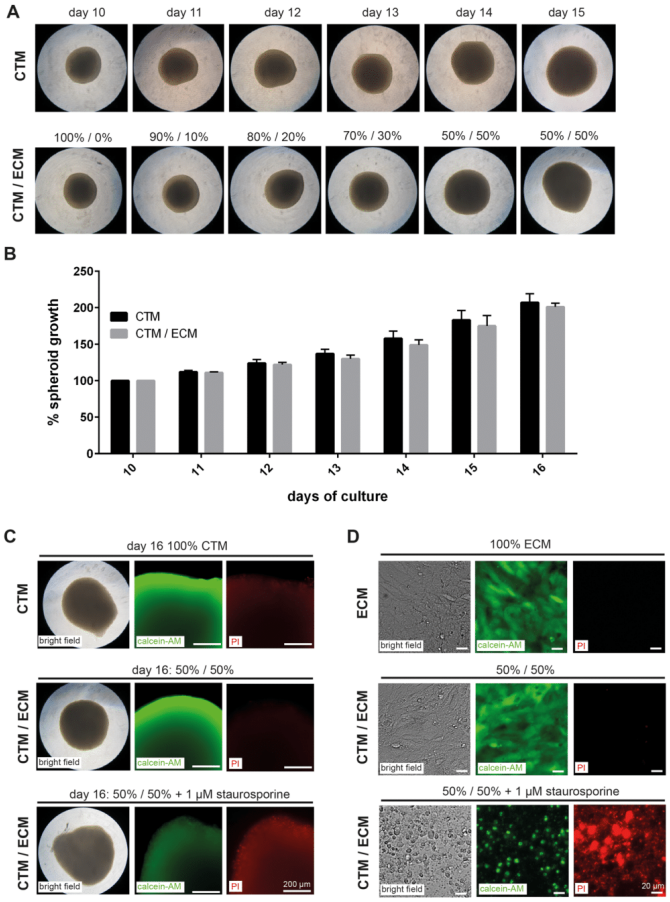

FIG. 3. Adaption of hCMEC/D3 cells and cortical spheroid growth to CTM/ECM medium. (a) Bright field images of cortical spheroids grown from day 10 to day 15 in ECM and CTM/ECM cell culture medium. (b) Changes in the diameter of spheroids grown in CTM and CTM/ECM medium. The diameter at day 10 was normalized to 100%. The mean of the measurements is shown. Error bars indicate the standard deviation of three independent experiments. (c) and (d) Bright field microscopy images and fluorescence microscopy images of calcein-AM (green) and propidium iodide (PI, red) staining of spheroids at day 16 (c) and hCMEC/D3 cultured in ECM and CTM/ECM medium (d). Treatment with 1 μM staurosporine for 24 h served as control for viability and cell death analyses. (a), (c), and (d) Representative data of three independent experiments performed in 96-well plates are shown.

At day 11, spheroids were adapted to adjusted CTM/ECM medium as described in Table I and cultured for additional two days in final 50/50 CTM/ECM medium composition. No difference in the expression levels of the indicated neural differentiation markers was observed between spheroids cultured in CTM or CTM/ECM. In both media, spheroids showed a sustained and defined expression of Tbr1, Tbr2, and Pax6 (Figure 4(a)).

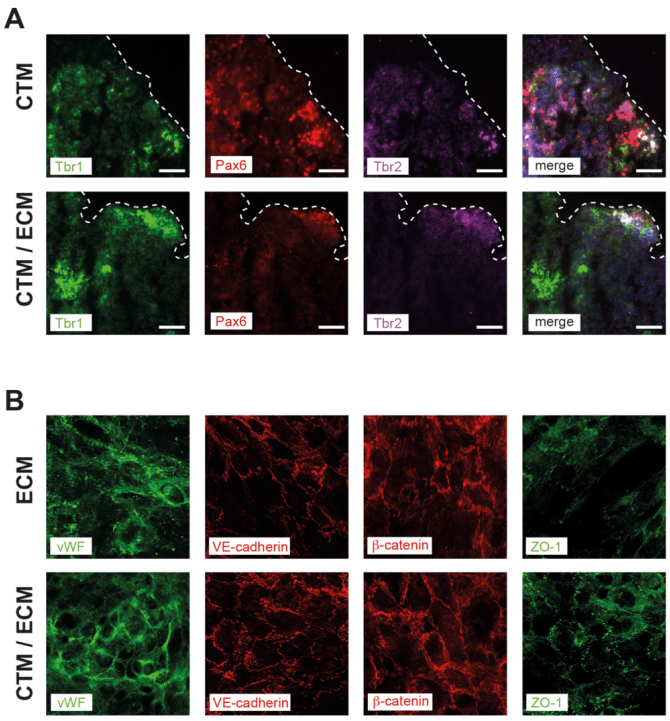

FIG. 4. Expression of cell differentiation markers in cortical spheroids and hCMEC/D3 cells cultured in ECM or CTM/ECM medium. (a) Cortical spheroids at day 16 of spheroid culture were stained for neural differentiation markers Tbr1 (green), Pax6 (red), and Tbr2 (magenta). In the merged image, cell nuclei are stained with DAPI (blue). Dashed lines indicate the borders of the spheroid cross-sections. (b) Expression of endothelial cell marker proteins von Willebrand factor (vWF, green), VE-cadherin (red), β-catenin (red), and ZO-1 (green) expressed in hCMEC/D3 cells. Representative images of three independent experiments are shown. Imaging was performed with fixed cells on membranes cut out from the biochips after perfusion.

In hCMEC/D3 cell layers, we analysed the expression of von Willebrand factor (vWF), a protein that is involved in regulation of coagulation and moreover is a central regulator of permeability and flexibility of the endothelial cell layer within the BBB.[18] In addition, we examined the expression of VE-cadherin and β-catenin, proteins required for the maintenance of endothelial barrier integrity and CNS homeostasis,[19] as well as the tight junction protein ZO-1. We observed no alterations in the protein expression of these proteins during adaption and subsequent culture of CMEC in CTM/ECM medium compared with ECM medium (Figure 4(b)).

Modulation of endothelial barrier integrity with a pro-inflammatory cytokine mix

As a next step, co-culture of hCMEC/D3 cells and cortical spheroids within the microfluidically supported biochip was established. HCMEC/D3 cells adapted to CTM/ECM medium were seeded at the top membrane and cultured for 2 days to allow full confluence and formation of a tight endothelial barrier. Cortical spheroids were subsequently transferred into the

micro-cavities of the lower membrane via micro-channel 2 of the biochip. Inflammation in response to LPS is associated with BBB disruption and the release of the pro-inflammatory cytokines TNF, IL-1β, and IFNγ derived from pericytes.[20–23] These cytokines can act synergistically at the individual cell types of the BBB modulating its function during neuroinflammation.[22] To simulate a LPS-induced neuroinflammation in our biochip model in the absence of pericytes, a mixture of cytokines was added to the perfusion medium in the micro-channel 1. See supplementary Figure 2 (Ref. 14) for a scheme of cytokine stimulation via micro-channel 2. The final concentration of cytokines in the perfusion medium was 50 ng/ml TNF, 10 ng/ml IL-1β, 10 ng/ml IFNγ, and 100 ng/ml LPS.

The cytokine mix was added only to the medium that perfused the apical side of the endothelial cell layer. In this setting, cortical spheroids should only be affected by the cytokine mix upon preceding disruption of the endothelial barrier.

To determine the endothelial cell layer permeability, 3 kDa FITC-dextran was added to the perfusion medium and the intensity of fluorescence signals in the lower chamber of the biochip was assessed. Aliquot sampling was performed via the sample port S2 of the biochip (Figure 1). After 24 h of cytokine-mix perfusion of the endothelial BBB layer and subsequent incubation with 10 mg/ml FITC-dextran for 30 min, we observed a considerable increase in the fluorescence signal indicating a cytokine-induced impairment of the endothelial barrier integrity (Figure 5(a)). The increased permeability was associated with a reduced viability and an increased cell death of hCMEC/D3 cells determined by calcein-AM and PI staining, respectively (Figures 5(b) and 5(c)). We further observed reduced endothelial expression of vWF, VE-cadherin, and ZO-1 in response to cytokine treatment (Figures 5(d)–5(f)). By contrast, the expression of β-catenin was not altered by cytokine stimulation of the endothelial cell layer (Figure 5(f)).

Disruption of the endothelial barrier is associated with a diminished expression of neural differentiation marker expression in cortical spheroids

After transfer into the biochip, cortical spheroids remained stable, were viable, and showed no signs of increased cell death (Figure 6(a)). However, in response to cytokine treatment of the endothelial cell layer, signs of spheroid disintegration and an attenuated viability similar to staurosporine treatment were detectable at the levels of reduced density of cortical spheroids in bright field microscopy, as well as a diminished calcein-AM staining and increased PI fluorescence signals (Figure 6(b)). Furthermore, the defined expression of neocortex differentiation regulators Tbr1, Tbr2, and Pax6 was lost upon perfusion of the endothelial barrier with the cytokine mix medium.

DISCUSSION

The majority of published BBB models so far uses static cell culture approaches.[24] Recently, a three-dimensional model of the BBB comprising RBE4 rat brain endothelial cell layers wrapped inside a cylindrical lumen of a hollow collagen gel was reported. This model was shown to be sensitive to mediators of neuroinflammation.[25] A similar approach has also been chosen in a study by Herland *et al.*,[26] in which human brain microvascular endothelial cells (hBMECs) were co-cultured with pericytes and astrocytes. Here, the BBB was responsive to stimulation with pro-inflammatory TNF as detected by the release of G-CSF and IL-6 in the supernatant of the culture medium. In addition, a model with human umbilical vein endothelial cells (HUVECs) has been reported revealing an increased endothelial cell layer tightness when HUVECs were co-cultured with astrocytes.[27] However, only a few microfluidically supported BBB models with the ability to mimic physiological shear stress conditions were reported so far. Booth and Kim recently described the establishment of the so-called μBBB model consisting of a co-culture of murine CMECs and astrocytes on a permeable membrane. The authors report that the co-culture of both cell types results in a significant increase in TEER values and tightness of the BBB, which was further increased by application of physiological shear stress to the endothelial cell layer.[28] Similar results have been reported by Prabhakarpandian *et al.* for the Sym-BBB model, in which shear stress stimulation and astrocyte-conditioned medium result

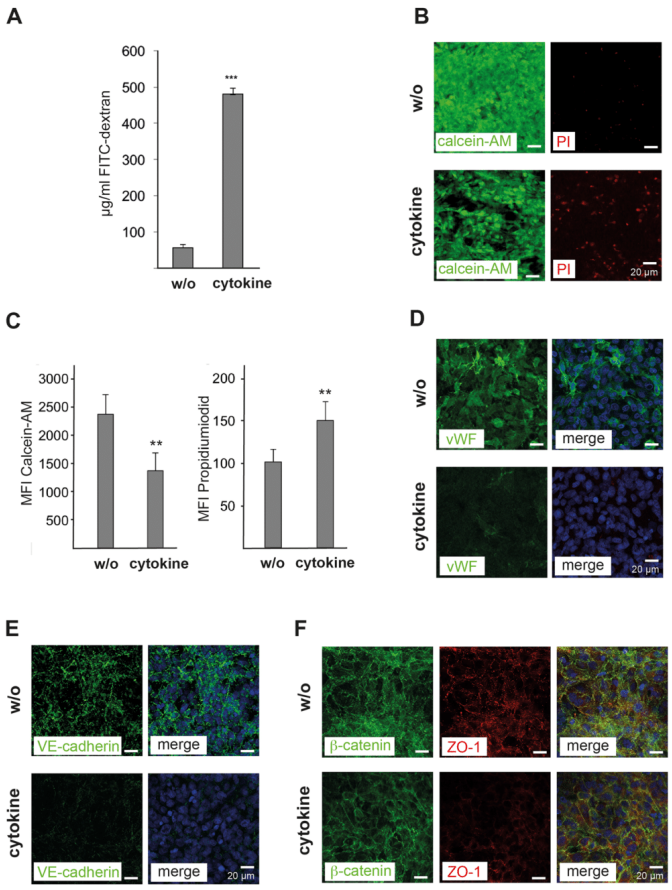

FIG. 5. Modulation of the endothelial integrity in response to cytokine treatment. (a) Measurement of the permeability of hCMEC/D3 cell layers co-cultured with cortical spheroids in the biochip using 3 kDa FITC-dextran beads. The amount of labelled dextran beads (μg/ml) permeating from the apical to the basal side of the endothelial cell layer was quantified by fluorescence spectrometry. (b) Immunofluorescence microscopic images of hCMEC/D3 cell layers without (w/o) and with cytokine-mix (cytokine) treatment for 24 h. Stainings with calcein-AM (green) and propidium iodide (PI, red) are shown. (c) Quantification of calcein-AM and PI signals in hCMEC/D3 cells. (d)–(f) Fluorescence microscopic images of hCMEC/D3 cells treated as described in (b) and stained for (d) von Willebrand factor (vWF, green), (e) VE-cadherin (green), (f) β-catenin (green), and ZO-1 (red). (d)–(f) In the merged images, cell nuclei were stained with DAPI (blue). (a) and (c) The mean values of three independent measurements are shown; error bars indicate the standard deviation. Statistical significance was calculated using student's t-test (** $p < 0.01$, *** $p < 0.001$). (b)–(f) Representative data of three independent experiments are shown.

in an increased tight junction protein expression and enhanced tightness of RBE4 cell layers.[29] Recently, a novel microfluidic bioreactor ("NeuroVascular Unit," NVU) for the co-culture of endothelial cells, astrocytes, and pericytes under flow conditions has been reported. Within this bioreactor, a microenvironment is provided that favours the paracrine signalling between the

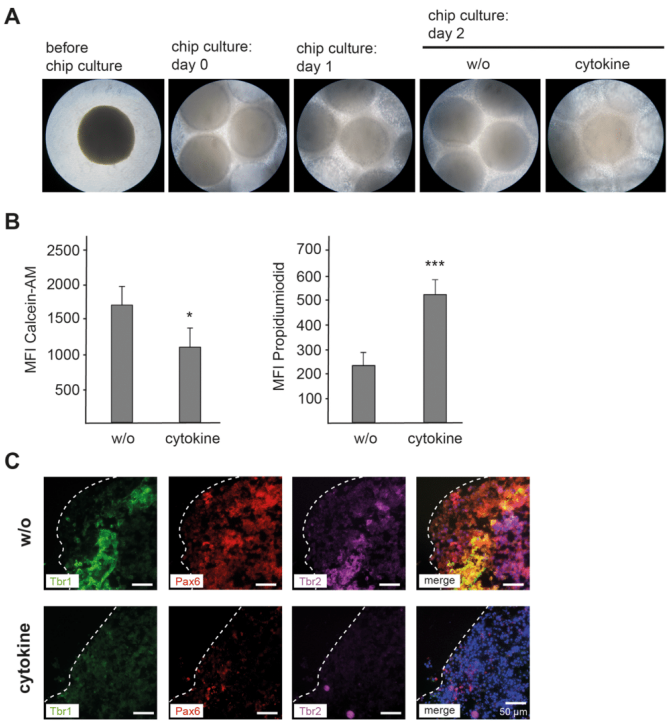

FIG. 6. Impact of endothelial barrier disruption on cortical spheroid growth and expression of neural differentiation markers in response to cytokine mix treatment. (a) Bright field microscopic images of cortical spheroids before transfer into the biochip (before chip culture), and co-culture with an endothelial hCMEC/D3 cell layer immediately after transfer into the biochip (chip culture: day 0), after 24 h culture in the biochip (chip culture: day 1), after 48 h culture in the biochip (chip culture: day 2, w/o), and after 48 h culture in the biochip with 24 h of cytokine mix treatment (chip culture: day 2, cytokine). (b) Fluorescence microscopical analyses of calcein-AM and propidium iodide stainings of spheroids at day 16 of co-culture with hCMEC/D3 cells without (w/o) and 24 h of cytokine mix treatment (cytokine). Mean values of three independent measurements are shown. Error bars indicate standard deviations. Statistical significance was calculated using student's t-test (* $p < 0.05$, *** $p < 0.001$). (c) Expression of cell differentiation markers in cortical spheroids co-cultured in the biochip cultured as described in (b). Cortical spheroids at day 16 of spheroid culture were stained for neural differentiation markers Tbr1 (green), Pax6 (red), and Tbr2 (magenta). In the merged image, cell nuclei are stained with DAPI (blue). Dashed lines indicate the borders of the spheroid cross-sections. (a) and (c) Representative data of three independent experiments are shown.

co-cultured cell types needed for the long-term stable differentiation of the BBB and growing human neurons.[30]

An important feature of the hCMEC/D3 cell line used in our study, however, is the formation of a physiological barrier already in the absence of glia cells or astrocytes.[8,31] We therefore omitted inclusion of additional cell types in the endothelial layer. However, future studies to improve our model should include astrocytes and pericytes. Most of the current microfluidically supported BBB models were established in polydimethylsiloxane (PDMS)-based systems. PDMS is often utilized because of its straightforward application in rapid prototyping.[32] However, the use of PDMS comprises some important drawbacks, such as hydrophobic molecules can easily

get adsorbed to the chip surface.[33,34] Moreover, uncrosslinked free PDMS monomers leach out into the media and affect cellular behaviour.[33,34] In addition, PDMS is known to be permeable to gases and water vapour and induces changes in the osmolarity of cell culture media.[35] We therefore selected polystyrene as chip bulk material. This polymer is used since decades as a reliable cell culture substrate allows simple surface modifications and does not interfere with bright field or fluorescence microscopy.

Here, we demonstrated that our biochip-based model allows the co-culture of endothelial hCMEC/D3 cell layers and cortical tissue spheroids under physiological perfusion conditions. By stepwise adaption to an adjusted CTM/ECM medium, we were able to culture both cell types in a mutual cell culture medium without affecting the expression levels or distribution of the endothelial or neural cell marker proteins analysed. HCMEC/D3 cell layers expressed central marker proteins known to regulate BBB integrity and flexibility *in vivo*, such as vWF, VE-cadherin, ZO-1, and β-catenin.[4–6,9,10,18,19] Furthermore, this model is able to reflect critical aspects of neuroinflammation, as depicted by its ability to specifically reproduce a cytokine-induced disruption of the endothelial barrier associated with subsequent alterations in neural cell morphology, increased neural cell death, and diminished expression of neural differentiation marker proteins. Our results are in agreement with the findings from studies in mice that analysed the development of the neocortex under inflammatory conditions. Similar to the *in vivo* model, we also observed a reduced expression of the neocortex development regulators Tbr1,[36] Tbr2,[37] and Pax6[38] in response to inflammation and pro-inflammatory cytokines. The data thus show that our *in vitro* model of an endothelial barrier co-cultured with neural tissue spheroids is able to reflect crucial aspects of neuroinflammation during neocortex formation.

However, we are also aware of the limitations of our model. Our biochip-based system currently lacks the option of direct measurements of TEER generated by the endothelial cell layer as electrodes between the endothelial cell layer and spheroids potentially affect spheroid growth and interfere with spheroid transfer into the biochip. Moreover, the distance between the endothelial barrier and the top of microcavity-embedded neural spheroids is approximately 0.7 mm forming a total media volume of approximately 160 μl between both cellular compartments. These dimensions are considerably larger than in the *in vivo* situation and thus may affect endocrine and paracrine signalling between the endothelial and neural tissue.

Another limitation of our model is the absence of pericytes and astrocytes. However, the current approach was chosen to have a first proof-of-principle with a simple cellular setup and a sustainable co-culture of different cell types within the biochip. Follow-up studies will be performed to test whether a co-culture of cerebral microvascular endothelial cells together with astrocytes and/or pericytes can be established to bring our model even closer to the physiological conditions. In this context, it is worth to note that human brain microvascular endothelial cells (hBMECs) generated from induced pluripotent stem cells have also been co-cultured with astrocytes, pericytes, and neural cells. In this co-culture model of the BBB, a significant tightness and the expression of tight and adherence junction proteins as well as multidrug-resistance proteins were demonstrated.[39,40]

CONCLUSIONS

To the best of our knowledge, we here describe for the first time a microfluidically supported biochip that integrates a model of cerebral microvascular endothelial barrier and cortical tissue spheroids. The model resembles physiological shear stress conditions at the endothelial barrier and allows a direct assessment of neuroinflammatory effects on cortical tissue differentiation and viability. It thus represents a novel tool to screen drugs affecting cerebral microvascular endothelial barrier integrity and mediating neuroinflammatory effects. In addition, the new biochip design allows the integration of single cell layers and spheroidal cell aggregates within an integrative microfluidically supported biochip. Moreover, this biochip design is adaptable to other organ-on-a-chip models that rely on integration of an endothelial cell layer resembling the vasculature and spheroid cultures resembling organ specific tissue.

From our data, we conclude that the presented new biochip model is able to mimic an inflammation-related impairment of the cerebral microvascular endothelial barrier concomitantly affecting expression of neural cell differentiation markers and cell viability in response to cytokine treatment. This model thus represents a valuable tool mimicking the cerebral vascular system in its cross-talk with cortical tissue under neuroinflammatory conditions *in vitro*. However, more work is required to fully characterize its potential in, e.g., toxicological or pharmaceutical screening studies.

ACKNOWLEDGMENTS

We are grateful to the excellent technical assistance of Fatina Siwczak and Margot Voigt at the University Hospital Jena as well as to Birgitta Slawik and Konrad Gulich at the BfR for providing technical support in generation of cortical organoids. The authors acknowledge support of this work by a grant from the German Federal Institute of Risk Assessment (Grant No. 1329-533).

[1]W. M. Pardridge, NeuroRx **2**, 3 (2005).
[2]S. N. Bhatia and D. E. Ingber, *Microfluidic Organs-on-Chips* (Nature Publishing Group, 2014), pp. 760–772.
[3]N. S. Bhise, J. Ribas, V. Manoharan, Y. S. Zhang, A. Polini, S. Massa, M. R. Dokmeci, and A. Khademhosseini, J. Controlled Release **190**, 82 (2014).
[4]C. G. Galbraith, R. Skalak, and S. Chien, "Shear stress induces spatial reorganization of the endothelial cell cytoskeleton," Cell Motil. Cytoskeleton **40**(4), 317–330 (1998).
[5]L. Cucullo, P.-O. O. Couraud, B. Weksler, I.-A. A. Romero, M. Hossain, E. Rapp, and D. Janigro, J. Cereb. Blood Flow Metab. **28**, 312 (2008).
[6]M. Raasch, K. Rennert, T. Jahn, S. Peters, T. Henkel, O. Huber, I. Schulz, H. Becker, S. Lorkowski, H. Funke, and A. Mosig, Biofabrication **7**, 15013 (2015).
[7]Y. Persidsky, S. H. Ramirez, J. Haorah, and G. D. Kanmogne, J. Neuroimmune Pharmacol. **1**, 223 (2006).
[8]B. Weksler, I. A. Romero, and P.-O. Couraud, *The hCMEC/D3 Cell Line as a Model of the Human Blood Brain Barrier* (BioMed Central Ltd., 2013), p. 16.
[9]B. R. Stevenson, J. D. Siliciano, M. S. Mooseker, and D. A. Goodenough, J. Cell Biol. **103**, 755 (1986).
[10]L. M. Griep, F. Wolbers, B. De Wagenaar, P. M. Ter Braak, B. B. Weksler, I. A. Romero, P. O. Couraud, I. Vermes, A. D. Van Der Meer, and A. Van Den Berg, Biomed. Microdevices **15**, 145 (2013).
[11]K. A. Frankola, N. H. Greig, W. Luo, and D. Tweedie, "Targeting TNF-α to elucidate and ameliorate neuroinflammation in neurodegenerative diseases," CNS Neurol Disord Drug Targets **10**(3), 391–403 (2011).
[12]C. Mc Guire, R. Beyaert, and G. van Loo, "Death receptor signalling in central nervous system inflammation and demyelination," Trends Neurosci. **34**(12), 619–628 (2011).
[13]K. M. Park and W. J. Bowers, "Tumor necrosis factor-alpha mediated signaling in neuronal homeostasis and dysfunction," Cell Signal. **22**(7), 977–983 (2010).
[14]See supplementary material at http://dx.doi.org/10.1063/1.4955184 for structures of the biochip with indicated lengths and heights and a scheme of cytokine stimulation via micro-channel 2 of the biochip.
[15]M. Eiraku and Y. Sasai, Nat. Protoc. **7**, 69 (2011).
[16]S. Giselbrecht, T. Gietzelt, E. Gottwald, C. Trautmann, R. Truckenmüller, K. F. Weibezahn, and A. Welle, Biomed. Microdevices **8**, 191 (2006).
[17]M. W. van der Helm, A. D. van der Meer, J. C. T. Eijkel, A. van den Berg, and L. I. Segerink, Tissue Barriers **4**, e1142493 (2016).
[18]G. L. Suidan, A. Brill, S. F. De Meyer, J. R. Voorhees, S. M. Cifuni, J. E. Cabral, and D. D. Wagner, Arterioscler., Thromb., Vasc. Biol. **33**, 2112 (2013).
[19]K. A. Tran, X. Zhang, D. Predescu, X. Huang, R. F. Machado, J. R. Göthert, A. B. Malik, T. Valyi-Nagy, and Y.-Y. Zhao, Circulation **133**(2), 177–186 (2016).
[20]D. a. Edelman, Y. Jiang, J. G. Tyburski, R. F. Wilson, and C. P. Steffes, J. Trauma **62**, 89 (2007).
[21]A. Ghosh, T. Birngruber, W. Sattler, T. Kroath, M. Ratzer, F. Sinner, and T. R. Pieber, PLoS One **9**, 3 (2014).
[22]D. Jansson, J. Rustenhoven, S. Feng, D. Hurley, R. L. Oldfield, P. S. Bergin, E. W. Mee, R. L. Faull, and M. Dragunow, J. Neuroinflammation **11**, 104 (2014).
[23]W. A. Banks, A. M. Gray, M. A. Erickson, T. S. Salameh, M. Damodarasamy, N. Sheibani, J. S. Meabon, E. E. Wing, Y. Morofuji, D. G. Cook, and M. J. Reed, J. Neuroinflammation **12**, 223 (2015).
[24]D. B. Stanimirovic, M. Bani-Yaghoub, M. Perkins, and A. S. Haqqani, Expert Opin. Drug Discovery **10**, 141 (2015).
[25]H. Cho, J. H. Seo, K. H. K. Wong, Y. Terasaki, J. Park, K. Bong, K. Arai, E. H. Lo, and D. Irimia, Sci. Rep. **5**, 15222 (2015).
[26]A. Herland, A. D. van der Meer, E. A. FitzGerald, T.-E. Park, J. J. F. Sleeboom, and D. E. Ingber, PLoS One **11**, e0150360 (2016).
[27]J. H. Yeon, D. Na, K. Choi, S.-W. Ryu, C. Choi, and J.-K. Park, Biomed. Microdevices **14**, 1141 (2012).
[28]R. Booth and H. Kim, "Characterization of a microfluidic *in vitro* model of the blood-brain barrier (μBBB)," Lab Chip **12**(10), 1784 (2012).
[29]B. Prabhakarpandian, M.-C. Shen, J. B. Nichols, I. R. Mills, M. Sidoryk-Wegrzynowicz, M. Aschner, and K. Pant, "SyM-BBB: A microfluidic blood brain barrier model," Lab Chip **13**(6), 1093–1101 (2013).
[30]J. A. Brown, V. Pensabene, D. A. Markov, V. Allwardt, M. Diana Neely, M. Shi, C. M. Britt, O. S. Hoilett, Q. Yang, B. M. Brewer, P. C. Samson, L. J. McCawley, J. M. May, D. J. Webb, D. Li, A. B. Bowman, R. S. Reiserer, and J. P. Wikswo, Biomicrofluidics **9**, 054124 (2015).

[31]B. B. Weksler, E. A. Subileau, N. Perrière, P. Charneau, K. Holloway, M. Leveque, H. Tricoire-Leignel, A. Nicotra, S. Bourdoulous, P. Turowski, D. K. Male, F. Roux, J. Greenwood, I. A. Romero, and P. O. Couraud, FASEB J. **19**, 1872 (2005).
[32]E. W. Young and C. A. Simmons, "Macro- and microscale fluid flow systems for endothelial cell biology," Lab Chip **10**(2), 143–160 (2010).
[33]M. W. Toepke and D. J. Beebe, "PDMS absorption of small molecules and consequences in microfluidic applications," Lab Chip **6**(12), 1484–1486 (2006).
[34]K. J. Regehr, M. Domenech, J. T. Koepsel, K. C. Carver, S. J. Ellison-Zelski, W. L. Murphy, L. A. Schuler, E. T. Alarid, and D. J. Beebe, "Biological implications of polydimethylsiloxane-based microfluidic cell culture," Lab Chip **9**(15), 2132–2139 (2009).
[35]R. Thuenauer, E. Rodriguez-Boulan, and W. Römer, "Microfluidic approaches for epithelial cell layer culture and characterisation," Analyst **139**, 3206–3218 (2014).
[36]P. A. Carpentier, U. Haditsch, A. E. Braun, A. V. Cantu, H. M. Moon, R. O. Price, M. P. Anderson, V. Saravanapandian, K. Ismail, M. Rivera, J. M. Weimann, and T. D. Palmer, J. Neurosci. **33**, 16874 (2013).
[37]A. A. Tronnes, J. Koschnitzky, R. Daza, J. Hitti, J. M. Ramirez, and R. Hevner, Reprod. Sci. **23**(6), 771–778 (2016).
[38]H. Soumiya, H. Fukumitsu, and S. Furukawa, J. Neurosci. Res. **89**, 1575 (2011).
[39]E. S. Lippmann, S. M. Azarin, J. E. Kay, R. A. Nessler, H. K. Wilson, A. Al-Ahmad, S. P. Palecek, and E. V. Shusta, "Derivation of blood-brain barrier endothelial cells from human pluripotent stem cells," Nat. Biotechnol. **30**(8), 783–791 (2012).
[40]E. S. Lippmann, A. Al-Ahmad, S. M. Azarin, S. P. Palecek, and E. V. Shusta, Sci. Rep. **4**, 4160 (2014).

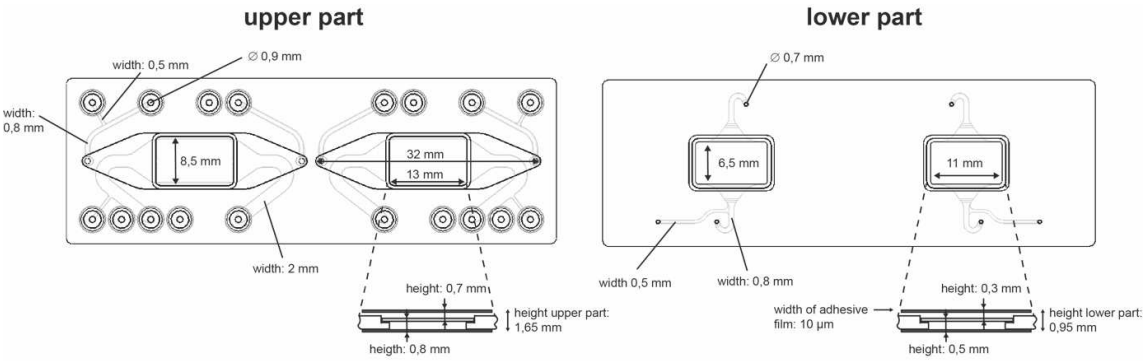

Supplementary Figure 1. Technical drawing of the upper and lower parts of the biochip specifying the sizes of individual structures. All micro-channels have a depth of 0.4 mm. In the indicated zoomed sections (dashed lines) the height from the membrane to respective bonding foil of each part of the biochip is shown.

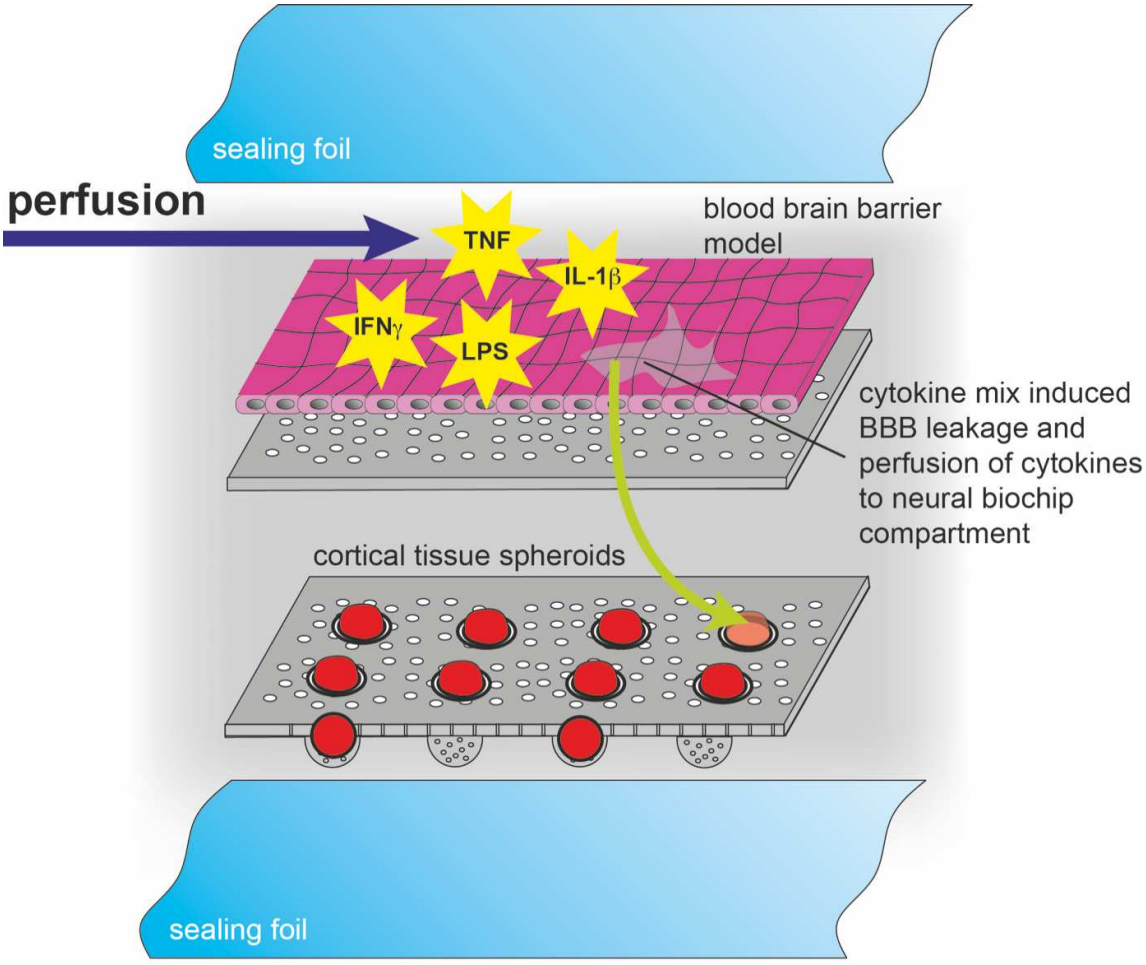

Supplementary Figure 2. Scheme of the cytokine-induced leakage of the endothelial barrier and diffusion of cytokines to the neural spheroid comportment of the biochip.

Manuscript IV

Crossing the blood-brain barrier: Glutathione-conjugated poly(ethylene imine) for gene delivery

Englert, C., Trützschler, A. K., Raasch, M., Bus, T., Borchers, P., Mosig, A. S., Träger, A. and Schubert, U. S. (2016)

Journal of Controlled Release 241: 1-14

The targeted drug delivery to the central nervous system represents one of the major challenges that pharmaceutical research must deal with. Glutathione (GSH) was recently identified as potential candidate to facilitate receptor-mediated transcytosis of nanocarriers. The previously published simplified model of the BBB based in an improved MOTiF biochip design was tested in an application study. Different pDNA polyplex forming L-GSH-coupled poly (ethylene imine) (PEI) polymers were analysed regarding microvascular interaction and translocation. The study emphasises on (i) the influence of GSH-decorated polymer composition on basic polyplex characteristics, (ii) GSH loading and synthesis strategy-dependent amino group class on cellular interaction and (iii) the ability to cross the BBB and deliver fluorescently labelled genetic material. We demonstrated that BBB passage depends on amine side chains used and GSH ratio within the polymers with improved performance for secondary amines. We further proofed the feasibility of GSH-coupling to enhance nanocarrier passage through the BBB and outline this technique as promising tool for targeted gene delivery to the central nervous system.

author contribution (25 %): hCMEC cell culture, preparation of biochip, preparation of polyplex stocks, performing biochip polyplex perfusion experiments, time-dependent sampling, immunofluorescence staining and microscopy, analysis of data, preparation of figures, co-writing the manuscript.

Journal of Controlled Release 241 (2016) 1–14

Contents lists available at ScienceDirect

Journal of Controlled Release

journal homepage: www.elsevier.com/locate/jconrel

Crossing the blood-brain barrier: Glutathione-conjugated poly(ethylene imine) for gene delivery

Christoph Englert [a,b,1], Anne-Kristin Trützschler [a,b,1], Martin Raasch [c,d], Tanja Bus [a,b], Philipp Borchers [a,b], Alexander S. Mosig [b,c,d,*], Anja Traeger [a,b,**], Ulrich S. Schubert [a,b,***]

[a] Laboratory of Organic and Macromolecular Chemistry (IOMC), Friedrich Schiller University Jena, Humboldtstrasse 10, 07743 Jena, Germany
[b] Jena Center for Soft Matter (JCSM), Friedrich Schiller University Jena, Philosophenweg 7, 07743 Jena, Germany
[c] Institute of Biochemistry II, Jena University Hospital, Nonnenplan 2-4, 07743 Jena, Germany
[d] Center for Sepsis Control and Care, Jena University Hospital, Erlanger Allee 101, 07747 Jena, Germany

ARTICLE INFO

Article history:
Received 29 June 2016
Received in revised form 24 August 2016
Accepted 28 August 2016
Available online 30 August 2016

Keywords:
Poly(ethylene imine)
Blood-brain barrier
Microfluidic biochip
L-Glutathione
Non-viral gene delivery

ABSTRACT

The targeted drug delivery to the central nervous system represents one of the major challenges in pharmaceutical formulations since it is strictly limited through the highly selective blood-brain barrier (BBB). L-Glutathione (GSH), a tripeptide and well-known antioxidant, has been studied in the last years as potential candidate to facilitate the receptor-mediated transcytosis of nanocarriers. We thus tested whether GSH decoration of a positively charged polymer, poly(ethylene imine), with this vector enables the transport of genetic material and, simultaneously, the passage through the BBB. In this study, we report the synthesis of GSH conjugated cationic poly(ethylene imine)s *via* ecologically desirable thiol-ene photo-addition. The copolymers, containing 80% primary or secondary amine groups, respectively, were investigated concerning their bio- and hemocompatibility as well as their ability to cross a hCMEC/D3 endothelial cell layer mimicking the BBB within microfluidically perfused biochips. We demonstrate that BBB passage depends on the used amino-groups and on the GSH ratio. Thereby the copolymer containing secondary amines showed an enhanced performance. We thus conclude that GSH-coupling represents a feasible and promising approach for the functionalization of nanocarriers intended to cross the BBB for the delivery of drugs to the central nervous system.

1. Introduction

Discovered by Paul Ehrlich in 1885 and named by Max Lewandowsky in 1900, the blood-brain barrier (BBB) is known as one of the most challenging obstacles concerning the delivery of drugs and therapeutic nucleic acids [1,2]. Within the BBB, specialized endothelial cells of the cerebral vasculature (cerebral microvascular endothelial cell, CMEC) form an endothelial layer that strictly regulates the passage of small molecules. The tightness of the BBB is furthermore regulated by astrocytes and pericytes that are in direct contact with the CMECs [3]. The BBB passage of molecules depends on several parameters, including the molecular size, lipid solubility, hydrophilicity, and the degree of dissociation. The passage of macromolecules as well as of 98% of small molecules (<400 g mol^{-1}) is prevented under physiological conditions [4]. Besides the passive transport, which comprises the diffusion of small molecules [5], the active transport of amino acids and macromolecules such as transferrin is described to be mediated by carrier proteins or transcytosis [6]. While the transport of different amino acids is well-investigated [7], the transport of L-glutathione (GSH), a tripeptide which is known as antioxidant that lowers the oxidative stress level within the brain, is currently under investigation [8–10].

In order to circumvent the BBB, several methods including the invasive direct injection into the central nervous system (CNS) and the non-invasive nasal delivery of nanoparticular and liposomal carriers as well as of covalently targeted small molecules have been investigated [11,12]. However, nasal delivery possesses the difficulty to adjust the therapeutic delivery due to individually varying absorption profiles, limited volume and long term side effects [11].

Introducing targeting molecules to nanocarriers is the key to benefit from the active transporting systems and to enable also the passage of larger drugs. Non-viral receptor- and adsorptive-initiated transcytosis, as well as carrier-mediated transport can be used for an active transcellular vector-based drug delivery. By using larger biomolecules like antibodies and peptides [13,14], additional surface modifications like PEGylation and polysorbate 80 ("Tween 80" or polyoxyethylene(20)

* Correspondence to: A.S. Mosig, Center for Sepsis Control and Care, Jena University Hospital, Erlanger Allee 101, 07747 Jena, Germany.
** Correspondence to: A. Traeger, Jena Center for Soft Matter (JCSM), Friedrich Schiller University Jena, Philosophenweg 7, 07743 Jena, Germany.
*** Correspondence to: U.S. Schubert, Laboratory of Organic and Macromolecular Chemistry (IOMC), Friedrich Schiller University Jena, Humboldtstrasse 10, 07743 Jena, Germany.
E-mail addresses: alexander.mosig@med.uni-jena.de (A.S. Mosig), anja.traeger@uni-jena.de (A. Traeger), ulrich.schubert@uni-jena.de (U.S. Schubert).
[1] The authors contributed equally to this work.

http://dx.doi.org/10.1016/j.jconrel.2016.08.039
0168-3659/

sorbitan monooleate) [15] or small molecule conjugation (such as GSH), BBB passage could be revealed successfully [16–19]. The latter has been successfully used to modify nanoparticles for drug delivery resulting in an enhanced passaging ability of the BBB [20,21]. Recently, Grover et al. combined two known techniques to create a novel nanoparticle system (PEGylation and GSH coating), while Gaillard *et al.* showed the improvement of the BBB passage using liposomal carrier systems [20,21]. The 2-BBB company has already started with two clinical trials regarding liposomal based PEGylated and GSH decorated particles bearing doxorubicin and methylprednisolone [22]. At the end of 2014 positive results from phase 1 were announced showing a BBB passage and anti-tumor properties. This reveals that the decoration with GSH seems to be a promising targeting approach also for other carrier systems. While the choice of targeting molecules influences the transcytosis efficiency, the nanocarrier material should be adopted to the transported drug. Therefore, synthetic as well as natural polymers (*e.g.* polysaccharides, proteins) have been used for the transport of drugs and genetic material [23]. Among others, polybutylacrylate (polysorbate 80) [24] and PLA/PGA or PLGA (TAT [25] or polysorbate 80 [26]) have been successfully established in *in vivo* tests for the encapsulation of hydrophobic drugs. In order to enable nucleic acid delivery to the central nervous system (as novel treatment option of neuronal-related diseases), there is an urgent need for appropriate binding nanocarriers. Cationic polymers, in particular poly(ethylene imine) (PEI), represent a class of suitable candidates for the complexation of genetic material by electrostatic interactions [27]. Due to its superior buffering ability enabling endosomal escape, PEI is known as the gold standard of polymeric carriers for gene delivery *in vitro* [28]. However, its potential is accompanied with high cytotoxicity and non-biodegradability [29]. The functionalization of the linear PEI backbone [30] and the addition of side chains, creating copolymers, represent a powerful strategy to overcome these limitations and have been extensively studied attaching various carbohydrates [31–33] or polymers like poly(ethylene glycol) [34].

However, these *in vitro* studies were based on standard cell culture techniques under static culture conditions. Shear forces as observed *in vivo* and their impact on endothelial cells [35] as first cells to come in contact with administered drugs have not been addressed. Microfluidics can serve as a tool to reduce this transferability gap. Recently, we reported a microfluidically supported biochip model of the BBB with the proof-of-concept of the modulation of the BBB permeability by inflammatory cytokines [36]. To mimic the cerebral endothelial cell layer of the BBB, hCMEC/D3 cell layers have been used that specifically express cerebral endothelial marker proteins including cell adhesion and tight junction proteins as well as CNS related transporter proteins. *In vitro* the cell line forms a tight endothelial cell layer that shows similarities with the BBB even in the absence of astrocytes or pericytes [37–39]. Thus HCEMC/D3 cells were already used in various BBB models [40,41] for mechanistically studies on leukocyte transmigration [42], nanoparticle uptake and transcytosis [43,44].

In this study, we describe for the first time a nanocarrier design that combines vector as well as charge optimized properties for crossing the BBB and that enables complexation of nucleic acids. We focused on the installation of GSH moieties on the backbone of high molar mass linear PEI. A post-polymerization functionalization process was applied to obtain double bond functionalities and defined quantities of cationic ethylene imine units. Since reduced GSH provides a free thiol end group, thiol-ene photo-addition was used to modify the PEI backbone avoiding potentially hazardous metal catalysts. Comparable amounts of primary amine groups in the polymer side chain were installed in a second approach on the PEI backbone for an enhanced polyplex stability. The copolymers were characterized concerning their polyplex formation, toxicity, hemocompatibility and their potential to deliver nucleic acids across the BBB. We want to demonstrate that polyplexes, formed by GSH-modified PEI-based polymers and plasmid DNA, are able to cross an endothelial cell model of the BBB under physiological shear stress of 4 dyn cm^{-2}.

2. Results and discussion

To conjugate GSH to a cationic polymer backbone (using a poly(ethylene imine)-derivative), the thiol-ene photo-addition reaction was utilized. It can be performed under mild conditions (no thermal energy, no toxic metal catalysts) without generating harmful side products. The solubility properties of GSH limits the click reaction to water. To investigate the influence of different amine functionalities on the balance between stable polyplex formation and BBB passage, materials either containing solely secondary amines or bearing additional primary amines were synthesized.

2.1. Polymer synthesis

The homopolymer poly(2-ethyl-2-oxazoline) (PEtOx) was synthesized according to literature procedure [9]. For this purpose, the cationic ring-opening polymerization (CROP) of the monomer 2-ethyl-2-oxazoline was performed in a microwave reactor. The precursor revealed a degree of polymerization of 575 (calculated from the tosylate ^{1}H-NMR signal integrals of MeOTos before purification) and a dispersity of 1.3 (SEC: DMAc, 0.21% LiCl, calibration: polystyrene). PEtOx was further treated with half-concentrated hydrochloric acid and heated to reflux overnight [45]. The resulting linear poly(ethylene imine) (**P1**) exhibited a degree of hydrolysis of > 95% (calculated from ^{1}H-NMR). **P1** served as the main polymer for the installation of all functionalities including the GSH moieties. To investigate the influence of different cationic charges on the biocompatibility and the DNA binding affinity, primary as well as secondary amine functionalities were introduced to the polymer backbone besides the GSH functionalities [46]. This versatile approach required two different synthesis pathways (see Scheme 1).

The first one comprises of the partial functionalization of linear poly(ethylene imine) (**P1**) with *N*-succinimidyl-4-pentenate to introduce double bond functionalities yielding the P(EI-*stat*-ButEnOx) copolymer (**P2**) (see Scheme 1a, strategy I) [47]. Since the homopolymer poly(2-butenyl-2-oxazoline) (which can be synthesized by a CROP of the respective monomers) does not withstand the conditions of acidic or basic hydrolysis, the mentioned post-polymerization modification strategy was applied. Preliminary studies of copolymers consisting of varying contents of ethylene imine (EI) and 2-butenyl-2-oxazoline units (ButEnOx) resulted in a critical amount of EI units required for the formation of stable polyplexes [47]. Therefore, a ButEnOx content of 27% was installed onto the backbone of **P1**, resulting in an EI content of 78% (**2**) (see Table 1). The introduction of GSH (reduced state, for the schematic representation of the structure see Scheme 1) was performed by a thiol-ene photoaddition while maintaining a constant EI content of 78% (Scheme 1c). Since GSH shows only limited solubility properties, the click reaction was performed in water utilizing the photoinitiator Irgacure® 2959. The full conversion resulted in the copolymer P($EI_{73\%}$-*stat*-$GluButOx_{27\%}$) (**3**).

In a second approach primary amine moieties were installed on the polymer backbone to investigate their influence on the interaction with DNA. While primary amine groups are known to promote superior complexation of nucleic acids [48,49], secondary amines reveal an enhanced buffer capacity resulting in a fast endosomal release [50]. The previously mentioned modification strategy was used (Scheme 1a, strategy II) to synthesize a fully functionalized poly(2-butenyl-2-oxazoline) (**P4**). Subsequently, the protected aminothiol was added to **P4** under UV irradiation (Scheme 1b) to yield the copolymer P(bocAmButOx$_{82\%}$-*stat*-ButEnOx$_{18\%}$) (**P5**) (Table 1). In a second photo-addition step, reduced GSH was introduced to the backbone of **P5** analog to the previously described first synthesis route (Scheme 1c, strategy II). Under these conditions, the conversion of the double bonds was incomplete (56% of the origin double bond functionalities remained), even after an additional functionalization step. Almost certainly, the content of flexible side chains containing sterically demanding protection groups hinders the full modification. Furthermore, the introduction of a defined amount

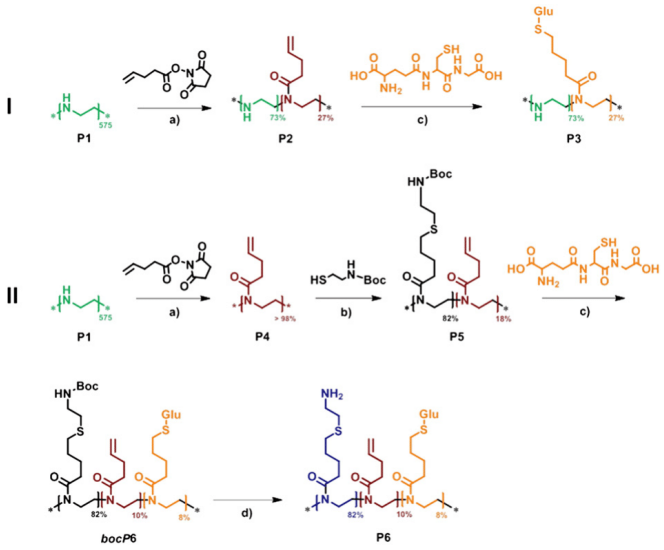

Scheme 1. Schematic representation of the synthesis of I) P(EI-*stat*-GluButOx) (**P3**) and II) P(AmButOx-*stat*-ButEnOx-*stat*-GluButOx) (**P6**), respectively. a) Functionalization of linear poly(ethylene imine) (**P1**). b) Thiol-ene photo-addition of *tert*-butyl-(2-mercaptoethyl)carbamate to the copolymer backbone. c) Thiol-ene photo-addition of L-glutathione to the copolymer backbone. d) Deprotection of primary amine side chains.

of bulky GSH (~8%) could result in an additional hindrance, which limits the degree of functionalization. The deprotection of ***boc*P6** (Scheme 1d) resulted in the final polymer P(AmButOx$_{82\%}$-*stat*-ButEnOx$_{10\%}$-*stat*-GluButOx$_{8\%}$) (**P6**). Focusing on the amount of amine groups within the copolymers, a comparison of **P3** and **P6** concerning this point is part of further investigations.

Characterization by ^{1}H-NMR spectroscopy (Fig. 1) confirmed the almost complete hydrolysis of PEtOx revealing one main signal for the backbone of **P1** between 3.70 and 3.20 ppm (NR—CH_2—CH_2, A). In addition, 5% remaining 2-ethyl-2-oxazoline units can be found. The appearance of the double bond signals for **P2** at 5.81 ppm (CH_2═CH—, E) and 4.95 ppm (CH_2═CH—, F) confirm the successful functionalization with *N*-succinimidyl-4-pentenate. The former signal is compared to the unaffected ethylene imine backbone to determine the composition of the formed copolymer **P2** (degree of functionalization: 27%). The disappearance of the double bond signals after the thiol-ene photoaddition confirmed the complete functionalization with GSH. Besides the additional protons observed after the click reaction (E′ and F′), the signals of GSH can be assigned to the respective protons (see Fig. 1). The very specific GSH signal for the CH group of the cysteine unit appears at 4.54 ppm (NR—CH—CH_2—S, H).

The complete functionalization of **P1** resulted in polymer **P4**, indicated by the disappearance of the signals assigned to the ethylene imine backbone (between 3.70 and 3.20 ppm) (see Fig. 2). Instead, the signals assigned to the double bonds at 5.8 ppm (CH_2═CH—, D) and 4.96 ppm (CH_2═CH—, E) as well as to the backbone (3.45–3.53, NR—CH_2—CH_2, A) could be observed. The successful attachment of side chains bearing primary amine groups and GSH moieties is shown by the CH_2 signals nearby the amine group around 2.8 ppm (NH_2—CH_2—CH_2), the signal of the *boc*-protecting group which disappears after deprotection (1.4 ppm, CH_3 boc) and the specific GSH protons of **P6**.

The composition of the prepared polymers (and respective intermediates) is depicted in Table 1. Asymmetric flow field-flow fractionation (AF4) was utilized to determine the molar masses of the starting polymer **P1** and the final products **P3** and **P6**. Since the intermediates reveal different solubility behaviors, another characterization method had to be chosen. Therefore, size exclusion chromatography (SEC) was used to determine the molar masses of **P2**, **P4**, **P5** and ***boc*P6**. However, in both cases the presence of cationic amine units (primary or secondary) and/or double bond functionalities resulted in undesired column and membrane interactions and, therefore, a change in the elution behavior (increased dispersities) [51,52]. Although the obtained values indicate lower molar masses compared to the calculated values, a trend is visible.

To confirm the successful photo-addition of GSH and the formation of a single (polymeric) species (**P3**, **P6**), diffusion-ordered NMR spectroscopy (DOSY NMR) was performed. GSH clearly revealed a higher diffusion coefficient compared to the polymeric species. The decreasing values for the GSH decorated **P2** indicate an increase of the hydrodynamic radius of **P3** in solution (Fig. 3A). This can be explained by the bulky GSH moiety. Comparable results are obtained for **P6** (Fig. 3B).

2.2. Bio- and hemocompatibility

Biocompatibility represents a critical parameter for potential non-viral vectors in biomedical applications. *In vitro* studies were performed using the precursor **P2** and the final GSH-conjugated polymers **P3** and **P6** in comparison to the linear PEI (**P1**) to evaluate their bio- and hemocompatibility (Fig. 4A and Supporting information Fig. S1). **P4** and **P5** were excluded due to their insolubility in aqueous media. **P1** exhibited a high cytotoxicity at low polymer concentrations (IC_{50} of ~4 μg mL^{-1}) because of its high molar mass and cationic charge density (leading to membrane damages followed by the possible initiation of apoptosis [53,54]). Interestingly, the attachment of 27% GSH resulted in a strong reduction of the cytotoxicity. **P3** revealed an IC_{50} value of

Table 1
Composition and molar masses for (*co*-)polymers **P1** to **P6**.

		Composition[a]			NMR[b]	AF4		SEC[c,d]	
		X	Y	Z	Mn	Mn	Đ	Mn	Đ
Abr.	Name	[%]	[%]	[%]	[gmol^{-1}]	[gmol^{-1}]		[gmol^{-1}]	
P1	$LPEI_x$	>98	0	0	24,800	9900	1.4	n.d.	n.d.
P2	$P(EI_x$–*stat*–$ButEnOx_y)$	73	27	0	37,500	n.d.	n.d.	31,400[c]	1.2
P3	$P(EI_x$–*stat*–$GluButOx_z)$	73	0	27	85,200	21,000	2.0	n.d.	n.d.
P4	$PButEnOx_y$	0	>98	0	71,900	n.d.	n.d.	44,000[c]	1.5
P5	$P(bocAmButOx_x$–*stat*–$ButEnOx_y)$	82	18	0	155,300	n.d.	n.d.	23,400[d]	1.9
***boc*P6**	$P(bocAmButOx_x$–*stat*–$ButEnOx_y$–*stat*–$GluButOx_z)$	82	10	8	169,500	n.d.	n.d.	38,400[d]	1.7
P6	$P(AmButOx_x$–*stat*–$ButEnOx_y$–*stat*–$GluButOx_z)$	82	10	8	122,300	63,300	1.8	n.d.	n.d.

[a] Determined by ^{1}H NMR (calculated from the ratio of x, y and z signals)

[b] Determined by ^{1}H NMR (calculated from tosylate signals of MeOTos before purification)

[c] SEC 1: $CHCl_3$/*i*PrOH/NEt_3 94:2:4, polystyrene calibration

[d] SEC 2: DMAc, 0.21% LiCl, polystyrene calibration

n.d. – not determined. All polymers soluble in aqueous media and /or insoluble in organic solvents were measured at AF4 – MALS system.

~270 µg mL^{-1} and even polymer concentrations up to 150 µg mL^{-1} revealed nearly no cytotoxic effects (relative viability ≥ 85%). The precursor **P2** also exhibited a lower cytotoxicity compared to **P1** (see Supporting information Fig. S1A). The replacement of the ethylene imine units by flexible primary amine containing side chains for **P6** led to an increased cytotoxicity (IC_{50} value of ~44 µg mL^{-1}) compared to **P3**. Furthermore, the incomplete thiol-ene photoaddition resulted in a lower content of GSH and, likewise, unmodified double bond functionalities, which could both influence the biocompatibility. However,

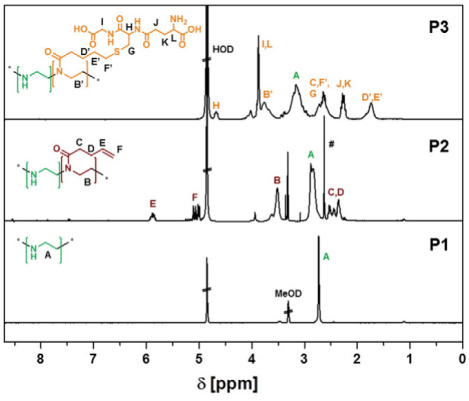

Fig. 1. Comparison of ^{1}H-NMR spectra of **P1** to **P3** (# side product *N*-hydroxysuccinimide) (400 MHz, D_2O/MeOD).

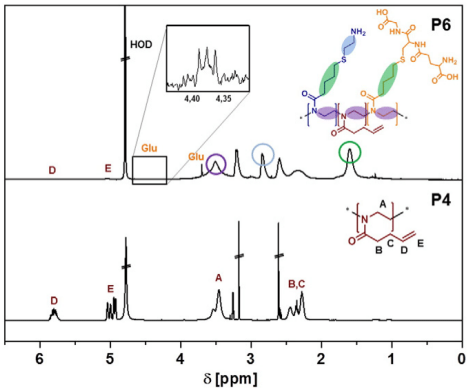

Fig. 2. Comparison of ^{1}H-NMR spectra of **P4** and **P6** (400 MHz, D_2O/MeOD and D_2O).

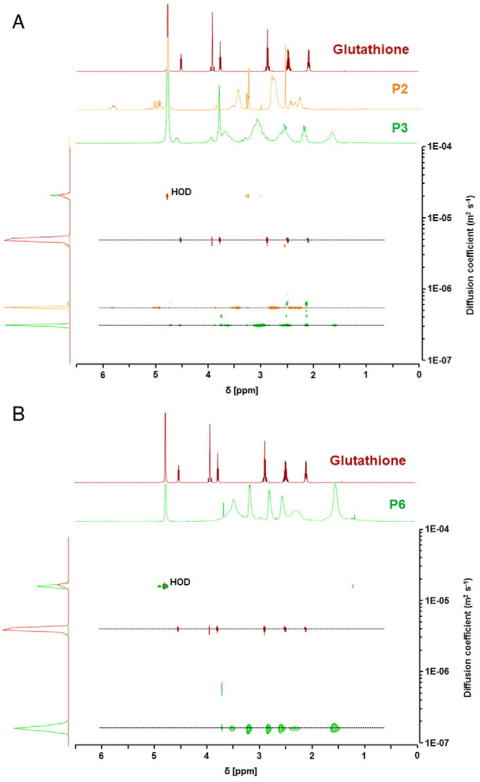

Fig. 3. Diffusion ordered NMR spectra of: A) **P2**, **P3** and L-glutathione and B) **P6** and L-glutathione (400 MHz, D_2O).

polymer concentrations of **P3** and **P6** from 2 to 5 μg mL^{-1} were used for the preparation of polyplexes, which are in an acceptable range beyond the cytotoxicity-inducing concentrations. The cytotoxicity test was not only performed with L292 cells according to the ISO protocol 10993-5 but the assay was also performed with HEK as well as hCMEC/3D cells for a detailed determination of the causal relation of toxicity and related interactions (see Supporting information Fig. S2 A). In static culture the hCMEC revealed a different performance during cytotoxicity tests and showed only 10% relative viability for **P1** at a concentration of 2 μg mL^{-1} and also a decreased viability for **P6** whereas **P3** revealed no cytotoxic effects up to 500 μg mL^{-1}. While the IC_{50} values of **P1** and **P6** decreased up to a 2-fold higher concentration, **P3** showed no cytotoxic effect at all independent of the used cell line (Fig. S2B).

To investigate the blood compatibility of **P2**, **P3** and **P6**, the hemolytic activity as well as the aggregation of erythrocytes was assessed (Fig. 4B, Supporting information Figs. S3 and S4). All investigated copolymers did not show any hemolytic activity in a concentration range from 10 to 100 μg mL^{-1}. **P1** as well as **P2** (SI Fig. S1B) revealed a slightly hemolytic activity at higher concentrations (50 to 100 μg mL^{-1}) indicated by a hemoglobin releases of 2% as well as strong agglomeration of erythrocytes (see Supporting information, Fig. S3). While no agglomeration for **P3** was observed, indicating a good hemocompatibility, **P6** showed distinct interactions with cellular membranes of erythrocytes leading to aggregation. Obviously, the type of amines within the polymer side chain represents a crucial factor for the interaction with cells, in particular with the plasma membrane, and is therefore linked to the biocompatibility properties. This fact was also assumed by Dekie et al. concluding this from glutamic acid derivatives [55]. However, Fischer et al. mentioned that these effects have to be mentioned relative to the polymer class and can also be influenced by factors like charge density (number of amines and three dimensional arrangements) [54].

As reported earlier, primary amines revealed an increased affinity to cellular membranes compared to secondary amines, indicated by a higher toxicity [56]. Tripathi et al. demonstrated the successful reduction of the cytotoxicity by pyridoxyl derivatization of primary amines of branched PEI [57]. This behavior supports the findings observed for **P3** and **P6**.

2.3. Characterization of the polyplexes

An efficient delivery of nucleic acids, like plasmid DNA, into cells depends on several parameters. They comprise of the compact condensation of the genetic material, the masking of negative charges, the prevention of degradation and the efficient dissociation from the vector after transfer into the cellular cytoplasm or nucleus. PEI derivatives, in particular PEI disulfide linked rabies virus glycoprotein, have been shown to enable the delivery of neurogenic microRNA into the brain [58]. To investigate the binding affinity of **P1**, **P2** (SI Fig. S1C), **P3** as

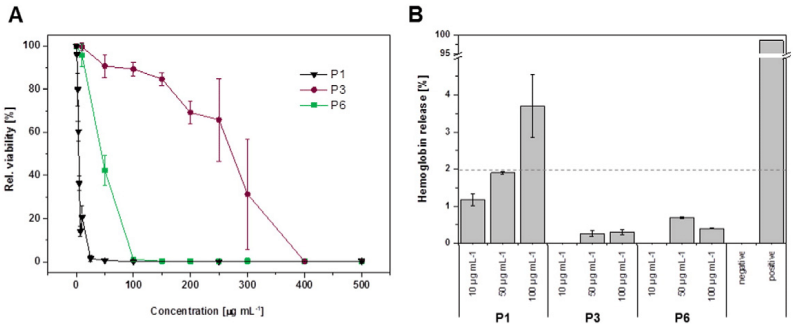

Fig. 4. Bio- & hemocompatibility. A) Relative viability of L929 cells after 24 h incubation with the respective polymers at indicated concentrations. B) Hemolysis assay of erythrocytes after incubation with polymers at indicated concentrations. Triton X-100 was used as positive and PBS as negative control. A value < 2% hemolysis is classified as non-hemolytic, 2–5% as slightly hemolytic and values > 5% as hemolytic. Values represent the mean ± S.D. (n = 3).

well as **P6** with plasmid DNA as model system, the ethidium bromide quenching assay (EBA) was utilized. Polyplexes were formed at different nitrogen (polymer) to phosphate (DNA) ratios (N/P). Due to the electrostatic and hydrophobic interactions between the polymer and the pDNA, ethidium bromide is excluded from its binding sites within the oligonucleotides resulting in a reduction of fluorescence intensity [59,60].

All polymers revealed a decreasing fluorescence intensity with increasing N/P ratios that resulted in a plateau, indicating stable polyplex formation (Fig. 5A and Supporting information Fig. S1D). While the positive control **P1** exhibited a fast polyplex formation starting at N/P 5, **P2**, **P3** and **P6** revealed a stable polyplex formation at higher N/Ps from 20 to 40 reaching 60%, 45% and 30% relative fluorescence units (RFU), respectively. A possible explanation for the slightly lower binding affinity could be the ethylene imine units which are shielded by the bulky GSH moieties as well as a lower zeta potential of **P3** (4.06 mV) compared to **P6** (28.4 mV) (see Table S5). For **P6**, primary amine groups are attached through flexible side chains, which are easier accessible for the pDNA. Additionally primary amines are known to promote pDNA compensation [61].

The heparin dissociation assay was used to analyze the stability and the dissociation behavior of the formed polyplexes [62,63]. Heparin is a natural polyanion with one of the highest density of negative charges and can effectively bind to the positive charged polymers **P3** and **P6**. It competes with the pDNA within the polyplex and forces the release of the nucleic acid. The free nucleic acid is able to rebind free ethidium bromide (added in the same concentration as for the EBA) causing an increase of the fluorescence intensity (Fig. 5B). In the case of the **P3** and **P6** polyplexes, the pDNA was released very fast at low heparin concentrations. While **P3** revealed a reversible binding, reaching 90% dissociation at 10 U mL^{-1} heparin, **P6** showed full dissociation (~100% RFU at 10 U mL^{-1}). In contrast, **P1** required higher concentrations of heparin (40 U mL^{-1}) for almost full release (~95% RFU), which underlines the stability of **P1**/pDNA polyplexes and is in accordance to literature data [46].

An efficient delivery, comprising of the internalization of polyplexes into cells *via* endocytic pathways, requires defined sizes and charges of the complexes. Therefore, critical sizes of polymeric carriers up to 200 nm are recommended [64]. As shown in Table 2, the formed polyplexes of **P3** and **P6** revealed z-averages of 282 nm and 117 nm at a N/P ratio of 20, respectively, which are calculated from the correlation function. Since the intensity of the particle scattering is proportional to the sixth power of its diameter (Rayleigh approximation), larger particles or agglomerates of free polymer chains result in comparatively more light scattering and higher intensity than smaller ones. Therefore, the intensity-weighted diameters (z-averages) determined by dynamic light scattering are supplemented by the number-weighted sizes revealing a calculated number percentage over 95. Although the calculated sizes can only be seen as informative basis, they are in good agreement with the favorable size of polyplexes. The zeta potential changes during the synthesis from well-known positive charged **P1** (28.4 mV) to the GSH bearing conjugate **P3** (−6.9 mV). In this case, a potential explanation could be that the positive charge of the former PEI backbone is complexing the DNA meanwhile the GSH carboxylic acid moieties are present at the outside of the polyplex resulting in a negative value of −6.9 mV while the precursor **P2** showed comparable size and zeta potential as **P1**. The results of **P2** can be found in the Supporting information, Table S6. The change in charge cannot be observed in the case of **P6**. Here, the lower content of GSH and the side chains with more flexible primary amines reduce the effect of the GSH functionalities.

Table 2
Size and zeta potential measured in 20 mM 4-(2-hydroxethyl) piperazine-1-ethanesulfonic acid (HEPES) and 5% (w/v) glucose, pH 7.2 of pDNA complexes of **P1**, **P3** and **P6** at N/P 20 measured by dynamic light scattering.

Polymeric system	z-Average [d/nm]	PDI	Number-weighted size [d/nm]	Zeta potential [mV]
P1	132 ± 28	0.24	61 ± 18	28.4 ± 2.7
P3	282 ± 5	0.38	109 ± 18	−6.9 ± 0.1
P6	117 ± 1	0.31	61 ± 16	33.2 ± 1.5

2.4. Uptake efficiency

To investigate the potential of the different polymers to deliver nucleic acids, cellular uptake studies were performed with adherent human embryonic kidney (HEK) cells as well as hCMEC/3D in OptiMEM and EndoGro media (see Supporting information, Figs. S7 and S8). For this purpose, YOYO-1 labeled pDNA was used for the polyplex formation at N/P 20 to detect the time-depended cellular internalization by flow cytometry. A fast polyplex uptake in HEK cells was revealed for **P6** polyplexes exhibiting ~50% internalization after 15 min, >80% internalization after 1 h, and a nearly complete uptake of polyplexes after 2 to 4 h similar to **P1**. Taking the aggregation data of **P6** into account, the strong interaction with the cellular membrane, led to enhanced uptake efficiency. In contrast, **P3** polyplexes exhibited only poor uptake efficiencies with <10% of HEK cells positive for internalized **P3** polyplexes (Fig. 6A). These results were also confirmed by life cell imaging after 1 h (Fig. 6B). Interestingly, the precursor of **P3** without GSH, **P2**, exhibited

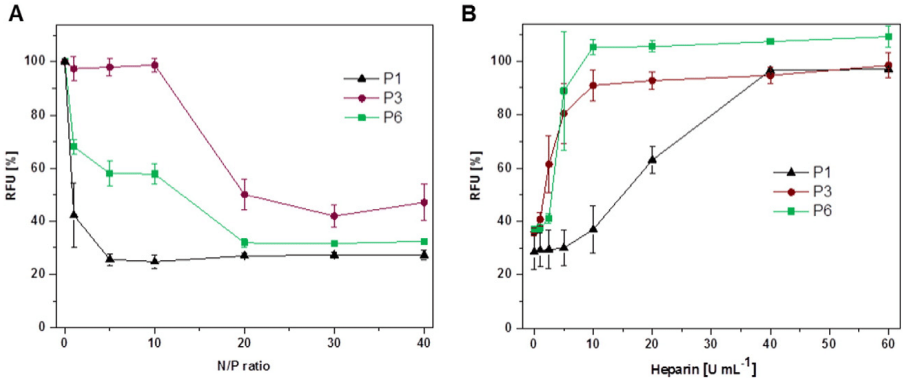

Fig. 5. Polyplex formation and stability with pDNA using the polymers **P1**, **P3** and **P6**. A) Complexation affinity (ethidium bromide quenching assay) of respective polymers at indicated N/P ratios. B) Dissociation assay of polyplexes formed at N/P 40 using heparin (0 to 60 U mL^{-1}). Values represent the mean ± S.D. (n = 3).

an enhanced polyplex uptake comparable to **P6** (see Supporting information, Fig. S1E). Compared to HEK cell experiments the uptake of **P6** decreased in hCMEC/3D cells independently from the culture media used to 20 to 40%. In contrast, the results of **P1** and **P3** uptake did not changed significantly.

Taking the MFI of uptaken pDNA into account, comparable results were also obtained for the transfection efficiencies of the polymers **P1**, **P3** and **P6 in HEK cells**. A transfection efficiency of over 60% of HEK cells was achieved for **P1**, whereas reduced transfection efficiencies were found for **P3** and **P6** of around 30% and 5%, respectively (see Supporting information, Fig. S9).

2.5. Blood-brain barrier passaging performance within the biochip approach

The GSH modified polyplexes were subsequently investigated towards their ability to cross the endothelial layer of the BBB. HCMEC/D3 cells resembling the cerebral endothelial cell layer of the BBB were cultured on a suspended membrane within MOTiF biochips that were recently shown to enable an improved culture of endothelial cells under physiological perfusion conditions [65]. Here, the membrane serves as a cell substrate that is perfused from the apical side of the endothelial cell layer. The cells were grown until full confluence to form a densely packed layer (see Supporting information, Fig. S10). Additionally, immunofluorescence staining for characteristic adherens and tight junction proteins was performed to confirm the integrity of the microvascular endothelial layer before perfusion (see Fig. 7, first row). HCMEC exhibit prominent staining of VE-Cadherin, a key component of adherens endothelial junction and mediator of Claudin-5 expression [66]. Claudin-5 is the main claudin-class protein expressed in BBB endothelial cells and a key regulator of its permeability [67]. Another VE-Cadherin regulated protein is β-Catenin, which plays an important role in maintenance of the BBB integrity and related signaling [68,69]. In addition, we investigated the distribution of occludin, another protein important for tight junction formation and for regulating paracellular permeability [70]. Occludin is associated with cytoplasmic scaffolding and regulatory protein ZO-1 [3]. Claudin-5, β-Catenin, ZO-1 and occludin were found all expressed and localized to intercellular junctions formed by hCMEC. Perfusion with precursor polymer **P1** resulted in a significant loss of endothelial junctional markers (see Fig. 7). Arrowheads indicate a reduced staining of the proteins at the intercellular contacts. This observation is in accordance to the results obtained for the biocompatibility of **P1** on L929 cells (see Fig. 4A) as well as on hCMEC (see Supporting information S2). In flow experiments hCMEC seem to be rendered more susceptible to PEI uptake since already a concentration of 0.1 μg mL^{-1} revealed a strong impact on the cell viability (see Fig. 4A). In 2006 Mennesson et al. already showed that an increase in the polyplex-cell membrane interaction and binding capabilities under flow conditions is altered by shear and sedimentation velocity forces [71]. As demonstrated in hemocompatibility tests, **P1** leads to erythrocyte aggregation and, therefore, to strong membrane interactions. We speculate that in the presence of flow this interaction could

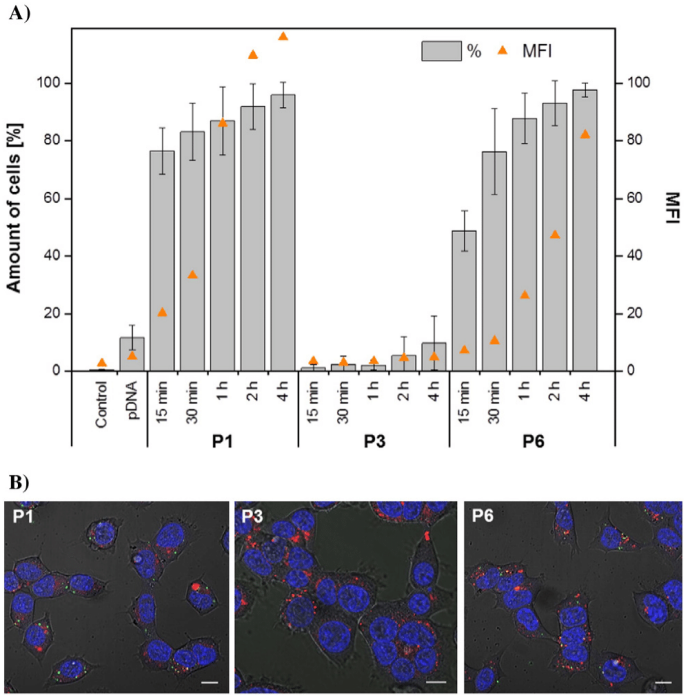

Fig. 6. Cellular uptake study of **P1**, **P3** and **P6** polyplexes (N/P 20) using YOYO-1 labeled pDNA. A) HEK cells were treated with polyplexes for 15 min to 4 h and uptake was analyzed *via* flow cytometry (MFI – mean fluorescence intensity). Values represents the mean ± S.D. (n = 3). B) Confocal microscopy of HEK cells, which were incubated for 1 h with polyplexes (green). Cell nuclei were stained with Hoechst (blue), lysosomes with LysoTracker Red (red). Scale bar = 10 μm.

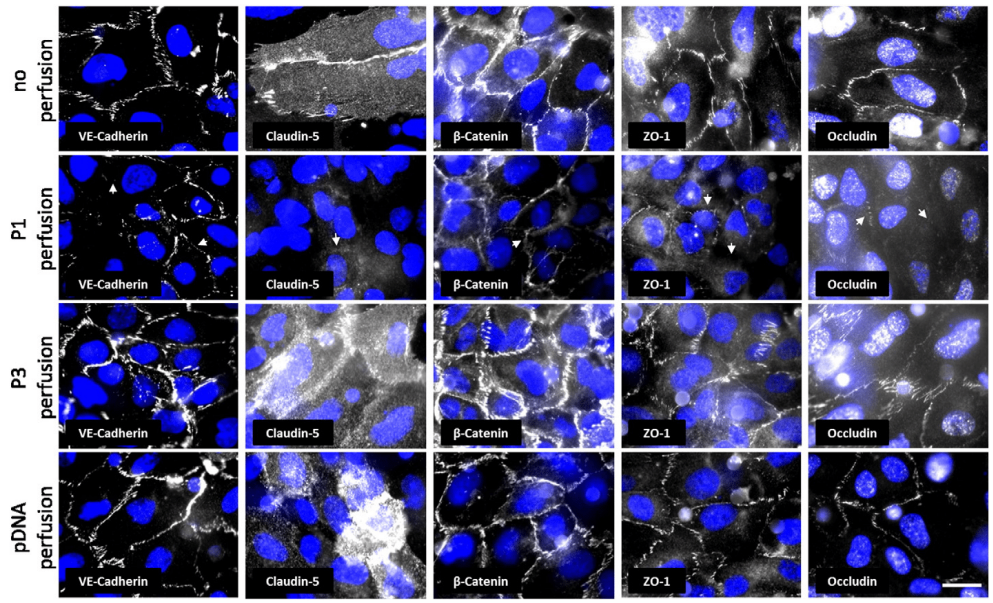

Fig. 7. Expression of BBB relevant junctional marker proteins before and after polyplex perfusion. pDNA served as control group. Arrowheads show breakdown or diminished expression of adherens (VE-Cadherin) and tight junction components evoked by polyplex **P1**. Nuclei are stained in blue (scale bar 20 nm, n = 3).

be promoted which results in a disruption of tight junctions and increased cytotoxicity. In contrast, perfusion with polyplex **P3** as well as free pDNA, serving as control, revealed no impact on adherens or tight junction formation (see Fig. 7). We thus conclude that under flow conditions the tightness of the hCMEC layers is not impaired by the polyplexes, except for polyplex **P1**.

The biochip design allows the quantification of nanoparticles taken up by the endothelial layer through fluorescence measurements as well as the exact determination of the total amount of polyplexes that crossed the endothelial barrier. The imperviousness of the model system, in particular for the endothelial cell layer, was proven for YOYO-1 labeled pDNA without nanocarrier (see Supporting information, Fig. S11). In order to demonstrate the need of glutathione moieties for a successful passage, the precursor **P2** was investigated for comparison reasons. For the polyplex **P6**, we observed the highest uptake into the endothelial cell layer that was associated with a polyplex aggregation (Fig. 8A; see also Supporting information Fig. S3), which was also observed in kinetic studies using HEK cells. In contrast, polyplexes **P1** and **P2** show a lower enrichment at the endothelial layer. **P3** exhibited the weakest enrichment within the endothelial layer compared to other polymers. An image analysis of the quantitative uptake revealed that the internalization of the polyplex **P6** within the endothelial barrier was significantly higher compared to the internalization of the polyplexes **P1** and **P2**, respectively (Fig. 8B). Interestingly, the highest difference in the endothelial uptake of all polyplexes tested was observed for **P3,** even with a significant difference regarding the GSH free precursor **P2** (see Fig. S12).

To further elucidate the trans-endothelial transport of the different polyplexes, we measured its enrichment in the lower chamber underneath the endothelial barrier of the biochip (Fig. 8C). GSH was reported to facilitate a crossing of the nanocarriers through the BBB [21]. We thus tested whether pDNA bound to **P3** could be delivered through the endothelial barrier more efficiently than polyplexes **P1**, **P2** or **P6** (high uptake efficiency and strong interaction with endothelial layer). After 30 min of perfusion we observed a significant increase of polyplex **P1** translocation through the endothelial that remained at this level up to 60 min of perfusion. A viability test revealed that **P1** was toxic already at low concentrations (Fig. 4A). A similar effect was further confirmed by immunofluorescence staining of several endothelial adherens and tight junction proteins involved in maintenance of barrier integrity. Accordingly, **P1** induced a leakage of hCMEC/D3 cell layers under flow conditions. The difference in our observations under flow conditions compared to static culture conditions, where the final concentration of 0.5 μg mL^{-1} was still in an acceptable range, can likely be explained by a significantly increased total amount of polyplexes presented to the cells within the similar incubation time compared to the static cell culture. This could be an explanation to the unexpected polyplex passage after 30 min. In contrast, we observed a continuously increasing transport of the polyplex **P3** through the endothelial layer reaching a maximum at 60 min. Indeed, a significantly difference is observed compared to the non-passaging precursor polyplex **P2** without glutathione modification. Taking the results of the uptake studies into account, a highly "active" polymer like **P6** within HEK cells can perform in a different way compared to microvascular endothelial cell interactions. It is not beneficial for a passage through the BBB due to its strong interaction with any kind of cells, independent of proper uptake or not. These results indicate that *in vivo* **P6** would probably adhere to and might be partly internalized by endothelial blood vessel cells, followed by cargo release instead of passing the cell layer. Importantly, the pure pDNA, the precursor polyplex using **P2** without GSH and **P6** containing only 8%

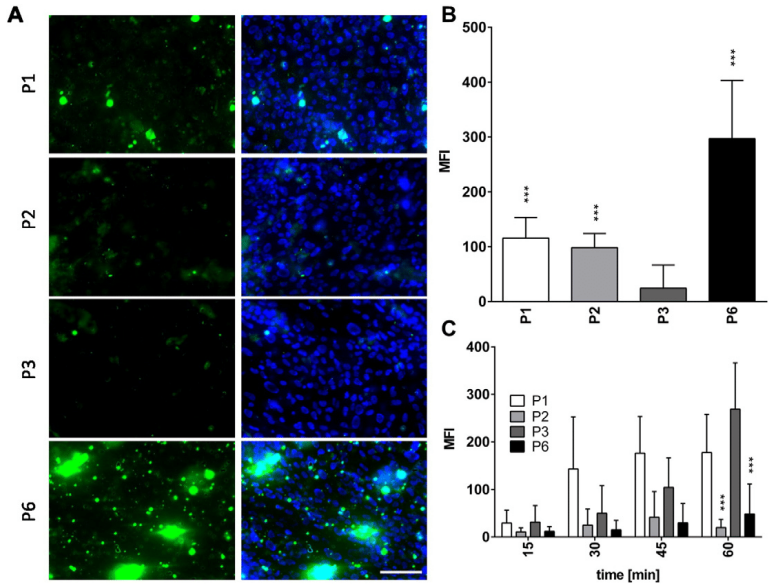

Fig. 8. Performance of the GSH-conjugated polyplexes **P1**, **P2**, **P3** and **P6** in a microfluidically supported biochip assay mimicking permeability of the BBB. A) Microscopic images display polyplex uptake (green) with the hCMEC/D3 cells (nuclei stained with DAPI (blue)) under a physiologic shear stress of 4 dyn cm^{-2}. B) Quantificational analysis of polyplexes at the cellular barrier. C) Passage of polyplexes **P1**, **P2**, **P3** and **P6** through BBB-like hCMEC/D3 cell layer over time. * significances *vs.* **P3**; ***$p < 0.001$; $n = 3$; scale bar 100 nm.

coupled GSH were virtually prevented from crossing the endothelial layer. Only **P3** showed no interaction neither with HEK cells nor endothelia cells, but was able to pass the BBB and, therefore, was identified as a promising candidate as BBB nanocarrier. These results further indicate the strong influence of the polymer design/composition for a BBB carrier balancing the GSH content, DNA binding potential and cellular interactions.

3. Conclusion

In this study, the synthesis of L-glutathione (GSH) bearing cationic polymers is described. To enable the transport of genetic material, ~80% amine functionalities of different nature (primary amines in side chains and secondary amine groups in polymer backbones) were installed within a poly(ethylene imine) derivative. A post-polymerization modification technique followed by a thiol-ene photo-addition in water was used to attach the GSH moieties. The cationic polymers investigated in this study exhibited cytotoxic side effects. The insertion of different types of amines in combination with GSH improved the cell viability compared to poly(ethylene imine). While the presence of primary amines in **P6** still revealed adverse effects on the cell viability combined with a strong interaction with cellular membranes, **P3** exhibited a superior cell viability as well as a good hemocompatibility. Despite the functionalization with negatively charged GSH, the copolymers were able to bind and release plasmid DNA. These features supported the potential application as attractive gene delivery agents for the passage of the BBB.

Studies with biochip embedded cerebral microvascular endothelial cell layers perfused under physiological shear stress conditions revealed a significantly enhanced passage of the BBB for the GSH modified candidate containing secondary amine functionalities. Interestingly, the primary amines led to strong interactions with cells combined with remarkable high uptake efficiency independent of the utilized cell types. However, this functionalization likely mediates an intracellular incorporation within the BBB and, thus, renders the nanocarriers (**P6**) unsuitable to efficiently cross the endothelial layer of the BBB. While **P1** showed an unexpected cell layer passaging effect which is probably due to a reduced tightness of the cell layer, the nanocarrier precursor (**P2**) as well as the uncomplexed plasmid DNA nanocarriers revealed significantly reduced ability to cross the endothelial BBB compared to GSH-coupled nanocarriers with higher GSH amounts (**P3**). The GSH-coupling of nanocarriers thus represents a promising approach to efficiently cross the BBB while avoiding cellular toxicity as shown in this first proof-of-concept study *in vitro*. However, follow-up studies are required to further characterize trans-endothelial transport across the BBB. To proof the feasibility of GSH-coupled nanocarriers as novel therapeutic option for drug-delivery to the CNS also more complex *in vivo* models will be investigated in the future.

4. Experimental part

4.1. Materials

Unless otherwise stated, the chemicals were used without further purification. Trifluoroacetic acid, ethanol, methanol, Irgacure® 2959, *tert*-butyl-(2-mercaptoethyl)carbamate and reduced L-glutathione were purchased from Sigma Aldrich. The following chemicals were ordered from the suppliers in brackets: 2-Ethylen-2-oxazoline (Acros Organics), 4-dimethylaminopyridine (Merck Millipore), 2,2-dimethoxy-1,2-diphenylethan-1-one (TCI America), hydrochloric acid (VWR Chemicals). *N*-succinimidyl-4-pentenate was synthesized according to literature procedures [72]. AlamarBlue, YOYO-1 iodide, Hoechst 33342 trihydrochloride (10 mg mL^{-1} solution) as well as LysoTracker Red

DND-99 were obtained from Life Technologies (Thermo Fisher, Germany). If not stated otherwise, cell culture media and supplements (L-glutamine, antibiotics) were obtained from Lonza (Basel, Switzerland) and Biochrom (Merck Millipore, Germany), respectively. All other chemicals were purchased from standard suppliers and used without further purification.

4.2. General methods and instrumentation

An Initiator Sixty single-mode microwave synthesizer from Biotage, equipped with a noninvasive IR sensor (accuracy: 2%), was used for polymerization under microwave irradiation.

Proton (^{1}H) nuclear magnetic resonance (NMR) spectra were recorded in deuterated water or methanol, at room temperature using a Bruker Advance I (300 MHz) or a Bruker Advance III HD (400 MHz) spectrometer; chemical shifts (δ) are expressed in parts per million relative to TMS. Size exclusion chromatography (SEC) was measured on a Agilent 1200 series system equipped with a PSS degasser, a G1310A pump, a G1362A refractive index detector and a PSS GRAM guard column running with dimethylacetamide (DmAc) with 0.21% of lithium chloride. For further measurements a Shimadzu system using a SCL-10A VP controller equipped with a DGU-14A degasser, a LC-10AD VP pump, a RID-10A refractive index detector and a PSS SDV guard and linear S column running with chloroform/*iso*-propanol/triethylamine (94:2:4) was utilized. The Techlab oven used for both systems was set to 40 °C and the molar masses were calculated using polystyrene (PS) standards. Asymmetric flow field-flow fractionation (AF4) was performed on an AF2000 MT system (Postnova Analytics, Landberg, Germany) coupled to an UV (PN3211, 260 nm), RI (PN3150), MALS (PN3070, 633 nm) detector. The eluent is delivered by two different pumps (tip and focus-flow) and the sample is injected by an autosampler (PN5300) into the channel. The channel has a trapezoidal geometry and an overall area of 31.6 cm^2. The nominal height of the spacer was 500 μm and a regenerated cellulose membrane with a molar mass cut-off of 10,000 g mol^{-1} (M_n) was used as the accumulation wall. All experiments were carried out at 25 °C and the eluent was 20 mM NaCl in 25 mM sodium acetate buffer at pH 3.5. The detector flow rate was set to 0.5 mL min^{-1} for all samples and 50 μL (10 mg mL^{-1}) were injected with an injection flow rate of 0.2 mL min^{-1} for 7 min. For all samples the cross-flow was set to 2 mL min^{-1}. After the focusing period and a transition time of 1 min, the cross flow was kept constant for 1 min and was then decreased under a power function gradient 0.40 to zero within 15 min. Afterwards the cross-flow was kept constant at zero for 20 min to ensure complete elution. For the calculation of the molar mass a Zimm plot was used. The refractive index increment (d*n*/d*c*) of all samples was measured by manual injection of a known concentration directly into the channel without any focusing or cross-flow. The d*n*/d*c* was calculated as the average of at least three injections from the area under the RI curve. The cytotoxicity studies as well as ethidium bromide and heparin assays were performed using a microplate reader (Tecan Infinite M200 Pro, Crailsheim, Germany). For the uptake studies of HEK-293 and hCMEC/D3 cells a flow cytometer, Cytomics FC 500 (Beckman Coulter, Krefeld, Germany) and a confocal laser scanning microscope LSM880 (Carl Zeiss, Jena, Germany) were used (see below).

*4.3. Synthesis of linear poly(ethylene imine) (**P1**)*

The polymerization of the monomer 2-ethyl-2-oxazoline using the initiator methyl tosylate was performed in a microwave synthesizer according to literature procedures [9]. The resulting poly(2-ethyl-2-oxazoline) (**PEtOx**, DP = 575, 5.0 g) was further hydrolyzed in 6 M hydrochloric acid (HCl) at 100 °C for 16 h under heating to reflux [73]. The excess of HCl and formed propionic acid was removed under reduced pressure. After dissolving in water, the solution was neutralized by the addition of 3 M sodium hydroxide (pH > 8). The precipitated linear poly(ethylene imine) was filtered off and, subsequently, redissolved in 15 mL *N*,*N*-dimethylformamide to remove the formed salt. After repeated precipitation in 400 mL ice-cold diethyl ether, the obtained product was dried under reduced pressure at 85 °C for three days. ^{1}H-NMR was used to determine the degree of hydrolysis of the resulting polymer **1** (yield: 1.85 g, 85%).

PEtOx: DP = 575. ^{1}H-NMR (300 MHz, D_2O): δ 3.70–3.20 (—NR—CH_2—CH_2), 2.41–2.08 (CH_2—CH_3), 1.09–0.79 (CH_2—CH_3) ppm.
P1: EtOx:EI [%] = 5:95. ^{1}H-NMR (300 MHz, MeOD): δ 3.58–3.41 (NR—CH_2—CH_2), 2.91–2.61 (NH—CH_2—CH_2), 2.56–2.36 (CH_2—CH_3), 1.18–1.06 (CH_2—CH_3) ppm. AF4: M_n = 9900 g mol^{-1}, Đ = 1.4.

*4.4. Synthesis of P(EI-stat-ButEnOx) (**P2**, **P4**)*

Double bond functionalities were installed on the backbone of **P1** by a post-polymerization modification process. For this purpose, **P1** (for **P2**: 751 mg, for **P4**: 765 mg) and the catalyst 4-*N*,*N*-dimethylaminopyridine (DMAP, for **P2**: 120 mg, 0.98 mmol, for **P4**: 360 mg, 2.95 mmol) were dissolved in pyridine (V = 5 mL) at 80 °C. In a second vial, *N*-succinimidyl-4-pentenate (for **P2**: 707 mg, for **P4**: 4.012 g) was dissolved in pyridine (V = 5 mL) and heated to 80 °C. The two solutions were combined to a 5 wt% mixture (5 mL pyridine were added) of **P1**. The reaction mixture was stirred for 21 h at 80 °C. The polymer solution was precipitated in 500 mL ice-cold diethyl ether. The filtered product was washed with 50 mL diethyl ether and dried under reduced pressure to constant weight (yield: **P2**: 0.83 g, 73%, **P4**: 1.29 g, 58%).

P2: EI:ButEnOx [%] = 73:27. ^{1}H-NMR (400 MHz, D_2O): δ 2.28–2.46 (m, CH_2 ButEnOx), 2.63–2.85 (m, NH—CH_2—CH_2), 3.35–3.62 (m, NR—CH_2—CH_2), 4.9–5.0 (dd, CH_2═CH—), 5.76–5.86 (m, CH_2═CH—) ppm. SEC ($CHCl_3$/iPrOH/NEt_3): M_n = 31,400 g mol^{-1}, Đ = 1.20.
P4: EI:ButEnOx [%] = 0:100. ^{1}H-NMR (400 MHz, D_2O): δ 2.27–2.44 (m, CH_2 ButEnOx), 3.45–3.53 (m, NR—CH_2—CH_2), 4.92–5.04 (dd, CH_2═CH), 5.76–5.84 (m, CH_2═CH) ppm. SEC ($CHCl_3$/iPrOH/NEt_3): M_n = 44,000 g mol^{-1}, Đ = 1.53.

*4.5. Synthesis of P(EI-stat-GluButOx) via thiol-ene photo-addition (**P3**)*

In a microwave vial, P($EI_{73\%}$-*stat*-$ButEnOx_{27\%}$) (**P2**: 740 mg) and a 1.2-fold excess per double bond of reduced L-glutathione (1.11 g, 3.6 mmol) were dissolved in 15 mL Milli-Q water (5 wt% of **P2**). The radical photoinitiator Irgacure® 2959 (100 mg, 0.45 mmol) was added and the reaction mixture was degassed with argon for 30 min. The clear solution was stirred in a UV-chamber (λ = 365 nm) for 17 h and, subsequently, dialyzed against water using Spectra/Por 1 dialysis membrane (6000 to 8000 g mol^{-1} cut-off). The product **P3** was lyophilized and obtained as a yellowish powder (yield: 770 mg, 44%).

P3: EI:GluButOx [%] = 73:27. ^{1}H-NMR (400 MHz, D_2O): δ 1.60–1.71 (m, CH_2—CH_2—S—), 2.12 (q, NCH—CH_2—CH_2—C═O), 2.45–2.64 (m, NCH—CH_2—CH_2—C═O, CH_2 ButOx), 2.87–3.30 (m, CH_2—S—CH_2—CH_2, NH—CH_2—CH_2), 3.63–3.95 (m, NR—CH_2—CH_2, NR—CH_2—COOH, NH_2—CH), 4.54 (m, NR—CH—CH_2—S) ppm. AF4: M_n = 21,000 g mol^{-1}, Đ = 2.0.

*4.6. Synthesis of P(bocAmButOx-stat-ButEnOx) via thiol-ene photo-addition (**P5**)*

In a similar procedure, PButEnOx (**P4**, 1.13 g) and 2-(*boc*-amino)ethanethiol (1.19 g, 6.7 mmol) were dissolved in 15 mL methanol (7.5 wt% of **P4**). 2,2-Dimethoxy-2-phenylacetophenone (DMPA, 88 mg, 0.40 mmol) was added as photoinitiator and the reaction

mixture was degassed with argon for 30 min. Subsequently, the solution was stirred in a UV-chamber (λ = 365 nm) for 17 h. Precipitation in 400 mL ice-cold diethyl ether, washing with 50 mL of diethyl ether and drying under reduced pressure for three days resulted in a yellowish powder **P5** (yield: 1.94 g, 80%).

P5: *boc*AmButOx:ButEnOx [%] = 82:18. ^{1}H-NMR (300 MHz, MeOD): δ 1.42 (s, *CH*$_3$ boc), 1.65 (s, *CH*$_2$—S—CH$_2$—*CH*$_2$—NR), 2.37–2.63 (m, m, *CH*$_2$ ButEnOx, S—CH$_2$—*CH*$_2$—NR), 3.50 (m, NR—*CH*$_2$—*CH*$_2$, S—*CH*$_2$—CH$_2$—NR), 4.96–5.09 (dd, *CH*$_2$═CH), 5.84 (m, CH$_2$═*CH*) ppm. SEC (DMAc, 0.21% LiCl): M_n = 23,400 g mol^{-1}, Đ = 1.86.

4.7. Synthesis of P(bocAmButOx-stat-ButEnOx-stat-GluButOx) via thiolene photo-addition (boc*P6*)

The conjugation of reduced L-glutathione (GSH) to the copolymer **P5** was performed similar to the conjugation to **P3**. For this purpose, **P5** (1.01 g) was dissolved in 17 mL ethanol (6 wt% of **P5**). The photoinitiator Irgacure® 2959 (321 mg, 1.4 mol) and a 1.2-fold excess per double bond of GSH (252 mg, 0.82 mmol) was added, the reaction mixture was degassed with argon for 30 min and stirred in a UV-chamber (λ = 365 nm) for 48 h. An aliquot of 50 μL was taken and characterized *via* ^{1}H-NMR. Due to still incomplete photo-addition, additional GSH (150 mg, 0.49 mmol) was added to the reaction mixture and irradiated for further 48 h. The copolymer was purified by dialysis against ethanol using Spectra/Por 1 dialysis membrane (6000 to 8000 g mol^{-1} cut-off) and dried under reduced pressure for four days (yield: 735 mg, 67%).

***boc*P6**: *boc*AmButOx:ButEnOx:GluButOx [%] = 82:10:8. ^{1}H-NMR (300 MHz, MeOD): δ 1.32–1.48 (s, *CH*$_3$ boc), 1.67 (m, *CH*$_2$—S—CH$_2$—CH$_2$—NR), 2.20 (m, NCH—*CH*$_2$—CH$_2$—C═O), 2.17–2.60 (m, NCH—*CH*$_2$—CH$_2$—C═O, CH$_2$ ButOx), 3.08–3.91 (m, *CH*$_2$—S—CH$_2$—CH$_2$, NR—*CH*$_2$—*CH*$_2$, NR—*CH*$_2$—COOH, NH$_2$—*CH*), 4.58 (m, NR—*CH*—CH$_2$—S), 5.02 (*CH*$_2$═CH), 5.34 (CH$_2$═*CH*) ppm. SEC (DMAc, 0.21% LiCl): M_n = 38,400 g mol^{-1}, Đ = 1.74.

4.8. Synthesis of P(AmButOx-stat-ButEnOx-stat-GluButOx) via deprotection (*P6*)

The protected copolymer ***boc*P6** (615 mg) was dissolved in dichloromethane (24 mL) and trifluoroacetic acid (40 mL) was added. The reaction mixture was stirred for 20 h at room temperature and, subsequently, precipitated in 300 mL ice-cold diethyl ether. The residue was filtered off, washed with 30 mL diethyl ether, re-dissolved in methanol and shaken overnight with Amberlyst® A21 (free base) (~0.5 mg). After filtration, the solvent was removed and the copolymer **P6** lyophilized.

P6: AmButOx:ButEnOx:GluButOx [%] = 82:10:8. ^{1}H-NMR (400 MHz, D$_2$O): δ 1.60 (*CH*$_2$—S—CH$_2$—CH$_2$—NR), 2.05 (NCH—*CH*$_2$—CH$_2$—C═O), 2.32–3.73 (NCH—*CH*$_2$—CH$_2$—C═O, CH$_2$ ButOx, *CH*$_2$—S—CH$_2$—CH$_2$, NR—*CH*$_2$—*CH*$_2$, NR—*CH*$_2$—COOH, NH$_2$—*CH*$_2$—*CH*$_2$), 4.38 (NR—*CH*—CH$_2$—S), 5.06 (*CH*$_2$═CH), 5.84 (CH$_2$═*CH*) ppm. AF4: M_n = 63,300 g mol^{-1}, Đ = 1.82.

4.9. Determination of the cytotoxicity

Cytotoxicity studies were performed with the mouse fibroblast cell line L929 (CCL-1, ATCC), as recommended by ISO10993-5 as well as with HEK-293 and hCMECs/D3 cells. The cells were routinely cultured in Dulbecco's modified eagle's medium (DMEM, Lonza) supplemented with 10% fetal calf serum (FCS), 100 U mL^{-1} penicillin and 100 μg mL^{-1} streptomycin at 37 °C in a humidified 5% (v/v) CO_2 atmosphere. In detail, cells were seeded at 10^4 cells per well in a 96-well plate and incubated for 24 h, whereas no cells were seeded in the outer wells. Afterwards, the substances to be tested (polymers) at indicated concentrations (from 10 μg mL^{-1} to 500 μg mL^{-1}) were added to the cells and the plates were incubated for further 24 h. Control cells were incubated with fresh culture medium. Subsequently, the medium was replaced by a mixture of fresh culture medium and Alamar-Blue solution, prepared according to the manufacturer's instructions. After an additional incubation of 4 h at 37 °C, the fluorescence was measured at Ex 570/Em 610 nm, with untreated cells on the same well plate serving as negative controls. The negative control was standardized as 0% of metabolism inhibition and referred as 100% viability. Cell viability below 70% was considered indicative of cytotoxicity. Data are expressed as mean ± S.D. of three determinations.

4.10. Hemolysis assay

The interaction of polymers with cellular membranes was examined by analyzing the release of hemoglobin from erythrocytes. Blood from sheep, collected in heparinized tubes, were provided by the Institute of Laboratory Animal Science and Animal Welfare, Friedrich Schiller University Jena. The blood was centrifuged at 4500 × *g* for 5 min, and the pellet was washed three times with cold 1.5 mM phosphate buffered saline (PBS, pH 7.4). After dilution with PBS in a ratio of 1:7, aliquots of erythrocyte suspension were mixed 1:1 with the polymer solution and incubated in a water bath at 37 °C for 60 min. After centrifugation at 2400 × *g* for 5 min, the hemoglobin release into the supernatant was determined spectrophotometrically using a microplate reader at 544 nm wavelength. Complete hemolysis (100%) was achieved using 1% Triton X-100 serving as positive control. Pure PBS was used as negative control (0% hemolysis). The hemolytic activity of the polycations was calculated as follow (Eq. (1)):

$$\%\text{Hemolysis} = 100 * \frac{(A_{Sample} - A_{Negative\ \ control})}{A_{Positive\ \ control}} \quad (1)$$

A value < 2% hemolysis rate was considered as non-hemolytic, 2 to 5% as slightly hemolytic and values > 5% as hemolytic. Experiments were run in triplicates and were performed with three different batches of donor blood.

4.11. Erythrocyte aggregation

The erythrocyte suspension was mixed 1:1 with the polymer solutions (100 μL total volume) in a clear flat bottomed 96-well plate. The cells were incubated at 37 °C for 2 h, and the absorbance was measured at 645 nm in a microplate reader. Cells, which were treated with PBS served as negative control and 25 kDa bPEI (50 μg mL^{-1}, Polyscience) was used as positive control. Absorbance values of the test solutions lower than the negative control were regarded as aggregation. Experiments were run in triplicates and were performed with three different charges of donor blood from sheep.

4.12. Polyplex preparation

Polyplexes of pDNA and polymers were prepared by mixing stock solutions of 15 μg mL^{-1} pDNA and different amounts of polymers (1 mg mL^{-1}) to obtain various N/P ratios (nitrogen of polymer to phosphate of pDNA) in HBG buffer (20 mM 4-(2-hydroxethyl) piperazine-1-ethanesulfonic acid (HEPES) and 5% (w/v) glucose, pH 7.2). The solutions were vortexed for 10 s at maximal speed and incubated at room temperature for 20 min to ensure complex formation.

4.13. Ethidium bromide quenching assay

The formation of polyplexes with pDNA was examined by quenching of the ethidium bromide fluorescence as described previously [56]. Briefly, 15 μg mL^{-1} pDNA in a total volume of 100 μL HBG buffer

(HEPES buffered glucose) were incubated with ethidium bromide (0.4 μg mL^{-1}) for 10 min at room temperature. Afterwards, polyplexes with increasing amounts of indicated polymers (regarding N/P ratio) were prepared in black 96-well plates (Nunc Thermo Fisher). The samples were incubated at room temperature for 15 min before fluorescence measurements. The fluorescence of the samples was measured at an excitation wavelength of 525 nm and an emission wavelength of 605 nm using a microplate reader. A sample solely containing pDNA and EtBr was used to calibrate the device to 100% fluorescence against a background of 0.4 μg mL^{-1} of EtBr in HBG solution. The percentage of dye displaced upon polyplex formation was calculated using Eq. (2):

$$\mathrm{RFU}\,[\%] = \frac{F_{sample} - F_0}{F_{pDNA} - F_0} * 100 \quad (2)$$

RFU is defined as the relative fluorescence and F_{sample}, F_0, and F_{pDNA} are the fluorescence intensities of a given sample, the ethidium bromide in HBG alone, and the ethidium bromide intercalated into pDNA alone.

4.14. Heparin dissociation assay

To investigate the release of pDNA from the polyplexes, the heparin dissociation assay was performed. Polyplexes with a N/P ratio of 40 were prepared as described above in a total volume of 100 μL HBG buffer containing ethidium bromide (0.4 μg mL^{-1}). After incubation in the dark at room temperature for 15 min, the polyplexes were transferred into a black 96-well plate, and heparin of indicated concentrations was added. The solution was mixed and incubated for further 30 min at 37 °C in the dark. The fluorescence of ethidium bromide was measured at Ex 525 nm/Em 605 nm with a Tecan microplate reader. The percentage of intercalated ethidium bromide was calculated as described before.

4.15. Dynamic and electrophoretic light scattering

Dynamic light scattering (DLS) was performed on a Zetasizer Nano ZS (Malvern Instruments, Herrenberg) with a He-Ne laser operating at a wavelength of $\lambda = 633$ nm. All measurements (30 runs, triplicate) were carried out at 25 °C after an equilibration time of 120 s. The counts were detected at an angle of 173°. The mean particle size was approximated as the effective (z-average) diameter and the width of the distribution as the polydispersity index of the particles (PDI) obtained by the cumulants method assuming a spherical shape. Electrophoretic light scattering (ELS) was used to measure the zeta potential (ζ). The measurement was performed on a Zetasizer Nano ZS (Malvern Instruments, Herrenberg, Germany) by applying laser Doppler velocimetry. For each measurement, 20 runs were carried out using the slow-field reversal and the fast-field reversal mode at 150 V. Each experiment was performed in triplicate a 25 °C. The zeta potential was calculated from the electrophoretic mobility (μ) according to the Henry Equation. Henry coefficient f(ka) was calculated according to Oshima.

4.16. Polyplex uptake

HEK-293 cells (CRL-1573, ATCC) were cultured in RPMI 1640 medium supplemented with 10% FCS, 100 μg mL^{-1} streptomycin, 100 IU mL^{-1} penicillin and 2 mM L-glutamine at 37 °C in a humidified 5% (v/v) CO_2 atmosphere. For uptake studies, cells were seeded at a density of 10^5 cells per mL in 24-well plates and cultured for 24 h. One hour prior to the addition of the polyplexes, the medium was changed to OptiMEM (Thermo Fisher, Germany). For the uptake kinetic study within 4 h, pDNA was labeled with YOYO-1 iodide prior to the polyplex preparation. For labeling of 1 μg pDNA, 0.026 μL of 1 M YOYO-1 solution was mixed with pDNA and incubated for 20 min at 4 °C protected from light. Afterwards, HBG buffer and the polymers were added at the indicated N/P ratio and the polyplexes were formed as described previously. The cells were harvested 15 min, 30 min, 1 h, 2 h and 4 h after polyplex addition and 10% trypan blue was added to quench the outer fluorescence of the cells. To determine the relative uptake of the polyplexes, 10,000 cells were measured by flow cytometry using a Cytomics FC 500 (Beckman Coulter) and the amount of viable cells showing YOYO-1 signal were gated. Dead cells were identified *via* counterstaining with propidium iodide. The experiments were performed at least three times independently. The uptake studies of hCMECs were performed in OptiMEM and EndoGro media, respectively. For live cell imaging HEK cells (10^5 cells mL^{-1}) were seeded in glass-bottomed, 4-chamber dishes (CELLVIEW, Greiner Bio-One, Germany) and cultured for 24 h. One hour prior to polymer addition, the cells were rinsed with phosphate buffered saline (PBS) and the media were changed to OptiMEM. Polyplexes were prepared at N/P 20 as described above and incubated for further 1 h. Afterwards, the media were replaced with fresh culture media supplemented with LysoTracker Red DND-99 and Hoechst 33342 for lysosome and nucleus staining, respectively. The living cells were imaged with a LSM880 using the following excitation wavelengths/laser lines 405 nm (for Hoechst), 488 nm (for YOYO-1) and 561 nm (for LysoTracker Red).

4.17. Transfection of adherent cells

For transfection of adherent HEK-293 cells, the cells were seeded at a density of 10^5 cells mL^{-1} in 24-well plates and incubated for 24 h at 37 °C, 5% (v/v) CO_2. One hour prior to transfection, the cells were washed with PBS and supplemented with serum-reduced media (OptiMEM). Polyplexes were prepared as described above, and were added to the cells (50 μL per well). After an incubation time of 4 h at 37 °C, the supernatant was replaced by fresh growth medium and the cells were further incubated for 20 h. For analysis *via* flow cytometry (Cytomics FC 500, Beckman Coulter), the cells were harvested by trypsinization and 10^4 cells were analyzed. For determination of the viability during flow cytometry, dead cells were identified *via* counterstaining with propidium iodide. For determination of the transfection efficiency, viable cells expressing EGFP were gated. The experiments were performed independently three times.

4.18. Immunofluorescence microscopy.

Cells were fixed with ice cold methanol for 10 min at −20 °C, permeabilized with 0.1% Saponin and blocking was done with 3% normal donkey serum. Antibody staining was performed using mouse-anti-human VE-Cadherin, mouse-anti-human β-Catenin (both BD Biosciences, Heidelberg, Germany), mouse-anti-human Claudin-5, rabbit-anti-human ZO-1 and rabbit-anti-human Occludin (all Life Technologies, Karlsruhe, Germany) overnight. Secondary antibodies donkey-anti-rabbit Cy3 (Dianova, Hamburg, Germany) and donkey-anti-mouse AlexaFluor647 (Life Technologies) as well as DAPI (Life Technologies) were applied for 1 h at room temperature. Samples were embedded in fluorescence mounting medium (Dako, Hamburg, Germany) and imaged on an Axio Observer.Z1 fluorescence microscope (Carl Zeiss AG, Jena, Germany). Image analysis was performed using ImageJ2 software (Fiji).

4.19. Dynamic cell culture assay

MOTiF biochips were made by injection moulding of polystyrene and manufactured by microfluidic Chip Shop (Jena, Germany) as described previously [65]. Chip geometry and embedded structures are shown in Supporting information, Fig. S10. The human cerebral microvascular endothelial cell line hCMEC/D3 (BIOZOL, Eching, Germany) was cultured in EndoGRO-MV Basal Medium supplemented with 5% (v/v) FCS, 0.2% (v/v) EndoGRO-LS supplement, 5 ng/mL recombinant human epidermal growth factor, 10 mM L-glutamine, 1 μg mL^{-1} hydrocortisone-hemisuccinate, 0.75 U mL^{-1} heparin-sulfate, 50 μg mL^{-1}

ascorbic acid (all additives were obtained from Merck-Millipore, Darmstadt, Germany), and 100 U mL^{-1} penicillin and 100 μg mL^{-1} streptomycin at 37 °C in a humidified 5% (v/v) CO_2 atmosphere. The membrane within the biochip was coated with 150 μg mL^{-1} collagen A (Biochrom, Berlin, Germany) for at least 1 h prior to cell seeding. hCMEC/D3 were seeded at a density of 0.75×10^5 cm^{-2} in the upper channel to grow on top of the membrane. Cells were cultured until fully confluent after four to five days. Afterwards, biochips were connected to an Ismatec peristaltic pump (Cole Parmer, Wertheim, Germany) *via* gas permeable silicon tubing (Cole Parmer and microfluidic Chip Shop) at 37 °C in a humidified 5% (v/v) CO_2 atmosphere and accustomed to flow conditions with a flow rate of 175 μL min^{-1} (corresponding shear stress of 2 dyn cm^2) for 30 min. Meanwhile polyplex formation at a N/P ratio of 20 was performed in hCMEC/D3 cell culture medium as stated above with additionally applying YOYO-1 as reporter dye. As corresponding controls polyplex solutions without dye were used. Subsequently shear stress was increased to 4 dyn cm^2 and polyplex solutions were applied for 1 h. For sampling 30 μL from the lower channel system were taken whereas the first 15 μL were discarded to ensure sampling from under the membrane and not just from the microchannels. Samples were taken every 15 min. Afterwards, cells were washed gently by flushing the upper and lower microchannels three times with PBS. Nuclei were stained with Hoechst 33342. Membranes and supernatants were analyzed using an Axio Observer.Z1 fluorescence microscope (Carl Zeiss AG, Jena, Germany) applying a filter with 470 nm excitation and 525 nm emission wave lengths. At least three images per sample were taken. Fluorescence images were analyzed with the ImageJ2 software whereas controls were subtracted for quantification.

4.20. Statistical analysis

The values represent the mean ± S.D. Direct comparison of two different groups was done with two-tailed, non-paired student's test. For multiple comparisons analysis by two-way ANOVA was performed using Turkey's multiple testing as post-test. Statistical significant was defined with p-values of <0.05.

Acknowledgment

The authors would like to thank Carolin Fritzsche for the support with the bio assays and Gabriele Sentis and Dr. Peter Bellstedt for nuclear magnetic resonance measurements. We gratefully acknowledge Dr. Johannes C. Brendel for helpful discussions. The funding of the collaborative research center ChemBioSys (SFB 1127) by the Deutsche Forschungsgemeinschaft (DFG), the Carl Zeiss Foundation (scholarship for AT), the German Federal Ministry of Education and Research (BMBF # 031A518B Vectura) and the German Federal Institute of Risk Assessment (grant number 1329-533) are highly acknowledged. The LSM880 ELYRA PS.1 was further founded with a grant from the DFG.

Appendix A. Supplementary data

Supplementary figures and tables S1–S12. This material is available free of charge *via* the Internet at http://pubs.acs.org. Supplementary data associated with this article can be found in the online version, at http://dx.doi.org/10.1016/j.jconrel.2016.08.039.

References

[1] P. Ehrlich, Das Sauerstoffbedürfnis des Organismus, eine farbenanalytische Studie, Hirschwald, Berlin, 1885.
[2] M. Lewandowsky, Zur Lehre von der Cerebrospinalflüssigkeit, Z. Klin. Med. 40 (1900) 480–494.
[3] N.J. Abbott, A.A.K. Patabendige, D.E.M. Dolman, S.R. Yusof, D.J. Begley, Structure and function of the blood–brain barrier, Neurobiol. Dis. 37 (2010) 13–25, http://dx.doi.org/10.1016/j.nbd.2009.07.030.
[4] V.A. Levin, Relationship of octanol/water partition coefficient and molecular weight to rat brain capillary permeability, J. Med. Chem. 23 (1980) 682–684, http://dx.doi.org/10.1021/jm00180a022.
[5] X. Liu, M. Tu, R.S. Kelly, C. Chen, B.J. Smith, Development of a computional approach to predict blood-brain barrier permeability, Drug Metab. Dispos. 32 (2004) 132–139, http://dx.doi.org/10.1124/dmd.32.1.132.
[6] C.C. Visser, L.H. Voorwinden, D.J.A. Crommelin, M. Danhof, A.G. de Boer, Characterization and modulation of the transferrin receptor on brain capillary endothelial cells, Pharm. Res. 21 (2004) 761–769, http://dx.doi.org/10.1023/B:PHAM.0000026425.69874.8e.
[7] B.V. Zlokovic, The blood-brain barrier in health and chronic neurodegenerative disorders, Neuron 57 (2008) 178–201, http://dx.doi.org/10.1016/j.neuron.2008.01.003.
[8] R. Kannan, R. Chakrabarti, D. Tang, K.J. Kim, N. Kaplowitz, GSH transport in human cerebrovascular endothelial cells and human astrocytes: evidence for luminal localization of Na+-dependent GSH transport in HCEC1, Brain Res. 852 (2000) 374–382, http://dx.doi.org/10.1016/S0006-8993(99)02184-8.
[9] M. Bauer, C. Lautenschlaeger, K. Kempe, L. Tauhardt, U.S. Schubert, D. Fischer, Poly(2-ethyl-2-oxazoline) as alternative for the stealth polymer poly(ethylene glycol): comparison of in vitro cytotoxicity and hemocompatibility, Macromol. Biosci. 12 (2012) 986–998, http://dx.doi.org/10.1002/mabi.201200017.
[10] R. Kannan, J.F. Kuhlenkamp, E. Jeandidier, H. Trinh, M. Ookhtens, N. Kaplowitz, Evidence for carrier-mediated transport of glutathione across the blood-brain barrier in the rat, J. Clin. Invest. 85 (1990) 2009–2013, http://dx.doi.org/10.1172/JCI114666.
[11] C.M. Berlin, D.G. May-McCarver, D.A. Notterman, R.M. Ward, D.N. Weismann, G.S. Wilson, J.T. Wilson, Alternative routes of drug administration—advantages and disadvantages, Pediatrics 100 (1997) 143–152, http://dx.doi.org/10.1542/peds.100.1.143.
[12] A. Mistry, S. Stolnik, L. Illum, Nanoparticles for direct nose-to-brain delivery of drugs, Int. J. Pharm. 379 (2009) 146–157, http://dx.doi.org/10.1016/j.ijpharm.2009.06.019.
[13] X. Wen, K. Wang, Z. Zhao, Y. Zhang, T. Sun, F. Zhang, J. Wu, Y. Fu, Y. Du, L. Zhang, Y. Sun, Y. Liu, K. Ma, H. Liu, Y. Song, Brain-targeted delivery of trans-activating transcriptor-conjugated magnetic PLGA/lipid nanoparticles, PLoS One 9 (2014) e106652, http://dx.doi.org/10.1371/journal.pone.0106652.
[14] B. Oller-Salvia, M. Sanchez-Navarro, E. Giralt, M. Teixido, Blood-brain barrier shuttle peptides: an emerging paradigm for brain delivery, Chem. Soc. Rev. (2016), http://dx.doi.org/10.1039/C6CS00076B.
[15] J. Kreuter, Nanoparticulate systems for brain delivery of drugs, Adv. Drug Deliv. Rev. 47 (2001) 65–81, http://dx.doi.org/10.1016/S0169-409X(00)00122-8.
[16] L. Nobs, F. Buchegger, R. Gurny, E. Allémann, Surface modification of poly(lactic acid) nanoparticles by covalent attachment of thiol groups by means of three methods, Int. J. Pharm. 250 (2003) 327–337, http://dx.doi.org/10.1016/S0378-5173(02)00542-2.
[17] K. Kafedjiiski, M. Werle, F. Föger, A. Bernkop-Schnürch, Synthesis and in vitro characterization of a novel poly(acrylic acid)-glutathione conjugate, J. Drug. Deliv. Sci. Tech. 15 (2005) 411–417, http://dx.doi.org/10.1016/S1773-2247(05)50081-9.
[18] S.S. More, R. Vince, Design, synthesis and biological evaluation of glutathione peptidomimetics as components of anti-parkinson prodrugs, J. Med. Chem. 51 (2008) 4581–4588, http://dx.doi.org/10.1021/jm800239v.
[19] N. Raval, T. Mistry, N. Acharya, S. Acharya, Development of glutathione-conjugated asiatic acid-loaded bovine serum albumin nanoparticles for brain-targeted drug delivery, J. Pharm. Pharmacol. 67 (2015) 1503–1511, http://dx.doi.org/10.1111/jphp.12460.
[20] A. Grover, A. Hirani, V. Sutariya, Blood-barin barrier permeation of glutathione-coated nanoparticle, J. Pharm. Pharm. Sci 1 (2014), http://dx.doi.org/10.15226/2374-6866/1/1/00103.
[21] P.J. Gaillard, C.C.M. Appeldoorn, J. Rip, R. Dorland, S.M.A. van der Pol, G. Kooij, H.E. de Vries, A. Reijerkerk, Enhanced brain delivery of liposomal methylprednisolone improved therapeutic efficacy in a model of neuroinflammation, J. Control. Release 164 (2012) 364–369, http://dx.doi.org/10.1016/j.jconrel.2012.06.022.
[22] P.J. Gaillard, C.C.M. Appeldoorn, R. Dorland, J. van Kregten, F. Manca, D.J. Vugts, B. Windhorst, G.A.M.S. van Dongen, H.E. de Vries, D. Maussang, O. van Tellingen, Pharmacokinetics, brain delivery, and efficacy in brain tumor-bearing mice of glutathione pegylated liposomal doxorubicin (2B3-101), PLoS One 9 (2014) e82331, http://dx.doi.org/10.1371/journal.pone.0082331.
[23] T. Patel, J. Zhou, J.M. Piepmeier, W.M. Saltzman, Polymeric nanoparticles for drug delivery to the central nervous system, Adv. Drug Deliv. Rev. 64 (2012) 701–705, http://dx.doi.org/10.1016/j.addr.2011.12.006.
[24] J. Kreuter, R.N. Alyautdin, D.A. Kharkevich, A.A. Ivanov, Passage of peptides through the blood-brain barrier with colloidal polymer particles (nanoparticles), Brain Res. 674 (1995) 171–174, http://dx.doi.org/10.1016/0006-8993(95)00023-J.
[25] K.S. Rao, M.K. Reddy, J.L. Horning, V. Labhasetwar, TAT-conjugated nanoparticles for the CNS delivery of anti-HIV drugs, Biomaterials 29 (2008) 4429–4438, http://dx.doi.org/10.1016/j.biomaterials.2008.08.004.
[26] S.A. Kulkarni, S.-S. Feng, Effects of surface modification on delivery efficiency of biodegradable nanoparticles across the blood–brain barrier, Nanomedicine 6 (2011) 377–394, http://dx.doi.org/10.2217/nnm.10.131.
[27] J. Wang, Z. Lu, M.G. Wientjes, J.L.-S. Au, Delivery of siRNA therapeutics: barriers and carriers, AAPS J. 12 (2010) 492–503, http://dx.doi.org/10.1208/s12248-010-9210-4.
[28] M.A. Mintzer, E.E. Simanek, Nonviral vectors for gene delivery, Chem. Rev. 109 (2009) 259–302, http://dx.doi.org/10.1021/cr800409e.
[29] J.H. Jeong, S.H. Song, D.W. Lim, H. Lee, T.G. Park, DNA transfection using linear poly(ethylenimine) prepared by controlled acid hydrolysis of poly(2-ethyl-2-oxazoline), J. Control. Release 73 (2001) 391–399, http://dx.doi.org/10.1016/S0168-3659(01)00310-8.
[30] C. Englert, M. Hartlieb, P. Bellstedt, K. Kempe, C. Yang, S.K. Chu, X. Ke, J.M. García, R.J. Ono, M. Fevre, R.J. Wojtecki, U.S. Schubert, Y.Y. Yang, J.L. Hedrick, Enhancing the biocompatibility and biodegradability of linear poly(ethylene imine) through con-

trolled oxidation, Macromolecules 48 (2015) 7420–7427, http://dx.doi.org/10.1021/acs.macromol.5b01940.
[31] K. Kunath, A. von Harpe, D. Fischer, T. Kissel, Galactose-PEI–DNA complexes for targeted gene delivery: degree of substitution affects complex size and transfection efficiency, J. Control. Release 88 (2003) 159–172, http://dx.doi.org/10.1016/S0168-3659(02)00458-3.
[32] W. Cheng, C. Yang, J.L. Hedrick, D.F. Williams, Y.Y. Yang, P.G. Ashton-Rickardt, Delivery of a granzyme B inhibitor gene using carbamate-mannose modified PEI protects against cytotoxic lymphocyte killing, Biomaterials 34 (2013) 3697–3705, http://dx.doi.org/10.1016/j.biomaterials.2013.01.090.
[33] C. Englert, M. Fevre, R.J. Wojtecki, W. Cheng, Q. Xu, C. Yang, X. Ke, M. Hartlieb, K. Kempe, J.M. García, R.J. Ono, U.S. Schubert, Y.Y. Yang, J.L. Hedrick, Facile carbohydrate-mimetic modifications of poly(ethylene imine) carriers for gene delivery applications, Polym. Chem. (2016), http://dx.doi.org/10.1039/c6py00940a (in press).
[34] M. Ogris, S. Brunner, S. Schüller, R. Kircheis, E. Wagner, PEGylated DNA/transferrin-PEI complexes: reduced interaction with blood components, extended circulation in blood and potential for systemic gene delivery, Gene Ther. 6 (1999) 595–605.
[35] B.J. Ballermann, A. Dardik, E. Eng, A. Liu, Shear stress and the endothelium, Kidney Int. 54 (1998) 100–108, http://dx.doi.org/10.1046/j.1523-1755.1998.06720.x.
[36] M. Raasch, K. Rennert, T. Jahn, C. Gärtner, G. Schönfelder, O. Huber, A. Seiler, A. Mosig, An integrative microfluicically supported in vitro model of an endothelial barrier combined with cortical spheroids simulates effects of neuroinflammation in neocortex development, Biomicrofluidics 10 (2016), http://dx.doi.org/10.1063/1.4955184 (in press).
[37] B.B. Weksler, E.A. Subileau, N. Perrière, P. Charneau, K. Holloway, M. Leveque, H. Tricoire-Leignel, A. Nicotra, S. Bourdoulous, P. Turowski, D.K. Male, F. Roux, J. Greenwood, I.A. Romero, P.O. Couraud, Blood-brain barrier-specific properties of a human adult brain endothelial cell line, FASEB J. 19 (2005) 1872–1874, http://dx.doi.org/10.1096/fj.04-3458fje.
[38] B. Weksler, I.A. Romero, P.-O. Couraud, The hCMEC/D3 cell line as a model of the human blood brain barrier, Fluids Barriers CNS 10 (2013) 1–10, http://dx.doi.org/10.1186/2045-8118-10-16.
[39] B. Poller, H. Gutmann, S. Krähenbühl, B. Weksler, I. Romero, P.-O. Couraud, G. Tuffin, J. Drewe, J. Huwyler, The human brain endothelial cell line hCMEC/D3 as a human blood-brain barrier model for drug transport studies, J. Neurochem. 107 (2008) 1358–1368, http://dx.doi.org/10.1111/j.1471-4159.2008.05730.x.
[40] L. Cucullo, P.-O. Couraud, B. Weksler, I.-A. Romero, M. Hossain, E. Rapp, D. Janigro, Immortalized human brain endothelial cells and flow-based vascular modeling: a marriage of convenience for rational neurovascular studies, J. Cereb. Blood Flow Metab. 28 (2008) 312–328, http://dx.doi.org/10.1038/sj.jcbfm.9600525.
[41] L.M. Griep, F. Wolbers, B. de Wagenaar, P.M. ter Braak, B.B. Weksler, I.A. Romero, P.O. Couraud, I. Vermes, A.D. van der Meer, A. van den Berg, BBB on chip: microfluidic platform to mechanically and biochemically modulate blood-brain barrier function, Biomed. Microdevices 15 (2013) 145–150, http://dx.doi.org/10.1007/s10544-012-9699-7.
[42] B.P. Daniels, L. Cruz-Orengo, T.J. Pasieka, P.-O. Couraud, I.A. Romero, B. Weksler, J.A. Cooper, T.L. Doering, R.S. Klein, Immortalized human cerebral microvascular endothelial cells maintain the properties of primary cells in an in vitro model of immune migration across the blood brain barrier, J. Neurosci. Methods 212 (2013) 173–179, http://dx.doi.org/10.1016/j.jneumeth.2012.10.001.
[43] D. Ye, M.N. Raghnaill, M. Bramini, E. Mahon, C. Aberg, A. Salvati, K.A. Dawson, Nanoparticle accumulation and transcytosis in brain endothelial cell layers, Nanoscale 5 (2013) 11153–11165, http://dx.doi.org/10.1039/C3NR02905K.
[44] D. Ye, K.A. Dawson, I. Lynch, A TEM protocol for quality assurance of in vitro cellular barrier models and its application to the assessment of nanoparticle transport mechanisms across barriers, Analyst 140 (2015) 83–97, http://dx.doi.org/10.1039/C4AN01276C.
[45] H.M.L. Lambermont-Thijs, F.S. van der Woerdt, A. Baumgaertel, L. Bonami, F.E.D. Prez, U.S. Schubert, R. Hoogenboom, Linear poly(ethylene imine)s by acidic hydrolysis of poly(2-oxazoline)s: kinetic screening, thermal properties, and temperature-induced solubility transitions, Macromolecules 43 (2010) 927–933, http://dx.doi.org/10.1021/ma9020455.
[46] T. Bus, C. Englert, M. Reifarth, P. Borchers, M. Hartlieb, A. Vollrath, S. Hoeppener, A. Traeger, U.S. Schubert, 3rd Generation Poly(ethylene imine)s for Gene Delivery, 2016 (submitted).
[47] C. Englert, L. Tauhardt, M. Hartlieb, K. Kempe, M. Gottschaldt, U.S. Schubert, Linear poly(ethylene imine)-based hydrogels for effective binding and release of DNA, Biomacromolecules 15 (2014) 1124–1131, http://dx.doi.org/10.1021/bm4017572.
[48] M. Neu, D. Fischer, T. Kissel, Recent advances in rational gene transfer vector design based on poly(ethylene imine) and its derivatives, J. Gene Med. 7 (2005) 992–1009, http://dx.doi.org/10.1002/jgm.773.
[49] S.K. Samal, M. Dash, S. Van Vlierberghe, D.L. Kaplan, E. Chiellini, C. van Blitterswijk, L. Moroni, P. Dubruel, Cationic polymers and their therapeutic potential, Chem. Soc. Rev. 41 (2012) 7147–7194, http://dx.doi.org/10.1039/C2CS35094G.
[50] J.C. Sunshine, D.Y. Peng, J.J. Green, Uptake and transfection with polymeric nanoparticles are dependent on polymer end-group structure, but largely independent of nanoparticle physical and chemical properties, Mol. Pharm. 9 (2012) 3375–3383, http://dx.doi.org/10.1021/mp3004176.
[51] B. Wittgren, A. Welinder, B. Porsch, Molar mass characterization of cationic methyl methacrylate–ethyl acrylate copolymers using size-exclusion chromatography with online multi-angle light scattering and refractometric detection, J. Chromatogr. A 1002 (2003) 101–109, http://dx.doi.org/10.1016/S0021-9673(03)00729-5.
[52] R. Roemling, K. Tokunaga, H. Monyama, Analysis of cationic polymers by size exclusion chromatography (SEC), LC-GC Europe (2008) 47–48.
[53] S.M. Moghimi, P. Symonds, J.C. Murray, A.C. Hunter, G. Debska, A. Szewczyk, A two-stage poly(ethylenimine)-mediated cytotoxicity: implications for gene transfer/therapy, Mol. Ther. 11 (2005) 990–995, http://dx.doi.org/10.1016/j.ymthe.2005.02.010.
[54] D. Fischer, Y. Li, B. Ahlemeyer, J. Krieglstein, T. Kissel, In vitro cytotoxicity testing of polycations: influence of polymer structure on cell viability and hemolysis, Biomaterials 24 (2003) 1121–1131, http://dx.doi.org/10.1016/S0142-9612(02)00445-3.
[55] L. Dekie, V. Toncheva, P. Dubruel, E.H. Schacht, L. Barrett, L.W. Seymour, Poly-L-glutamic acid derivatives as vectors for gene therapy, J. Control. Release 65 (2000) 187–202, http://dx.doi.org/10.1016/S0168-3659(99)00235-7.
[56] A.C. Rinkenauer, L. Tauhardt, F. Wendler, K. Kempe, M. Gottschaldt, A. Traeger, U.S. Schubert, A cationic poly(2-oxazoline) with high in vitro transfection efficiency identified by a library approach, Macromol. Biosci. 15 (2015) 414–425, http://dx.doi.org/10.1002/mabi.201400334.
[57] S.K. Tripathi, N. Gupta, M. Mahato, K.C. Gupta, P. Kumar, Selective blocking of primary amines in branched polyethylenimine with biocompatible ligand alleviates cytotoxicity and augments gene delivery efficacy in mammalian cells, Colloids Surf. B 115 (2014) 79–85, http://dx.doi.org/10.1016/j.colsurfb.2013.11.024.
[58] D.W. Hwang, S. Son, J. Jang, H. Youn, S. Lee, D. Lee, Y.-S. Lee, J.M. Jeong, W.J. Kim, D.S. Lee, A brain-targeted rabies virus glycoprotein-disulfide linked PEI nanocarrier for delivery of neurogenic microRNA, Biomaterials 32 (2011) 4968–4975, http://dx.doi.org/10.1016/j.biomaterials.2011.03.047.
[59] J.B. Lepecq, C. Paoletti, Federation of european biochemical societies 3rd meeting: a fluorescent complex between ethidium bromide and nucleic acids, J. Mol. Biol. 27 (1967) 87–106, http://dx.doi.org/10.1016/0022-2836(67)90353-1.
[60] A.J. Geall, I.S. Blagbrough, Rapid and sensitive ethidium bromide fluorescence quenching assay of polyamine conjugate–DNA interactions for the analysis of lipoplex formation in gene therapy, J. Pharm. Biomed. Anal. 22 (2000) 849–859, http://dx.doi.org/10.1016/S0731-7085(00)00250-8.
[61] A.C. Rinkenauer, S. Schubert, A. Traeger, U.S. Schubert, The influence of polymer architecture on in vitro pDNA transfection, J. Mater. Chem. B 3 (2015) 7477–7493, http://dx.doi.org/10.1039/C5TB00782H.
[62] S. Sundaram, S. Viriyayuthakorn, C.M. Roth, Oligonucleotide structure influences the interactions between cationic polymers and oligonucleotides, Biomacromolecules 6 (2005) 2961–2968, http://dx.doi.org/10.1021/bm0502314.
[63] A. Kwok, S.L. Hart, Comparative structural and functional studies of nanoparticle formulations for DNA and siRNA delivery, Nanomed. Nanotechnol. 7 (2011) 210–219, http://dx.doi.org/10.1016/j.nano.2010.07.005.
[64] R. Luxenhofer, G. Sahay, A. Schulz, D. Alakhova, T.K. Bronich, R. Jordan, A.V. Kabanov, Structure-property relationship in cytotoxicity and cell uptake of poly(2-oxazoline) amphiphiles, J. Control. Release 153 (2011) 73–82, http://dx.doi.org/10.1016/j.jconrel.2011.04.010.
[65] R. Martin, R. Knut, J. Tobias, P. Sven, H. Thomas, H. Otmar, S. Ingo, B. Holger, L. Stefan, F. Harald, M. Alexander, Microfluidically supported biochip design for culture of endothelial cell layers with improved perfusion conditions, Biofacrication 7 (2015) 015013, http://dx.doi.org/10.1088/1758-5090/7/1/015013.
[66] J. Gavard, J.S. Gutkind, VE-cadherin and claudin-5: it takes two to tango, Nat. Cell Biol. 10 (2008) 883–885, http://dx.doi.org/10.1038/ncb0808-883.
[67] W. Jia, R. Lu, T.A. Martin, W.G. Jiang, The role of claudin-5 in blood-brain barrier (BBB) and brain metastases (review), Mol. Med. Rep. 9 (2014) 779–785, http://dx.doi.org/10.3892/mmr.2013.1875.
[68] E. Dejana, F. Orsenigo, M.G. Lampugnani, The role of adherens junctions and VE-cadherin in the control of vascular permeability, J. Cell Sci. 121 (2008) 2115–2122, http://dx.doi.org/10.1242/jcs.017897.
[69] S. Liebner, M. Corada, T. Bangsow, J. Babbage, A. Taddei, C.J. Czupalla, M. Reis, A. Felici, H. Wolburg, M. Fruttiger, M.M. Taketo, H. von Melchner, K.H. Plate, H. Gerhardt, E. Dejana, Wnt/β-catenin signaling controls development of the blood–brain barrier, J. Cell Biol. 183 (2008) 409–417, http://dx.doi.org/10.1083/jcb.200806024.
[70] T. Hirase, J.M. Staddon, M. Saitou, Y. Ando-Akatsuka, M. Itoh, M. Furuse, K. Fujimoto, S. Tsukita, L.L. Rubin, Occludin as a possible determinant of tight junction permeability in endothelial cells, J. Cell Sci. 110 (1997) 1603–1613 (doi:).
[71] E. Mennesson, P. Erbacher, M. Kuzak, C. Kieda, P. Midoux, C. Pichon, DNA/cationic polymer complex attachment on a human vascular endothelial cell monolayer exposed to a steady laminar flow, J. Control. Release 114 (2006) 389–397, http://dx.doi.org/10.1016/j.jconrel.2006.06.006.
[72] A. Gress, A. Völkel, H. Schlaad, Thio-click modification of poly[2-(3-butenyl)-2-oxazoline], Macromolecules 40 (2007) 7928–7933, http://dx.doi.org/10.1021/ma071357r.
[73] J.C. Fernandes, X. Qiu, F.M. Winnik, M. Benderdour, X. Zhang, K. Dai, Q. Shi, Linear polyethylenimine produced by partial acid hydrolysis of poly(2-ethyl-2-oxazoline) for DNA and siRNA delivery in vitro, Int. J. Nanomedicine 8 (2013) 4091–4102, http://dx.doi.org/10.2147/IJN.S47413.

SUPPORTING INFORMATION:

Glutathione-conjugated Poly(ethylene imine) for Passage of Blood-Brain Barrier

Christoph Englert,[a,b,†] Anne-Kristin Trützschler,[a,b,†] Martin Raasch,[c,d] Tanja Bus,[a,b] Philipp Borchers,[a,b] Alexander S. Mosig,[b,c,d,] Anja Traeger,[a,b,*] Ulrich S. Schubert[a,b,*]*

[a] *Laboratory of Organic and Macromolecular Chemistry (IOMC), Friedrich Schiller University Jena, Humboldtstrasse 10, 07743 Jena, Germany*

[b] *Jena Center for Soft Matter (JCSM), Friedrich Schiller University Jena, Philosophenweg 7, 07743 Jena, Germany*

[c] *Institute of Biochemistry II, Jena University Hospital, Nonnenplan 2-4, 07743 Jena, Germany*

[d] *Center for Sepsis Control and Care, Jena University Hospital, Erlanger Allee 101, 07747 Jena*

[†] *The authors contributed equally to this work*

Email: ulrich.schubert@uni-jena.de, anja.traeger@uni-jena.de, alexander.mosig@med.uni-jena.de

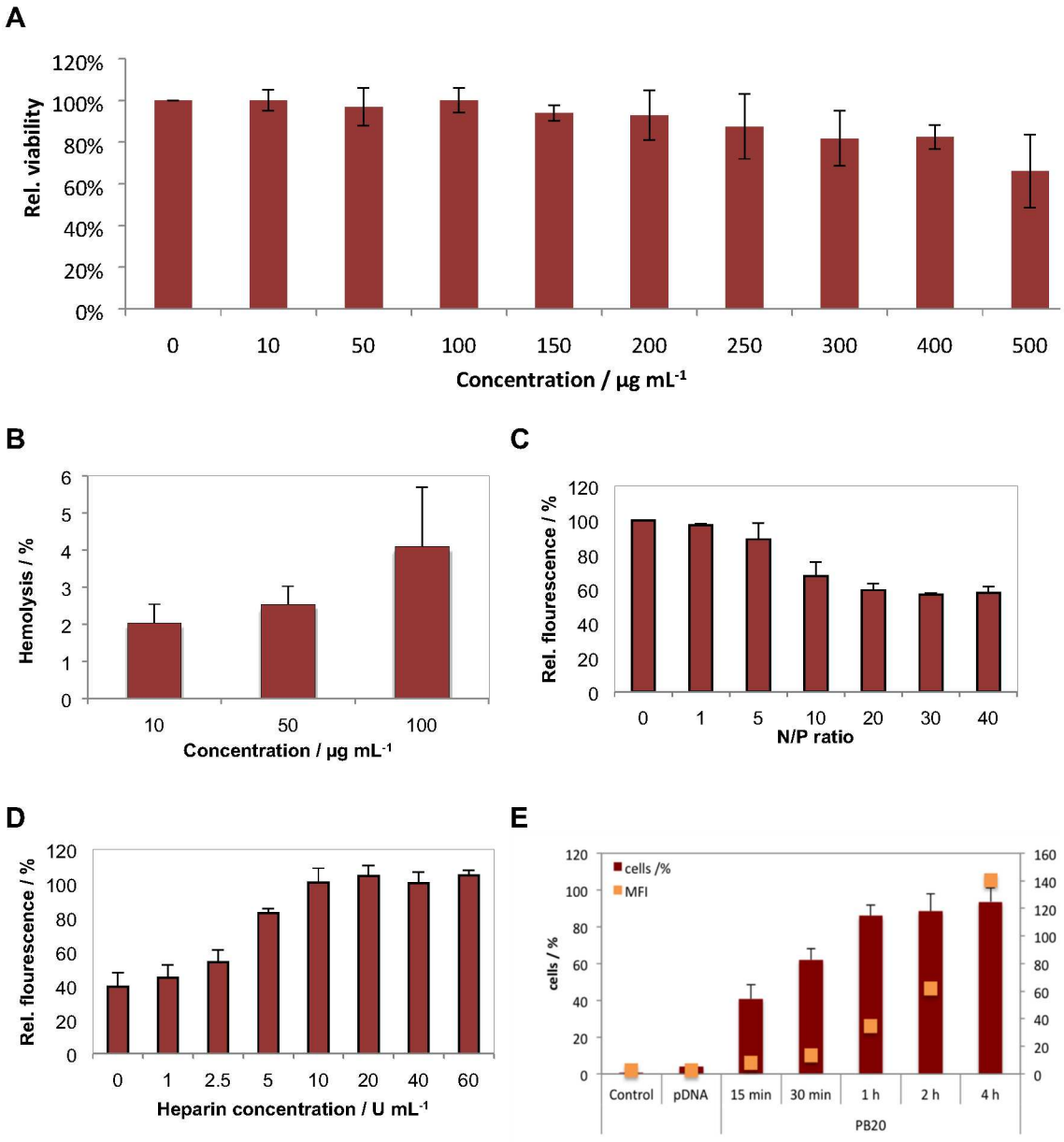

Figure S1. A) Cytotoxicity assay of **P2** using alarmaBlue. Non-treated cells served as 100% relative viability. B) Erythrocyte aggregation assay of **P2** at indicated concentrations. BPEI served as positive control and PBS as negative control. C) Hemolysis assay of erythrocytes after incubation with **P2** at indicated concentrations. Triton X-100 served as positive control (100% hemolysis) and PBS as negative control (1.99%). A value less than 2% hemolysis rate was classified as non-hemolytic, 2 to 5% as slightly hemolytic and values > 5% as hemolytic. Values represent the mean ± S.D. (n=3). D) Complexation affinity of **P2** with plasmid DNA at indicated N/P ratios (ethidium bromide quenching assay). E) Dissociation assay of **P2** polyplexes formed at N/P 20 using heparin (0 to 60 U mL^{-1}). Values represent the mean ± S.D. (n=3).

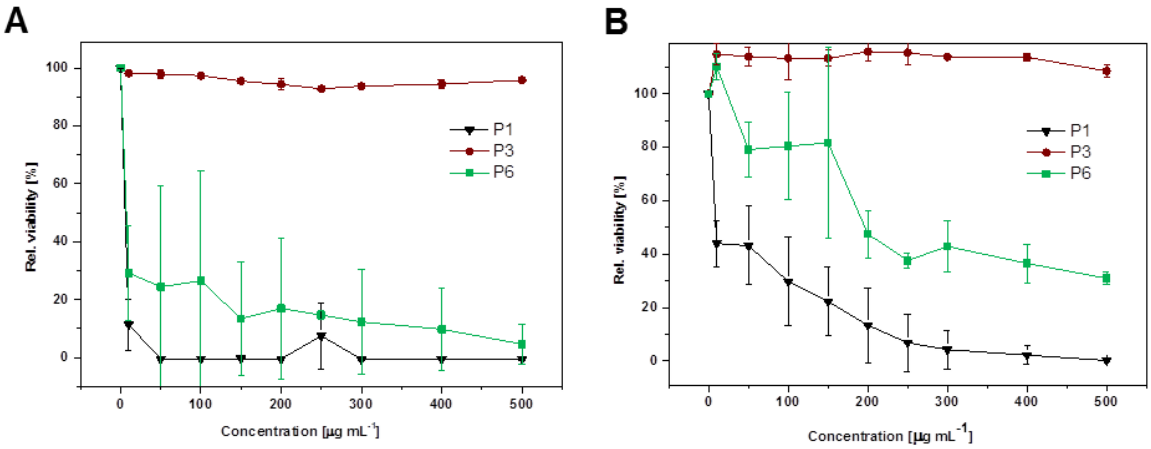

Figure S2. Biocompatibility. A) Relative viability of hCMEC cells after 24 h incubation with the respective polymers at indicated concentrations. B) Relative viability of HEK cells after 24 h incubation with the respective polymers at indicated concentrations.

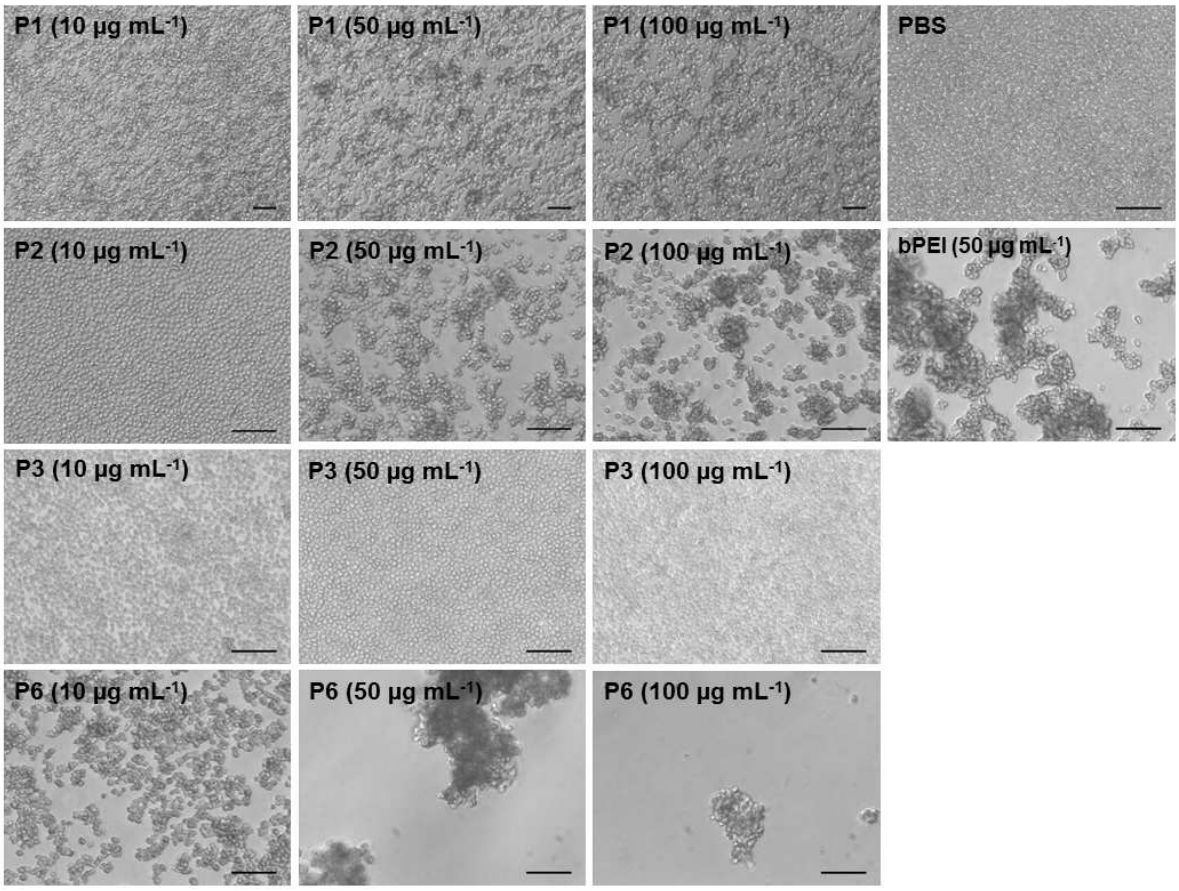

Figure S3. Light microscopy of erythrocyte aggregation of the polymers **P1**, **P3** and **P6**. PBS served as negative control, while bPEI (25kDa) was served as positive control. Scale bar = 20 µm.

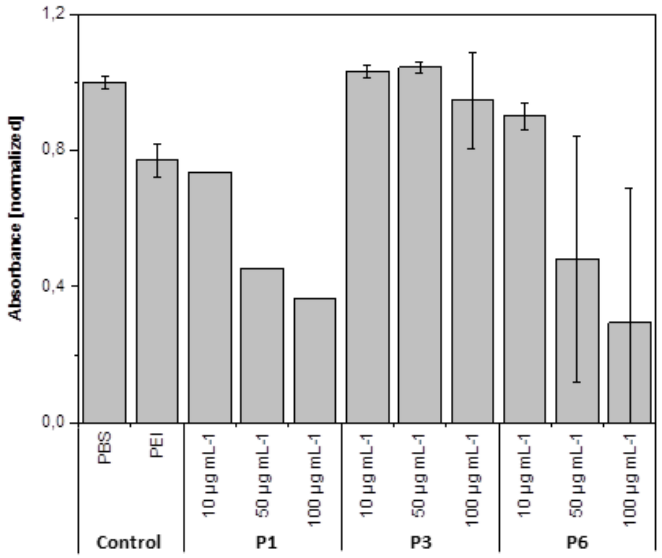

Figure S4. A) Hemolysis assay of erythrocytes after incubation with polymers at the indicated concentrations. Triton X-100 served as positive control and PBS as negative control. A value less than 2% hemolysis rate was classified as non-hemolytic, 2 to 5% as slightly hemolytic and values >5% as hemolytic. Values represent the mean ± S.D. (n=3). B) Erythrocyte aggregation of the tested polymers at indicated concentrations. bPEI (25 kDa) served as positive control resulting in high aggregation formation and PBS as negative control. Values represent the mean ± S.D. (n=3).

Table S5. Size and zeta potential of polymer **P1**, **P2**, **P3** and **P6** in HBG buffer measured by dynamic and electrophoretic light scattering.

Polymeric system	z-Average [d/nm]	PDI	Number-weighted size [d/nm]	Zeta potential [mV]
P1	450 ± 7	0.51	< 1	10.4 ± 0.5
P2	328 ± 27	0.66	< 1	4.9 ± 0.4
P3	233 ± 11	0.40	< 1	4.0 ± 1.4
P6	140 ± 23	0.58	26	28.4 ± 0.6

Table S6. Size and zeta potential of pDNA complexes of **P2** at N/P 20 in HBG buffer measured by dynamic and electrophoretic light scattering.

Polymeric system	z-Average [d/nm]	PDI	Number-weighted size [d/nm]	Zeta potential [mV]
P2	264 ± 11	0.35	109 ± 33	24.3 ± 1.1

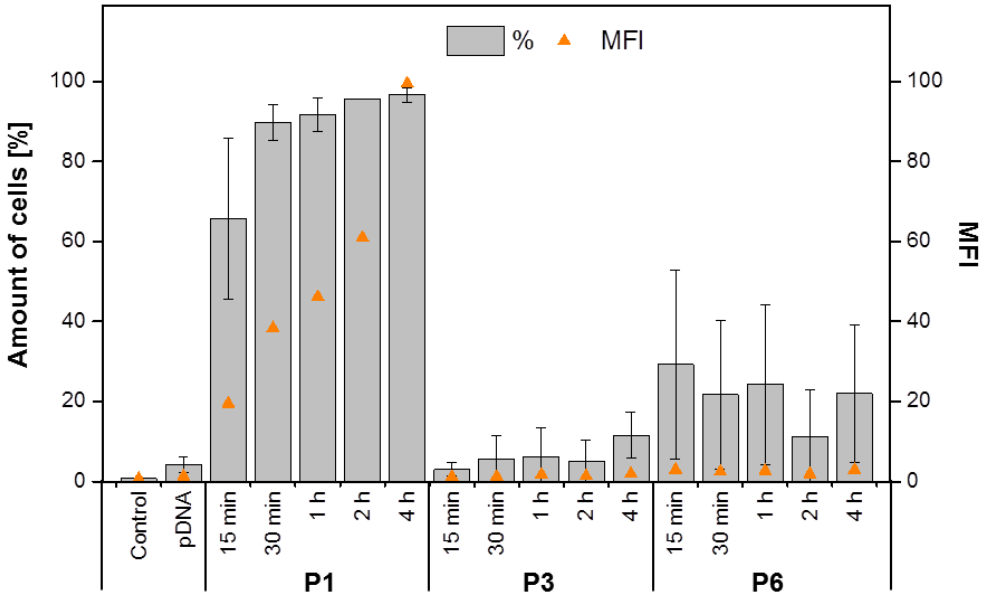

Figure S7. Cellular uptake study of **P1**, **P3** and **P6** polyplexes (N/P 20) using YOYO-1abeled pDNA. hCMEC cells were treated in EndoGro media with polyplexes for 4 h and uptake was analyzed via flow cytometry (MFI – Mean fluorescence intensity). Values represents the mean ± S.D. (n=3).

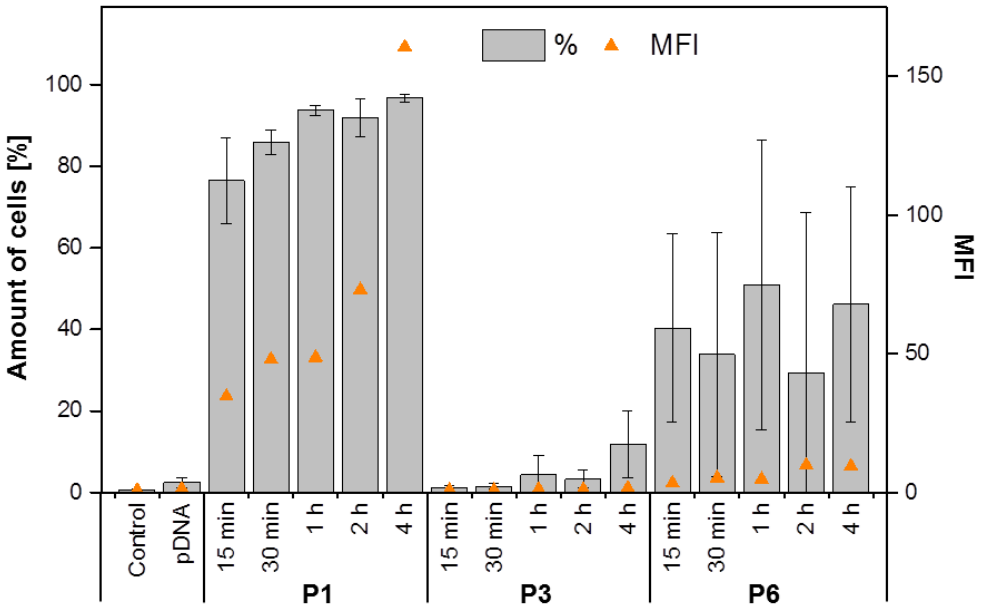

Figure S8. Cellular uptake study of **P1**, **P3** and **P6** polyplexes (N/P 20) using YOYO-1abeled pDNA. hCMEC cells were treated in OptiMEM with polyplexes for 4 h and uptake was analyzed via flow cytometry (MFI – Mean fluorescence intensity). Values represents the mean ± S.D. (n=3).

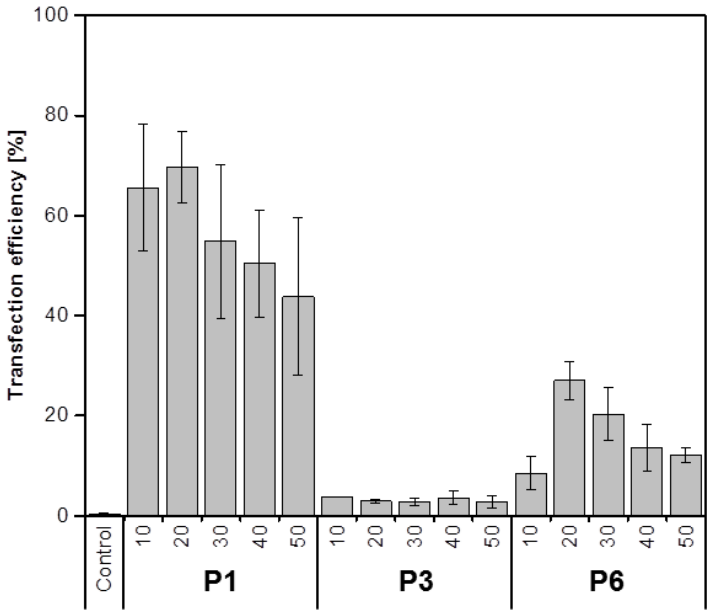

Figure S9. Transfection efficiency of copolymers **P1** to **P3** and **P6** for adherent HEK cells in OptiMEM at different N/P ratios after 24 h. Values represent the mean ± S.D. (n = 3).

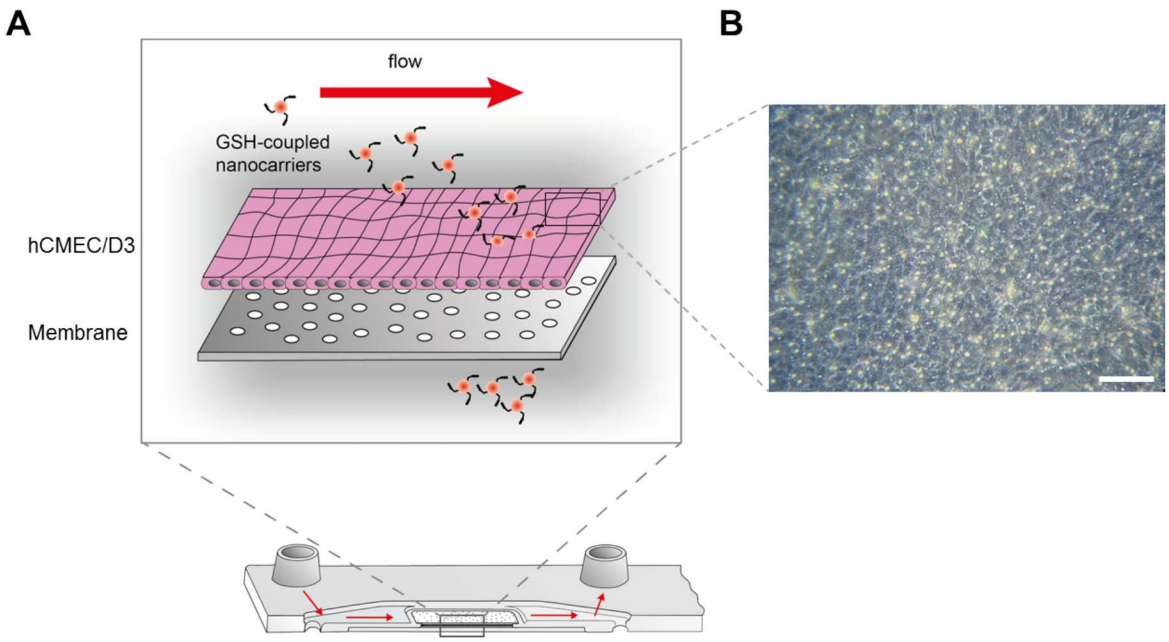

Figure S10. Chip geometry and dynamic cell culture setting. A) Schematic illustration of hCMEC/D3 cultured on top of a porous membrane within the chip. GSH-coupled nanocarriers are perfused on the apical side and passage through the cell layer was investigated basolateral. B) Microscopic image of confluent and tight hCMEC/D3 layer cultured within the chip. Membrane pores appear as bright round spots shining through the cell layer (scale bar 100 nm).

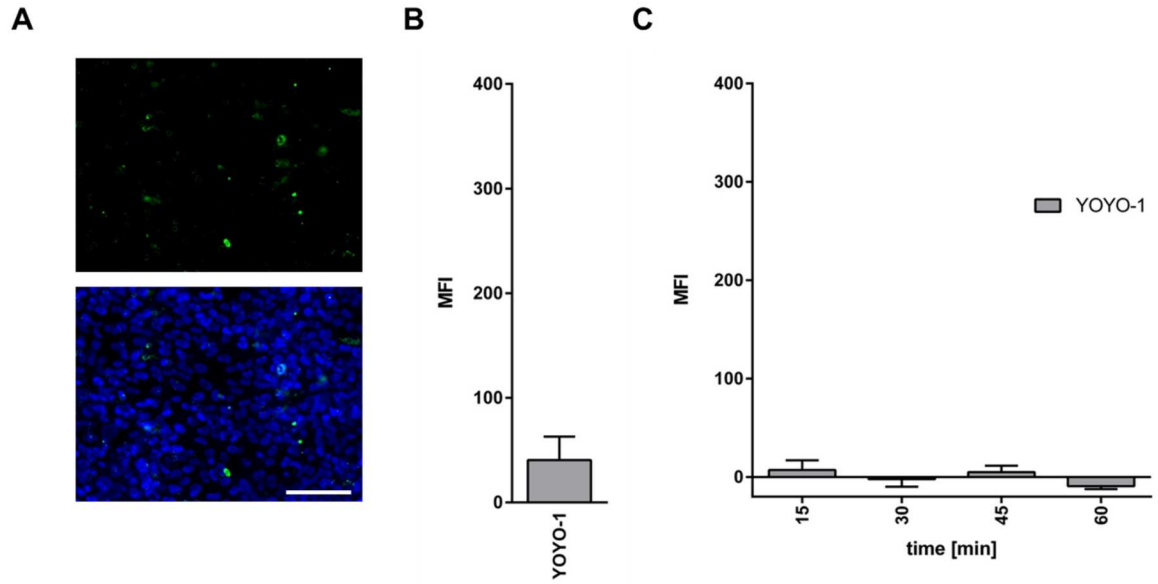

Figure S11. Negative control without polymer induced polyplex formation. A) Fluorescence images of YOYO-1 residues (green) on hCMEC/D3 (nuclei in blue). Only slight interaction can be observed. B) Quantification of YOYO 1 residues on hCMEC/D3 layer. C) Analysis of possible passage through hCMEC/D3 layer over time. No markable fluorescence was detectable. (scale 100 nm; n=3)

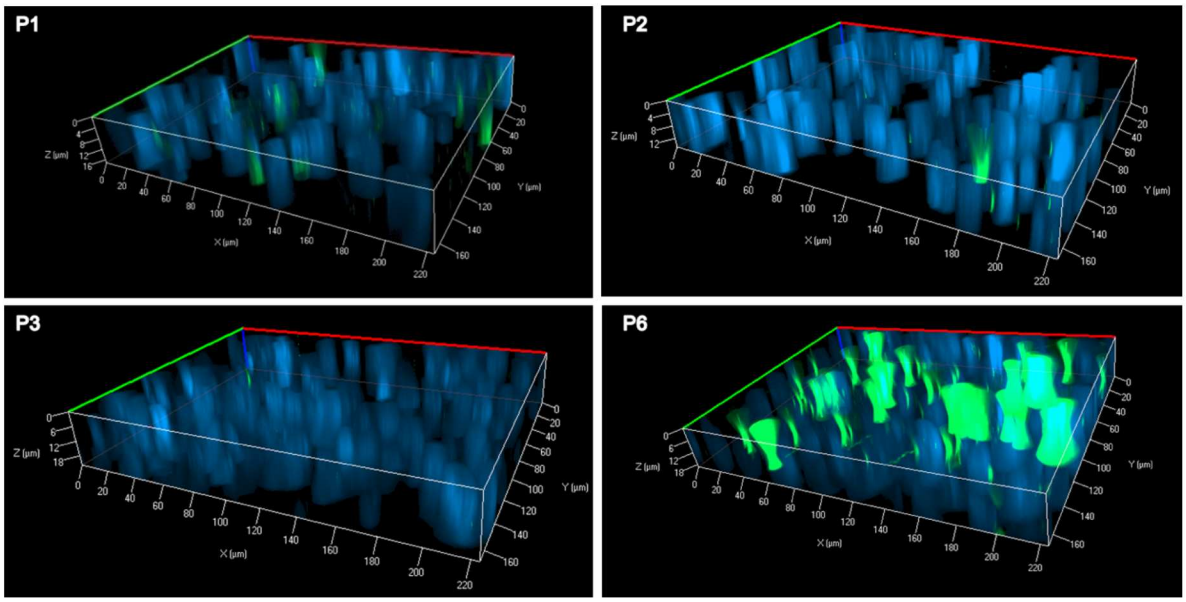

Figure S12. Three dimensional projection of z-stack images showing polyplex uptake (green) through localization at same levels as cell nuclei (blue) can be observed.

4. Discussion

The focus of my thesis is the establishment, characterisation and improvement of microfluidically perfused EC cultures within microfludically perfused MOTiF biochips. Based on this work a MPS recreating the BBB has been established. The perfused endothelial layers and the BBB model were further used in screening experiments with nanocarriers intended as potential novel therapeutic option of precise drug delivery. Research in human cell culture still relies on the use of classical petri dish approaches as standard cell culture technique. Physiologic conditions, especially microenvironmental cues such as shear and stretch are mostly neglected, though there is evidence for a need of these cues to enable physiological cellular behaviour *in vitro* [130, 131]. In examples it has been demostrated that vascular ECs improve morphologically [47, 79] and vascular smooth muscle cell (SMC) phenotype [132, 133]. The *in vitro* exchange of metabolic and catabolic substrates is performed at intervals creating a non-physiological sawtooth-like change of metabolite and nutrient levels in the cell culture medium. Further, cellular crosstalk is often not sufficiently considered. It was shown that isolated vascular smooth muscle cells (SMCs) lose their contractile, fully differentiated phenotype in *in vitro* in a mono-cell culture [134], but this altered secretory SMC phenotype is less distinctive in endothelial co-culture [135]. Hence, a loss in paracrine signalling as well as cell-matrix interaction can lead to cellular dedifferentiation [136]. Due to such unwanted and to a certain degree uncontrollable *in vitro* cellular behaviour and the lack of sophisticated models, more complex research and drug testing is solely achieved using cost and time consuming animal models, lastingly challenged by ethical values [137-140]. That there soon will be no common agreement on the moral dilemma how extensively animal models should be used, lies in the diverse nature of human beliefs as Foëx reasonably outlines [141]. However, if pursuing animal experimentation, the most challenging issue for researchers remains the transferability gap between species. Not only dose extrapolation is a matter of dispute [142], but approaches relying solely on animal models are challenged since translation of research strikingly fails. For instance only 8 % of cancer drug candidates pass clinical trial phase I [143]. First of all, one might think of toxic side effects, but non-predictive nature regarding bioavailability and that there is a high rate of non-correlation between species is also problematic [144]. In a NIH director's blog entry, current director Collins refers to different linkages between human genes addressing sepsis, trauma and burns compared to genes in mice. A circumstance which lead to about 150 drugs failed-by-design in humans [145]. Despite it is known that human patients may be exposed to severe unknown side effects, animal models for clinical research interfere establishing appropriate predictive models [146]. In a 2015 released article Green enumerates clearly a lot of attributable reasons for both issues: bias in study design, in data analysis, from data over-interpretation, from irreproducibility, in

reporting, in publication and validation of animal models as well as economic facts [147]. Meta-analysis of reported methods and data might help to re-evaluate suitability of animal models in narrow question-specific contexts, yet it is highly time consuming. Most urgent problems to humans so far result from data over-interpretation, which might result in false assumptions and lead to ineffective drugs, non-specific target structures and mechanisms, as well as from drugs with unknown harmful side effects. To overcome these problems there is a requirement for new evaluation strategies in pre-clinical screening techniques. This may affect all fields in designing drugs: screening for promising structures and selecting candidates as leading structures, screening for highly specific target sites on cellular and protein level, screening for appropriate carrier polymers, ADME/tox assays (absorption, distribution, metabolism, excretion), which can be addressed by the use of MPS. In contrast to the above-mentioned status quo of cell culture approaches it is possible to closely resemble microenvironments of different sites of the human body in a complex fashion. Driven by the application of of flow and related flow mechanics of several body fluids the field has evolved into linking cellular crosstalk, scaffolding, shear stress and spatiotemporal molecular gradients into MPS (fig. 8) [148].

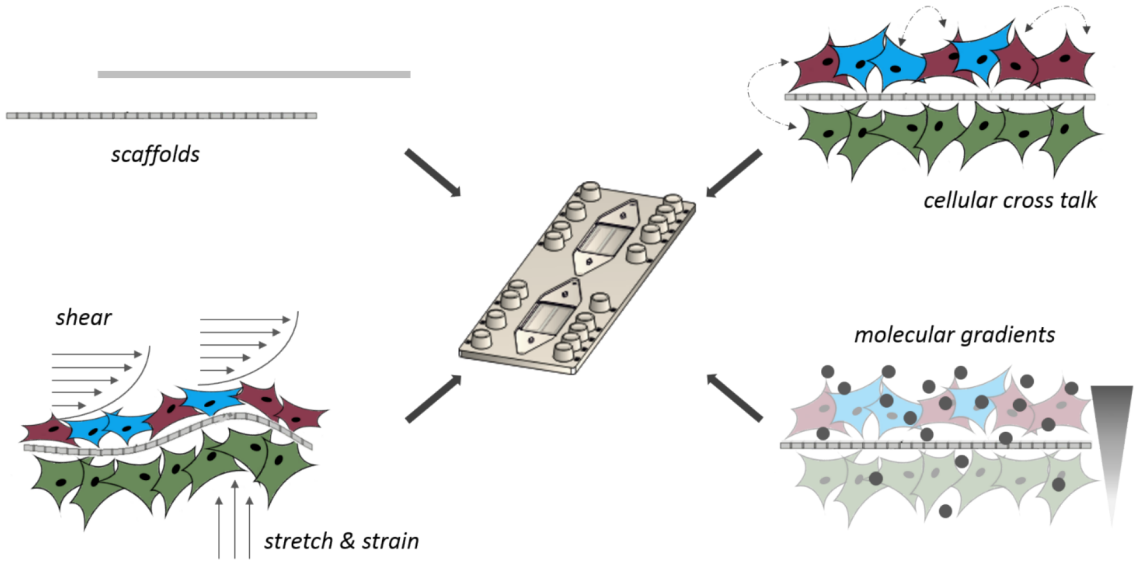

Figure 8. *MPS linking material sciences, physics and biology.* Microfluidic devices with multiple layers enable a complex interplay between materials, physical forces and cell biology. It represents a new technology to perform human *in vitro* cell culture in a more comprehensive way.

ECs represent the cell type under most influence of fluid shear stress and mechanical stretching through the pulsatile movement of the blood stream (extensively reviewed in [57]). Davies and colleagues showed the inherent nature of morphological alignment of ECs when exposed to shear stress *in vitro* [80]. Extensive studies on that phenomenon and subcellular structures were performed since then [40, 44, 47, 79, 149, 150]. Regarding the establishment of microfluidic cell culture within the MOTiF biochip choosing ECs as model system for this

thesis had several important advantages. They are easy to culture *in vitro*. Changes in response to flow culture are already observable on a macroscale level through cellular alignment. Since directly in contact with the blood flow *in vivo* ECs are the first cells to encounter xenobiotics and to get in contact with immune cells. Thereby they regulate important functions of the vascular bed: restrictive barrier [151, 152], immune cell adhesion, migration and infiltration [153] of underlying tissues, molecule passage [28, 152] and uptake of drugs [154]. A simple mimicry of the vasculature is also important for nutritional renewal in MPS since a lot of organ tissue specific cell types do not experience high flow and shear rates within the human body and may react very sensitive to it. Yet, diffusion distances for oxygen and nutrients are small before totally consumed. A rapid supply without impairing the cells must be ensured.

4.1 MOTiF biochip design enables innovative *in vitro* endothelial cell culture

Biochip-based systems are on the verge to revolutionise *in vitro* cell culture and pre-clinical drug testing. A smart design enables the overall control of cellular microenvironments with focus on the replication of *in vivo* like settings to maintain an *in vivo* like cell phenotype [148]. Simple approaches use commercially available two-dimensional perfusion chambers. Despite perfusion of cells, more complex biologic processes like cell layer permeability studies, cellular transmigration, vertically applied molecular gradients and directed secretion of chemokines achieved through cell polarity cannot be studied. Subdividing the perfusion channel by a porous membrane horizontally within the MOTiF biochip overcomes these limitations and additionally enables basal cellular perfusion (3D perfusion). Furthermore, the free hanging membrane is more flexible than rigid surfaces and additionally supports cellular adjustment to mechanostimulatory cues transduced by the substrate. Contact angle measurements and computational fluid dynamic simulations revealed a laminar flow profile within the MOTiF biochip. A laminar flow profile is of high importance for a healthy EC phenotype [50, 155]. It is shown that ECs exposed to oscillatory or turbulent flow exhibit a polygonal morphology [156, 157], increased cellular turnover [40, 95] and that they show different global gene expression patterns [158] and higher secretion levels of MCP-1 and IL-8 [159]. In the literature, these observations are consistently discussed by linking altered flow profiles with atherosclerosis [6, 95, 160]. Given the integrated key feature of the porous membrane subdividing the perfusion channel, we also perfused EC layers three-dimensionally, i.e. from the apical and basal side of the cells. This resulted in a high remodelling of cytoskeleton and exhibited an increased cellular height compared to standard flow chambers. Moreover, we observed an increased expression of vWf in MOTiF biochips independently form shear stress with highest expression in areas of high pore-density. The formation of *in vivo*-like high molecular weight vWf strings [161, 162] was also detectable. A neutral extracellular pH-value influences vWf string formation in WPBs [163] and is promoted by the continuous nature of perfused EC culture. Von

Willebrand factor exocytosis is furthermore regulated through VEGF-receptor 2 signalling by mechanostimulation [164]. Three-dimensional flow conditions might stretch the membrane thereby triggering the ECs to release vWf. *In vivo* these vWf strings remain temporarily associated with the cells [165, 166] and contribute to a healthy endothelium [167]. Increased cellular heights could also be found in other perfusion models of renal tubular epithelial cells [104, 124]. It seems to be a common characteristic of perfused endothelial and epithelial cells. But nutritional supply and catabolite removal by only apical perfusion in standard perfusion chambers restricts cellular growth and height and does not have such great impact on EC phenotype as could be shown with 3D perfusion conditions. Another innovation within the MOTiF biochip design relies strictly on the use of the plastic cell culture substrates such as COC and PS and the integration of PET membranes. Most similar applications are made of PDMS, mainly because soft-lithography based methods for an easy fabrication and rapid prototyping are well established [168, 169]. However, this material bears some disadvantages for (EC) cell culture (cf. 1.3.2). It should be added, that it absorbs small [101] and hydrophobic [109] molecules rendering the material impractical for substance and drug testing. Compared to other chip designs, the MOTiF biochip is modular. It is possible to attach a second chip body underneath the first modifying the former second level to a membranous structure thereby creating a third level for cell culture and perfusion. This was done for the development of a BBB-like model (cf. manuscript III) enabling complex 3D cell culture. The new channel height of 1.1 mm in the middle of the modular biochip enables the integration of pre-cultured tissue spheroids, which were immobilised on a porous membrane containing microcavities of 800 µm. In general, different cell supporting surfaces can be easily integrated by replacing membranes. However, throughout all experiments PET membranes with 8 µm pore diameter and a pore density of 10^5 / cm² were used for EC culture establishment. Taken together, the MOTiF biochip design sets up favourable culture conditions for endothelial cells: individual two-dimensional and 3D perfusion, precise control of shear stress, a membrane as scaffold additionally allowing mechanostimulation and a chip bulk material suitable for substance and particle testing.

4.2 Microfluidically perfused endothelial cell layers benefit morphologically and on the molecular level

4.2.1 Improved perfusion conditions support endothelial cell biology

ECs are exposed to various stimulatory cues throughout the vasculature: shear forces, different types of flow profiles (laminar, oscillatory or turbulent), mechanostimulatory stretch, interaction with perfused cells of the blood and immune system. They all show a strong impact on endothelial physiology [10, 11]. As pointed out above, MOTiF biochips are suitable for

endothelial perfusion in a 3D fashion. This should lay the foundation for establishing flow culture for this thesis and for further research projects. To test, if EC layers within MOTiF biochips behave like it is reported in the literature for endothelial flow culture, ECs were perfused for 24 h. Different shear stress rates of 0.07 Pa (0.7 dyn / cm²) and 1 Pa (10 dyn / cm²) were chosen to characterize cellular adaption to altered environmental conditions. Results were additionally compared to standard flow chambers and static culture conditions (cf. manuscript I). Initially, improved perfusion conditions resulted in a more viable cell layer in MOTiF biochips compared to standard flow chambers. We hypothesize that this might be triggered by an improved removal of catabolites and supply with nutrition related to bidirectional apical and basal perfusion of ECs. As expected, morphological adaption of cells to shear stress and flow have been observed. Cell shape index (CSI) analysis revealed significant differences between perfusion in standard flow chambers and MOTiF biochips with significant lower values in the latter indicating more stretched and aligned ECs. This was accompanied by extensive cytoskeletal remodelling and higher cell densities in the MOTiF biochip. This was indicated through prominent F-actin expression and stress fibre formation in MOTiF biochips additionally promoting changes in cellular alignment and a decrease in CSI. Results obtained for static as well as standard flow chamber experiments differed in CSI and F-actin expression intensity and pattern with inferior results. This might be due to chip design and the nature of materials chosen as cell culture surface: flexible membrane in MOTiF biochips vs. rigid channel surface in standard perfusion channels (cf. 4.1). Additional stretch of at least 4 % applied to ECs enhances cellular alignment in flow direction, stretch of at least 7 % also cellular elongation. Moreover, this correlates positively with prominent F-actin stress fibre formation when stretch forces and shear stress increase [170]. Although we can only speculate, this type of mechanostimulation might be responsible for a more distinct endothelial phenotype with strong F-actin fibres and might result in stronger endothelial attachment since cell numbers in MOTiF biochips increase with applied forces. This is in contrast to data from standard Boyden chambers, in which EC numbers decrease. The only obvious difference can be seen in the surface condition and 3D perfusion. The enhancement of vWf expression independently from shear stress can be regarded as further evidence for mechanostimulatory cues coming from the flexible membrane surface, again emphasising how the newly developed MOTiF biochip supports EC culture (cf. 4.1). Interestingly, ultra large vWf strings seem to be important for the initial pathogenic step of *S. aureus*-induced endocarditis in patients with a healthy endothelium [171]. Since the exact mechanisms of vWf string formation still remain to be uncovered, endothelial cell culture in MOTiF biochips represents an interesting approach to study vWF biology and its interaction with immune cells under flow conditions.

4.2.2 Endothelial barrier modulation and immune cell recruitment: recreation of inflammatory events within MOTiF biochips

The maintenance and regulation of the endothelial barrier is crucial for endothelial interactions with immune cells in health and disease. Among others, EC junctional integrity is regulated by PECAM-1 [23]. It was found to be significantly upregulated in MOTiF biochips when EC layers were perfused three-dimensionally. This was accompanied by elevated ZO-1 levels under high shear stress. ZO-1 also contributes to endothelial barrier formation [3]. Elevated levels of both proteins contribute to a tighter endothelial barrier within MOTiF biochips. Moreover, thickened endothelial layers mediated by extensive cytoskeletal remodelling enhance barrier formation in perfused biochip cell culture. Similar observations were made on renal tubular epithelial cells in biochip models of the human kidney [104, 124]. To test barrier functionality and modulation, pro-inflammatory cytokines TNF and IFNγ were applied basally. It is reported that PECAM-1 is downregulated and redistributed during inflammatory events [172] leading to an impairment of endothelial barrier function [173]. ZO-1 responds to IFNγ treatment with decreasing protein levels and subcellular localization [174]. Cytokine stimulation of ECs resulted not only in a loss of PECAM-1 and ZO-1 protein expression as could be shown by immunofluorescence staining. An overall cellular elongation was observable additionally. Stroka et al. were able to show that this enhanced elongation observed in TNF treated ECs is accompanied with dynamic shifts in cytoskeleton and reduced cell stiffness [175]. Thus, a barrier breakdown and leakage visualised by FITC-dextran passage is a combination of decreased protein levels and reduced cellular cytoskeletal stiffness. Impaired endothelial barrier function contributes to various diseases such as sepsis and associated inflammatory syndromes leading to bacterial translocation [30], and it also contributes to injury like trauma and burns [29]. In the context of inflammatory processes, we then investigated the expression of cell adhesion molecules on perfused EC layers in MOTiF biochips. TNF treatment furthermore activates the endothelium, which also includes an altered cell adhesion molecule expression linked to inflammatory processes [31, 176, 177]. In MOTiF biochips it was found that ECs exhibit a characteristic cell adhesion molecule expression profile in response to shear stress. In agreement with data from previous work ECs adapt to high shear stress rates by upregulation of ICAM-1 and VCAM-1 [51, 178]. Upon TNF treatment ECs showed decreased levels of ICAM-1, VCAM-1 and E-selectin under shear stress when compared to static cell culture. Laminar shear stress attenuates the expression of VCAM-1 and E-selectin after TNF treatment by NF-κB signalling pathways [179, 180] as well as does flow-mediated release of nitric oxide [181]. However, in these studies ICAM-1 upregulation was shown in response to TNF treatment within flow conditions. This might be due to different stimulation times used in all these studies [179, 180]. Stressing that point again, endothelial layers within MOTiF biochips are exposed to low

stretching due to membrane flexibility, it is possible that this mechanostimulation contributes to the observed reduction of ICAM-1 expression. In another study TNF treated ECs show diminished ICAM-1, VCAM-1 and E-selectin expression when exposed to 1.5 Pa shear stress and 100 mmHg hydrostatic pressure [182], which is in accordance to the results obtained in our study. Altered CAM expression could be further successfully tested for functional relevance regarding immune cell adhesion under perfusion conditions. The application of shear stress revealed significantly less immune cell adhesion on ECs without TNF treatment compared to static condition. But there was still a decrease in THP-1 adhesion with increasing shear stress observable which was in accordance with the observed CAM expression profile after 24 h. The first of the three basic steps in cell adhesion involves selectin-mediated rolling along the endothelium, the second is characterized by integrin activation and the third involves integrin mediated adhesion to CAMs [17, 183, 184]. The balance between these adhesive forces and additionally applied dispersive hydrodynamic forces determines cell adhesion [185]. *In vivo* diminished expression of these molecules in response to flow might help keeping the balance in a healthy state, even during inflammatory processes, preventing massive immune cell recruitment and detrimental immune cell activation. Flow-mediated cell adhesion is not only crucial for immune cell recruitment and migration. The concept of flow mediated distribution of cells and subsequent adherence at particularly exposed sites of the vasculature is highly important in cancer cell metastasis. Tumour cell-endothelial and tumour cell-matrix interactions determine their metastatic potential [184]. A multifactorial analysis is of high importance since not only receptor-ligand interactions influence cell adhesion but different kinds of shear stress at different sites throughout the vasculature also strongly contribute as could be demonstrated. Hence, improved perfused EC cultures in MOTiF biochips could contribute to studies of vascular inflammation and vascular tumour cell interaction.

EC biology relies strongly on culture methods chosen as could be shown in manuscript I. Cellular growth regarding cell densities, cellular heights, cellular shape and alignment as well as molecular configuration strongly depends on applied shear forces and perfusion regime. These shear forces simulate *in vivo*-like conditions helping to create target-oriented microenvironments of different kinds of vascular beds. Even the nature of applied forces (two-dimensional vs. 3D perfusion; rigid vs. flexible substrate surfaces) results in strong differences and reveals cues about the importance of multifactorial cell culture techniques. Functional effects can be seen on the molecular level with different expression patterns for endothelial marker proteins, adherens and tight junction molecules corresponding to barrier functionality, CAMs and related cellular interactions and recruitment. Hence, EC layers benefit morphologically and on the molecular level when cultured under flow conditions. These perfused EC layers could further improve studies on vascular inflammation, EC barrier modulation and tumour cell adhesion.

4.3 Distinct microenvironmental modulation mediates endothelial-nanoparticle interaction

4.3.1 Mechanomodulatory cues influence endothelial cell nanoparticle uptake

Microenvironmental conditions influenced by non-biological – at least in context of *ex vivo* culturing – factors such as shear stress and mechanostimulation as well as culture surface materials and geometric design of novel culture devices have strong impact on EC outcome. Distinctive results of shear stress influence on endothelial culture (cf. manuscript I) lead to a follow up study on NP uptake under different shear forces and with different polymer compositions (cf. manuscript II) as part of this thesis. Based on the shear stress-mediated alterations in endothelial biology on morphological and molecular levels, we hypothesised a strong impact in a pharmaceutical screening context. ECs are the first cells throughout the circulation to encounter xenobiotics. Furthermore, polymer-based NP drug delivery gets more into research focus due to improved pharmacological properties, higher efficacies and reduced side effects compared to direct drug application [64]. Nanoparticle uptake is affected by size, shape, surface charge and protein corona [67, 74]. These factors influence and challenge biodistribution and determine the interaction with the RES. Further, predictions concerning uptake and clearance remain challenging tasks, especially when translating *in vitro* data into *in vivo* research [186, 187]. These concerns were addressed by investigating the uptake behaviour of a well-designed NP library with different characteristics under a range of shear forces in perfused EC culture. Initially, NP composition and applied shear stress were of interest, that's why a simple standard flow culture design was chosen to not elaborate study design too much. First, NPs consisting of different compositions of 3 % PMAA and 13 % PMAA or 20 % PDMAEMA were characterised in size, shape and charge by colleagues before subjecting them to flow-based uptake studies on ECs. Batches of 200 nm in particle size were selected where endocytosis could be assumed as internalisation mechanism. Four different kind of shear stresses were chosen: 0.07 Pa (0.7 dyn / cm²) representing basal medium exchange with low stimulating effects on endothelial biology and is assumed to be present in the human hepatic sinusoid, 0.3 Pa (3 dyn / cm²) and 0.6 Pa (6 dyn / cm²) in human veins and venules [6], the latter one also in human suprarenal aorta and 1 Pa (10 dyn / cm²) representing conditions to be found in human common carotid artery [116]. Our initial hypothesis would have expected to reveal a decreasing NP uptake with increasing shear forces. Keeping experimental parameters defining shear stress steady, such as medium viscosity and channel properties, higher shear forces are only obtained by an increase in flow rate (cf. eq.1, 1.3.3). We hypothesised a shorter interaction time between particles and cells would lead to an impaired uptake rate. All three NP compositions falsified this assumption by showing a positive

correlation between increasing shear stress and the total amount of internalised NPs. These results indicate a strong interaction, adhesion and internalisation with ECs even at high shear forces for the chosen type of particles. On the one hand, endothelial uptake is positively modulated by high shear forces. Endothelial permeability for macromolecules such as LDL increases [41] and most likely may an altered endocytosis profile influence NP uptake. On the other hand, the observed uptake profile might be a NP material-dependent observation. A review of the literature supports the initial assumptions since other studies investigating SiO_2-NPs or PS-based NPs showed reduced uptake rates under increasing shear stress conditions, even in the presence of targeting antibodies [154, 188, 189]. These findings suggest enough cell-target interaction *in vivo* for the methacrylate-based particle compositions. But uptake rates differed markedly among the particles from our library. Compared to static conditions a higher frequency of particle-cell interaction with increasing flow rates facilitated particle uptake with lowest uptake rates for 3 % PMAA and highest uptake rates for 20 % PDMAEMA in general. Interestingly, with the highest shear stress of 1 Pa endothelial-particle interaction changed and 20 % PDMAEMA particles showed less uptake efficiency than 13 % PMAA which stands in contrast to static and low shear stress observations. These effects might be most likely evoked by different surface protein expression patterns and EC responses to shear forces as the results from manuscript I suggest (cf. 4.2). As a conclusion shear forces applied in perfused EC layers emerge to be key features influencing NP uptake and represent an important screening characteristic. Differences between static and dynamic culture conditions emphasise these assumptions. Most importantly, in comparison to the literature, perfused EC layers might reveal unique EC-NP interactions (elevated or reduced) that are not visible in static culture.

4.3.2 Tissue-resident macrophages dampen endothelial nanoparticle uptake rates

It was important not just to reflect conditions present along the vasculature, but also to address liver sinusoidal physiology with emphasis to shear forces and phagocyting cells. The liver plays an important role in drug and NP clearance metabolizing 73 % of the most common drugs [190]. Most responsible for this clearance capacity is the cytochrome P450 enzyme group [191] and tissue resident macrophages known as Kupffer cells, respectively. These cells line the walls of the liver sinusoid, reside within its lumen among ECs and are as well highly programmed to phagocyte particles from the blood stream [192, 193]. Moreover, cell-cell interactions, especially between different type of cells, have strong impact on cellular behaviour. Thus, in a second step macrophages were introduced into endothelial chip culture for studying NP fate upon perfusion with respect to physiologic implications in a heterogeneous cell environment. Also, in the presence of macrophages, a shear stress dependent increased uptake of methacrylate-based NPs was observable in both ECs as well as macrophages. As

expected, due to their phagocyting nature macrophages showed higher uptake rates than ECs, but with same tendencies for strongest interaction with 20 % PDMAEMA particles. Interestingly, macrophages seemed to impair endothelial NP uptake intensely in co-cultures compared to endothelial mono-culture. It is not likely that this was just an effect by an increased uptake rate of macrophages since an excess of NPs was applied and local concentration gradients formed by uptake processes must have been outbalanced easily by perfusion. This finding gains most importance regarding high perfusion conditions where most prominent differences in endothelial mono-culture were observable. It might be hypothesised that macrophages influence ECs in co-culture via paracrine signalling pathways thereby impairing their particle uptake behaviour (fig. 9).

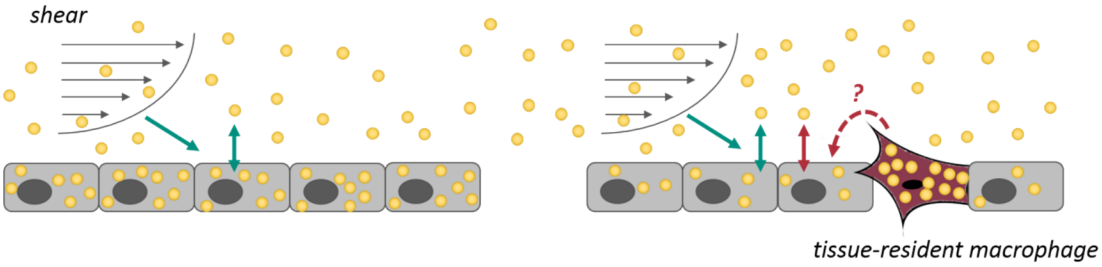

Figure 9. *Influences on EC-NP interaction.* ECs are influenced on a functional level by physical and biological components of their microenvironment. Shear stress modulates EC-NP interaction and uptake dynamics. Tissue-resident macrophages seem to dampen EC-NP interaction and uptake by yet unknown paracrine signaling.

The NP uptake profile could also be recapitulated by colleagues in a mouse model using intravital microscopy. Fastest uptake was observed for 20 % PDMAEMA followed by 13 % PMAA. Slowest uptake was exhibited by low-charged 3 % PMAA NPs. Furthermore, Kupffer cells showed a strong interaction and uptake with all particles compared to the endothelial lining within the sinusoidal structures. In general, the experimental outcome of *in vivo* administration and particle distribution between endothelial and macrophage cell types support the results obtained in the perfused EC culture experiments. Previously it was shown that *in vitro* studies underestimate effects and effectiveness of NP uptake and clearance *in vivo* [194]. In the case of endothelial macrophage co-culture further studies are required to fully elucidate possible signalling events which impair other cell types in NP uptake when macrophages are present. These findings arise importance in NP therapies. More complex cellular and perfused *in vitro* culture models might lead to a better understanding and predictability of NP administration and effectiveness, especially in tumour therapy. The question arises if tumour-associated macrophages are able to modulate NP uptake in cancer cells leading to a reduced effectiveness in therapies or if these observations are restricted to the vascular endothelium [195]. Taken together, distinct microenvironmental control applied in these series of

experiments mediates endothelial behaviour towards *in vivo*-like settings.

4.4 Perfused endothelial cell layers contribute to the design of complex microphysiologic systems

MOTiF biochip models incorporating multiple cellular growth and perfusion dimensions, bare the possibility to emerge as promising tools to recapitulate diverse biologic processes like cellular growth, ADME processes of particles and substances as well as cellular cross-communication. A free hanging membrane further subdividing culture cavities in separate but interacting compartments thereby providing scaffolding surfaces, facilitates these new advantages. These settings provide the technical setting to build up organ-like structures and mimic organ-like functions on a microscale: the concept of MPS [96, 196].

4.4.1 MOTiF biochips support the culture of various endothelial cell types and enable molecular cross-talk between compartments

In MOTiF biochips, characterised EC layers may serve well as a simplified structure mimicking the vascular bed under perfusion conditions. ECs of various origins can be easily cultivated in MOTiF biochips and adapted to microenvironmental cues such as shear stress. Cell cultures opposite of the membrane can be designed in an organotypic microanatomy by mixing up or layering cell types in appropriate arrangements. We used this approach to create a BBB-like MPS combining the hCMEC/D3 cell line with murine cortical spheroids derived from embryonic stem cells (cf. manuscript III). The MOTiF biochip design was improved by introduction of a lower shell attached to the upper basic part via adhesive films. The integration of a second membrane beneath the original membrane of the upper part divided the chip into three microchannels with each bearing the option for cell culture and perfusion. The newly introduced membrane comprises thermo-formed micro-cavities with a diameter of 800 µm and pores with a diameter of 5 µm and allows the immobilization of cortical spheroids. Flow-induced shear stress substantially benefits to microvascular endothelial morphology, tight junction formation, receptor and transporter protein expression resulting in an improved BBB tightness and functionality [85]. Up to date, most published *in vitro* models of the BBB use static cell culture approaches [197], commonly in a transwell-design [198, 199]. The transwell assay has proven to be useful studying transport processes across tissue barriers [200], but was so far not perfusable. Thus, microfluidic chip-based solutions were developed. Herland *et al.* co-cultured human brain microvascular ECs (hBMECs) with pericytes and astrocytes in a semi-perfused approach. Their model did not undergo a microfluidic priming and adaption as cells were perfused only for some hours for analytical purposes. In this model, the BBB was responsive to stimulation with TNF as indicated by the release of G-CSF and IL-6 into the culture medium

[103]. Besides that, only a few studies have been reported to be microfluidic-based [201], thereby mimicking physiological shear stress conditions. One of the earliest models was the μBBB published by Booth and Kim [105]. Like most BBB models [202, 203], cells of rodent origin were used. Murine CMECs were co-cultured under perfusion with astrocytes which they reported to result in a significant increase in transendothelial electrical resistance (TEER) values. Similar observations were made in the Sym-BBB model of Prabhakarpandian and colleagues. Astrocyte- conditioned medium and shear stress resulted in an increased tight junction expression and decreased permeability of the endothelial layer [202]. Recently, more complex models included pericytes [203, 204]. In a novel microfluidic bioreactor, Brown *et al*. recreated the setting of a neuro-vascular unit by co-culturing ECs, astrocytes, pericytes and neurons. They tried to provide a micro-environment that favours the paracrine signalling between the cell types needed for the long-term stable differentiation of the BBB [204]. Subsequent analysis revealed substantial improvements in barrier formation regarding increasing TEER values, increasing protein expression of β-Catenin, decreasing permeability [203] as well as increasing tight junction formation [203, 204]. For a first approach, we chose the hCMEC/D3 cell line, which is reported to form a physiological barrier already in the absence of glia cells, astrocytes or pericytes [205, 206]. However, we additionally integrated complex neural tissue cultures. In our model, we demonstrate that our biochip-based approach allows the co-culture of endothelial hCMEC/D3 cell layers and cortical tissue spheroids under physiological perfusion conditions. Endothelial hCMEC/D3 layers still expressed central marker proteins known to regulate BBB integrity and flexibility *in vivo* such as vWf, VE-Cadherin, ZO-1 and β-Catenin [207-212]. Neural differentiation markers Tbr1, Tbr2 and Pax6 representing regulators of neocortical development [213-218] did not show significant differences in their expression levels when spheroids were cultured in the biochip setting.

Additionally, we performed functional testing under inflammatory conditions. It is crucial to combine an endothelial barrier with neural tissue in respect to the investigation of neuro-inflammatory processes and how both cellular environments affect each other. In this context, most microfluidic based BBB models are also designed in a PDMS chip environment. This enables highest flexibility for researchers in study but bears important disadvantages in experiment quality (cf. 1.3.2). Most importantly it adsorbs small and hydrophobic molecules rendering a BBB-like cellular environment impractical for substance and drug testing. However, barrier regulation and modulation by agents as well as substance passage are the most important issues in BBB models. We specifically can reproduce cytokine induced cellular damage such as the disruption of the endothelial barrier function with a nearly tenfold increase in 3 kDa FITC-Dextran leakage accompanied by subsequent alterations in neural cell morphology, increased neural cell death, diminished spheroid tissue integrity and decreased expression of neocortical developmental markers. These observations are in agreement with

findings from studies in other microfluidically perfused BBB models focusing on barrier integrity and modulation [210, 219] as well as studies made in mice regarding neocortical development under inflammatory conditions [220-222]. The data thus show that the presented *in vitro* model comprising an endothelial hCMEC/D3 barrier and cortical tissue spheroids can reflect crucial aspects of neuroinflammation during neocortex formation. This model however bears certain limitations. Of particular importance is the absence of astrocytes and pericytes. Both cell types are reported to improve microvascular endothelial barrier functionality [202-204] via paracellular signalling [223]. Moreover, resembling the setting of a neurovascular unit with endothelial, glia and neural components as well as basal lamina and ECM embedding is more favourable because of diverse interactions as well as the comprehensive impact of BBB modulation on neural tissue and vice versa. Such an approach would reflect the highly complex setup to be found at the neurovascular unit more physiologically [224]. This would render the system more predictable in relation to inflammatory condition modelling as well as for studies of drug applications regarding BBB passage and uptake capabilities at neural target sites. However, the current approach was chosen to have a first proof-of-principle with a simple cellular setup and a sustainable co-culture of different cell types and of different origins in the biochip. Follow-up studies will focus on an inclusion of astrocytes and/or pericytes as well as neurons or neural tissue of human origin to improve this first approach. Moreover, our biochip-based system currently lacks the ability to directly measure TEER values generated by the EC layers as electrodes between the cortical tissue spheroids and microvascular EC layer may affect spheroid growth as well as spheroid introduction into the biochip. Another point is the relatively large distance of 0.7 mm and the resulting volume of 160 µl between the co-cultured cells. This might influence endocrine and paracrine signalling between microvascular ECs and the neural tissue. Relatively large distances between neural tissue and microvascular ECs could be overcome by embedding interneurons and astrocytes in an ECM-like collagen gel to close the rather wide gap. However, to the best of our knowledge we reported for the first time a biochip-based model supporting the co-culture of a cerebral microvascular endothelial barrier and cortical tissue spheroids. The model resembles physiological shear stress conditions and allows a direct assessment of neuroinflammatory effects on vascular and neural tissue components. In conclusion, this model represents a valuable tool of the cerebral vascular crosstalk for suitable for further applications. It bears the option to study microvascular endothelial barrier integrity under the influence of drug or drug carrier administration (cf. manuscript IV and 4.4.2). Further, tissue integrity during as well as molecular mechanisms of diseases such as ischemia, trauma, brain tumours and brain infections could be investigated with further development of the model. Additionally, the results from manuscript III underline the feasibility of the MOTiF biochip for EC cultures of different origins and for developing more complex MPS.

4.4.2 Microphysiologic endothelial tissue barriers support *in vitro* drug screening

Microvascular endothelial barrier integrity plays an important role in drug administration and displays one of the most challenging obstacles regarding drug and nucleic acid delivery in the pharmaceutical industry [27]. The BBB is highly selective and passage of small molecules is strictly regulated [21] in a bi-directional way through several transport mechanisms [28, 225]. The functionalisation of nanocarriers with target moieties displays a key strategy to benefit from the active transport system to transport larger molecules. In this context, GSH-modified nanocarriers have been designed to demonstrate a facilitated transport of nucleic acids for therapeutic gene delivery across the BBB (cf. manuscript IV). Glutathione has already been reported to successfully cross the BBB in *in vivo* rat models and *in vitro* transwell assays [226, 227] as well as being used as NP coating agent [228-231]. The polyplex nanocarriers tested in this study have been investigated under physiological shear stress conditions of 0.4 Pa within a simplified human model of the BBB biochip system. We could already show that dynamic cell culture and shear stress has a profound impact on EC-NP interaction (cf. manuscript II and section 4.3) We could demonstrate the feasibility of microfluidically perfused endothelial layers to evaluate EC-NP interaction also for testing of peptide-decorated nanocarriers. Similar to results obtained in the study “Comparison of the uptake of methacrylate-based nanoparticles in static and dynamic *in vitro* systems as well as *in vivo”* (cf. manuscript II), it was shown that perfusion has a profound impact on nanoparticle uptake. In static control experiments (cf. suppl. information manuscript IV), two polyplex candidates showed superior interaction with microvascular hCMEC/D3 cells over the third candidate which was eventually evaluated to be best suited for transendothelial passage in perfusion experiments. Further, sustained endothelial barrier integrity for the lead candidate was demonstrated by immunofluorescence staining of tight and adherence junction proteins. Both approaches verified the favourable characteristics of diminished EC-NP interaction and increased barrier passage while preserving barrier integrity. With this study, we further showed the suitability of the MOTiF biochip for basic research as well as for nanocarrier screening purposes regarding uptake, trans-endothelial passage and toxic effects. One of the earliest microfluidic chip-based BBB models, the μBBB model [105], was used to study permeability of FITC-Dextran of different sizes in an murine EC and astrocyte co-culture approach to show the models suitability for drug delivery studies to some extent. This was further proven by a follow-up study using seven known neuroactive drugs including Ethosuximide (antiseizure medication) and Sertraline (antidepressant) for trans-endothelial passage [232]. Prabharkapandian *et al.* exemplarily demonstrated the application of the rat EC based sym-BBB model in an efflux study with rhodamine 123 and known L-type calcium channel blocker Verapamil to inhibit P-glycoprotein efflux transporter [202]. Brown *et al.* demonstrated the feasibility for such models by investigating the active trans-endothelial transport of ascorbate

across human brain microvascular ECs [204]. Most of the established models so far use cells of animal origin and neither of them has been used to study nanocarrier interaction at the BBB or nanocarrier transendothelial passage. This might be due to the early stage of the field of microfluidic *in vitro* BBB models concomitant with limitations taken into account as has been reviewed by Åberg [233]. To date, NP studies considering microenvironmental cues including shear stress and blood flow characteristics have been performed *in vivo* (comprehensively reviewed in [234]). Here, we report for the first time a novel nanocarrier with GSH moieties to cross the BBB which was designed for gene delivery within a microfluidic biochip-based model with microvascular ECs forming a BBB surrogate. *In vivo* models are suitable to finally examine nanocarrier distribution throughout the whole body as well as nanocarrier metabolism and excretion which cannot be achieved yet by MPS [199]. However, animal models on the other hand are very expensive, need a high level of expertise in handling and are time consuming to operate [199]. Thus, perfused endothelial layers from various sites of the vasculature or in particular MPS of the BBB represent valuable tools to preselect carrier design and polymer formulations regarding tissue target sites, cellular interaction, transendothelial passage capabilities and cytotoxicity on human cells in a more physiologic cellular microenvironment. Now, microfluidic chip-based models just evolve to substantially replace animal testing eventually some day in the future with still a lot of effort to put in for refinement and further development. However, with the investigation of perfused endothelial cell layers recreating microphysiological conditions of the vasculature, we could demonstrate that they are on their way to already complete scientific tools for improved recapitulation of EC biology (cf. manuscript I), to study influences of cellular crosstalk (cf. manuscript II), to establish more sophisticated MPS (cf. manuscript III) and for improved screenings under physiologically more relevant conditions (cf. manuscripts II and IV). On the long-term they might bare the ability to close interspecies data transferability gaps.

4.5 Further developmental potential regarding the improvement of endothelial and vascular *in vitro* research

The thesis shows the implication of a microfluidically perfused biochip for endothelial vascular layers in mono-cell culture and several co-culture strategies with tissue-resident macrophages or adjacent neural tissue. Further, its additional value for PMAA-based NP and GSH-coupled nanocarrier screening could be successfully demonstrated. The selection of a defined microenvironment, especially the inclusion of shear stress but also of other cell types, has a strong impact on endothelial outcome and performance within uptake studies. The biochip approach itself and the concept of a membrane as cell culture scaffold within the biochip thereby creating two single perfusable channels comprise a high potential for further developmental effort (I) to improve the system on a technical and (II) cellular basis as well as

(III) to integrate endothelial / vascular cell layers into other MPS.

4.5.1 Technical improvement strategies for perfused vascular endothelial cell culture

4.5.1.1 Quantification of endothelial barrier integrity

Endothelial barrier integrity plays an important role in maintaining vascular homeostasis. ECs form a restrictive barrier to regulate tissue fluid homeostasis, nutritional supply of adjacent tissue and immune cell infiltration / transmigration [151, 152] (cf. 1.1.2). Endothelial barrier integrity can be evaluated easily by fluorescence-labelled molecule diffusion, i.e. FITC-Dextran, but also by TEER measurement providing an even more precise readout for assessment of barrier integrity. Leaky cell layers with gaps are less detectable by simple molecule diffusion than by electrical resistance measurement. Substantial increase in TEER can be monitored already on a molecular level in a confluent EC layer when tight junctions start to form and begin to close intercellular space. TEER values depend also on endothelial localization within the vascular bed, thus being heavily influenced by endothelial function. HUVECs display TEER values between 6-20 $\Omega \cdot cm^2$ [235, 236] whereas hCMEC/D3 are able to generate TEER values up to 1200 $\Omega \cdot cm^2$ under pulsatile perfusion which is in accordance with data on microvascular ECs obtained *in vivo* [206]. Thus, the biochip-based EC culture approach presented in this thesis would benefit from the integration of electrodes to measure TEER values. One possible implementation without extensive redesign of the biochip body would be using conductive materials for the biochip bonding. Indium tin oxide (ITO) is a promising candidate as it assures electrical conductivity to external electrodes while being transparent for monitoring cell culture in the biochip or performing live cell imaging under perfusion conditions [237]. First experiments have already been conducted.

4.5.1.2 Modulating flow profiles and membrane flexibility

Flow profiles are of major importance regarding EC culture under physiological aspects *in vitro*. Detailed data presented in this thesis on apical and basal perfusion as well as on applying different shear stress rates to EC layers emphasise the impact on cellular morphology and performance. Laminar or laminar pulsatile shear stress is related to the development of a healthy endothelial phenotype [39, 41]. In contrast, oscillatory or turbulent flow are linked to atherosclerotic processes in the vascular bed [6, 95, 160]. Besides laminar flow, ECs are among the cell types with the strongest exposure to mechanical stretching [57]. Cellular stretching improves ECs on a molecular and functional level [164, 170]. Moreover, mechanostimulative stretch positively influences SMC outcome of the vascular bed including cell orientation, phenotype and functionality [133]. Thus, developing pulsatile flow profiles by precisely regulating alternating flow with short increases in velocity would benefit to induce

slight membranal stretching. Further the inclusion of more flexible membranes would benefit the EC and overall vascular biology. Hydrogel-based membranes [238, 239], bioinspired polymer membranes [240] or cellulose-based constructs [241] could be applied. Stretch as well as changes in hydrostatic pressure help to approximate the *in vivo* micro-environment of the vascular bed more precisely. Further, both would contribute to study lung and gut vascular cell biology more accurately as tissue stretch and relaxation are immanent characteristics.

4.5.1.3 Online monitoring of physiologic parameters

Non-invasive / non-destructive real-time assessment of cellular parameters is one benefit of microfluidic biochip-based cell culture compared to animal experimentation. Devices needed for monitoring have less impact on *in vitro* cell cultures than on whole organisms where altered behaviour and high stress levels are most likely to influence measurements. Live cell imaging is a method which is already practicable without further adjustments to the biochip. This enables real-time monitoring of cellular interaction, adhesion and transmigration processes. Introducing TEER measurements to the biochip represents only one possibility for further technological development regarding online monitoring. Integration of chemiluminescent sensor spots into biochip channels enable the real-time measurement of parameters like pH, pO_2 or glucose consumption. Techniques to successfully apply sensitive sensor films to synthetic foils have already been established [242] and can be routinely integrated into microfluidic chips and be readout by colour CCD-camera technology [243]. Lab members have already demonstrated the feasibility in monitoring pO_2 during microfluidic perfusion culture [120]. Establishing sensor spots based on pH measurement within the MOTiF biochip would be most beneficial for controlling endothelial phenotype. A neutral extracellular pH-value influences vWf string formation [163] observed in healthy endothelium *in vivo* [161, 162]. Monitoring glucose consumption would improve medium exchange protocols as well as it would give insight in basic cellular metabolism during studies.

4.5.1.4 Introducing surface modifications

ECs further rely on strong surface adhesion and proper formation of a confluent cell layer to withstand shear stress and mechanical forces in *in vitro* microfluidic biochip cell culture. Surface modifications represent possible strategies to facilitate endothelial adhesion and growth. Oxygen plasma treatment for surface hydrophilization is routinely implemented into the final fabrication steps of the MOTiF biochip. Shen *et al.* demonstrated that hydrophilic surfaces could enhance the expression of focal adhesion protein associated with EC adhesion [244]. Furthermore, surface treatment with natural ECM-derived coating agents like collagen I or IV, fibronectin and poly-L-lysine has already been implemented into cell seeding protocols. With regard to the biochip body itself, surface patterning is one elaborate technique not only

to support endothelial adhesion and growth but also to facilitate physiologic alignment processes. Hu *et al.* demonstrated good EC adhesion and superior cellular alignment when seeding and culturing ECs on micro-wavy patterns [245]. Oligopeptide surface patterning comprising of a motif of arginine-alanine-aspartate-serine (RADS) important for native cell adhesion recognition has also been applied successfully to support cellular adhesion and defined alignment [246]. Hatano *et al.* have focused on generating wrinkled micro- and nano-topographical surfaces to mimic topographical structures of ECM components for guided EC culture [247]. Thus, approaches for surface pattering would be most beneficial for microfluidic EC culture, especially for studies and applications under high shear stress.

4.5.2. Cellular improvement strategies for microfluidic vascular endothelial cell culture

4.5.2.1 Integration of key vascular cell types

ECs line the inner surface of the vascular bed[2], yet, ECs in mono-cell culture represent only a simplified approach to set up a vascular layer within MPS applications. The vasculature consists at least of ECs supported by ECM components and, depending on the site of the vascular bed, additionally SMCs, pericytes and fibroblasts arranged in several layers [248]. As it could be demonstrated in this thesis, the co-culture with tissue-resident macrophages as immune-modulating components further influences shear stress dependent uptake behaviour of NPs through ECs. Endothelial-macrophage co-culture further helps to refine vascular cell culture and MPS as it enables the study of inflammation dependent processes and tissue responses and has been successfully applied in infection models [249, 250]. Endothelial monocyte recruitment and tissue macrophage co-culture has also become apparent regarding inflammatory processes of the vasculature itself like it is observed in atherosclerotic events [251, 252]. Embedding macrophages and recruiting monocytes in microfluidic models has further been used to demonstrate macrophage polarization state-dependent control over tumour cell line MCF-7 by applying chondramide A as tumour cell cytotoxic agent and actin-targeting compound [253].

Smooth muscle cells act as main constitutor of the media in large blood vessels and are located underneath the endothelium. They are in direct interaction with ECs through either immediate contact or the release of mediators into the surrounding tissue and medium [254]. EC-SMC interaction key regulates crucial processes of the vasculature like vascular tone, SMC differentiation, SMC recruitment and influences cellular viability [254], SMC morphology [255, 256] and orientation [257], SMC collagen synthesis [135] and gene regulation in both cell types [258]. Although not in direct contact to the medium (blood), SMCs are also exposed to cyclic stretch and shear forces [259]. Importantly, EC-SMC signalling results in atheroprotective communication via miRNAs between both cell types [260, 261], key processes which should

be considered in developing MPS to investigate inflammatory events. Cellular compositions vary depending on the site of the vascular bed. Barrier functionality is critically regulated by ECs, but depends also on other co-cultured cell types like pericytes which cover between 10 % and 50 % of the endothelial abluminal side and substitute partially SMCs [262]. Within brain micro-vessels, pericytes have their highest distribution in total absence of SMCs and ECs are in close contact to them [262]. Pericytes play important roles in tightening microvascular EC layers [263, 264] also together with astrocytes [223]. These synergistic processes of co-culture and microfluidic shear stress application are thus important for further vascular tissue designs within MPS and should be carefully considered.

4.5.2.2 Implementing induced pluripotent stem cells and addressing personalised medicine

Not only the consideration and inclusion of specific cell types to recreate the vascular tissue in MPS more precisely, but also the origin of cell types is an important factor. Microphysiological systems emerge as research and screening tools. Compared to animal studies, these systems bare the possibility of faster and partially cheaper research studies with a broader range of technical variability [126]. This will become even more obvious when implementing induced pluripotent stem cells (IPSCs), a field just emerging in MPS design and application. Induced pluripotent stem cells have the advantage of being nearly indefinitely available and they can be differentiated into nearly every cell type of the human body [265]. Protocols to generate ECs and pericytes [266], vascular SMCs [267] and fibroblasts [268] have already been established. Even endothelial subsets considering endothelial heterogeneity have been established to differentiate from iPSC via the application of different amounts of VEGF [269, 270]. Hence, vascular tissue constructs can be generated from cells with a uniform genetic background excluding study bias. Further, iPSCs can be generated with moderate effort from various cell types and any person thereby lowering the costs to investigate rare diseases or enabling personalised medicine.

4.5.2.3 Extracellular matrix, cell polarity and adaptation of *in vivo* cell arrangements

Cellular arrangement plays an important role when mixing different cell types in co-culture approaches. For proper cellular function, they depend on cell-cell contact formation thereby regulating overall tissue maintenance and function [271], polarity formation [272] and in particular epithelial-endothelial barrier functionality [273]. Furthermore, polarity establishment also depends on molecular gradients and the application of certain amounts of anisotropic strain on cells [274]. In the human body tissues of all kinds are composed of different cell types arranged in a layer like fashion [214, 248, 275-279]. Components of the ECM provide crucial environmental cues for cellular organisation [280, 281] and polarisation [282]. Thus, further development of vascular endothelial structures in MPS should strongly consider layering

different vascular cell types in an organo- / tissue- typic approach including the incorporation of ECM components by extrinsic or intrinsic means. When layering different cell types for vascular tissue generation such as fibroblasts, SMCs or ECs, simultaneous or successive application of ECM components such as collagens, laminins and fibronectins is feasible. Moreover, shown by studies of De Clerck *et al.* from the early 1980s, ascorbic acid can be applied during cell layer formation and cell culture to intrinsically stimulate ECM production in SMCs as well as ECs [283]. Cell sheet generation and ECM dependent cell sheet stabilisation has been successfully applied by using thermoresponsive polymer technology for tissue engineering [284-287]. The concept of layered cells has also already been predominantly applied in more complex microfluidic cell co-cultures [102, 257, 259, 288, 289]. Although early experiments for this thesis using thermoresponsive polymer surfaces for cell sheet layering with subsequent transfer into a former version of the MOTiF biochip were rather unsatisfactory, abstraction of *in vivo*-like concepts for the development of endothelial biochip culture to vascular biochip culture using cell layering techniques seems to be the most favourable approach to generate complex 3D microenvironments. These microenvironments are in turn able to self-organise, to differentiate and to structure endothelial-epithelial cell culture [110].

4.5.3. Implementation of vascular endothelial cell layers into microfluidic tissue models and microphysiological systems

EC culture benefits from microfluidically perfused culture as could be demonstrated in this thesis. Further, in discussing developmental potential of MOTiF biochip approaches, layered vascular tissue may represent a future key feature for more complex 3D MPS emulating tissue and organ functions. Vascular tissue procures and regulates complex functions like barrier integrity, immune cell recruitment, nourishment of and establishing gradients in adjacent tissues. Endothelial layers mimicking a vascular bed have been integrated into a variety of microfluidic applications of the liver [289], lung [102], in tumour models [253, 290], in models of angiogenesis [106] or the blood-brain barrier [204, 232]. Some of the aforementioned microfluidic models have already been used to study inflammation and immune cell recruitment in the context of sepsis and liver functionality [289] as well as macrophage polarisation state-dependent tumour cell decay [253, 290]. The integration of vascular components into MPS becomes necessary when thinking about the usage of MPS for disease modelling and comprehension. This is imminent with recapitulating atherosclerotic processes [157, 291] or break down of inflammation-dependent endothelial-epithelial barriers of gut [292, 293] and lung [293, 294]. Disease modelling for mechanistic studies in basic research and pharmaceutical drug development through the industry is a major point and focus in MPS development. Furthermore, there is the near goal to develop microfluidic biochip-based multi-organ applications establishing axes of gut – liver, liver – brain or lung – brain to study systemic

processes. There is also the great vision to create a “human- / body-on-a-chip” in its very basic functions [295, 296]. In this context, implementing vascular endothelial layers into more complex and more sophisticated models becomes necessary as it will serve as an interconnecting structure and an individual organ-like unit similar to the vascular bed of the human body [297]. Based on the concept of mimicking *in vivo* microenvironments it seems more reasonable than solely to rely on artificial channel and/ or tubing structure. Additionally, vascularisation of channel and tubing structures might help to establish more physiologic surface-to-volume ratios [295]. Regarding organ-targeted nanocarrier uptake studies it is crucial to estimate the role of the vascular circulation system with reference to aspects of unfavoured uptake and inflammation-associated endothelial and macrophage activation. Endothelial heterogeneity will gain more importance in complex devices as well to fully comprehend *in vitro* targeted vascular or microvascular barrier permeation under *in vivo*-like parameters. The underlying concept of organoid design was performed within other follow-up studies of our group [120, 253, 289, 290]. The initial characterization of endothelial layers within biochips and its application (cf. manuscripts I and II, cf. 4.2 and 4.3) and the further gained knowledge from this thesis served well in further study designs and will help to implement vascular units into MPS applications for basic research and drug screening systems.

5. References

1. Sumpio, B.E., J.T. Riley, and A. Dardik, *Cells in focus: endothelial cell.* Int J Biochem Cell Biol, 2002. **34**(12): p. 1508-12.
2. Davies, M.G. and P.O. Hagen, *The vascular endothelium. A new horizon.* Ann Surg, 1993. **218**(5): p. 593-609.
3. Schnittler, H.J., *Structural and functional aspects of intercellular junctions in vascular endothelium.* Basic Res Cardiol, 1998. **93 Suppl 3**: p. 30-9.
4. Aird, W.C., *Phenotypic heterogeneity of the endothelium: I. Structure, function, and mechanisms.* Circ Res, 2007. **100**(2): p. 158-73.
5. Ballermann, B.J., et al., *Shear stress and the endothelium.* Kidney Int Suppl, 1998. **67**: p. S100-8.
6. Malek, A.M., S.L. Alper, and S. Izumo, *Hemodynamic shear stress and its role in atherosclerosis.* JAMA, 1999. **282**(21): p. 2035-42.
7. Ku, D.N., et al., *Pulsatile flow and atherosclerosis in the human carotid bifurcation. Positive correlation between plaque location and low oscillating shear stress.* Arteriosclerosis, 1985. **5**(3): p. 293-302.
8. Bhagat, K., *Endothelial function and myocardial infarction.* Cardiovasc Res, 1998. **39**(2): p. 312-7.
9. Pearson, J.D., *Normal endothelial cell function.* Lupus, 2000. **9**(3): p. 183-8.
10. Minami, T. and W.C. Aird, *Endothelial cell gene regulation.* Trends Cardiovasc Med, 2005. **15**(5): p. 174-84.
11. Aird, W.C., *Endothelium as an organ system.* Crit Care Med, 2004. **32**(5 Suppl): p. S271-9.
12. Goncharov, N.V., et al., *Markers and Biomarkers of Endothelium: When Something Is Rotten in the State.* Oxid Med Cell Longev, 2017. **2017**: p. 9759735.
13. Ordonez, N.G., *Immunohistochemical endothelial markers: a review.* Adv Anat Pathol, 2012. **19**(5): p. 281-95.
14. Woodfin, A., M.B. Voisin, and S. Nourshargh, *PECAM-1: a multi-functional molecule in inflammation and vascular biology.* Arterioscler Thromb Vasc Biol, 2007. **27**(12): p. 2514-23.
15. Newman, P.J., *The biology of PECAM-1.* J Clin Invest, 1997. **99**(1): p. 3-8.
16. Huang, A.J., et al., *Effects of human neutrophil chemotaxis across human endothelial cell monolayers on the permeability of these monolayers to ions and macromolecules.* J Cell Physiol, 1988. **135**(3): p. 355-66.
17. Springer, T.A., *Traffic signals for lymphocyte recirculation and leukocyte emigration: the multistep paradigm.* Cell, 1994. **76**(2): p. 301-14.
18. Tousoulis, D., et al., *The role of nitric oxide on endothelial function.* Curr Vasc Pharmacol, 2012. **10**(1): p. 4-18.
19. Luscher, T.F. and M. Barton, *Biology of the endothelium.* Clin Cardiol, 1997. **20**(11 Suppl 2): p. II-3-10.
20. van Hinsbergh, V.W. and G.P. van Nieuw Amerongen, *Intracellular signalling involved in modulating human endothelial barrier function.* J Anat, 2002. **200**(6):

p. 549-60.

21. Ballabh, P., A. Braun, and M. Nedergaard, *The blood-brain barrier: an overview: structure, regulation, and clinical implications.* Neurobiol Dis, 2004. **16**(1): p. 1-13.

22. Dvorak, A.M. and D. Feng, *The vesiculo-vacuolar organelle (VVO). A new endothelial cell permeability organelle.* J Histochem Cytochem, 2001. **49**(4): p. 419-32.

23. Wallez, Y. and P. Huber, *Endothelial adherens and tight junctions in vascular homeostasis, inflammation and angiogenesis.* Biochim Biophys Acta, 2008. **1778**(3): p. 794-809.

24. Bazzoni, G. and E. Dejana, *Endothelial cell-to-cell junctions: molecular organization and role in vascular homeostasis.* Physiol Rev, 2004. **84**(3): p. 869-901.

25. Dejana, E. and F. Orsenigo, *Endothelial adherens junctions at a glance.* J Cell Sci, 2013. **126**(Pt 12): p. 2545-9.

26. Bazzoni, G., *Endothelial tight junctions: permeable barriers of the vessel wall.* Thromb Haemost, 2006. **95**(1): p. 36-42.

27. Pardridge, W.M., *The blood-brain barrier: bottleneck in brain drug development.* NeuroRx, 2005. **2**(1): p. 3-14.

28. Abbott, N.J., et al., *Structure and function of the blood-brain barrier.* Neurobiol Dis, 2010. **37**(1): p. 13-25.

29. Wei, X.N., et al., *An integrated mathematical model of thrombin-, histamine-and VEGF-mediated signalling in endothelial permeability.* BMC Syst Biol, 2011. **5**: p. 112.

30. Chen, D.C., *Sepsis and Intestinal Microvascular Endothelial Dysfunction.* Chin Med J (Engl), 2017. **130**(10): p. 1137-1138.

31. Pober, J.S. and W.C. Sessa, *Evolving functions of endothelial cells in inflammation.* Nat Rev Immunol, 2007. **7**(10): p. 803-15.

32. Barbieri, S.S., et al., *Suppressing PTEN activity by tobacco smoke plus interleukin-1beta modulates dissociation of VE-cadherin/beta-catenin complexes in endothelium.* Arterioscler Thromb Vasc Biol, 2008. **28**(4): p. 732-8.

33. Ince, C., et al., *The Endothelium in Sepsis.* Shock, 2016. **45**(3): p. 259-70.

34. Choi, J.J., et al., *Molecules of various pharmacologically-relevant sizes can cross the ultrasound-induced blood-brain barrier opening in vivo.* Ultrasound Med Biol, 2010. **36**(1): p. 58-67.

35. *Alternative routes of drug administration--advantages and disadvantages (subject review). American Academy of Pediatrics. Committee on Drugs.* Pediatrics, 1997. **100**(1): p. 143-52.

36. Oller-Salvia, B., et al., *Blood-brain barrier shuttle peptides: an emerging paradigm for brain delivery.* Chem Soc Rev, 2016. **45**(17): p. 4690-707.

37. Kreuter, J., *Nanoparticulate systems for brain delivery of drugs.* Adv Drug Deliv Rev, 2001. **47**(1): p. 65-81.

38. Pardridge, W.M., *Drug targeting to the brain.* Pharm Res, 2007. **24**(9): p. 1733-44.

39. Chatzizisis, Y.S., et al., *Role of endothelial shear stress in the natural history of coronary atherosclerosis and vascular remodeling: molecular, cellular, and*

vascular behavior. J Am Coll Cardiol, 2007. **49**(25): p. 2379-93.

40. Davies, P.F., et al., *Turbulent fluid shear stress induces vascular endothelial cell turnover in vitro.* Proc Natl Acad Sci U S A, 1986. **83**(7): p. 2114-7.

41. Davies, P.F., *How Do Vascular Endothelial Cells Respond to Flow?* Vol. 4. 1989. 22-25.

42. Li, Y.S., J.H. Haga, and S. Chien, *Molecular basis of the effects of shear stress on vascular endothelial cells.* J Biomech, 2005. **38**(10): p. 1949-71.

43. Silkworth, J.B., W.E. Stehbens, and D. Phil, *The Shape of Endothelial Cells in En Face Preparations of Rabbit Blood Vessels.* Angiology, 1975. **26**(6): p. 474-487.

44. Nerem, R.M., M.J. Levesque, and J.F. Cornhill, *Vascular endothelial morphology as an indicator of the pattern of blood flow.* J Biomech Eng, 1981. **103**(3): p. 172-6.

45. Flaherty, J.T., et al., *Endothelial nuclear patterns in the canine arterial tree with particular reference to hemodynamic events.* Circ Res, 1972. **30**(1): p. 23-33.

46. Karlon, W.J., et al., *Measurement of orientation and distribution of cellular alignment and cytoskeletal organization.* Ann Biomed Eng, 1999. **27**(6): p. 712-20.

47. Girard, P.R. and R.M. Nerem, *Shear stress modulates endothelial cell morphology and F-actin organization through the regulation of focal adhesion-associated proteins.* J Cell Physiol, 1995. **163**(1): p. 179-93.

48. Malek, A.M. and S. Izumo, *Mechanism of endothelial cell shape change and cytoskeletal remodeling in response to fluid shear stress.* J Cell Sci, 1996. **109 (Pt 4)**: p. 713-26.

49. Nerem, R.M., et al., *The study of the influence of flow on vascular endothelial biology.* Am J Med Sci, 1998. **316**(3): p. 169-75.

50. Dimmeler, S., et al., *Shear stress inhibits apoptosis of human endothelial cells.* FEBS Lett, 1996. **399**(1-2): p. 71-4.

51. Morigi, M., et al., *Fluid shear stress modulates surface expression of adhesion molecules by endothelial cells.* Blood, 1995. **85**(7): p. 1696-703.

52. Nagel, T., et al., *Shear stress selectively upregulates intercellular adhesion molecule-1 expression in cultured human vascular endothelial cells.* J Clin Invest, 1994. **94**(2): p. 885-91.

53. Sampath, R., et al., *Shear stress-mediated changes in the expression of leukocyte adhesion receptors on human umbilical vein endothelial cells in vitro.* Ann Biomed Eng, 1995. **23**(3): p. 247-56.

54. Chappell, D.C., et al., *Oscillatory shear stress stimulates adhesion molecule expression in cultured human endothelium.* Circ Res, 1998. **82**(5): p. 532-9.

55. Chistiakov, D.A., A.N. Orekhov, and Y.V. Bobryshev, *Effects of shear stress on endothelial cells: go with the flow.* Acta Physiol (Oxf), 2017. **219**(2): p. 382-408.

56. Collins, N.T., et al., *Cyclic strain-mediated regulation of vascular endothelial occludin and ZO-1: influence on intercellular tight junction assembly and function.* Arterioscler Thromb Vasc Biol, 2006. **26**(1): p. 62-8.

57. Davies, P.F., *Flow-mediated endothelial mechanotransduction.* Physiol Rev, 1995. **75**(3): p. 519-60.

58. Conway, D. and M.A. Schwartz, *Lessons from the endothelial junctional mechanosensory complex.* F1000 Biol Rep, 2012. **4**: p. 1.

59. Silberman, M., et al., *Shear stress-induced transcriptional regulation via hybrid promoters as a potential tool for promoting angiogenesis.* Angiogenesis, 2009. **12**(3): p. 231-42.

60. Zhou, J., et al., *Force-specific activation of Smad1/5 regulates vascular endothelial cell cycle progression in response to disturbed flow.* Proc Natl Acad Sci U S A, 2012. **109**(20): p. 7770-5.

61. Barakat, A. and D. Lieu, *Differential responsiveness of vascular endothelial cells to different types of fluid mechanical shear stress.* Cell Biochem Biophys, 2003. **38**(3): p. 323-43.

62. Chiu, J.J. and S. Chien, *Effects of disturbed flow on vascular endothelium: pathophysiological basis and clinical perspectives.* Physiol Rev, 2011. **91**(1): p. 327-87.

63. Singhal, A.K., et al., *Role of Endothelial Cells in Myocardial Ischemia-Reperfusion Injury.* Vasc Dis Prev, 2010. **7**: p. 1-14.

64. Wang, A.Z., R. Langer, and O.C. Farokhzad, *Nanoparticle delivery of cancer drugs.* Annu Rev Med, 2012. **63**: p. 185-98.

65. Cicha, I., *Strategies to enhance nanoparticle endothelial interactions under flow.* Journal of Cellular Biotechnology, 2016. **1**(2): p. 191-208.

66. Singh, R. and J.W. Lillard, Jr., *Nanoparticle-based targeted drug delivery.* Exp Mol Pathol, 2009. **86**(3): p. 215-23.

67. Frohlich, E., *The role of surface charge in cellular uptake and cytotoxicity of medical nanoparticles.* Int J Nanomedicine, 2012. **7**: p. 5577-91.

68. Wilczewska, A.Z., et al., *Nanoparticles as drug delivery systems.* Pharmacological Reports, 2012. **64**(5): p. 1020-1037.

69. Ghorbani, H.R., *A Review of Methods for Synthesis of Al Nanoparticles.* Oriental Journal of Chemistry, 2014. **30**(4).

70. Kralj, S. and D. Makovec, *Magnetic Assembly of Superparamagnetic Iron Oxide Nanoparticle Clusters into Nanochains and Nanobundles.* ACS Nano, 2015. **9**(10): p. 9700-9707.

71. Sun, Y. and Y. Xia, *Shape-controlled synthesis of gold and silver nanoparticles.* Science, 2002. **298**(5601): p. 2176-9.

72. Berg, J.M., et al., *The relationship between pH and zeta potential of ~ 30 nm metal oxide nanoparticle suspensions relevant to in vitro toxicological evaluations.* Nanotoxicology, 2009. **3**(4): p. 276-283.

73. De Jong, W.H. and P.J. Borm, *Drug delivery and nanoparticles:applications and hazards.* Int J Nanomedicine, 2008. **3**(2): p. 133-49.

74. Treuel, L., X. Jiang, and G.U. Nienhaus, *New views on cellular uptake and trafficking of manufactured nanoparticles.* J R Soc Interface, 2013. **10**(82): p. 20120939.

75. Perry, J.L., et al., *PRINT: a novel platform toward shape and size specific nanoparticle theranostics.* Acc Chem Res, 2011. **44**(10): p. 990-8.

76. Derry, M.J., L.A. Fielding, and S.P. Armes, *Polymerization-induced self-assembly of block copolymer nanoparticles via RAFT non-aqueous dispersion polymerization.* Progress in Polymer Science, 2016. **52**: p. 1-18.

77. Cole, A.J., V.C. Yang, and A.E. David, *Cancer theranostics: the rise of targeted magnetic nanoparticles.* Trends Biotechnol, 2011. **29**(7): p. 323-32.

78. Nakamura, Y., et al., *Nanodrug Delivery: Is the Enhanced Permeability and*

Retention Effect Sufficient for Curing Cancer? Bioconjugate Chemistry, 2016. **27**(10): p. 2225-2238.

79. Levesque, M.J. and R.M. Nerem, *The elongation and orientation of cultured endothelial cells in response to shear stress.* J Biomech Eng, 1985. **107**(4): p. 341-7.

80. Dewey, C.F., Jr., et al., *The dynamic response of vascular endothelial cells to fluid shear stress.* J Biomech Eng, 1981. **103**(3): p. 177-85.

81. Davies, P.F. and S.C. Tripathi, *Mechanical stress mechanisms and the cell. An endothelial paradigm.* Circ Res, 1993. **72**(2): p. 239-45.

82. Koo, A., C.F. Dewey, Jr., and G. Garcia-Cardena, *Hemodynamic shear stress characteristic of atherosclerosis-resistant regions promotes glycocalyx formation in cultured endothelial cells.* Am J Physiol Cell Physiol, 2013. **304**(2): p. C137-46.

83. Arisaka, T., et al., *Effects of shear stress on glycosaminoglycan synthesis in vascular endothelial cells.* Ann N Y Acad Sci, 1995. **748**: p. 543-54.

84. Yoshida, Y., et al., *Hemodynamic-force-induced difference of interendothelial junctional complexes.* Ann N Y Acad Sci, 1995. **748**: p. 104-20; discussion 120-1.

85. Cucullo, L., et al., *The role of shear stress in Blood-Brain Barrier endothelial physiology.* BMC Neurosci, 2011. **12**: p. 40.

86. Kang, T., et al., *Effects of shear stress on the cellular distribution of polystyrene nanoparticles in a biomimetic microfluidic system.* Journal of Drug Delivery Science and Technology, 2016. **31**: p. 130-136.

87. Torchilin, V.P., *Cell penetrating peptide-modified pharmaceutical nanocarriers for intracellular drug and gene delivery.* Biopolymers, 2008. **90**(5): p. 604-10.

88. Fang, I.J., et al., *Ligand conformation dictates membrane and endosomal trafficking of arginine-glycine-aspartate (RGD)-functionalized mesoporous silica nanoparticles.* Chemistry, 2012. **18**(25): p. 7787-92.

89. Antosova, A., et al., *Amino Acid Functionalized Superparamagnetic Nanoparticles Inhibit Lysozyme Amyloid Fibrillization.* Chemistry, 2019.

90. Kulandaisamy, A.J. and J.B.B. Rayappan, *Significance of Nanoparticles and the Role of Amino Acids in Structuring Them-A Review.* J Nanosci Nanotechnol, 2018. **18**(8): p. 5222-5233.

91. Raula, J., et al., *Preparation of amino acid nanoparticles at varying saturation conditions in an aerosol flow reactor.* Journal of Nanoparticle Research, 2012. **14**(7): p. 986.

92. Sun, E.Y., et al., *Development of Nanoparticle Libraries for Biosensing.* Bioconjugate Chemistry, 2006. **17**(1): p. 109-113.

93. Whitesides, G.M., *The origins and the future of microfluidics.* Nature, 2006. **442**(7101): p. 368-73.

94. Krueger, J.W., D.F. Young, and N.R. Cholvin, *An in vitro study of flow response by cells.* J Biomech, 1971. **4**(1): p. 31-6.

95. DePaola, N., et al., *Vascular endothelium responds to fluid shear stress gradients.* Arterioscler Thromb, 1992. **12**(11): p. 1254-7.

96. Bhatia, S.N. and D.E. Ingber, *Microfluidic organs-on-chips.* Nature Biotechnology, 2014. **32**(8): p. 760-772.

97. Lee, A., *The third decade of microfluidics.* Lab Chip, 2013. **13**(9): p. 1660-1.

98. Young, E.W. and C.A. Simmons, *Macro- and microscale fluid flow systems for endothelial cell biology.* Lab Chip, 2010. **10**(2): p. 143-60.

99. Huh, D., G.A. Hamilton, and D.E. Ingber, *From 3D cell culture to organs-on-chips.* Trends Cell Biol, 2011. **21**(12): p. 745-54.

100. van Midwoud, P.M., et al., *Comparison of biocompatibility and adsorption properties of different plastics for advanced microfluidic cell and tissue culture models.* Anal Chem, 2012. **84**(9): p. 3938-44.

101. Berthier, E., E.W. Young, and D. Beebe, *Engineers are from PDMS-land, Biologists are from Polystyrenia.* Lab Chip, 2012. **12**(7): p. 1224-37.

102. Huh, D., et al., *Reconstituting organ-level lung functions on a chip.* Science, 2010. **328**(5986): p. 1662-8.

103. Herland, A., et al., *Distinct Contributions of Astrocytes and Pericytes to Neuroinflammation Identified in a 3D Human Blood-Brain Barrier on a Chip.* PLoS One, 2016. **11**(3): p. e0150360.

104. Jang, K.J., et al., *Human kidney proximal tubule-on-a-chip for drug transport and nephrotoxicity assessment.* Integr Biol (Camb), 2013. **5**(9): p. 1119-29.

105. Booth, R. and H. Kim, *Characterization of a microfluidic in vitro model of the blood-brain barrier (muBBB).* Lab Chip, 2012. **12**(10): p. 1784-92.

106. Wong, K.H., et al., *Microfluidic models of vascular functions.* Annu Rev Biomed Eng, 2012. **14**: p. 205-30.

107. Eddington, D.T., J.P. Puccinelli, and D.J. Beebe, *Thermal aging and reduced hydrophobic recovery of polydimethylsiloxane.* Sensors and Actuators B-Chemical, 2006. **114**(1): p. 170-172.

108. Toepke, M.W. and D.J. Beebe, *PDMS absorption of small molecules and consequences in microfluidic applications.* Lab on a Chip, 2006. **6**(12): p. 1484-1486.

109. Regehr, K.J., et al., *Biological implications of polydimethylsiloxane-based microfluidic cell culture.* Lab on a Chip, 2009. **9**(15): p. 2132-2139.

110. Thuenauer, R., E. Rodriguez-Boulan, and W. Romer, *Microfluidic approaches for epithelial cell layer culture and characterisation.* Analyst, 2014. **139**(13): p. 3206-18.

111. Kutz, M., *Biomedical engineering and design handbook*. 2nd ed. 2009, New York: McGraw-Hill.

112. Ku, D.N., *Blood flow in arteries.* Annual Review of Fluid Mechanics, 1997. **29**: p. 399-434.

113. Reneman, R.S., T. Arts, and A.P. Hoeks, *Wall shear stress--an important determinant of endothelial cell function and structure--in the arterial system in vivo. Discrepancies with theory.* J Vasc Res, 2006. **43**(3): p. 251-69.

114. Papaioannou, T.G. and C. Stefanadis, *Vascular wall shear stress: basic principles and methods.* Hellenic J Cardiol, 2005. **46**(1): p. 9-15.

115. Le-Cong, P. and B.W. Zweifach, *In vivo and in vitro velocity measurements in microvasculature with a laser.* Microvasc Res, 1979. **17**(2): p. 131-41.

116. Cheng, C., et al., *Large variations in absolute wall shear stress levels within one species and between species.* Atherosclerosis, 2007. **195**(2): p. 225-35.

117. Gupta, N., et al., *Microfluidics-based 3D cell culture models: Utility in novel drug discovery and delivery research.* Bioeng Transl Med, 2016. **1**(1): p. 63-81.

118. Takayama, S., et al., *Subcellular positioning of small molecules.* Nature, 2001. **411**(6841): p. 1016.

119. Carraro, A., et al., *In vitro analysis of a hepatic device with intrinsic microvascular-based channels.* Biomed Microdevices, 2008. **10**(6): p. 795-805.

120. Rennert, K., et al., *A microfluidically perfused three dimensional human liver model.* Biomaterials, 2015. **71**: p. 119-131.

121. Imura, Y., et al., *A microfluidic system to evaluate intestinal absorption.* Anal Sci, 2009. **25**(12): p. 1403-7.

122. Kimura, H., et al., *An integrated microfluidic system for long-term perfusion culture and on-line monitoring of intestinal tissue models.* Lab Chip, 2008. **8**(5): p. 741-6.

123. Jang, K.J. and K.Y. Suh, *A multi-layer microfluidic device for efficient culture and analysis of renal tubular cells.* Lab Chip, 2010. **10**(1): p. 36-42.

124. Jang, K.J., et al., *Fluid-shear-stress-induced translocation of aquaporin-2 and reorganization of actin cytoskeleton in renal tubular epithelial cells.* Integr Biol (Camb), 2011. **3**(2): p. 134-41.

125. Russell, W.M.S. and R.L. Burch, *The principles of humane experimental technique*. 1959, London,: Methuen. 238 p.

126. Mosig, A.S., *Organ-on-chip models: new opportunities for biomedical research.* Future science OA, 2016. **3**(2): p. FSO130-FSO130.

127. Getz, G.S. and C.A. Reardon, *Animal models of atherosclerosis.* Arterioscler Thromb Vasc Biol, 2012. **32**(5): p. 1104-15.

128. Delire, B., P. Stärkel, and I. Leclercq, *Animal Models for Fibrotic Liver Diseases: What We Have, What We Need, and What Is under Development.* Journal of clinical and translational hepatology, 2015. **3**(1): p. 53-66.

129. Liu, T., F.G. De Los Santos, and S.H. Phan, *The Bleomycin Model of Pulmonary Fibrosis.* Methods Mol Biol, 2017. **1627**: p. 27-42.

130. Dinardo, C.L., et al., *Vascular smooth muscle cells exhibit a progressive loss of rigidity with serial culture passaging.* Biorheology, 2012. **49**(5-6): p. 365-73.

131. Macarak, E.J. and P.S. Howard, *Adhesion of endothelial cells to extracellular matrix proteins.* J Cell Physiol, 1983. **116**(1): p. 76-86.

132. Halka, A.T., et al., *The effects of stretch on vascular smooth muscle cell phenotype in vitro.* Cardiovasc Pathol, 2008. **17**(2): p. 98-102.

133. Shyu, K.G., *Cellular and molecular effects of mechanical stretch on vascular cells and cardiac myocytes.* Clin Sci (Lond), 2009. **116**(5): p. 377-89.

134. Chamley-Campbell, J., G.R. Campbell, and R. Ross, *The smooth muscle cell in culture.* Physiol Rev, 1979. **59**(1): p. 1-61.

135. Powell, R.J., et al., *Endothelial cell effect on smooth muscle cell collagen synthesis.* J Surg Res, 1997. **69**(1): p. 113-8.

136. Lauffenburger, D.A. and L.G. Griffith, *Who's got pull around here? Cell organization in development and tissue engineering.* Proc Natl Acad Sci U S A, 2001. **98**(8): p. 4282-4.

137. Locker, A., *[Animal testing ethics and human testing. Thoughts on our conduct with and our relationship to animals].* ALTEX, 2004. **21**(4): p. 221-6.

138. Nurunnabi, A., R. Afroz, and S. Alam, *Ethical Debate on Animal Research.* Bangladesh Journal of Bioethics, 2013. **4**(3): p. 11-18.

139. DeGrazia, D. and J. Sebo, *Necessary conditions for morally responsible animal research.* Camb Q Healthc Ethics, 2015. **24**(4): p. 420-30.

140. Buller, T., *Animal minds and neuroimaging--bridging the gap between science and ethics?* Camb Q Healthc Ethics, 2014. **23**(2): p. 173-81.

141. Foex, B.A., *The ethics of animal experimentation.* Emerg Med J, 2007. **24**(11): p. 750-1.

142. Reagan-Shaw, S., M. Nihal, and N. Ahmad, *Dose translation from animal to human studies revisited.* Faseb j, 2008. **22**(3): p. 659-61.

143. Mak, I.W., N. Evaniew, and M. Ghert, *Lost in translation: animal models and clinical trials in cancer treatment.* Am J Transl Res, 2014. **6**(2): p. 114-8.

144. Shanks, N., R. Greek, and J. Greek, *Are animal models predictive for humans?* Philos Ethics Humanit Med, 2009. **4**: p. 2.

145. Collins, F.S., *Of Mice, Men, and Medicine*. 2013.

146. Plenge, R.M., E.M. Scolnick, and D. Altshuler, *Validating therapeutic targets through human genetics.* Nat Rev Drug Discov, 2013. **12**(8): p. 581-94.

147. Green, S.B., *Can animal data translate to innovations necessary for a new era of patient-centred and individualised healthcare? Bias in preclinical animal research.* BMC Med Ethics, 2015. **16**: p. 53.

148. Andersson, H. and A. van den Berg, *Microfabrication and microfluidics for tissue engineering: state of the art and future opportunities.* Lab Chip, 2004. **4**(2): p. 98-103.

149. Davies, P.F., J. Zilberberg, and B.P. Helmke, *Spatial microstimuli in endothelial mechanosignaling.* Circ Res, 2003. **92**(4): p. 359-70.

150. Eskin, S.G., et al., *Response of cultured endothelial cells to steady flow.* Microvasc Res, 1984. **28**(1): p. 87-94.

151. Yuan, S.Y. and R.R. Rigor, *Regulation of Endothelial Barrier Function*. Regulation of Endothelial Barrier Function. 2010, San Rafael (CA).

152. Komarova, Y. and A.B. Malik, *Regulation of endothelial permeability via paracellular and transcellular transport pathways.* Annu Rev Physiol, 2010. **72**: p. 463-93.

153. Shi, C. and E.G. Pamer, *Monocyte recruitment during infection and inflammation.* Nat Rev Immunol, 2011. **11**(11): p. 762-74.

154. Lin, A., et al., *Shear-regulated uptake of nanoparticles by endothelial cells and development of endothelial-targeting nanoparticles.* J Biomed Mater Res A, 2010. **93**(3): p. 833-42.

155. Davies, P.F., *How Do Vascular Endothelial-Cells Respond to Flow.* News in Physiological Sciences, 1989. **4**: p. 22-25.

156. Shao, J., et al., *Integrated microfluidic chip for endothelial cells culture and analysis exposed to a pulsatile and oscillatory shear stress.* Lab Chip, 2009. **9**(21): p. 3118-25.

157. Estrada, R., et al., *Microfluidic endothelial cell culture model to replicate disturbed flow conditions seen in atherosclerosis susceptible regions.* Biomicrofluidics, 2011. **5**(3): p. 32006-3200611.

158. Garcia-Cardena, G., et al., *Biomechanical activation of vascular endothelium as a determinant of its functional phenotype.* Proc Natl Acad Sci U S A, 2001. **98**(8): p. 4478-85.

159. Cockcroft, N.Y., et al., *An in vitro perfusion system to examine the responses of endothelial cells to simulated flow and inflammatory stimulation.* Altern Lab Anim, 2009. **37**(6): p. 657-69.

160. Zarins, C.K., et al., *Carotid bifurcation atherosclerosis. Quantitative correlation of plaque localization with flow velocity profiles and wall shear stress.* Circ Res, 1983. **53**(4): p. 502-14.

161. Senis, Y.A., et al., *Changes in the pattern of distribution of von Willebrand factor in rat aortic endothelial cells following thrombin generation in vivo.* Br J Haematol, 1996. **93**(1): p. 195-203.

162. Sporn, L.A., V.J. Marder, and D.D. Wagner, *Inducible secretion of large, biologically potent von Willebrand factor multimers.* Cell, 1986. **46**(2): p. 185-90.

163. Valentijn, K.M., et al., *Multigranular exocytosis of Weibel-Palade bodies in vascular endothelial cells.* Blood, 2010. **116**(10): p. 1807-16.

164. Xiong, Y., et al., *Hypertensive stretch regulates endothelial exocytosis of Weibel-Palade bodies through VEGF receptor 2 signaling pathways.* Cell Res, 2013. **23**(6): p. 820-34.

165. Huang, R.H., et al., *Assembly of Weibel-Palade body-like tubules from N-terminal domains of von Willebrand factor.* Proc Natl Acad Sci U S A, 2008. **105**(2): p. 482-7.

166. Michaux, G., et al., *The physiological function of von Willebrand's factor depends on its tubular storage in endothelial Weibel-Palade bodies.* Dev Cell, 2006. **10**(2): p. 223-32.

167. Federici, A.B. and P.M. Mannucci, *Management of inherited von Willebrand disease in 2007.* Ann Med, 2007. **39**(5): p. 346-58.

168. McDonald, J.C. and G.M. Whitesides, *Poly(dimethylsiloxane) as a material for fabricating microfluidic devices.* Acc Chem Res, 2002. **35**(7): p. 491-9.

169. Melin, J. and S.R. Quake, *Microfluidic large-scale integration: The evolution of design rules for biological automation.* Annual Review of Biophysics and Biomolecular Structure, 2007. **36**: p. 213-231.

170. Zhao, S., et al., *Synergistic effects of fluid shear stress and cyclic circumferential stretch on vascular endothelial cell morphology and cytoskeleton.* Arterioscler Thromb Vasc Biol, 1995. **15**(10): p. 1781-6.

171. Pappelbaum, K.I., et al., *Ultralarge von Willebrand factor fibers mediate luminal Staphylococcus aureus adhesion to an intact endothelial cell layer under shear stress.* Circulation, 2013. **128**(1): p. 50-9.

172. Stewart, R.J., T.S. Kashour, and P.A. Marsden, *Vascular endothelial platelet endothelial adhesion molecule-1 (PECAM-1) expression is decreased by TNF-alpha and IFN-gamma. Evidence for cytokine-induced destabilization of messenger ribonucleic acid transcripts in bovine endothelial cells.* J Immunol, 1996. **156**(3): p. 1221-8.

173. Fernandez-Martin, L., et al., *Crosstalk Between Reticular Adherens Junctions and Platelet Endothelial Cell Adhesion Molecule-1 Regulates Endothelial Barrier Function.* Arteriosclerosis Thrombosis and Vascular Biology, 2012. **32**(8): p. E90-U141.

174. Capaldo, C.T. and A. Nusrat, *Cytokine regulation of tight junctions.* Biochimica Et Biophysica Acta-Biomembranes, 2009. **1788**(4): p. 864-871.

175. Stroka, K.M., J.A. Vaitkus, and H. Aranda-Espinoza, *Endothelial cells undergo morphological, biomechanical, and dynamic changes in response to tumor*

necrosis factor-alpha. Eur Biophys J, 2012. **41**(11): p. 939-47.

176. Madge, L.A. and J.S. Pober, *TNF signaling in vascular endothelial cells.* Exp Mol Pathol, 2001. **70**(3): p. 317-25.

177. Pober, J.S., *Endothelial activation: intracellular signaling pathways.* Arthritis Res, 2002. **4 Suppl 3**: p. S109-16.

178. Tsao, P.S., et al., *Fluid flow inhibits endothelial adhesiveness. Nitric oxide and transcriptional regulation of VCAM-1.* Circulation, 1996. **94**(7): p. 1682-9.

179. Chiu, J.J., et al., *Shear stress increases ICAM-1 and decreases VCAM-1 and E-selectin expressions induced by tumor necrosis factor-[alpha] in endothelial cells.* Arterioscler Thromb Vasc Biol, 2004. **24**(1): p. 73-9.

180. Partridge, J., et al., *Laminar shear stress acts as a switch to regulate divergent functions of NF-kappaB in endothelial cells.* FASEB J, 2007. **21**(13): p. 3553-61.

181. De Caterina, R., et al., *Nitric oxide decreases cytokine-induced endothelial activation. Nitric oxide selectively reduces endothelial expression of adhesion molecules and proinflammatory cytokines.* J Clin Invest, 1995. **96**(1): p. 60-8.

182. Nakadate, H., et al., *Combinations of Hydrostatic Pressure and Shear Stress Time-dependently Decrease E-selectin, VCAM-1 and ICAM-1 Expression Induced by Tumor Necrosis Factor-Alpha in Cultured Endothelial Cells.* Journal of Biomechanical Science and Engineering, 2012. **7**(2): p. 118-129.

183. Etzioni, A., *Adhesion molecules--their role in health and disease.* Pediatr Res, 1996. **39**(2): p. 191-8.

184. Khalili, A.A. and M.R. Ahmad, *A Review of Cell Adhesion Studies for Biomedical and Biological Applications.* Int J Mol Sci, 2015. **16**(8): p. 18149-84.

185. Gupta, V.K., et al., *Multi-scale simulation of L-selectin-PSGL-1-dependent homotypic leukocyte binding and rupture.* Biomechanics and Modeling in Mechanobiology, 2010. **9**(5): p. 613-627.

186. Chen, W.C., A.X. Zhang, and S.D. Li, *Limitations and niches of the active targeting approach for nanoparticle drug delivery* Eur J Nanomed, 2012. **4**(2-4): p. 89-93.

187. Dobrovolskaia, M.A., et al., *Preclinical studies to understand nanoparticle interaction with the immune system and its potential effects on nanoparticle biodistribution.* Mol Pharm, 2008. **5**(4): p. 487-95.

188. Samuel, S.P., et al., *Multifactorial determinants that govern nanoparticle uptake by human endothelial cells under flow.* International Journal of Nanomedicine, 2012. **7**: p. 2943-2956.

189. Yang, H., et al., *VCAM-1-targeted core/shell nanoparticles for selective adhesion and delivery to endothelial cells with lipopolysaccharide-induced inflammation under shear flow and cellular magnetic resonance imaging in vitro.* Int J Nanomedicine, 2013. **8**: p. 1897-906.

190. Di, L., *The role of drug metabolizing enzymes in clearance.* Expert Opin Drug Metab Toxicol, 2014. **10**(3): p. 379-93.

191. Zanger, U.M. and M. Schwab, *Cytochrome P450 enzymes in drug metabolism: regulation of gene expression, enzyme activities, and impact of genetic variation.* Pharmacol Ther, 2013. **138**(1): p. 103-41.

192. Dixon, L.J., et al., *Kupffer cells in the liver.* Compr Physiol, 2013. **3**(2): p. 785-97.

193. Bilzer, M., F. Roggel, and A.L. Gerbes, *Role of Kupffer cells in host defense and liver disease.* Liver Int, 2006. **26**(10): p. 1175-86.

194. Press, A.T., et al., *Cell type-specific delivery of short interfering RNAs by dye-functionalised theranostic nanoparticles.* Nat Commun, 2014. **5**: p. 5565.

195. Alizadeh, D., et al., *Tumor-associated macrophages are predominant carriers of cyclodextrin-based nanoparticles into gliomas.* Nanomedicine-Nanotechnology Biology and Medicine, 2010. **6**(2): p. 382-390.

196. An, F., et al., *Organ-on-a-Chip: New Platform for Biological Analysis.* Anal Chem Insights, 2015. **10**: p. 39-45.

197. Stanimirovic, D.B., et al., *Blood-brain barrier models: in vitro to in vivo translation in preclinical development of CNS-targeting biotherapeutics.* Expert Opin Drug Discov, 2015. **10**(2): p. 141-55.

198. He, Y., et al., *Cell-culture models of the blood-brain barrier.* Stroke, 2014. **45**(8): p. 2514-26.

199. Veszelka, S., et al., *Blood-brain barrier co-culture models to study nanoparticle penetration: focus on co-culture systems.* Acta Biologica Szegediensis, 2015. **59**(Suppl. 2): p. 157-168.

200. Wong, A.D., et al., *The blood-brain barrier: an engineering perspective.* Front Neuroeng, 2013. **6**: p. 7.

201. van der Helm, M.W., et al., *Microfluidic organ-on-chip technology for blood-brain barrier research.* Tissue Barriers, 2016. **4**(1): p. e1142493.

202. Prabhakarpandian, B., et al., *SyM-BBB: a microfluidic Blood Brain Barrier model.* Lab Chip, 2013. **13**(6): p. 1093-101.

203. Walter, F.R., et al., *A versatile lab-on-a-chip tool for modeling biological barriers.* Sensors and Actuators B-Chemical, 2016. **222**: p. 1209-1219.

204. Brown, J.A., et al., *Recreating blood-brain barrier physiology and structure on chip: A novel neurovascular microfluidic bioreactor.* Biomicrofluidics, 2015. **9**(5): p. 054124.

205. Weksler, B.B., et al., *Blood-brain barrier-specific properties of a human adult brain endothelial cell line.* FASEB J, 2005. **19**(13): p. 1872-4.

206. Weksler, B., I.A. Romero, and P.O. Couraud, *The hCMEC/D3 cell line as a model of the human blood brain barrier.* Fluids Barriers CNS, 2013. **10**(1): p. 16.

207. Galbraith, C.G., R. Skalak, and S. Chien, *Shear stress induces spatial reorganization of the endothelial cell cytoskeleton.* Cell Motil Cytoskeleton, 1998. **40**(4): p. 317-30.

208. Cucullo, L., et al., *Immortalized human brain endothelial cells and flow-based vascular modeling: a marriage of convenience for rational neurovascular studies.* J Cereb Blood Flow Metab, 2008. **28**(2): p. 312-28.

209. Stevenson, B.R., et al., *Identification of ZO-1: a high molecular weight polypeptide associated with the tight junction (zonula occludens) in a variety of epithelia.* J Cell Biol, 1986. **103**(3): p. 755-66.

210. Griep, L.M., et al., *BBB on chip: microfluidic platform to mechanically and biochemically modulate blood-brain barrier function.* Biomed Microdevices, 2013. **15**(1): p. 145-50.

211. Suidan, G.L., et al., *Endothelial Von Willebrand factor promotes blood-brain barrier flexibility and provides protection from hypoxia and seizures in mice.* Arterioscler Thromb Vasc Biol, 2013. **33**(9): p. 2112-20.

212. Tran, K.A., et al., *Endothelial beta-Catenin Signaling Is Required for Maintaining Adult Blood-Brain Barrier Integrity and Central Nervous System Homeostasis.* Circulation, 2016. **133**(2): p. 177-86.

213. Eiraku, M. and Y. Sasai, *Mouse embryonic stem cell culture for generation of three-dimensional retinal and cortical tissues.* Nat Protoc, 2011. **7**(1): p. 69-79.

214. Englund, C., et al., *Pax6, Tbr2, and Tbr1 are expressed sequentially by radial glia, intermediate progenitor cells, and postmitotic neurons in developing neocortex.* J Neurosci, 2005. **25**(1): p. 247-51.

215. Bayatti, N., et al., *Progressive loss of PAX6, TBR2, NEUROD and TBR1 mRNA gradients correlates with translocation of EMX2 to the cortical plate during human cortical development.* Eur J Neurosci, 2008. **28**(8): p. 1449-56.

216. Sansom, S.N., et al., *The level of the transcription factor Pax6 is essential for controlling the balance between neural stem cell self-renewal and neurogenesis.* PLoS Genet, 2009. **5**(6): p. e1000511.

217. Sessa, A., et al., *Tbr2 directs conversion of radial glia into basal precursors and guides neuronal amplification by indirect neurogenesis in the developing neocortex.* Neuron, 2008. **60**(1): p. 56-69.

218. Bedogni, F., et al., *Tbr1 regulates regional and laminar identity of postmitotic neurons in developing neocortex.* Proc Natl Acad Sci U S A, 2010. **107**(29): p. 13129-34.

219. Cho, H., et al., *Three-Dimensional Blood-Brain Barrier Model for in vitro Studies of Neurovascular Pathology.* Sci Rep, 2015. **5**: p. 15222.

220. Carpentier, P.A., et al., *Stereotypical alterations in cortical patterning are associated with maternal illness-induced placental dysfunction.* J Neurosci, 2013. **33**(43): p. 16874-88.

221. Tronnes, A.A., et al., *Effects of Lipopolysaccharide and Progesterone Exposures on Embryonic Cerebral Cortex Development in Mice.* Reprod Sci, 2016. **23**(6): p. 771-8.

222. Soumiya, H., H. Fukumitsu, and S. Furukawa, *Prenatal immune challenge compromises the normal course of neurogenesis during development of the mouse cerebral cortex.* J Neurosci Res, 2011. **89**(10): p. 1575-85.

223. Luissint, A.C., et al., *Tight junctions at the blood brain barrier: physiological architecture and disease-associated dysregulation.* Fluids Barriers CNS, 2012. **9**(1): p. 23.

224. Muoio, V., P.B. Persson, and M.M. Sendeski, *The neurovascular unit - concept review.* Acta Physiol (Oxf), 2014. **210**(4): p. 790-8.

225. Correale, J. and A. Villa, *Cellular elements of the blood-brain barrier.* Neurochem Res, 2009. **34**(12): p. 2067-77.

226. Kannan, R., et al., *Evidence for carrier-mediated transport of glutathione across the blood-brain barrier in the rat.* J Clin Invest, 1990. **85**(6): p. 2009-13.

227. Kannan, R., et al., *GSH transport in human cerebrovascular endothelial cells and human astrocytes: evidence for luminal localization of Na+-dependent GSH transport in HCEC.* Brain Res, 2000. **852**(2): p. 374-82.

228. Kafedjiiski, K., et al., *Synthesis and in vitro characterization of a novel poly(acrylic acid)-glutathione conjugate.* Journal of Drug Delivery Science and Technology, 2005. **15**(6): p. 411-417.

229. More, S.S. and R. Vince, *Design, synthesis and biological evaluation of glutathione peptidomimetics as components of anti-Parkinson prodrugs.* Journal

of Medicinal Chemistry, 2008. **51**(15): p. 4581-4588.

230. Raval, N., et al., *Development of glutathione-conjugated asiatic acid-loaded bovine serum albumin nanoparticles for brain-targeted drug delivery.* J Pharm Pharmacol, 2015. **67**(11): p. 1503-11.

231. Grover, A., A. Hirani, and V. Sutariya, *Blood-Brain Barrier Permeation of Glutathione-Coated Nanoparticle.* SOJ Pharm PharmSci, 2014. **1**(1): p. 4.

232. Booth, R. and H. Kim, *Permeability analysis of neuroactive drugs through a dynamic microfluidic in vitro blood-brain barrier model.* Ann Biomed Eng, 2014. **42**(12): p. 2379-91.

233. Berg, C., *Quantitative analysis of nanoparticle transport through in vitro blood-brain barrier models.* Tissue Barriers, 2016. **4**(1): p. e1143545.

234. Grabrucker, A.M., et al., *Nanoparticle transport across the blood brain barrier.* Tissue Barriers, 2016. **4**(1): p. e1153568.

235. Huang, A.J., et al., *Effects of Human Neutrophil Chemotaxis across Human-Endothelial Cell Monolayers on the Permeability of These Monolayers to Ions and Macromolecules.* Journal of Cellular Physiology, 1988. **135**(3): p. 355-366.

236. Patsch, C., et al., *Generation of vascular endothelial and smooth muscle cells from human pluripotent stem cells.* Nat Cell Biol, 2015. **17**(8): p. 994-1003.

237. van Beveren, L., et al. *Indium Tin Oxide film characterization using the classical Hall Effect*. in *CONFERENCE ON OPTOELECTRONIC AND MICROELECTRONIC MATERIALS AND DEVICES (COMMAD 2014)*. 2014.

238. Choi, E., et al., *Formation of hydrogel membranes in microchannels and its applications*. 2011.

239. Lou, Y.-R., et al., *The use of nanofibrillar cellulose hydrogel as a flexible three-dimensional model to culture human pluripotent stem cells.* Stem cells and development, 2014. **23**(4): p. 380-392.

240. Palivan, C.G., et al., *Bioinspired polymer vesicles and membranes for biological and medical applications.* Chem Soc Rev, 2016. **45**(2): p. 377-411.

241. Mayer-Wagner, S., et al., *Scaffold-free 3D cellulose acetate membrane-based cultures form large cartilaginous constructs.* J Tissue Eng Regen Med, 2011. **5**(2): p. 151-5.

242. Ehgartner, J., et al., *Low cost referenced luminescent imaging of oxygen and pH with a 2-CCD colour near infrared camera.* Analyst, 2014. **139**(19): p. 4924-33.

243. Ungerbock, B., et al., *Microfluidic oxygen imaging using integrated optical sensor layers and a color camera.* Lab Chip, 2013. **13**(8): p. 1593-601.

244. Shen, Y., et al., *Integrins-FAK-Rho GTPases pathway in endothelial cells sense and response to surface wettability of plasma nanocoatings.* ACS Appl Mater Interfaces, 2013. **5**(11): p. 5112-21.

245. Hu, J., et al., *Enhanced cell adhesion and alignment on micro-wavy patterned surfaces.* PLoS One, 2014. **9**(8): p. e104502.

246. Zhang, S., et al., *Biological surface engineering: a simple system for cell pattern formation.* Biomaterials, 1999. **20**(13): p. 1213-20.

247. Hatano, R., et al., *Endothelial cells derived from embryonic stem cells respond to cues from topographical surface patterns.* J Biol Eng, 2013. **7**: p. 18.

248. Tennant, M. and J.K. McGeachie, *Blood vessel structure and function: a brief update on recent advances.* Aust N Z J Surg, 1990. **60**(10): p. 747-53.

249. Tanabe, S. and D. Grenier, *Endothelial cell/macrophage cocultures as a model to study Streptococcus suis-induced inflammatory responses.* FEMS Immunol Med Microbiol, 2009. **55**(1): p. 100-6.

250. Lin, T.M., et al., *Monocyte-endothelial cell coculture enhances infection of endothelial cells with Chlamydia pneumoniae.* J Infect Dis, 2000. **181**(3): p. 1096-100.

251. Wada, Y., et al., *In vitro model of atherosclerosis using coculture of arterial wall cells and macrophage.* Yonsei Med J, 2000. **41**(6): p. 740-55.

252. Islam, K., et al., *Co-culture Methods Used to Model Atherosclerosis In Vitro Using Endothelial, Smooth Muscle and Monocyte Cells.* SM J Biomed Eng, 2016. **2**(1).

253. Pergola, C., et al., *Modulation of actin dynamics as potential macrophage subtype-targeting anti-tumour strategy.* Sci Rep, 2017. **7**: p. 41434.

254. Lilly, B., *We have contact: endothelial cell-smooth muscle cell interactions.* Physiology (Bethesda), 2014. **29**(4): p. 234-41.

255. Fillinger, M.F., et al., *Coculture of endothelial cells and smooth muscle cells in bilayer and conditioned media models.* J Surg Res, 1997. **67**(2): p. 169-78.

256. Williams, C. and T.M. Wick, *Endothelial cell-smooth muscle cell co-culture in a perfusion bioreactor system.* Ann Biomed Eng, 2005. **33**(7): p. 920-8.

257. Chiu, J.J., et al., *A model for studying the effect of shear stress on interactions between vascular endothelial cells and smooth muscle cells.* Journal of Biomechanics, 2004. **37**(4): p. 531-539.

258. Heydarkhan-Hagvall, S., et al., *Co-culture of endothelial cells and smooth muscle cells affects gene expression of angiogenic factors.* J Cell Biochem, 2003. **89**(6): p. 1250-9.

259. Truskey, G.A., *Endothelial Cell Vascular Smooth Muscle Cell Co-Culture Assay For High Throughput Screening Assays For Discovery of Anti-Angiogenesis Agents and Other Therapeutic Molecules.* Int J High Throughput Screen, 2010. **2010**(1): p. 171-181.

260. Hergenreider, E., et al., *Atheroprotective communication between endothelial cells and smooth muscle cells through miRNAs.* Nat Cell Biol, 2012. **14**(3): p. 249-56.

261. Boon, R.A., E. Hergenreider, and S. Dimmeler, *Atheroprotective mechanisms of shear stress-regulated microRNAs.* Thromb Haemost, 2012. **108**(4): p. 616-20.

262. Armulik, A., A. Abramsson, and C. Betsholtz, *Endothelial/pericyte interactions.* Circ Res, 2005. **97**(6): p. 512-23.

263. Armulik, A., G. Genove, and C. Betsholtz, *Pericytes: developmental, physiological, and pathological perspectives, problems, and promises.* Dev Cell, 2011. **21**(2): p. 193-215.

264. Fisher, M., *Pericyte signaling in the neurovascular unit.* Stroke, 2009. **40**(3 Suppl): p. S13-5.

265. Raasch, M., et al., *Microphysiological systems meet hiPSC technology - New tools for disease modeling of liver infections in basic research and drug development.* Adv Drug Deliv Rev, 2018.

266. Orlova, V.V., et al., *Generation, expansion and functional analysis of endothelial cells and pericytes derived from human pluripotent stem cells.* Nature Protocols, 2014. **9**: p. 1514.

267. Dash, B.C., et al., *Induced pluripotent stem cell-derived vascular smooth muscle cells: methods and application.* The Biochemical journal, 2015. **465**(2): p. 185-194.

268. Shamis, Y., et al., *Fibroblasts derived from human pluripotent stem cells activate angiogenic responses in vitro and in vivo.* PLoS One, 2013. **8**(12): p. e83755.

269. Rufaihah, A.J., et al., *Human induced pluripotent stem cell-derived endothelial cells exhibit functional heterogeneity.* American journal of translational research, 2013. **5**(1): p. 21-35.

270. Rosa, S., et al., *Functional characterization of iPSC-derived arterial- and venous-like endothelial cells.* Scientific Reports, 2019. **9**(1): p. 3826.

271. Campbell, H.K., J.L. Maiers, and K.A. DeMali, *Interplay between tight junctions & adherens junctions.* Exp Cell Res, 2017.

272. Honda, H., *The world of epithelial sheets.* Dev Growth Differ, 2017.

273. Campanale, J.P., T.Y. Sun, and D.J. Montell, *Development and dynamics of cell polarity at a glance.* J Cell Sci, 2017. **130**(7): p. 1201-1207.

274. Butler, M.T. and J.B. Wallingford, *Planar cell polarity in development and disease.* Nat Rev Mol Cell Biol, 2017.

275. Kwan, K.M., *Coming into focus: the role of extracellular matrix in vertebrate optic cup morphogenesis.* Dev Dyn, 2014. **243**(10): p. 1242-8.

276. Livesey, F.J. and C.L. Cepko, *Vertebrate neural cell-fate determination: lessons from the retina.* Nat Rev Neurosci, 2001. **2**(2): p. 109-18.

277. Hagios, C., A. Lochter, and M.J. Bissell, *Tissue architecture: the ultimate regulator of epithelial function?* Philos Trans R Soc Lond B Biol Sci, 1998. **353**(1370): p. 857-70.

278. Camazine, S., *Self-organization in biological systems*. Princeton studies in complexity. 2001, Princeton, N.J.: Princeton University Press. viii, 538 p., 8 p. of plates.

279. Bettahalli, N.M., et al., *Development of multilayer constructs for tissue engineering.* J Tissue Eng Regen Med, 2014. **8**(2): p. 106-19.

280. Hogrebe, N.J., J.W. Reinhardt, and K.J. Gooch, *Biomaterial microarchitecture: a potent regulator of individual cell behavior and multicellular organization.* J Biomed Mater Res A, 2017. **105**(2): p. 640-661.

281. Amenta, P.S. and D. Harrison, *Expression and potential role of the extracellular matrix in hepatic ontogenesis: a review.* Microsc Res Tech, 1997. **39**(4): p. 372-86.

282. Yonemura, S., *Differential sensitivity of epithelial cells to extracellular matrix in polarity establishment.* PLoS One, 2014. **9**(11): p. e112922.

283. de Clerck, Y.A. and P.A. Jones, *The effect of ascorbic acid on the nature and production of collagen and elastin by rat smooth-muscle cells.* Biochem J, 1980. **186**(1): p. 217-25.

284. Tsuda, Y., et al., *The use of patterned dual thermoresponsive surfaces for the collective recovery as co-cultured cell sheets.* Biomaterials, 2005. **26**(14): p. 1885-1893.

285. Harimoto, M., et al., *Novel approach for achieving double-layered cell sheets co-culture: overlaying endothelial cell sheets onto monolayer hepatocytes utilizing temperature-responsive culture dishes.* J Biomed Mater Res, 2002. **62**(3): p. 464-70.

286. Chen, G., et al., *Application of the cell sheet technique in tissue engineering.* Biomed Rep, 2015. **3**(6): p. 749-757.

287. Sakaguchi, K., T. Shimizu, and T. Okano, *Construction of three-dimensional vascularized cardiac tissue with cell sheet engineering.* J Control Release, 2015. **205**: p. 83-8.

288. Lee, P.J., P.J. Hung, and L.P. Lee, *An artificial liver sinusoid with a microfluidic endothelial-like barrier for primary hepatocyte culture.* Biotechnol Bioeng, 2007. **97**(5): p. 1340-6.

289. Groger, M., et al., *Monocyte-induced recovery of inflammation-associated hepatocellular dysfunction in a biochip-based human liver model.* Sci Rep, 2016. **6**: p. 21868.

290. Thomas, L., et al., *Selective upregulation of TNF alpha, expression in classically-activated human monocyte-derived macrophages (M1) through pharmacological interference with V-ATPase.* Biochemical Pharmacology, 2017. **130**: p. 71-82.

291. Zheng, W., et al., *An Early-Stage Atherosclerosis Research Model Based on Microfluidics.* Small, 2016. **12**(15): p. 2022-34.

292. Pastorelli, L., et al., *Central role of the gut epithelial barrier in the pathogenesis of chronic intestinal inflammation: lessons learned from animal models and human genetics.* Front Immunol, 2013. **4**: p. 280.

293. Balzan, S., et al., *Bacterial translocation: overview of mechanisms and clinical impact.* J Gastroenterol Hepatol, 2007. **22**(4): p. 464-71.

294. Matthay, M.A. and G.A. Zimmerman, *Acute lung injury and the acute respiratory distress syndrome: four decades of inquiry into pathogenesis and rational management.* Am J Respir Cell Mol Biol, 2005. **33**(4): p. 319-27.

295. Abaci, H.E. and M.L. Shuler, *Human-on-a-chip design strategies and principles for physiologically based pharmacokinetics/pharmacodynamics modeling.* Integr Biol (Camb), 2015. **7**(4): p. 383-91.

296. Skardal, A., T. Shupe, and A. Atala, *Organoid-on-a-chip and body-on-a-chip systems for drug screening and disease modeling.* Drug Discov Today, 2016. **21**(9): p. 1399-411.

297. Aird, W.C., *Endothelium as an organ system.* Critical Care Medicine, 2004. **32**(5): p. S271-S279.

VI. Theses

1. MOTiF biochip design supports EC culture and precise modulation of key physiologic parameters such as shear forces, mechanical stretch and nutritional supply

2. ECs benefit from improved perfusion conditions in MOTiF biochips in terms of morphology and maintaining their functionality

3. Spatially adjustable gradient concentrations enable endothelial cell barrier modulation and monitoring of immune cell recruitment

4. Microphysiologic systems simulate mechanomodulatory cues that influence the behaviour of NPs

5. Tissue resident macrophages modulate EC biology and have a profound impact on NP uptake behaviour.

6. The MOTiF biochip provides a new tool to investigate processes of neuro-inflammation and neocortex formation, e.g. within drug screening and toxicity studies

7. A microphysiologic model of the human BBB within MOTiF biochips allows the investigation of GSH functionalized nanocarriers for gene delivery

8. Microphysiologic systems bare the possibility to simulate the microenvironmental human *in vivo* situation more accurately. This new approach may help to bridge the gap between *in vitro* experiments, animal models and the human *in vivo* situation.

VII. Author contribution statement

Manuscript I

Raasch M, Rennert K, Jahn T, Peters S, Henkel T, Huber O, Schulz I, Becker H, Lorkowski S, Funke H, Mosig A. (2015)

Microfluidically supported biochip design for culture of endothelial cell layers with improved perfusion conditions.

Biofabrication. 7(1): p. 015013

author	**contribution**
M. Raasch	Cell culture and HUVEC isolation from umbilical cords, biochip preparation (sterilisation, cell seeding and maintenance), evaluation of culture conditions within the MOTiF biochip, performing biochip perfusion experiments, calculation of shear stress levels, immunofluorescence staining and microscopy, cell shape index analysis, permeability assays, THP-1 adhesion assays, flow cytometry analysis of CAMs, analysis of data, co-writing the manuscript **total contribution: 80 %**
K. Rennert	biochip design, cell culture, supervising experiments
T. Jahn, I. Schulz H. Becker	biochip design and fabrication
S. Peters	LSM analysis
T. Henkel	CFD analysis
O. Huber, H. Funke S. Lorkowski	scientific discussion, correction of manuscript
A. Mosig	study design, scientific discussion, writing the manuscript

Manuscript II

Rinkenauer AC, Press AT, **Raasch M**, Pietsch C, Schweizer S, Schworer S, Rudolph KL, Mosig A, Bauer M, Traeger A, Schubert US. (2015)
Comparison of the uptake of methacrylate-based nanoparticles in static and dynamic in vitro systems as well as in vivo.

J Control Release. 216: p. 158-68.

author	**contribution**
M. Raasch	HUVEC isolation from umbilical cords, performance of whole blood monocyte isolation, macrophage differentiation and fluorescence labelling, biochip preparation of HUVEC mono-cell and HUVEC-macrophage co-culture, performing biochip NP uptake studies, immunofluorescence microscopy, quantification of NP uptake, analysis of data, preparation of figures, co-writing the manuscript. **total contribution: 25 %**
A. C. Rinkenauer	NP preparation, static nanoparticle characterisation, flow cytometry, LSM analysis, writing the manuscript, study design
A. T. Press	LSM analysis, intravital microscopy, writing the manuscript, study design
C. Pietsch	polymer synthesis and characterisation
S. Schweizer	NP preparation
K. L. Rudolph, S. Schwörer, M. Bauer, U. S. Schubert	correction of manuscript
A. Träger, A. Mosig	study design, co-writing the manuscript, scientific discussion

Manuscript III

Raasch M, Rennert K, Jahn T, Gärtner C, Schönfelder G, Huber O, Seiler AE, Mosig AS. (2016)

An integrative microfluidically supported in vitro model of an endothelial barrier combined with cortical spheroids simulates effects of neuroinflammation in neocortex development. Biomicrofluidics. 10(4): p. 044102.

author	**contribution**
M. Raasch	cortical spheroid transport logistics**,** hCMEC cell culture and murine cortical spheroid differentiation, performance of medium adjustment to biochip assay co-culture medium, cortex model assembly, performing biochip perfusion experiments, viability assays, analysis and quantification of spheroid growth, permeability assays, immunofluorescence staining and microscopy, analysis of data, co-writing the manuscript. **total contribution: 80 %**
K. Rennert, O. Huber	scientific discussion, correction of manuscript
T. Jahn, C. Gärtner	biochip fabrication
G. Schönfelder, A. E. Seiler	provision of cortical spheroids, study design, correction of manuscript
A. S. Mosig	study design, scientific discussion, writing the manuscript

Manuscript IV

Englert C, Trutzschler AK, **Raasch M,** Bus T, Borchers P, Mosig AS, Traeger A, Schubert US. (2016)

Crossing the blood-brain barrier: Glutathione-conjugated poly(ethylene imine) for gene delivery.

J Control Release. 241: p.1-14.

author	**contribution**
M. Raasch	study design, hCMEC cell culture, preparation of biochip, preparation of polyplex stocks, performing biochip polyplex perfusion experiments, time-dependent sampling, immunofluorescence staining and microscopy, analysis of data, preparation of figures, co-writing the manuscript. **total contribution: 25 %**
C. Englert	study design, polymer synthesis and polymer characterisation, writing the manuscript, supervision of P. Borchers
A. K. Trützschler	study design, polymer characterisation, writing the manuscript
T. Bus	study design, tox and biocompatibility assays, correction of manuscript
P. Borchers	polymer synthesis
A. S. Mosig, A. Träger	study design, scientific discussion, correction of manuscript
U. S. Schubert	correction of manuscript

Jena, den 25.05.2020

Prof. Dr. med. Michael Bauer

IX. Declaration of Originality / Eigenständigkeitserklärung

Hiermit erkläre ich, dass mir die Promotionsordnung der Fakultät für Biowissenschaften der Friedrich-Schiller-Universität Jena bekannt ist, dass ich die Dissertation selbst angefertigt habe, dass keine Textabschnitte eines Dritten oder eigener Prüfungsarbeiten ohne Kennzeichnung übernommen wurden und dass alle von mir benutzten Hilfsmittel, persönlichen Mitteilungen und Quellen in meiner Arbeit ordnungsgemäß angegeben sind.

Ich versichere, dass ich die Hilfe eines Promotionsvermittlers nicht in Anspruch genommen habe und dass Dritte weder unmittelbar noch mittelbar geldwerte Leistungen von mir für Arbeiten erhalten haben, die im Zusammenhang mit dem Inhalt der vorgelegten Dissertation stehen.

Die vorliegende Dissertation wurde von mir bei keiner bisherigen Prüfungsarbeit für eine staatliche oder andere wissenschaftliche Prüfung eingereicht. Weiterhin versichere ich, dass ich die gleiche, eine in wesentlichen Teilen ähnliche oder eine andere Abhandlung nicht bei einer anderen Universität als Dissertation eingereicht habe.

Jena, den 25.05.2020

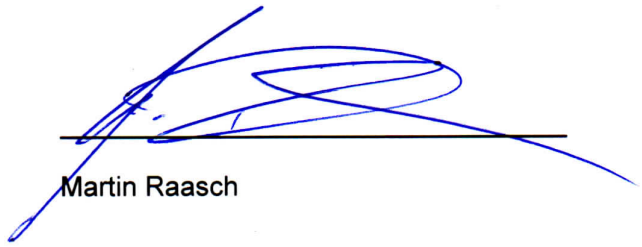

Martin Raasch

X. Academic Curriculum Vitae

Personal Details

Address:	Thomas-Müntzer-Str. 48
	99423 Weimar
Date of Birth:	05.05.1987
Marital Status:	not married
Mobile:	+49 160 92 16 22 87
E-Mail:	martin.raasch@med.uni-jena.de

Current Position

since 01/2017	Research Group INSPIRE (CSCC/ University Hospital Jena)
	pre-doctoral research fellow

Education

02/2012 – 12/2016	Research Group INSPIRE (CSCC/ University Hospital Jena)
	doctoral candidate
10/2009 – 09/2011	Leipzig University
	M.Sc. Biochemistry
10/2006 – 09/2009	Leipzig University
	B.Sc. Biochemistry

Research focus

human microphysiologic systems

microfluidic biochips

endothelial and vascular biology

induced pluripotent stem cells

sepsis

nanocarrier applications

Related Professional Experience

since 03/2018 CEO and Co-founder of Dynamic42 GmbH

2015 – 2018 Start-up idea “OrganiX”

Awards

2018 “EY PublicEyeAward” Audience Award

2018 “Thüringer Gründerpreis” Jury Award 3rd Place Businessplan

2017 „Thüringer Strategiewettbewerb für innovative Gründungen“ Jury Award

2017 „Science4Life“ (federal german competition) Jury Award 6th Place Businessplan

2016 „Thüringer Gründungsideenwettbewerb“ Jury Award Innovative Founding Idea 2016

2015 „Gründer- und Innovationstag Jena“ Jury Award Founding Champ 2015

Audience Award

Additional Qualification

2017 „Quality Management and Good Laboratory Practice“

PromoCell Academy Heidelberg

2017 Workshop „Induzierbare pluripotente Stammzellen (iPS) – Grundlagen und Kultur“

Charité Berlin

2015 Summer School “Gründungsmanagement”

University Friedrich Schiller Jena

2014 Project Management (advanced training)

Graduate Academy of University Friedrich Schiller Jena

Languages Englisch fluently (speaking and writing)

French basic

Memberships

since 2019 European Organ-On-Chip Society (EUROOCS)

since 2018 European Society For Alternatives To Animal Testing (EUSAAT)

since 2014 Center for Sepsis Control and Care (CSCC)

Conference Contributions

2019 EUROoC, Graz / Austria

"Challenges of human iPSC-derived microphysiological systems emulating human liver function" **(Poster**)

2018 EUSAAT, Linz / Austria

"Emulating the Gut-Liver Axis - Organ-on-chip as Translational Tool in Sepsis Research" (**Talk**)

"3D Models & Multi-Organ-Chips (MOC), Human-Organ-Chips (HOC) IV – Intestinal Systems" (**Session Chair**)

"Making drug screening visible: human iPSC-derived biochip-based models of the liver and kidney" (**Poster**)

2018 EUROoC, Stuttgart / Germany

"Emulating the Gut-Liver Axis - Organ-on-chip as Translational Tool in Sepsis Research" (**Talk**)

"Making drug screening visible: human iPSC-derived biochip-based models of the liver and kidney" (**Poster**)

2017 Sepsis Update Weimar, Weimar / Germany

"Dampening inflammation: Co2+ loaded block copolymer micelles as novel tools to trigger anti-inflammatory macrophage polarization" (**Poster**)

Publications

Maurer M, Gresnigt M, Last A, Wollny T, Berlinghof F, Pospich R, Cseresnyés Z, Medyukhina A, Graf K, Groeger M, **Raasch M**, Siwczak F, Nietzsche S, Jacobsen ID, Figge MT, Hube B, Huber O, Mosig AS. (2019)

A three-dimensional immunocompetent intestine-on-chip model as in vitro platform for functional and microbial interaction studies.

Biomaterials. 220: p. 119396. Journal Impact Factor: 10.273

Pein H, Ville A, Pace S, Temml V, Garscha U, **Raasch M**, Alsabil K, Viault G, Dinh CP, Guilet D, Troisi F, Neukirch K, König S, Bilancia R, Waltenberger B, Stuppner H, Wallert M, Lorkowski S, Weinigel C, Rummler S, Birringer M, Roviezzo F, Sautebin L, Helesbeux JJ, Séraphin D, Mosig AS, Schuster D, Rossi A, Richomme P, Werz O, Koeberle A. (2018)
Endogenous metabolites of vitamin E limit inflammation by targeting 5-lipoxygenase.
Nat Commun. 9(1): p. 3834. Journal Impact Factor: 11.878

Raasch M, Fritsche E, Kurtz A, Bauer M, Mosig AS. (2018)
Microphysiological systems meet hiPSC technology - New tools for disease modeling of liver infections in basic research and drug development.
Adv Drug Deliv Rev. 140: p. 51-67. Journal Impact Factor: 15.519

Rennert K, Nitschke M, Wallert M, Keune N, **Raasch M**, Lorkowski S, Mosig AS. (2017)
Thermo-responsive cell culture carrier: Effects on macrophage functionality and detachment efficiency.
J Tissue Eng. 8:2041731417726428. Journal Impact Factor: 4.148

Thomas L, Zhigang R, Gerstmeier J, **Raasch M**, Weinigel C, Rummler S, Menche D, Müller R, Pergola C, Mosig A, Werz O. (2017)
Selective upregulation of TNFα expression in classically-activated human monocyte-derived macrophages (M1) through pharmacological interference with V-ATPase.
Biochemical Pharmacology. 130: p. 71-82. Journal Impact Factor: 4.825

Pergola C, Schubert K, Pace S, Ziereisen J, Nikels F, Scherer O, Hüttel S, Zahler S, Vollmar A, Weinigel C, Rummler S, Müller R, **Raasch M**, Mosig A, Koeberle A, Werz O. (2017)
Modulation of actin dynamics as potential macrophage subtype targeting anti-tumour strategy.
Scientific Reports. 7: p. 41434. Journal Impact Factor: 4.011

Englert C, Trutzschler AK, **Raasch M,** Bus T, Borchers P, Mosig AS, Traeger A, Schubert US. (2016)
Crossing the blood-brain barrier: Glutathione-conjugated poly(ethylene imine) for gene delivery.
J Control Release. 241: p.1-14. Journal Impact Factor: 7.901

Raasch M, Rennert K, Jahn T, Gärtner C, Schönfelder G, Huber O, Seiler AE, Mosig AS. (2016)

An integrative microfluidically supported in vitro model of an endothelial barrier combined with cortical spheroids simulates effects of neuroinflammation in neocortex development.

Biomicrofluidics. 10(4): p. 044102. Journal Impact Factor: 2.531

Rinkenauer AC, Press AT, **Raasch M**, Pietsch C, Schweizer S, Schworer S, Rudolph KL, Mosig A, Bauer M, Traeger A, Schubert US. (2015)

Comparison of the uptake of methacrylate-based nanoparticles in static and dynamic in vitro systems as well as in vivo.

J Control Release. 216: p. 158-68. Journal Impact Factor: 7.901

Raasch M, Rennert K, Jahn T, Peters S, Henkel T, Huber O, Schulz I, Becker H, Lorkowski S, Funke H, Mosig A. (2015)

Microfluidically supported biochip design for culture of endothelial cell layers with improved perfusion conditions.

Biofabrication. 7(1): p. 015013 Journal Impact Factor: 7.236

VI. Acknowledgements

> "Almost every important human encounter boils down to the act, and the art, of asking."
>
> Amanda Palmer, The Art of Asking (2014)

And that is just what I did! Back in late 2011 I asked Dr. Mosig for a position as doctoral candidate in his group, even knowing there was no job posting. Half a year earlier, when I was still in Leipzig finishing my master's thesis, I read a portrait about his research group. I already knew alternatives to animal testing will be my thing, my goal that I want to pursue in research. To be honest, the topic about ethics and animal testing was shamefully neglected in the studies of biochemistry at Leipzig University, which bothered me tremendously. So, during my studies I already realised how I would like to put my future work into something meaningful.

Just by coincidence, I moved near Jena, so I gave it a shot and Dr. Mosig agreed to give me a position. I am still very thankful for that opportunity (and it should not have been the only one…)! I am also thankful to Dr. Mosig for being an excellent supervisor and mentor, for being always open for discussions, for encouraging me pursuing my ideas and for being so patient with me!

Further, I would like to thank Prof. Dr. med. Michael Bauer for being second supervisor during my work.

The following thesis is based on research that has been conducted between 2012 and 2016. And along the way I encountered a lot of people, I also would like to thank. To begin with Dr. Knut Rennert, who has been a great colleague and advisor. He thought me a lot about *in vitro* cell culture, and to be always critical with the data obtained. He became a valuable and reliable colleague as well as a trusted business partner. Further he is always in a good mood making work less stressful.

Further I like to thank Dr. Marko Gröger for being an excellent colleague in every way: for helping when another hand was needed, for constructive discussions and for making lab work so much fun! It bothered me a bit, that he started later with his doctoral thesis and finished earlier than me, but who could have known that both our work resulted in very fruitful *in vitro*

model applications accompanied by the second opportunity Dr. Mosig then offered to me: founding Dynamic42 GmbH, becoming CEO and having now the chance to translate years of work into products that will hopefully help to set new standards for *in vitro* research and drug testing.

I also like to thank all the rest of the Mosig lab group: Melanie Ulrich for being an excellent technician during the last four years and for sharing the best 80s music there ever was; also, Michelle Maurer for being a great colleague and Swen, Fatina, Nora and Tobi for the great lab support and atmosphere.

During 2015 everything got really exciting, when I started together with Dr. Nancy Blaurock-Möller, Dr. Knut Rennert and Dr. Mosig to actually work on our business idea. Thanks for the ride so far! Especially learning new things about business models, calculating revenues, talking about products and not research, taking part in business competitions, presenting in front of investors for money support and writing business plans was inspiring, exhausting and sometimes overwhelming. All new to a scientist, who initially chose science as career and not economics, and these overwhelming things contributed to the fact, that there was never the right time to finish writing my doctoral thesis.

I could not have coped with all the things on this journey if there were not some special people in my life who helped me not losing track. Now a big thank you goes to my mother, who always supported me, believed in me and had to wait a long time to see her son finishing his degree.

The biggest thank you goes to my partner and love of my life Christian Becker. You supported me every single day, motivated me, believed in me and you never let me down, no matter how complicated it has been. I cannot thank you enough for this! If necessary, you comforted me, made me laugh again and you brought me back down to earth and showed me never to forget the small, but beautiful things in life.

And of course, thank you to my crews in Weimar and Leipzig, especially Eileen and Thomas for being such great and lovely friends. Thank you to Laura for being there for Christian and me. Thank you to Julianna for always welcoming me in your home and on your couch in Leipzig when I needed some distance. And thank you to Clara and Niels, Tine, Maria, Filippo and Uwe who all became some valuable friends during that time!

Finally, thanks and lots of love to a person with a big heart who accompanied me on my way but is not among us anymore: Yella.